Mechanical properties of high density cellular polyurethanes

MECHANICAL PROPERTIES OF HIGH DENSITY CELLULAR POLYURETHANES

by

RONALD ERIC WHITTAKER, M.Phil., B.Sc.

A Thesis submitted for the award of the Degree of Doctor of Philosophy of the Loughborough University of Technology

September 1972

Supervisors: C. M. BLOW, Ph.D.
Institute of Polymer Technology

A. R. PAYNE, D.Sc.
Shoe and Allied Trades Research Association

Investigation undertaken at the Shoe and Allied Trades Research Association, Kettering, Northants, in Affiliation with Loughborough University of Technology

ABSTRACT

The use of cellular polyurethanes either as microporous foams in shoe upper materials (poromerics) or in closed cell form as soling materials has increased rapidly during the last few years in the footwear industry. Compared with vulcanised rubbers, these materials have high strength over an extended temperature range, high set and good resistance to cut growth. The research now presented has been concerned with determining the reasons for these mechanical properties of polyurethane as compared with compounded conventional vulcanised rubbers.

The supplementary contribution to the thesis presents a review of earlier work on the strength and reinforcement of crystalline, amorphous and filled vulcanised rubbers and includes a short section on the effect of crosslinking on ultimate failure properties of natural rubber. This study has been extended by the author into the effect of chain branching in polyurethane elastomers on the failure properties.

The viscoelastic properties of natural and artificial leathers are also discussed in order to demonstrate similarities between the different materials and show how a cellular polyurethane sheet has hysteresial properties similar to those of a natural material of fibrous structure.

It is shown that a cubical lattice model can be applied to explain the differences between such mechanical properties as modulus, tensile and tear strength of a cellular polyurethane and the corresponding solid material of the same polymer. This model, which has previously been applied to the mechanical properties of a natural rubber latex foam, indicates that the strength of cellular polyurethanes is due to the very high strength of the solid material.

An extensive investigation into the effect of time and temperature on the tensile properties of cellular and solid polyurethanes is presented in order to show that polyurethanes of the type used in poromerics have a very broad relaxation spectrum extending over 18 decades of time. Because of this response to deformation, the failure properties remain fairly constant over the temperature range from 21 - 160°C. Above 160°C, the tensile properties fall quite markedly. Stress softening in these polyurethanes is very high and can only be reversed by heating to temperatures above 160°C.

The cut growth and fatigue properties of cellular and solid polyurethanes are considered. Following a brief review of the investigation on cut growth and fatigue of vulcanised rubbers involving the use of tearing energy theory, it is shown that cut growth and hysteresis properties of vulcanised rubbers can be correlated. The lower limit of tearing energy (To) below which no cut growth takes place in the absence of chemical effects is found to be higher for polyurethanes than for vulcanised rubbers. Fatigue ~~life~~ failure of cellular polyurethanes is found to be due to cut growth from the largest pore in the sample. These data are also compared with measurements on other two phase elastomer systems such as styrene butadiene copolymer vulcanisates with high styrene content and polystyrene-polybutadiene thermoplastic rubbers.

From an extensive review of the literature on the structure of polyurethane elastomers, it is deduced that polyurethanes of the type used in poromerics consist of a segmented structure of long polyester chains connected to very minute (25Å) hard urethane segments. The cohesion of the hard segments is primarily due to hydrogen bonding and other physical forces.

It is concluded that the high strength, good cut growth resistance and broad relaxation spectrum of polyurethanes are due to the reinforcement given by the hard urethane segments which act as well dispersed minute filler particles in the polyester rubber matrix. The hydrogen bonding between the hard segments dissociates at approximately 170^{o}C so giving a degree of thermoplasticity which produces a very high permanent set.

An appendix discusses some of the practical applications in the footwear industry of the work presented, such as forming of poromerics, tearing from stitch-holes and flex cracking of solings.

ACKNOWLEDGEMENTS

The work described in this thesis was supervised jointly by Dr. C. M. Blow, Institute of Polymer Technology, University of Loughborough (University Supervisor) and Dr. A. R. Payne, Director, Shoe and Allied Trades Research Association (Industrial Supervisor). The author is indebted to his supervisors and to Professor R. J. W. Reynolds (University of Loughborough) for their helpful advice and encouragement throughout the course of this work.

The author is also indebted to the Shoe and Allied Trades Research Association for providing the opportunity and facilities for undertaking this research programme.

LIST OF CONTENTS

Appendix 2 continued

LIST OF SYMBOLS

SYMBOL	QUANTITY	UNITS (where appropriate)
a_T	Time-Temperature Shift Factor	
AK^2	Moment of Inertia	
c	Volume concentration	
C	Flaw size	cm
C_o	Initial flaw size	cm
$dc/_{dn}$	Rate of cut growth	cm/cycle
D	Diameter of struts in Model (Chap. 4)	
e	Extension of foam	
e'	Extension of solid	
e_c	Critical strain	
E_e	Equilibrium Modulus	kgf/cm^2
E_r	Breaking energy/unit vol.	J/cc
E_F	Energy density at failure in foam	J/cc
E(t)	Relaxation Modulus	kgf/cm^2
f(e)	Strain function	
F	Force	kgf
F(t)	Constant strain rate modulus	kgf/cm^2
g	Numerical Factor	
g(ε)	Strain function	
G_e	Equilibrium shear modulus	kgf/cm^2
h	Hysteresis ratio	
h_B	Hysteresis ratio at break	
H_1	Hysteresis in 1st cycle	J/cc
H_2	Hysteresis in 2nd cycle	J/cc
$H(\tau)$	Relaxation Spectrum	kgf/cm^2
H_B	Hysteresis at Break	J/cc
K	Cut growth constant (Table 6.1.)	
lo	Length of strut in Model (Chap. 4)	
L	Depth of flaw	cm
m	Cut growth power index	
N	Fatigue Life	cycles
N(e)	Fatigue Life (const. temp.)	cycles
N(t)	Fatigue Life (const. strain)	cycles
R	Gas Constant	

SYMBOL cont.	QUANTITY	UNITS (where appropriate)
R_1	Strain Rate	per sec.
S	Shape Factor	
t	Compressive Stress (Chap. 4 only)	kgf/cm^2
t	Time	sec.
t_B	Time to break	sec.
T	Temperature (Chap. 2,3 and 5)	^oK
T	Tearing Energy (Chap. 4 and 6)	kgf/cm
T_o	Standard Reference Temperature (Chap. 5 only)	^oK
T_o	Limiting tearing energy (Chap.6 only)	kgf/cm
T_F	Tearing energy for foam model	kgf/cm
T_g	Glass transition temperature	^oK
T_s	$T_g + 50\ ^oK$	^oK
U	Energy	
U_1	Energy input to 1st cycle	J/cc
U_2	Energy input to 2nd cycle	J/cc
U_B	Energy input to break	J/cc
V_e	Number network chains/unit volume	moles/cc
X	Strain Amplification factor	
Y	Young's Modulus for Solid	kgf/cm^2
Y_F	Young's Modulus for Foam	kgf/cm^2
β	Ratio diameter to length strut in model foam (Chap. 4)	
ε	Strain	
ε_B	Strain at Break	
σ_r	Reduced strain	
λ	Strain Ratio (1 + strain)	
σ	Stress	kgf/cm^2
σ_c	Critical stress	kgf/cm^2
σ_r	Reduced stress	kgf/cm^2
$\sigma(\varepsilon,t)$	Stress function	
τ	Relaxation Time	

SI Equivalent Units

$1\ kgf/cm^2 = 9.81 \times 10^{-2}\ MN/m^2$

$1\ kgf/cm = 9.81 \times 10^{-4}\ MN/m$

$1\ J/cc = 1\ MN/m^2$

CHAPTER 1

INTRODUCTION

1.1. USE OF POLYMERIC MATERIALS IN FOOTWEAR

1.1.1. Introduction

The traditional material used for centuries in the manufacture of footwear has been natural leather. In recent years leather has also been increasingly used in the manufacture of gloves, clothing and upholstery. The success of leather in these applications is due to the good comfort and hygiene properties offered to the wearer. It is also very tough yet reasonably flexible and has good durability.

Despite these good properties, however, it suffers from a number of disadvantages. It cannot, for example, be obtained in uniform continuous sheets and this has delayed automation in these industries. Variations in leather quality arise from the techniques of husbandry, environment type and age of the animal. Serious faults, for example, within leather are caused by insects and fungal infections. These faults however can be masked by the tanner but not always satisfactorily. A certain amount of wastage must result from this treatment and this is the main reason why footwear and clothing manufacturers have increasingly turned to synthetic materials which can be obtained in continuous sheets and also have fairly uniform physical properties.

Another reason for the emergence of synthetic leathers is the possibility of a supply gap existing in the next few years. By taking into account the increase in world population and also the increasing number of pairs of shoes per person, it is thought that the world output of hides will be at least 30% less than potential demand by 1980. These figures exclude the increasing use of natural leather in clothing. In 1960, 75% of total leather usage in Britain was in footwear, whereas in 1970 this figure was reduced to 58%.

Polymers[1] have been widely used as replacement materials for leather during the last 20 years. Only 7% of the footwear produced in the U.K. at present has leather soles. The rise in the use of polymeric based upper materials has not been as fast as soling materials but in 1970, 29% of the dress shoes produced in the U.K. had synthetic uppers.

1.1.2. Soling Materials

Polymers have been used as shoe soling materials for the last 40 years but the most successful have been resin rubber soling sheets and direct moulded rubber soles which were introduced around 1950. Resin rubber was found to be the first material that looked like leather but in addition was more durable, completely waterproof and cheaper. In order to produce a lighter sole, microcellular rubber was later introduced. During the 1960's the use of PVC increased as a soling material mainly due to the relative ease of processing but it offered little in improved performance in wear. During the last few years, however, microcellular polyurethane solings[1-4] have been introduced which have improved performance in wear over both rubber and PVC and are quite light in weight.

1.1.3. Upper Materials

The first group of materials to be used as substitutes for leather uppers in shoes were coated fabrics. Solid or cellular polyvinylchloride (PVC) coatings on a woven, non-woven or knitted base are the most widely used materials and are shown in the scanning electron microscope (SEM) photographs[5] in figures 1.1. and 1.2. PVC coated fabrics are satisfactory for use in certain types of footwear because the general appearance of leather is simulated and they also possess some similar properties. Their main disadvantage, however, is that they lack the ability to 'breathe' or transpire water vapour and air which is characteristic of leather and their use has therefore been restricted

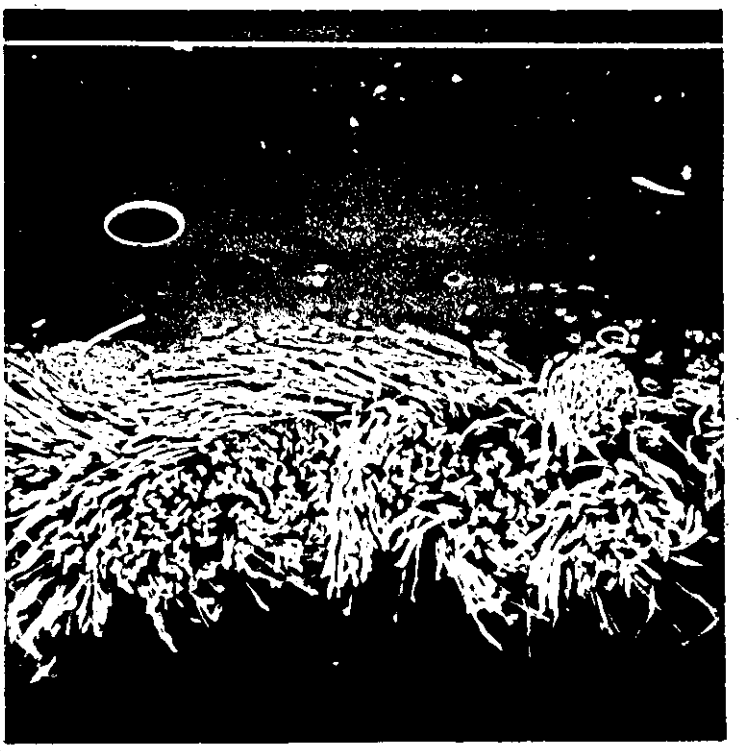

Figure 1.1.

SEM Cross-Section of Coated Fabric consisting of Solid PVC on woven fabric base. Magnification : 42 (After Hole and Whittaker[5]).

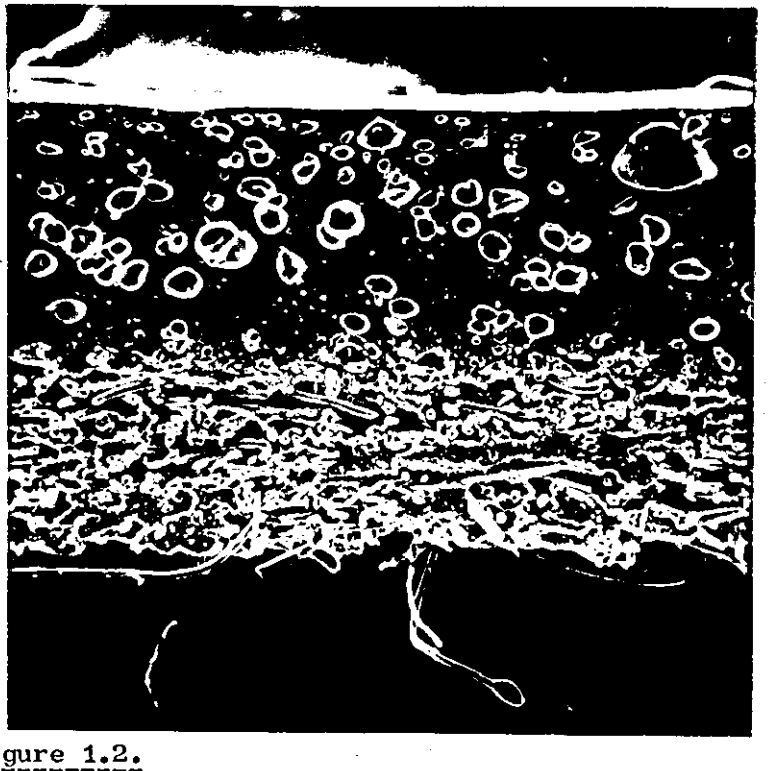

Figure 1.2.

SEM Cross-Section of Coated Fabric consisting of Cellular PVC on non-woven fabric base. Magnification : 40 (After Hole and Whittaker[5]).

to women's footwear of fairly open construction where these properties are not so important.

The outstanding moisture absorption and permeability properties of leather are due to the molecular and physical structure of its protein pre-cursor, collagen. Collagen is the main constituent of all structural tissue and is converted into leather by tanning with such agents as chromium salts, vegetable tannins and aldehydes.

The most hydrophilic man-made polymer yet manufactured, however, does not absorb more water than does leather itself. This fact has led many manufacturers to the idea of using collagen or leather fibres as a possible raw material for the manufacture of artificial leather[6]. This class of materials is known as collagenous poromerics. Since 1964, however, large financial investments have been made in the development and production of a completely man-made poromeric[5-7]. Up to present these have had better properties than the leather-based or collagenous types.

1.2. POROMERICS

1.2.1. Introduction

The manufacture of a completely synthetic material with moisture absorption and permeability properties similar to the natural leather was started in the late 1930s by E. I. Du Pont de Nemours Inc., U.S.A. Commercial production of the Du Pont product, under the trade name 'Corfam' was not started however until 1964, but as early as 1942, a U.S. patent[8] was taken out to describe a shoe upper material composed of flexible fabric coated with a synthetic linear polyamide. They initially used the term 'poromeric' to describe the material and defined it as 'A microporous, permeable, coriaceous sheet material comprising polyurethane reinforced with polyester'.

A number of new poromeric upper materials have come on to the market in recent years[5-7]. In view of the development of these materials, the Shoe and Allied Trades Research Association has had to widen the first definition given by Du Pont and now defines a poromeric material used in footwear as 'a man-made shoe upper material which is generally similar in nature and appearance to leather and in particular has a comparable permeability to water vapour'.

Most of the developments of poromerics have been based upon an attempt to imitate the fibrous structure of leather. This is shown by the comparison[5] of the scanning electron microscope photographs in figures 1.3. and 1.4. Figure 1.3. shows the structure of side leather and figure 1.4. shows the structure of poromeric 'Corfam' which has a high fibre density in the substrate. Leather consists also of a tightly packed fibre system but in contrast to the poromerics shows no large void spaces nor has any form of binder material between the fibres.

1.2.2. Structure of Poromerics

Poromerics in general have at least two discrete layers and some of the fibrous types such as 'Corfam', shown in figure 1.4. may have as many as five layers.

The layers are:

a) Finish (or top) layer

This is a very thin film applied to the otherwise complete poromeric. These finishes are commonly acrylic polymers but may sometimes be transparent polyurethane.

b) Surface skin

This is usually an integral part of the microporous layer, being formed as a result of fusion of the outermost cells. In some

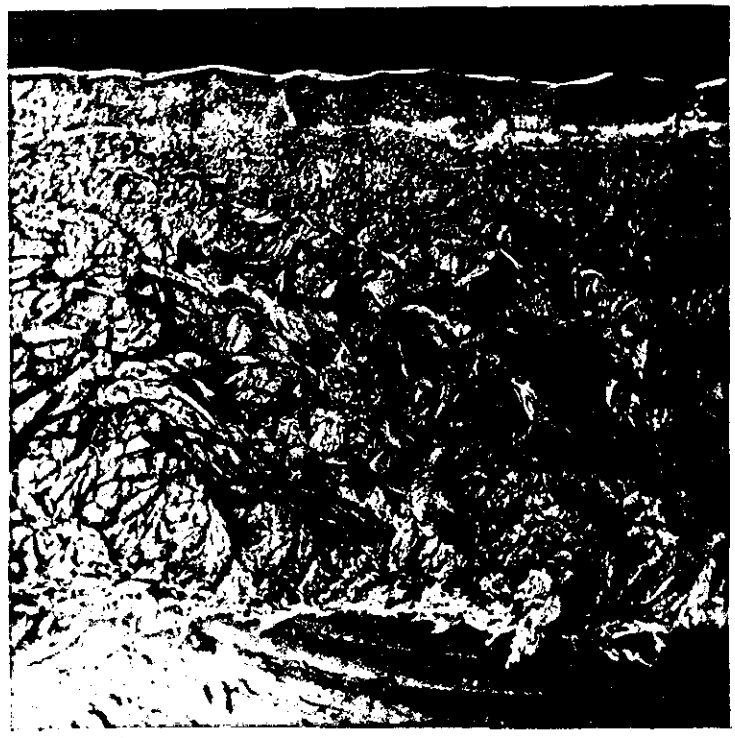

Figure 1.3.

SEM Cross-Section of Side Leather. Magnification : 35 (After Hole and Whittaker[5])

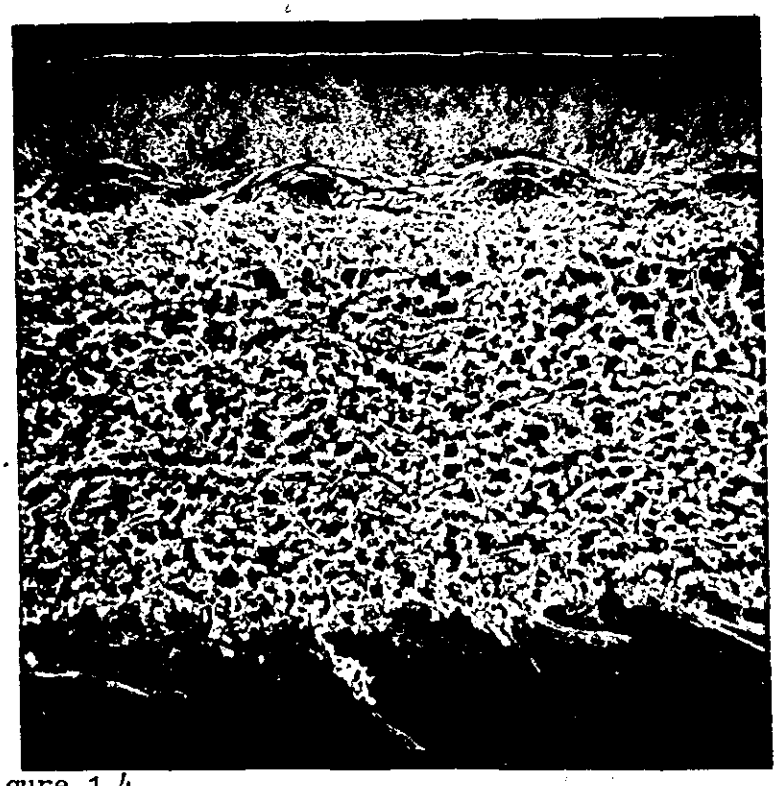

Figure 1.4.

SEM Cross-Section of "Corfam" poromeric. Magnification : 50 (After Hole and Whittaker[5]).

instances this surface is formed during a film release process and in others as part of the grain embossing process. The thickness and properties of this skin are very important because they affect the resistance to water penetration and the water vapour permeabilities of the poromeric, also its resistance to scuffing and snagging damage; in combination with the microporous coating, the skin determines the type of 'break' (wrinkle formation) that the material will form when folded.

c) Microporous layer

The thickness of the combined surface skin and microporous layer can vary from 16 - 44% of the overall thickness in commercial materials[7]. The microporous layer is generally a permeable polyurethane foam of small cell dimensions. The density is usually about 0.5 gm/cc and therefore amongst polyurethane foams would be considered as a high density material.

d) The interlayer

This is commonly a woven fabric which separates the microporous layer from the non-woven substrate in some materials. This component serves several purposes, e.g. increases tensile and tear strength (but reduces breaking extension); controls stretch and creep; masks surface uneveness effects when material is strained; places the neutral plane of the material close to the surface skin.

The interlayer fabric is polyester in 'Corfam', but other fibres are used in other poromerics. Although such interlayers provide the benefits listed above their use creates the problem of delamination which has caused some difficulties in shoe manufacture.

e) The substrate

This can be a non-woven, woven or knitted fabric all of which are impregnated to various extents with a polyurethane elastomeric

binder. However, in one instance, discussed below, the substrate is cellular polyurethane only.

In general, the impregnated substrates tend to behave like the fabric reinforcement which they contain, thus substrates with a non-woven matrix have a high breaking extension and tend to creep, whereas those substrates with woven fabrics have lower breaking extensions and tend not to creep; knitted substrates come somewhere between the two. The manufacture of poromerics has been discussed in several recent publications[7,9].

The five layers discussed above can be seen in 'Corfam' shown in figure 1.4. The density of fibres in this material is very much higher than in any other poromeric and approaches that found in natural leather. The polyurethane microporous layer in 'Corfam' differs from most of the other poromerics in that it is based on a polyether polyurethane rather than a polyester.

Figure 1.5. shows the structure of the poromeric 'Clarino' which is characterised by the absence of an interlayer. The other major difference between 'Clarino' and 'Corfam' is the much larger amount of foam elastomer in the substrate. It can be clearly seen from figure 1.5. how little adhesion is apparent between the fibres and the foam, an interesting departure from the usual non-woven structure. It is this absence of adhesion that contributes to the relatively good handle properties of 'Clarino'. The other significant feature in this connection is the small proportion of fibrous component in the substrate; it is much smaller in 'Clarino' than in any other fibrous based poromeric. The fibres in this material are nylon and viscose rayon.

Gradual development of poromerics has moved away from the "let's imitate leather" look and recently a new type of poromeric has appeared

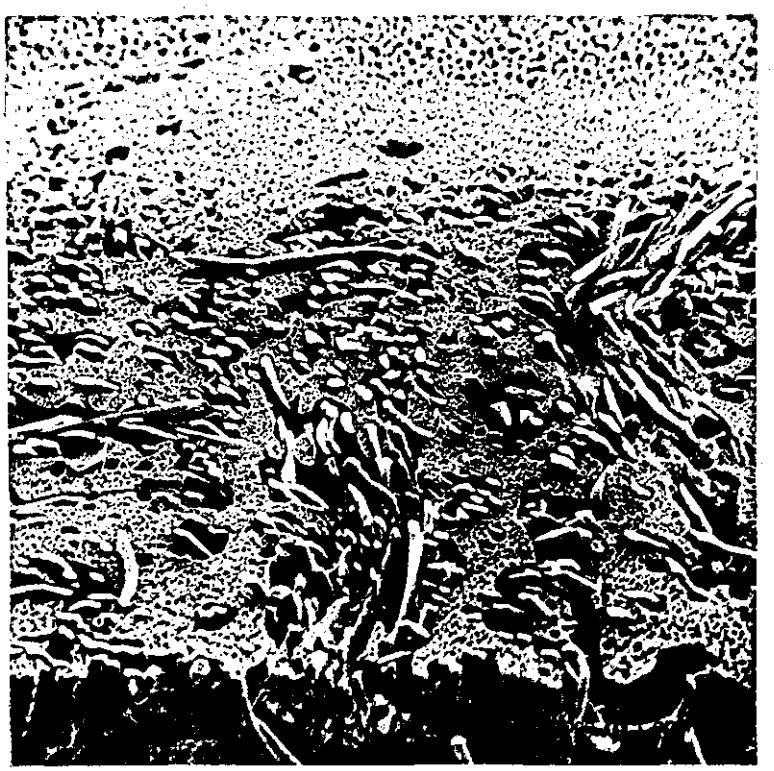

Figure 1.5.

SEM Cross-Section of "Clarino" poromeric. Magnification : 90 (After Hole and Whittaker[5]).

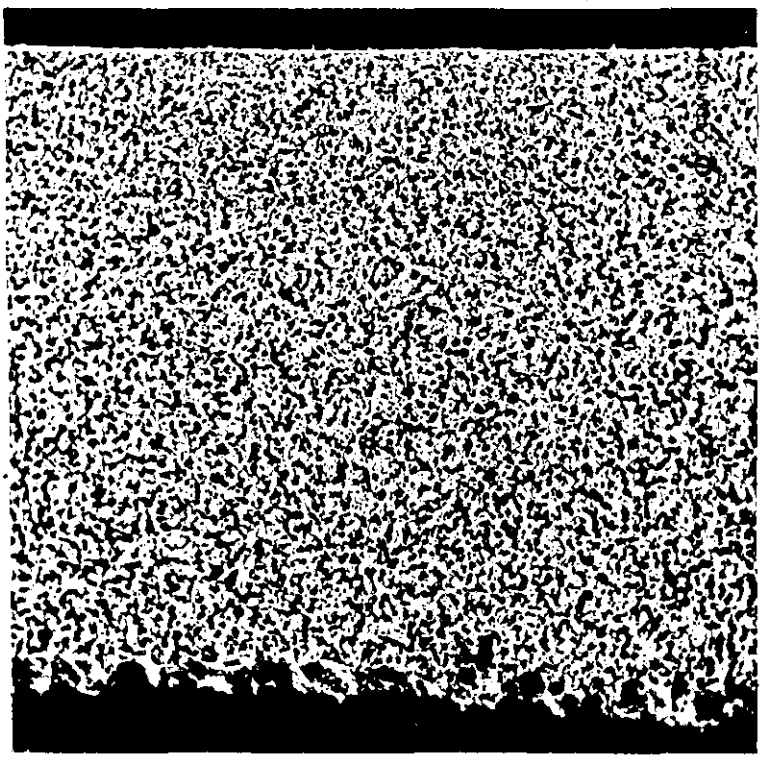

Figure 1.6.

SEM Cross-Section of "Porvair" poromeric. Magnification : 50 (After Hole and Whittaker[5])

which consists of just a surface skin and high density microporous polyurethane foam as shown by the scanning electron microscope photograph of 'Porvair' in figure 1.6. This material opens up a number of possibilities for process developments[10,11] within the footwear industry. The modulus of 'Porvair' is lower than ~~with~~ that of the fibrous poromerics, ~~and it~~ Porvair has good surface abrasion properties. The mechanical properties of this material are those of a polymer, and therefore are viscoelastic in nature, (i.e. dependent on time and temperature).

1.3. THE PROBLEM TO BE INVESTIGATED

The remarkable feature in the use of polyurethanes in footwear is that they are tough enough to replace a completely fibrous material. This is more particularly surprising when it is considered that the polyurethane is an unfilled cellular polymer of fairly low cross link density.

The strength of normal vulcanised elastomers has been the subject of a considerable amount of published work in recent years; in particular, reinforcement of rubber by the inclusion of filler particles such as carbon black. This subject has been partly investigated by the author[12-17] prior to the work presented in this thesis and a review paper on the strength and reinforcement of elastomers is included as a supplementary contribution.

In particular it has been found that the strength of a rubber is dependent on the hysteresis in the vulcanisate and quantitative relationships have been derived between energy input to break and hysteresis at break and secondly energy input to break and strain at break for both filled and unfilled elastomers. The addition of filler particles such as carbon black to rubber causes a shell of immobilised rubber to form around the filler particle. This results in the bulk rubber acquiring additional characteristic response times

which increased the viscoelastic hysteresis exhibited by the rubber in addition to the hydrodynamic increase in hysteresis caused by the addition of hard spherical particles to a viscous medium.

The subject under investigation in this thesis however is the strength and other mechanical properties of cellular polyurethanes used in the footwear industry, particularly the microporous foams used in poromerics. These results are compared with those of both unfilled and filled vulcanised rubbers in order to provide an explanation for the high strength and abrasion resistance and good cut growth properties of cellular polyurethanes.

One of the other characteristic features of the high density cellular polyurethanes used in the footwear industry is that in contrast to vulcanised rubbers, the high strength of the material is maintained over a fairly wide temperature range (from 21^{o}C to approximately 170^{o}C).

By the application of heat during conventional manufacture of shoes, it is possible to shape and completely set poromerics to a mould (last) shape. This would indicate that the polyurethanes used have a fairly wide distribution of relaxation times and this particular feature is studied in the present work.

If the cellular elastomeric polyurethane is heated to temperatures of approximately 160^{o}C or above, the material can be shaped to a mould by the application of pressure or vacuum. This behaviour indicates that the material is also thermoplastic in nature and this is further investigated in the thesis.

When used in footwear applications, cellular polyurethanes require a high resistance to cut growth. In the case of soling materials, polyurethane has to resist the growth of cracks from the penetration of sharp stones and flints whereas when used as

upper materials, the polyurethane has to resist the growth of cuts from stitch-holes and surface abrasion. The cut growth properties of these materials are discussed in this investigation in terms of the tearing energy theory developed for vulcanised rubbers. Practical applications of some of this work are considered in Appendix I.

CHAPTER 2

EFFECT OF CHAIN BRANCHING ON FAILURE PROPERTIES OF POLYURETHANES

2.1. INTRODUCTION

It has been found[12-14] in recent years that quantitative failure relationships can be obtained for amorphous rubbers between the energy input to break and hysteresis at break and secondly between the energy input and strain at break in a uniaxial tensile stress-strain test.

These failure relationships have also been applied to amorphous rubbers filled with carbon black when it was shown that under conditions of constant energy input, both the strains at break and the hysteresis at break of the filled rubbers could be corrected and unified with the gum rubber by use of a hydrodynamic factor.

Another investigation[17] showed that a strain-crystallizing rubber such as natural rubber diverged from the hysteresis failure law between 80 and 130°C. This divergence is due to the material between these two temperatures being in neither a uniformly crystalline nor totally amorphous state. Natural rubber was, however, found to obey the failure relationship between energy input to break and strain at break. This latter relationship[17] was also obeyed by several dicumyl peroxide-cured natural rubber vulcanisates of differing crosslink densities. Under conditions of constant energy input to break, the strains at break of the different crosslinked mixes, when corrected by a parameter from rubber elasticity theory become coincident.

Apart from this small study on NR vulcanisates, there has been little investigation into the effect of changing the degree of branching or crosslinking of the rubber on these failure relationships. As the polyurethane used in poromeric materials is generally reported to have

little crosslinking, an investigation by the author of the effect of changing the degree of branching associated with the polyol component in a range of known polyurethane elastomers is presented in this chapter in order to provide a more satisfactory base on which the properties of the elastomeric polyurethanes used in poromerics can be compared.

2.2. CAST POLYURETHANE ELASTOMERS

The elastomers used in this study were identical with those previously considered by Buist et al[18,19]. A usual procedure for the preparation of cast polyurethane elastomers with a lightly crosslinked structure is to use formulations containing at least one component with more than two reactive end-groups, such as the reaction of a diisocyanate with a lightly branched, or mixture of linear and branched, polyester or polyether. The properties of the elastomers are determined mainly by the chain structure and degree of branching of the polymeric intermediate and by the stoichiometric balance of the components.

Processing characteristics and properties of the products can be varied by use of more than one polyol component. This allows not only the degree of branching associated with the polyol component to be varied but by varying order of interaction of the polyols with the diisocyanate it is possible to vary processing factors such as temperature of reaction, viscosity and cure of casting mix; this also facilitates the incorporation of fillers. In addition to using polymeric polyol components, low molecular weight polyols may be included and branching can be introduced by use of a polyol such as glycerol or trimethylolpropane[18,19]. This system was adopted for the cast polyurethane mixes used in this investigation which are shown in Table 2.1.

Daltorol PR1* is a slightly branched polyester based on adipic acid and Suprasec PR* is toluene diisocyanate (TDI). The reaction of Daltorol PR1* with somewhat less than an equivalent of Suprasec PR* yields a soft elastomer but by including trimethylolpropane in the formulation, the hardness and tensile strength can be increased. Small amounts of trimethylolpropane increase resilience but high proportions give resinous products of low resilience and low ultimate elongation rather than elastomers.

The procedure used for preparation of the polyurethane sheets was to add trimethylolpropane to Daltorol PR1* at the start of the dehydration stage. At the end of the dehydration period before additions of the Suprasec PR* the mixtures were cooled to about 40°C. The sheets were supplied by Imperial Chemical Industries Ltd. (Dyestuffs Division) and were prepared by a simple casting technique.

TABLE 2.1.

FORMULATIONS OF CAST POLYURETHANE ELASTOMERS

(parts by weight)

Compound	A	B	C	D
Daltorol PR1*	100	100	100	100
Trimethylolpropane	3.5	7.0	10	13
Suprasec PR* (2,4 - 2,6/80/20/TDI)	16.2	22.9	29.0	34.9
Cure (hours at 110°C)	3	3	3	3

2.3. EXPERIMENTAL

The test pieces were in the form of rings with inner diameters of 23 mm and wall thickness of 2 mm. They were cut from sheets of rubber of approximately 2.5 mm thickness by use of a two blade rotating cutter shown in the photograph in Figure 2.1. Soap solution was sprayed on to

* Registered I.C.I. Ltd. Trade Names.

the rubber surface during cutting to obtain a clean cut.

Each ring test piece was weighed so that its cross-sectional area could be accurately calculated from the ring circumference and density. The samples were extended on a Table Model (TM-M) Instron Tensile Testing machine. The Instron was regularly serviced and checked throughout the whole of this work described in the thesis.

The test pieces were supported on double roller bearings shown in the photograph in Figure 2.2., one pair was attached to the load cell and the other to the crosshead. This type of support ensured that the ring test pieces were in a state of uniform tension and avoided the normal frictional forces that occur between a ring shaped test piece and support. Any differences in tension around the circumference of the test piece during extension were immediately removed by one or more of the rollers rotating.

The crosshead travelled in a chamber maintained at a constant temperature by air blown into it through a thermostatically controlled heater. The variation of temperature throughout the chamber was less than $\pm$ 1^{o}C. The samples were tested over a temperature range from 21 - 120^{o}C and the rate of strain was 250% per minute in every case. The test pieces remained in the constant temperature enclosure 5 minutes before straining at each temperature.

The experimental procedure to determine the energy input and hysteresis at break was to obtain, at each temperature, three tensile stress-strain curves up to failure on new samples. A fourth sample was then extended and the crosshead reversed just below the average breaking stress of the three samples. The energy input was obtained from the area under the extension curve and the hysteresis from the area between the extension

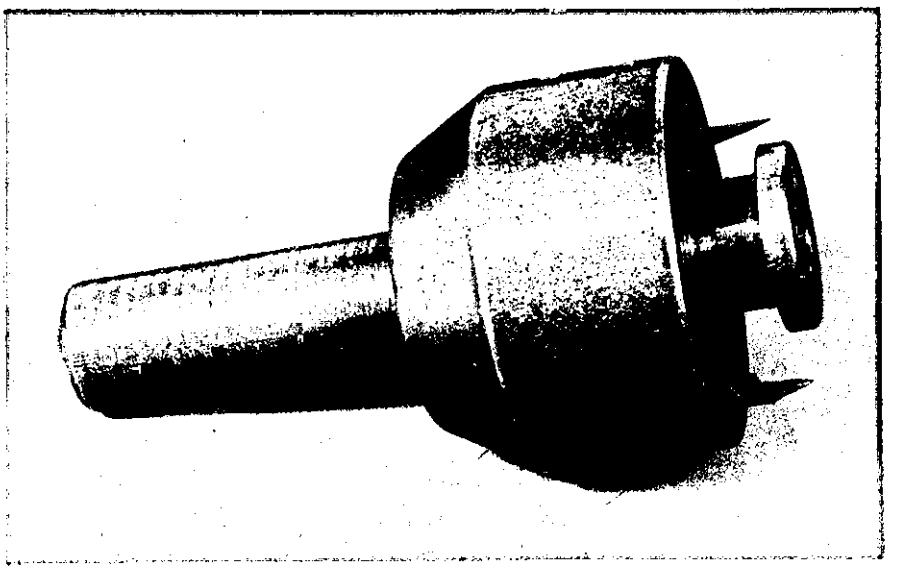

Figure 2.1.

Two blade rotating cutter used to cut ring samples from the rubber.

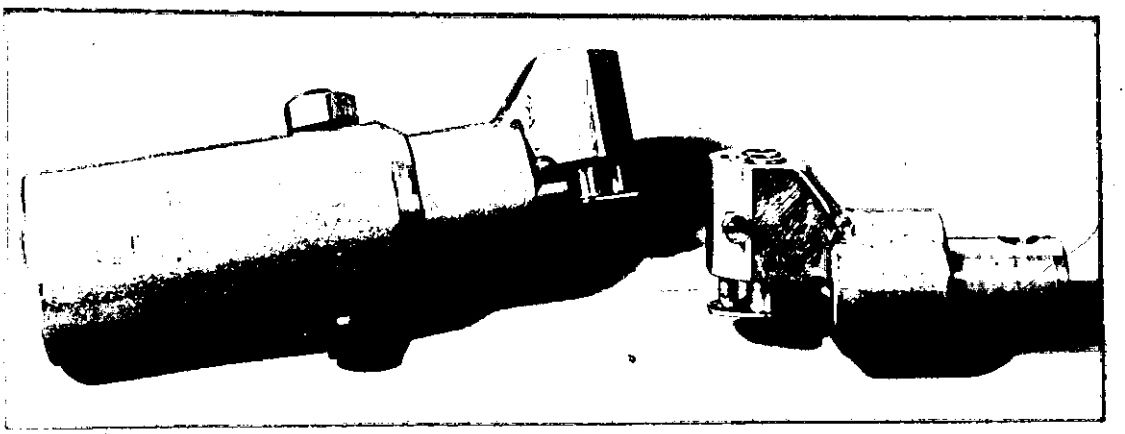

Figure 2.2.

Double roller bearing supports used for ring samples when strained in the Instron Tensile Tester.

and retraction curves directly by use of an integrator unit attached to the Instron tester.

2.4. EFFECT OF TEMPERATURE

The tensile strength and hysteresis of all the mixes were found to be very low. The hysteresis ratio at break (ratio of hysteresis at break to energy input to break) at 21°C was found to be 10.9% for mix D and approximately 4% for mixes A and B. The hysteresis was negligible at temperatures above 50°C and hence a full study on the effect of branching in polyurethanes on the energy at break/hysteresis at break failure criterion could not be carried out.

The effect of temperature on energy input to break for all the mixes is shown in Figure 2.3. where the average value of energy input to break for each of the four rubbers is plotted on semi-logarithmic paper against the reciprocal of absolute temperature.

Earlier studies[20,21] on normal crosslinked amorphous rubbers showed that the energy input to break was related to the reciprocal of absolute temperature by an equation which was considered analagous to the Van't Hoff isochore:

$$U_B = D\exp(G/T) \qquad 2.1.$$

where D and G are constants.

Straight lines have been drawn through the experimental points in Figure 2.3. and hence equation 2.1. is shown to be obeyed. The lines for the different compounds are also approximately parallel indicating that the constant G is independent of the degree of branching in the polyurethane and hence must be a parameter associated with the base constituents of the rubber. Similar results[21] were found on a series of SBR vulcanisates of differing crosslink densities.

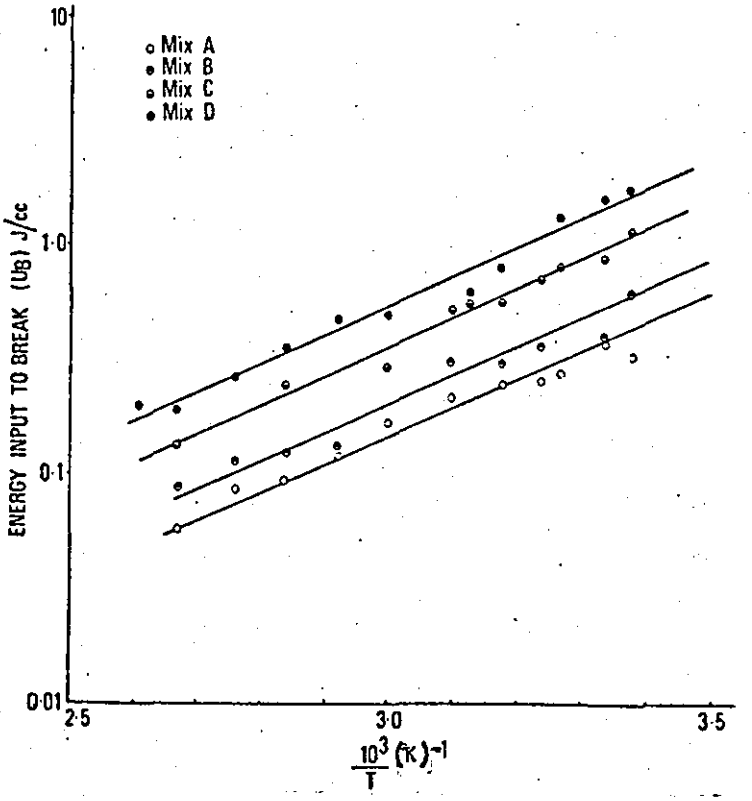

Figure 2.3.

Variation of energy input to break with reciprocal of absolute temperature for branched polyurethane elastomers.

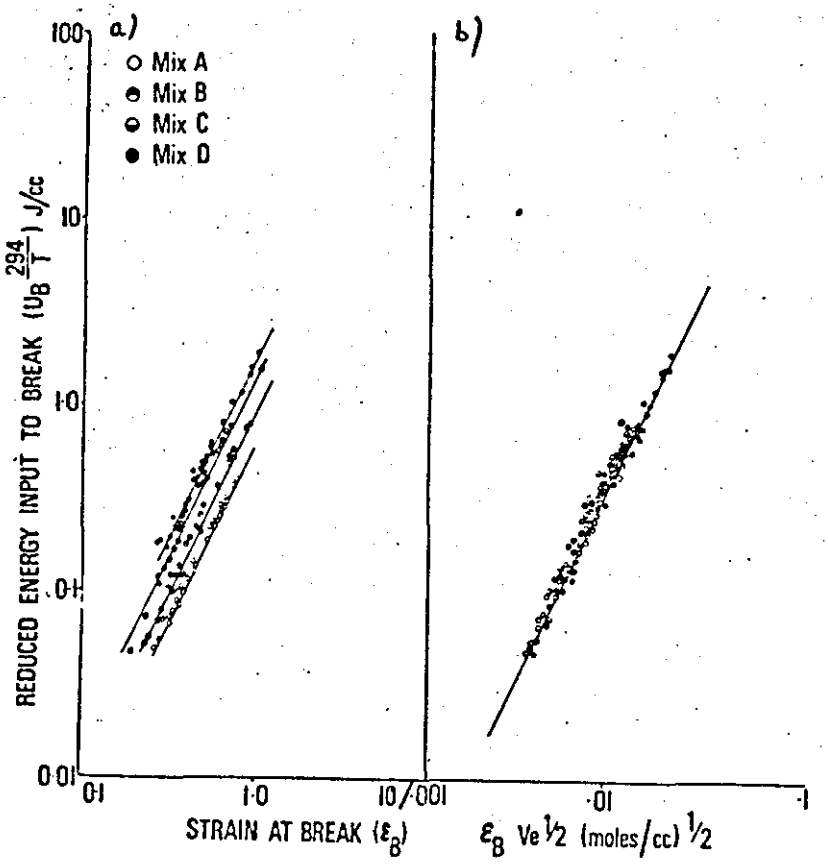

Figure 2.4.

Variation of reduced energy input to break for polyurethane elastomers with a) strain at break b) strain at break multiplied by $V_e^{\frac{1}{2}}$.

2.5. STRAIN AT BREAK

2.5.1. Experimental Results

Work[12-14,17] on both amorphous and strain-crystallising vulcanised rubbers has shown that the energy input to break (U_B) is related to the strain at break (ε_B) up to the maximum extensibility of the network (ε_B max) by an equation of the following form:

$$U_B \cdot \frac{294}{T} = A\ \varepsilon_B^2 \qquad 2.2.$$

where A is a constant and T is the temperature of test. The energy is reduced by the term 294/T to allow for the temperature dependence of rubberlike elasticity as predicted by the kinetic theory[22]. This relationship is a modification of the 'failure envelope' approach of Smith[23,24] and others[25] who plot stress or real stress at break against the strain at break. The use of the parameter, energy input to break, allows, however, a quantitative relationship between the failure parameters to be derived.

The variation of energy input to break with strain at break for the four polyurethane rubbers is shown in Figure 2.4a. The results as predicted by equation 2.2. produce a square law relationship, up to the maximum extensibility of the network (ε_B max), but are displaced along the strain axis.

Earlier work[17,21] on natural and styrene-butadiene rubber has shown that at the same energy input to break, the strains at break are in the ratio of their respective $V_e^{\frac{1}{2}}$ values provided that the strains are below the maximum extensibility of the network. V_e represents the number of network chains per unit volume of the rubber network and is usually expressed in mol/cm^3.

At very high temperatures, the amount of hysteresis for the

polyurethane was negligible and hence the rubbers could be considered as though they were in an equilibrium condition. The modulus at these high temperatures was therefore assumed to be the equilibrium modulus and was measured from the initial slope of the stress-strain curves.

The classical theory of rubberlike elasticity specifies[26-29] that the equilibrium shear modulus (Ge) is given by:

$$Ge = g\ V_e\ RT \qquad 2.3.$$

where R is the gas constant and g is a numerical factor having a value of approximately unity. The factor g includes the ratio r_e^2 / r_o^2 where r_e^2 is the mean square end to end distance of a strand and r_o^2 is the mean square end to end distance which strands of the same length would assume if not constrained by crosslinks[30,31] and other possible contributions[32-34].

In an idealized network V_e is the density of strands that are terminated both ends by chemical crosslinks, but it is rarely if ever possible to determine V_e accurately by independent means, hence the exact value of g remains in doubt. If it is assumed for the present study that g = 1 and that the equilibrium tensile modulus $E_e = 3Ge$, then equation 2.3. becomes:

$$E_e = 3\ V_e RT \qquad 2.4.$$

Values of $V_e^{\frac{1}{2}}$ were therefore obtained by use of equation 2.4. from measured values of equilibrium modulus and these are shown in Table 2.2. It is usually assumed for branched polymers that V_e includes chains between the branch points.

TABLE 2.2.

VALUES OF $V_e^{\frac{1}{2}}$

Mix	$V_e^{\frac{1}{2}}$ $(mol/cm^3)^{\frac{1}{2}}$
A	1.39×10^{-2}
B	1.66×10^{-2}
C	2.07×10^{-2}
D	2.36×10^{-2}

The strains at break of mixes A-D were multiplied by their respective $V_e^{\frac{1}{2}}$ values and the resulting graph is shown in Figure 2.4b. The agreement between the four mixes on this type of graph is shown to be remarkably good and therefore the equation to the line for different crosslink densities can be expressed as

$$U_B \cdot \frac{(294)}{(T)} = BV_e \varepsilon_B^2 \qquad 2.5.$$

where B is a constant.

2.5.2. Comparison with Vulcanised Rubbers

A similar graph to that shown in Figure 2.4a. was found in an earlier investigation[17] into the failure properties of natural rubber vulcanisates and this is shown in Figure 2.5a. It is found that a square law relationship predicted by equation 2.2. is obeyed for three vulcanisates cured with 1, 2 and 4 phr (phr = parts per hundred) dicumyl peroxide.

Values of V_e for these mixes was obtained from the data of Porter[35]. In this early investigation[17], agreement between the vulcanisates on this type of graph was obtained by multiplying the strains at break for the 2 and 4 phr dicumyl peroxide vulcanisates by the ratio of the respective $V_e^{\frac{1}{2}}$ value to the value of $V_e^{\frac{1}{2}}$ for the 1 phr dicumyl peroxide mix.

The results shown in Figure 2.5b. have, however, been obtained by multiplying the strain directly by $V_e^{\frac{1}{2}}$ and hence can be used as a direct comparison with branched polyurethane rubber results shown in Figure 2.4b.

A similar graph was obtained from work[21] on styrene-butadiene rubbers of differing crosslink densities and the composite plots for the three systems are compared in Figure 2.6. It is seen that the generalized failure relationship, equation 2.5., is approximately the same line for the three different polymer systems, amorphous, crystalline and branched, and is given by:

$$U_B \frac{294}{T} = (4.1 \times 10^3) V_e \varepsilon_B^2 \qquad 2.6.$$

if U_B is expressed in joules/cc.

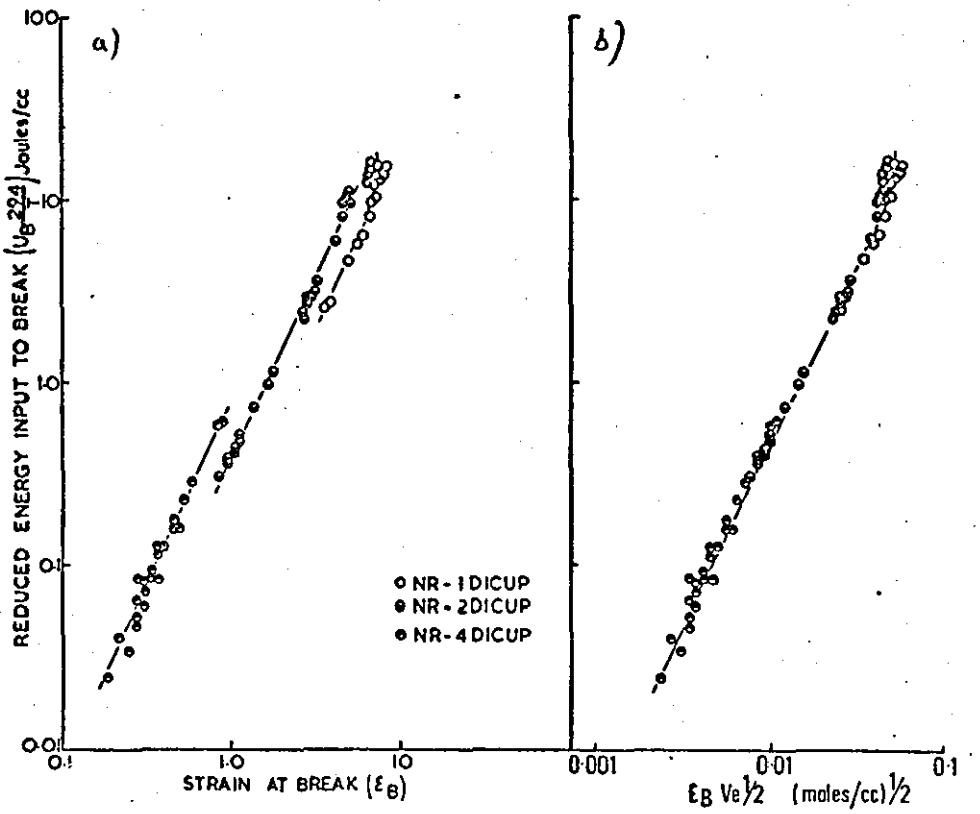

Figure 2.5.

Variation of reduced energy input to break for natural rubber-dicumyl peroxide vulcanisates from a previous study[17] with a) strain at break b) strain at break multiplied by $V_e^{\frac{1}{2}}$.

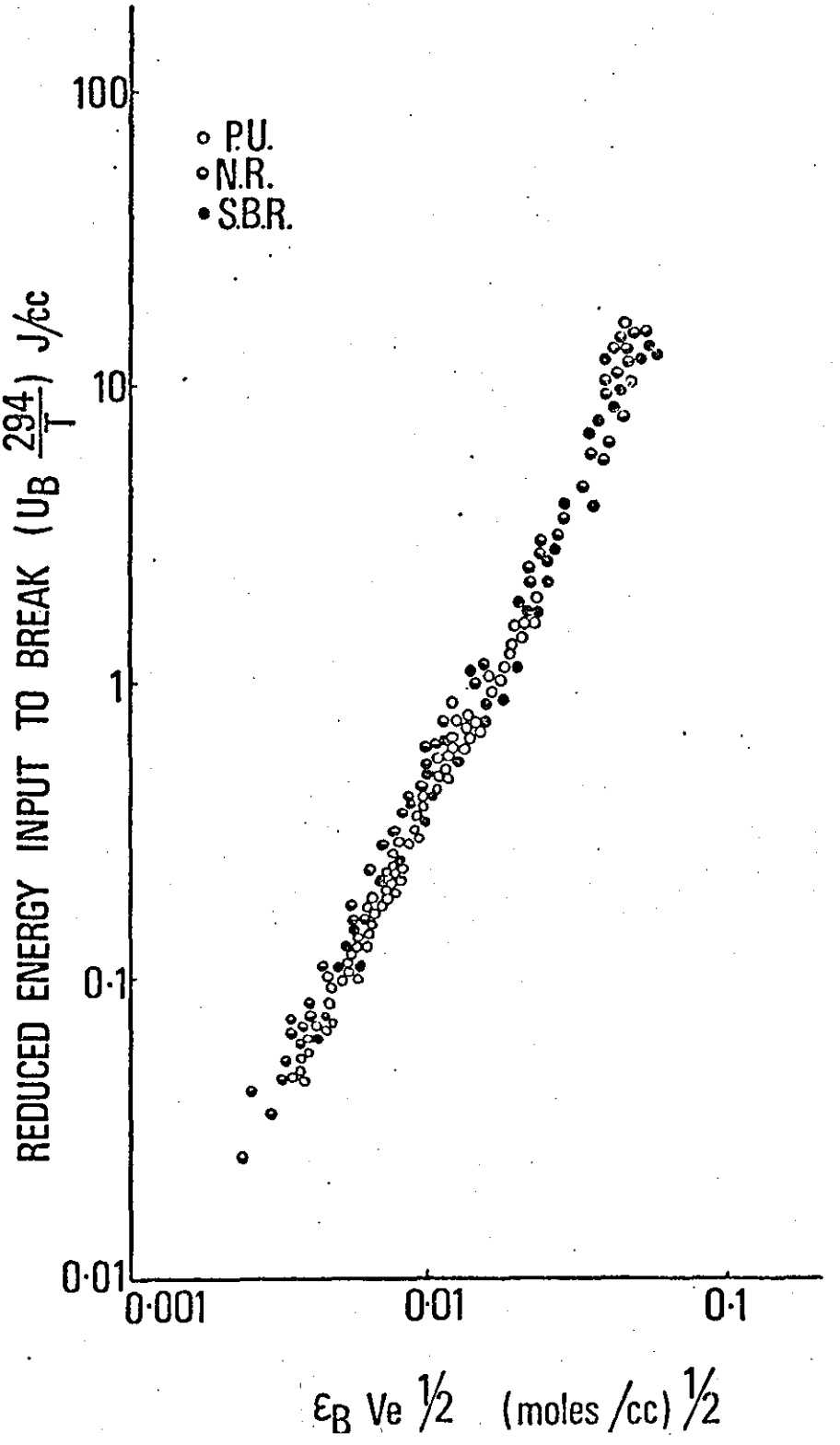

Figure 2.6.

Variation of reduced energy input to break with strain at break multiplied by $V_e^{\frac{1}{2}}$ for natural rubber-dicumyl peroxide cured vulcanisates, sulphur cured SBR vulcanisates and branched polyurethane elastomers.

The earlier work[12-14] on SBR and natural rubber showed that vulcanisates filled with various concentrations of carbon black could also be correlated on the energy input to break/strain at break graph by multiplying the strains at break of the filled vulcanisates by a hydrodynamic factor, (X) first derived by Guth and Gold[36] for expressing the viscosity of a liquid containing small spherical particles to that of the liquid alone and given by:

$$X = 1 + 2.5c + 14.1c^2 \qquad 2.7.$$

The general failure relationship then can be expressed as

$$U_B = (4.1 \times 10^3)\, V_e\, (X \varepsilon_B)^2 \qquad 2.8.$$

which is obeyed by amorphous, crystalline and branched polymers at different degrees of crosslinking, whether filled or unfilled.

2.6. CONCLUSIONS

The tensile failure properties of a typical branched polyester polyurethane have been compared with earlier work on natural rubber and styrene-butadiene rubber vulcanisates.

Although the low values of hysteresis at break excluded from the present investigation a comparison of the hysteresis properties and their effect on failure, a similar type of relationship to that found in vulcanised rubbers between energy input to break and reciprocal of absolute temperature has been established. The constant in this equation appeared to be independent of the degree of branching of the polyurethane.

The square law relationship between energy input and strain at break was found to be obeyed by polyurethane elastomers and correction by a parameter from rubber elasticity theory unified the results as found for both natural and styrene-butadiene rubber. The relationship was found, however, to be the same for the three polymer systems and hence must represent a basic material property.

CHAPTER 3

VISCOELASTIC PROPERTIES OF NATURAL AND ARTIFICIAL LEATHERS

3.1. INTRODUCTION

The study described in the previous chapter complements the earlier investigations into the strength and reinforcement of rubbers (reviewed in the supplementary contribution to the thesis) and this provides a firm basis for comparison with the experimental results on polyurethanes which are presented in Chapters 4 - 6.

Before studying in detail however, the mechanical properties of the polyurethanes used in poromerics, it is necessary to consider the properties of the various poromerics as a whole and compare these with the natural material, leather.

Because both leather and poromerics have to undergo similar shaping and setting operations in the manufacture of footwear, some similarities in their viscoelastic properties would be expected and this subject is considered in this chapter.

Measurements of the viscoelastic properties of leather fibres were reported as early as 1945 by Mitton[37] and in 1946 by Conabere and Hall[38]. They found that the extension of the fibres under constant load increased sharply with increased humidity. Subsequent drying of the fibre produced contraction but did not produce complete recovery of the samples to their original dimensions. The load-extension curve of leather fibres was, however, found to be independent of temperature. This latter result was confirmed by Grassman and Zeschitz[39] who measured the load-extension curve for leather fibres from -70° to $60^{\circ}C$.

The effects of moisture and temperature on the viscoelastic properties of leather were extensively studied and reviewed by Butlin[40] whilst developing the SATRA moist heat setting process in the early 1960's.

Following Butlin's work, Ward and Popplewell[41] showed in 1963 that the stress relaxation of leather was exponentially related to time, a result very similar to that obtained with vulcanised rubber. More recently stress-softening effects have been observed in both leather and poromerics[12,42,43] but no quantitative work has been presented up to present.

3.2. EXPERIMENTAL

Tensile test samples were cut parallel and perpendicular to the backbone in the usually accepted sampling area[41] of a standard full chrome willow side leather and a double buffed full chrome pearl split leather.

Tensile test samples were also cut perpendicular and parallel to the roll direction of a number of commercially available poromerics; 'Clarino', 'Corfam', 'Hi-Telac', 'Patora' and 'Porvair'. The structures of 'Corfam', 'Clarino' and 'Porvair' ~~was~~ are described in Chapter 1. 'Patora' contains a woven interlayer and ~~is~~ is similar in structure to 'Corfam' whereas 'Hi-Telac' is a 2-layer poromeric.

The test specimens used in the majority of the tensile tests for leathers and poromerics measured 100 mm x 10 mm. To achieve greater accuracy in tests where the materials were stressed to strains of less than 10%, the size of the test specimens was increased to 200 mm x 25 mm.

Tensile test results were obtained by use of an Instron Tensile Testing machine in a conditioned atmosphere of 65% r.h. and 21°C. In view of moisture and temperature effects on the tensile properties of leather, all the samples were placed in the conditioned atmosphere at least 24 hours before the tests were performed. Load-extension curves were automatically recorded on the chart recorder and hysteresis and energy density measurements were obtained by use of an integrator unit attached to the Instron chart recorder. The values of stress and strain

reported are referred to the original (before stressing) dimensions of the samples as is normally the convention with polymeric materials.

3.3. STRESS-STRAIN PROPERTIES

The stress-strain curves in Figure 3.1.(a) show three cycles obtained with double buffed full chrome pearl split leather cut parallel to the backbone; similar curves on 'Clarino' poromeric which is cut along the roll direction are shown in Figure 3.1.(b). In both cases, a considerable amount of energy is lost in the first cycle and a considerable amount of residual extension or set is retained in the material. Energy loss also occurs on the second and third cycles in both cases. Similar curves were found on the second leather and other poromerics. The curves illustrate the viscoelastic character of both leather and poromerics.

A number of recent investigations have been concerned with the shape of the load-extension curve for leathers up to about 2% strain in an attempt to relate these tensile properties to foot comfort. Upstone and Ward[44] found that at extensions up to 2% leather gave a non-linear stress-strain curve although they claimed the response of the material was almost entirely elastic. Mitton and Price[45] reported similar experiments but found that in contrast to Upstone and Ward, the stress-strain curve showed considerable viscoelastic behaviour up to about 2% extension. They further explained the non-linearity of the stress-strain curve in this region as due to inherent stresses in different layers of unstrained leather.

Figure 3.2.(a) and 3.2.(b) show three tensile cycles up to 2% extension for a full chrome willow side leather and for the homogeneous poromeric 'Porvair' respectively. It is seen that in both cases a measurable amount of hysteresis occurs in the first cycle of both materials which results in a certain residual extension or set.

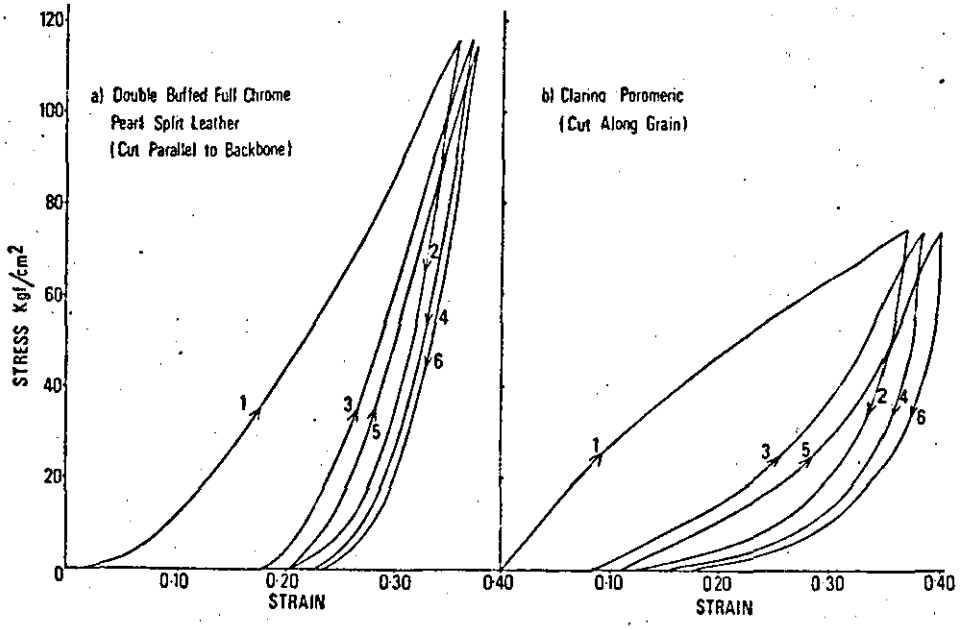

Figure 3.1.

(a) Stress strain curves obtained for double buffed full chrome pearl split leather cut parallel to backbone.

(b) Stress strain curves obtained with Clarino poromeric cut along grain.

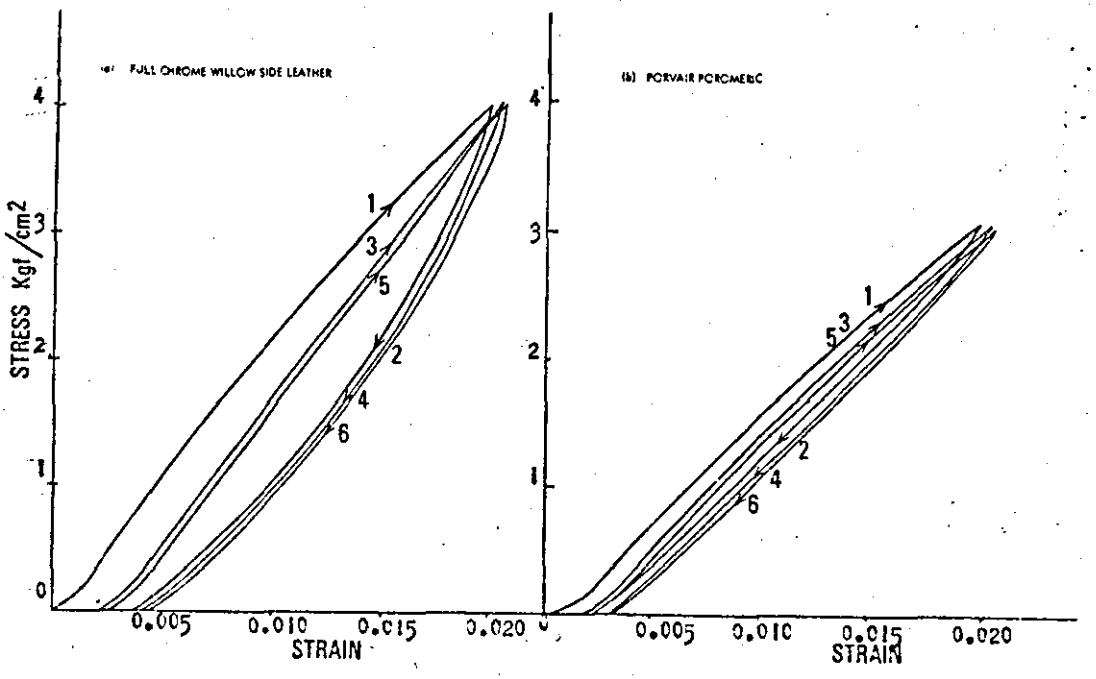

Figure 3.2.

(a) Stress strain curves up to 2% obtained for a full chrome willow side leather.

(b) Stress strain curves up to 2% obtained for the poromeric Porvair.

Considerable stress softening (difference between the stresses in the first and second extension curves at same strain) is also found in both materials at strains even as low as 2%. These results demonstrate the large viscous component in the tensile properties of leather and poromerics and hence support the conclusions reported by Mitton and Price[45].

3.4. ENERGY MEASUREMENTS

3.4.1. Hysteresis

The energy inputs to the first, second and third stress-strain cycles when taken to the same stress for all the poromerics and leathers were obtained from curves similar to those shown in Figures 3.1. and 3.2. This procedure was repeated at a number of strains. The energy input to the first cycle is plotted against the hysteresis in the first cycle at each particular strain on double logarithmic paper in Figure 3.3. for the five poromerics and two types of leather. It is seen that the results fall on a fairly good straight line which is common to all the poromerics and leathers. Some of the points at very low energy values arise from cycles taken to strains less than 2% whereas to obtain those at the very high energies strains up to about 400% were necessary. The points on Figure 3.3. also include results from samples taken, in the case of leather, parallel and perpendicular to the backbone of the animal and in the case of poromerics both along and across the roll directions. The equation to the line shown in Figure 3.3. is given by:

$$U_1 = 1.5\ H_1^{0.88} \qquad 3.1.$$

where U_1 is the energy input to the first cycle and H_1 is the energy lost or hysteresis in the first cycle.

It has been found[12-14] for amorphous vulcanised rubbers such as SBR that the energy input to break (U_B) is related to the hysteresis

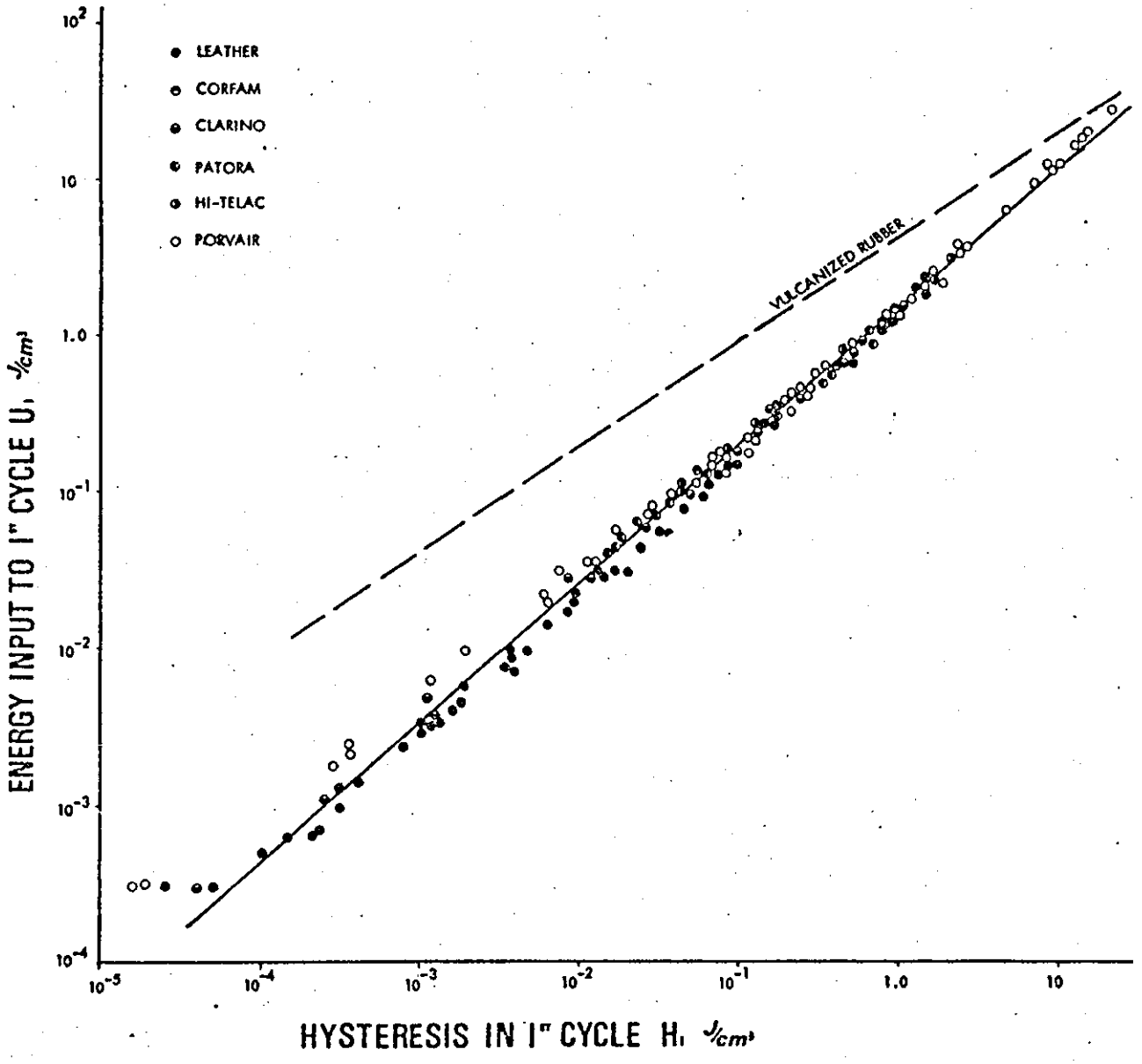

Figure 3.3.

Variation of energy input to first cycle with hysteresis in first cycle for a number of leathers and poromerics. Dotted line represents results for styrene butadiene rubber[12].

at break (H_B) by an equation of the following form

$$U_B \frac{294}{T} = K_1 H_B^{2/3} \qquad 3.2.$$

where K_1 is a constant and T is the temperature of test in ^oK. This relationship is dotted on Figure 3.3. for comparison. The interesting feature noticed here is that at any particular value of energy input, the hysteresis obtained in leather and poromerics is much larger than that obtained in vulcanised rubber. It is well known that normally crosslinked vulcanised rubber is too elastic to be used as a shoe upper material and hence it would appear that the relation represented by equation 3.1. is a necessary condition for all shoe upper materials. The materials shown to follow the correlation in Figure 3.3. vary in structure from the natural totally fibrous material to poromerics such as 'Corfam' and 'Patora' which incorporate a microporous polyurethane foam layer, a woven interlayer and a densely packed fibre base to the non-fibrous poromeric, 'Porvair' made entirely of cellular polyurethane. The correlation shown therefore is obeyed irrespective of the composition of the artificial leather material.

A similar correlation is found between the energy input to the second extension curve and hysteresis in the second extension cycle as shown in Figure 3.4. The equation of to the line is given by

$$U_2 = 1.8\ H_2^{0.86} \qquad 3.3.$$

The correlation shown in Figure 3.4. again indicates the basic similarity in viscoelastic properties of natural and artificial leathers.

3.4.2. Stress Softening

The energy difference between the first and second extension curves when extended to the same stress, which represents the amount of stress softening, was also measured for all the leather and poromerics considered. The variation of stress softening with energy input to the first cycle is shown in Figure 3.5. for double buffed full chrome pearl split leather,

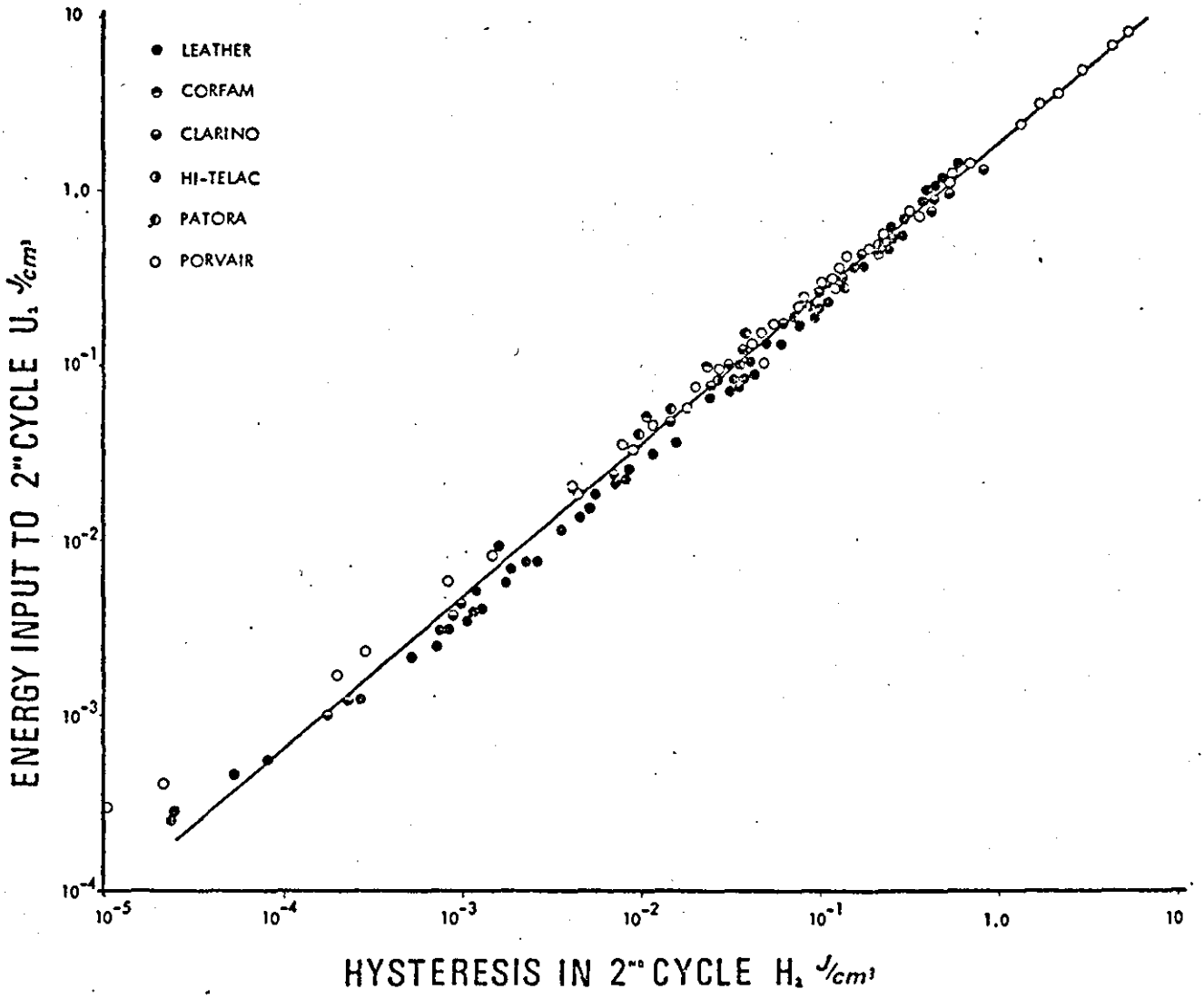

Figure 3.4.

Variation of energy input to second cycle with hysteresis in the second cycle for a number of leathers and poromerics.

full chrome willow side leather, the fibrous based poromeric 'Patora' and the homogenous poromeric 'Porvair'.

It is shown that the two leathers follow the same straight line on the logarithmic plot. The results for 'Patora' and 'Porvair' also follow reasonable straight lines but are slightly displaced from the line for leather. There is a slight departure at very high strains (above 35%) for leather and poromerics but these strains are well above those encountered in shoe manufacture or in wear.

The interesting feature here, however, is that at any particular value of energy input in the first cycle, the stress softening is much greater in the case of leather than the poromerics. The other fibrous poromerics considered in this study follow a very similar curve to that obtained with 'Patora' and these materials show slightly larger values of stress softening at the same energy input than the homogenous poromeric, 'Porvair'.

The difference in stress-softening properties between the two extreme materials of the range considered, i.e. leather and 'Porvair' is illustrated more clearly by the graph on linear scales shown in Figure 3.6. where the various parameters are plotted against energy input to the first cycle. As shown by Figure 3.3., the relationship between hysteresis and energy input to the first cycle for leathers and poromerics is similar. The difference between values of hysteresis and energy input give the amount of energy stored in the materials.

The major sources of hysteresis in footwear materials are firstly viscoelastic effects and secondly stress softening. Work on rubbers[12-14] has shown that a number of other contributions to hysteresis can occur including crystallisation of the polymer and breakage of weak cross links but these factors are thought to account for little hysteresis

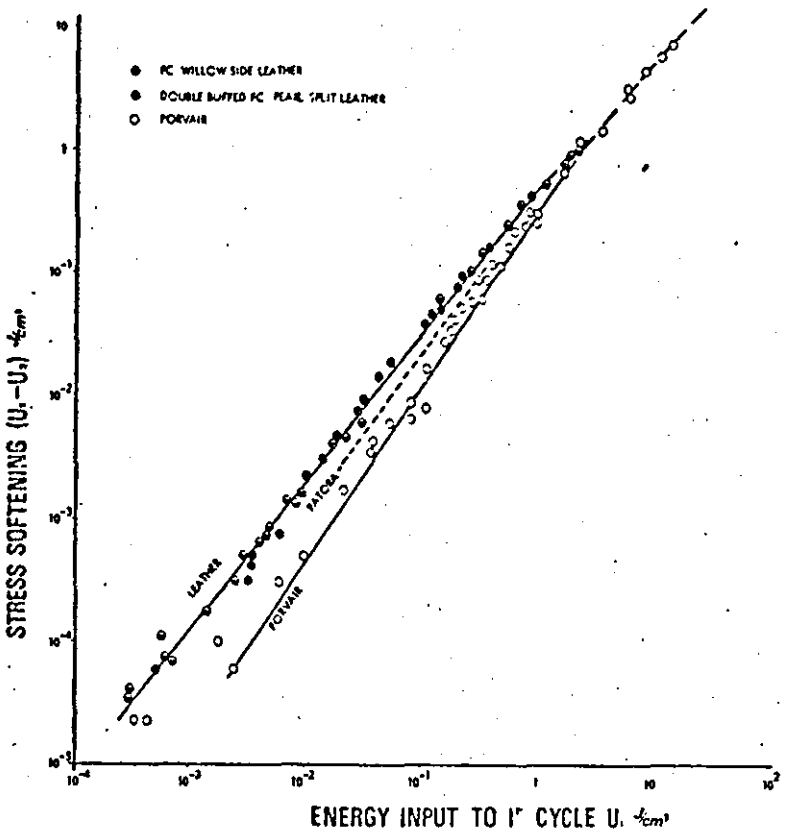

Figure 3.5.

Variation of stress softening measured as the energy difference between the first and second extension curves and the energy input to the first extension curve for two types of leather, poromerics Patora and Porvair.

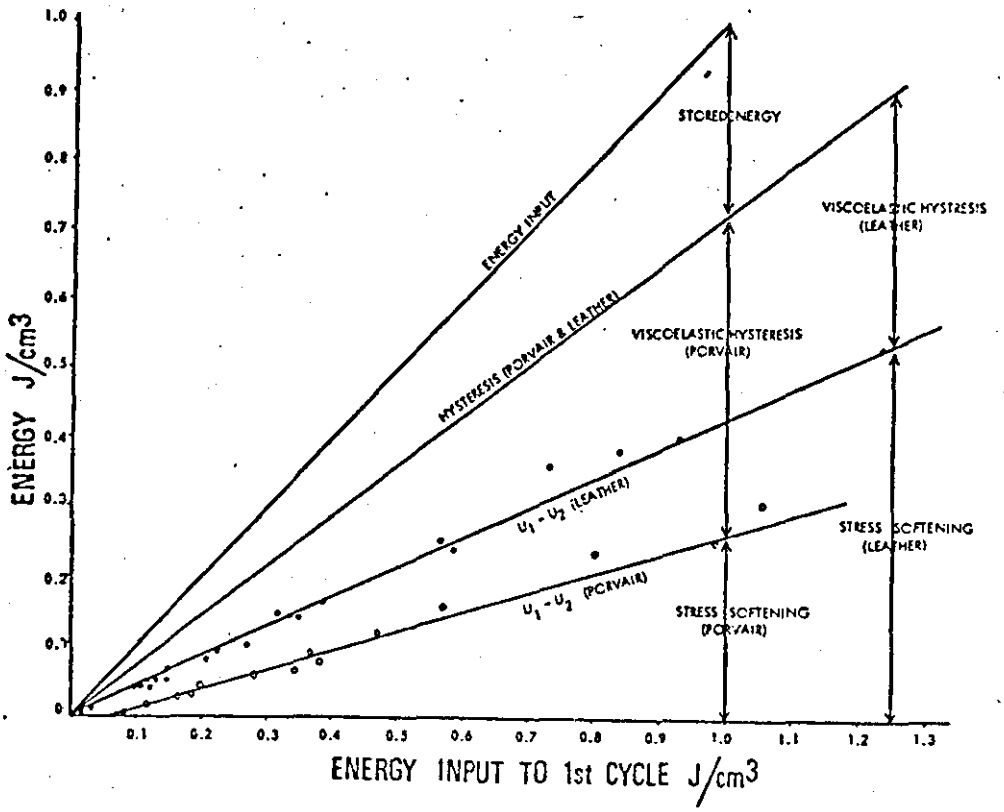

Figure 3.6.

Variation of hysteresis in first cycle and stress-softening in leather and Porvair with energy input to the first cycle.

in leatherlike materials. In leather some of the loss of energy attributed to stress softening would probably include contributions due to slip at fibre junctions and breakage of the individual leather fibres.

If it is assumed that the hysteresis for leather and poromerics can be separated into two components, viscoelastic and stress softening effects, Figure 3.6. shows that although hysteresis at the same energy input is the same for both leather and poromerics, the amount due to viscoelasticity is much greater in 'Porvair' than in natural leather. Conversely the amount of stress softening is greater in leather than 'Porvair'. The amount of stress-softening in the other fibrous based poromerics lies between the values for leather and 'Porvair' as shown in Figure 3.5.

3.5. TENSION SET

3.5.1. Correlation with other Parameters

When a viscoelastic material is extended to a particular strain and then retracted, the material does not return to its original length but retains a certain amount of residual extension. For the purpose of this investigation, the residual extension has been divided by the original length of the unstrained sample and termed "tension set". This particular property is considered important as it affects the shape retention and comfort of footwear.

Tension set is plotted as a function of strain on double logarithmic scales in Figure 3.7. for the double buffed full chrome pearl split leather, the full chrome willow side leather and the poromeric 'Porvair'. The two leathers follow a common straight line but the set at any particular strain for 'Porvair' is less than for leather. The set for 'Porvair' however still follows a logarithmic relationship with strain. The set results at any strain for the other fibrous poromerics fall

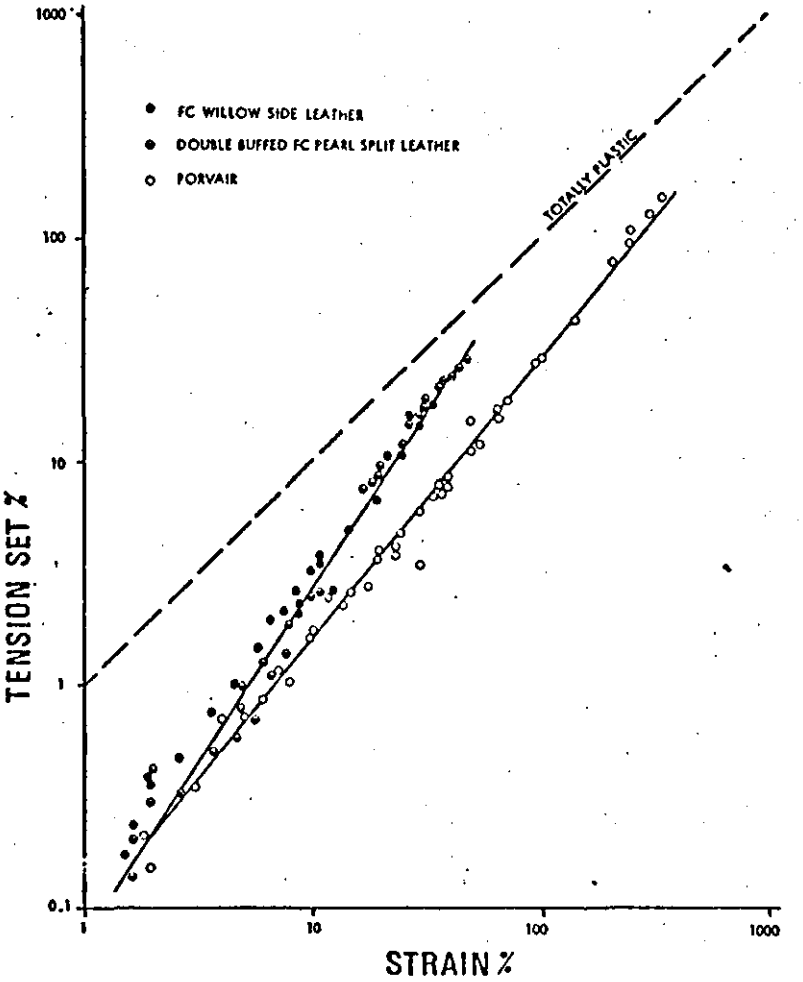

Figure 3.7.

Variation of tension set defined as residual extension divided by original length of sample with strain for two types of leather and Porvair.

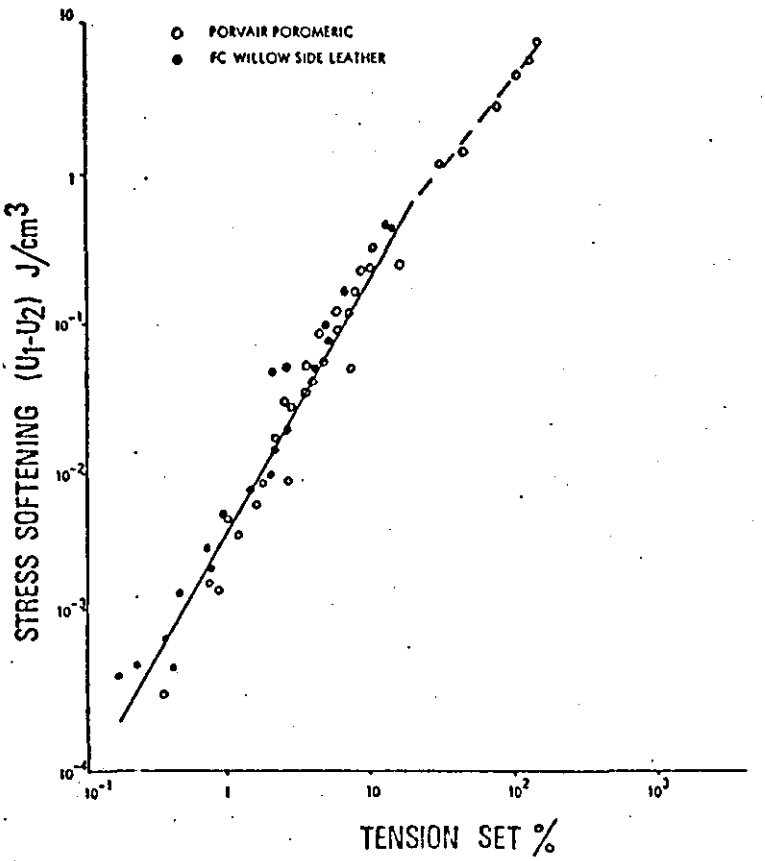

Figure 3.8.

Variation of stress softening with tension set for full chrome willow side leather and Porvair.

between leather and 'Porvair' and they have therefore, not been drawn on Figure 3.7. in order to aid clarity in presentation.

Figures 3.5. and 3.6. showed that stress softening at the same value of energy input was greater for leather than for poromerics and on comparison of the results shown in Figures 3.5. and 3.7. it would appear that tension set could be related to stress softening. The variation of tension set with stress softening for the two extreme materials of the range considered in this investigation, full chrome willow side leather and the cellular polyurethane poromeric 'Porvair' is shown in Figure 3.8. Over the range of strain considered in Figure 3.8. it appears that a reasonable correlation is obtained between tension set and stress softening.

3.5.2. Variation with Time

The tension set or residual extension developed in a material which displays some viscoelastic effects is partially recoverable with time. This section considers the variation of tension set for leather and poromeric upper materials with time of recovery.

Samples of full chrome willow side leather, 'Clarino' and 'Porvair' were stressed to various strains and then retracted. The residual extension was measured off the stress strain curve and was considered to be the tension set 1 sec. after the end of the test. The length of the strip was continually measured for about 4 weeks (over 10^7 secs). During this period they were left in a conditioned atmosphere at 65% r.h. and 21^{o}C.

The variation of tension set with time of recovery for samples of full chrome willow side leather is shown in Figure 3.9. After an initial period of fairly rapid recovery the tension set remains fairly steady with time and appears to reach a constant value. Similar results from stress relaxation measurements have been reported by Butlin[40].

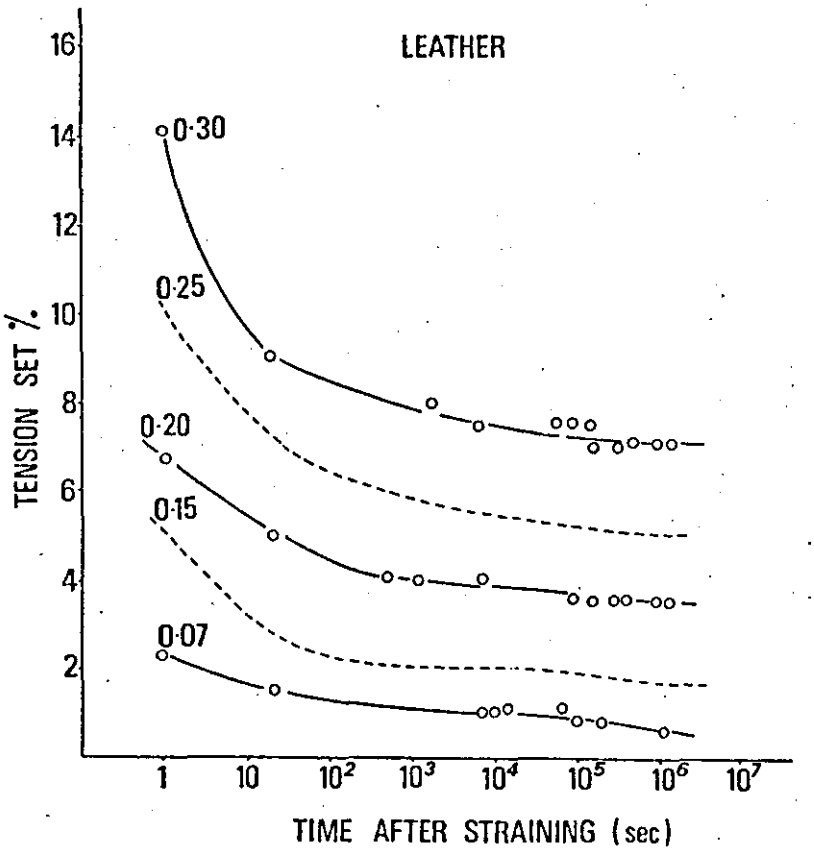

Figure 3.9.

Variation of tension set with time after straining for full chrome willow side leather taken to various strains.

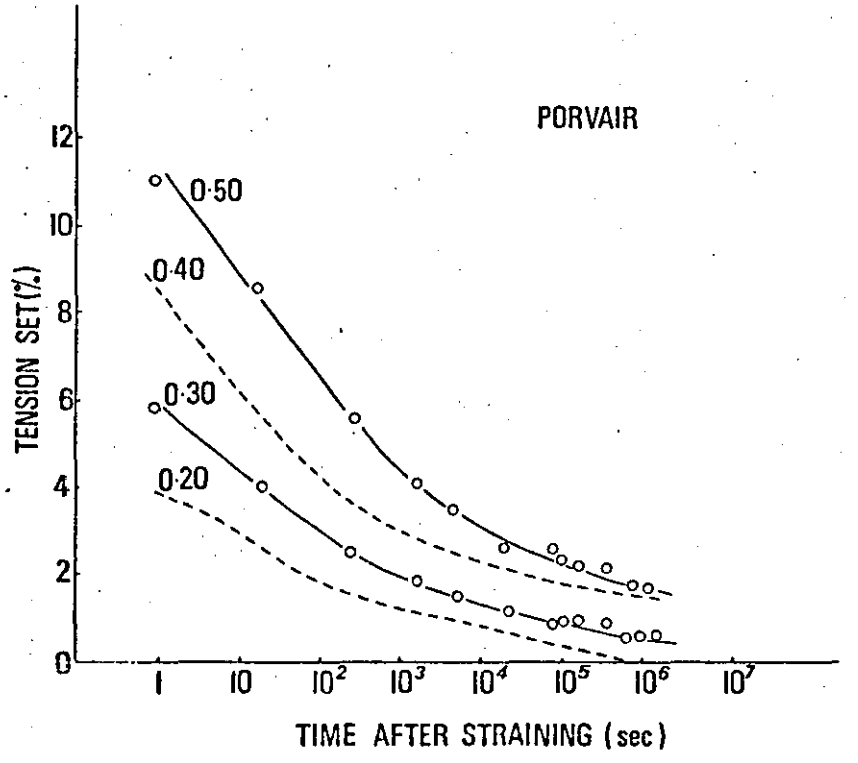

Figure 3.10.

Variation of tension set with time after straining for the poromeric Porvair taken to various strains.

In one case he showed that even over a recovery period of two years, the amount of set remained fairly constant.

A graph similar to Figure 3.9. is shown for 'Porvair' in Figure 3.10. As noted in the earlier graphs, a larger strain is required in 'Porvair' to obtain the same amount of tension set.

In order to compare the recovery rates of different materials, the recovery in residual extension between 1 and 10^7 secs. after straining is plotted against the actual strain in the cycle in Figure 3.11. for leather, 'Clarino' and 'Porvair'. Although the results for 'Porvair' are slightly displaced from leather and 'Clarino', the rates of recovery of these materials are not greatly different.

3.6. CONCLUSIONS

In this chapter, a number of common relationships between viscoelastic properties have been shown to occur in natural and artificial leathers. There is a general correlation between energy input and hysteresis in a stress-strain cycle and it would appear that this defines a condition for viscoelastic properties for all upper materials which are used in footwear. A second correlation has been found between the stress softening in a stress strain cycle and tension set. Some similarity is also shown between leather and poromeric materials in the recovery of tension set with time.

The most interesting feature in this analysis is that the various correlations between the viscoelastic properties are obeyed by materials which differ widely in structure from a natural totally fibrous material to a homogeneous cellular polyurethane elastomer. A more detailed investigation into the viscoelastic and mechanical properties of cellular polyurethane elastomers used in poromerics is presented in Chapter 4 - 6.

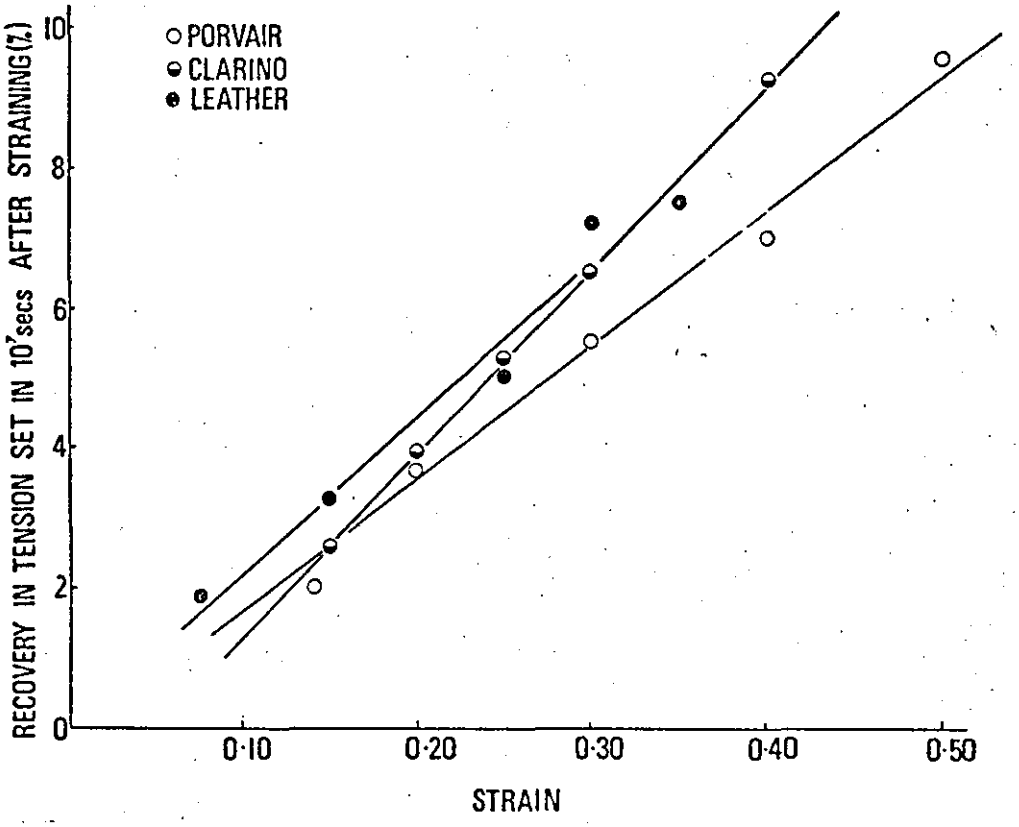

Figure 3.11.

Variation of amount of recovery of tension set in 10^7 seconds after straining with the strain in the cycle for full chrome willow side leather, Clarino and Porvair.

CHAPTER 4

RELATIONSHIP BETWEEN MECHANICAL PROPERTIES OF SOLID AND CELLULAR POLYURETHANES

4.1. INTRODUCTION

In the previous chapter, the mechanical properties of a homogeneous cellular polyurethane elastomer which is used as a poromeric have been compared with fibrous based poromerics. Before considering further the mechanical properties of polyurethane elastomers, it is necessary to determine how these properties are affected by the cellular structure.

The study of the mechanical properties of cellular or foamed polymers as distinct from solid materials was started in the late 1920's with the development of blown or expanded rubber. A number of early papers[46-48] discussed the physical properties such as density, hardness, tensile, hysteresis, damping, cell size, and insulation properties of these materials.

Latex foam rubber was developed in the early 1930's, and a number of investigations have been undertaken[49-52] into the tensile and compression properties of these materials. Most authors showed that the load-extension curves of foamed materials were sigmoidal, but little theoretical work analysing such deformations was reported although an extensive analysis[53-55] of the elastic properties of cork was made in 1946 and showed that the sigmoidal load-compression curves obtained with cork could be interpreted on the basis of collapsing of cell walls.

It was not until 1959 that a theory to describe the mechanical properties of foamed elastic materials such as modulus, compression, tear, and tensile was developed by Gent and Thomas[56-58]. This theory has now been developed further to describe viscoelastic[59] and permeability[60] properties of open-cell foamed materials and elastic

behaviour of closed-cell materials[58] and has been successfully applied to measurements on natural rubber foams. Little work, however, has been reported on the application of a theoretical model to the mechanical behaviour of cellular polyurethanes.

4.2. THEORETICAL MODEL

The fairly simple model proposed by Gent and Thomas[58] for a foamed material is shown in Figure 4.1., it consists of thin threads of unstrained length l_o and cross-sectional area D^2 joined together to form a cubical lattice. The intersections of cubical regions of volume D^3 are assumed to be essentially undeformable.

A fractional extension of the foam by an amount e' parallel to one set of threads is therefore associated with a larger extension e of the threads themselves, as follows:

$$\frac{e}{e'} = \frac{l_o + D}{l_o} = 1 + \beta \qquad 4.1.$$

The threads in the model occupy, for any cross section perpendicular to one set of threads, a fractional area of the total given by

$$\frac{D^2}{(D + l_o)^2} = \frac{\beta^2}{(1 + \beta)^2} \qquad 4.2.$$

The fractional volume V_r occupied by the solid material can be evaluated by considering a cube of side $(D + l_o)$ centered on one intersection, so that

$$V_r = \frac{3D^2 l_o + D^3}{(D + l_o)^3} = \frac{3\beta^2 + \beta^3}{(1 + \beta)^3}. \qquad 4.3.$$

The parameter β therefore gives a direct measure of the foam density, and the relationship is shown graphically in Figure 4.2.

4.3. EXPERIMENTAL

Samples of polyurethane foams were obtained from two commercially available poromerics: foam 1 was approximately 0.17 cm thick, while foam 2 was only 0.014 cm thick. It was necessary in the analysis of the results to obtain certain measurements on the solid polyurethane

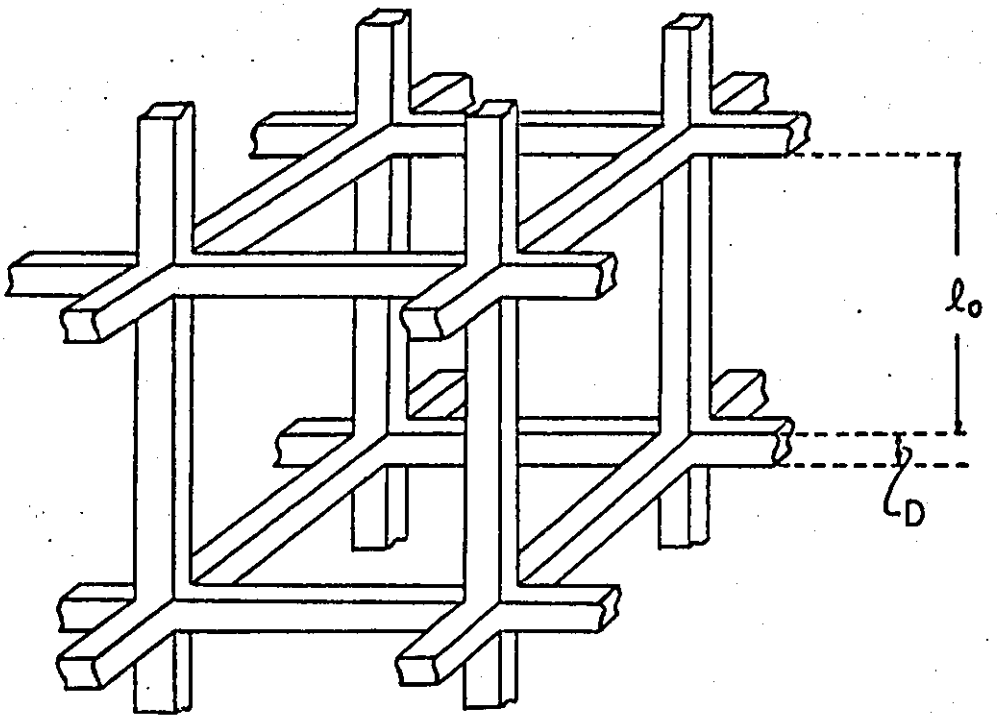

Figure 4.1.

Simple model of foamed material (After Gent and Thomas[58])

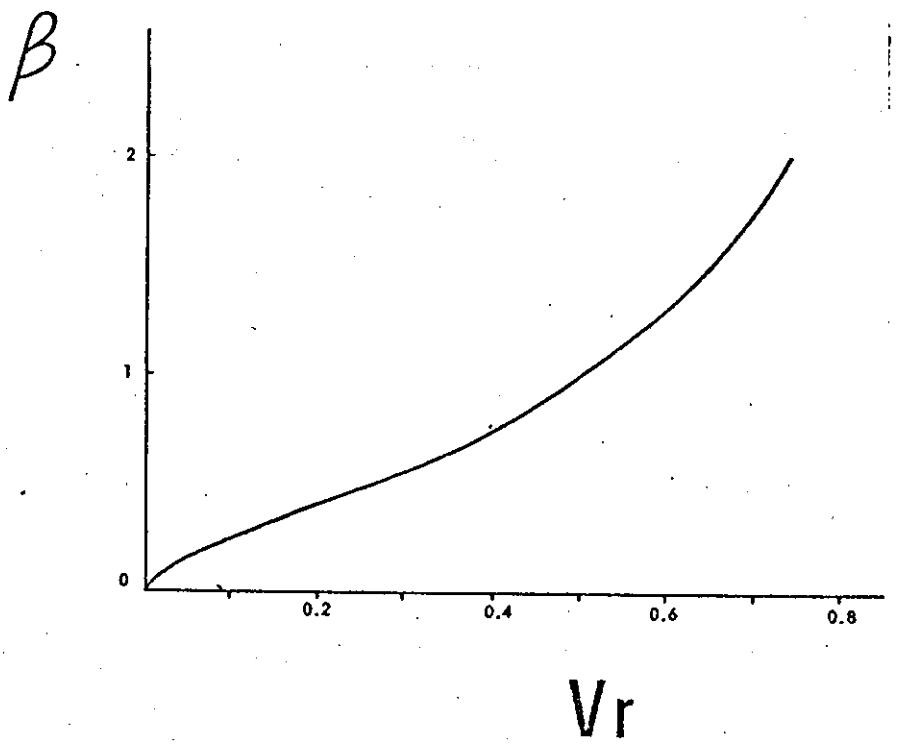

Figure 4.2.

Variation of parameter β with foam density from equation 4.3.

used in the foam. Unfortunately, it was not possible to obtain the solid polymer direct, and hence it was obtained by solution of the cellular material in a suitable solvent and casting a solid film. The solvent was then removed by heat treatment. The densities of the foam and solid were measured in both cases. Tensile, tear, and compression data on the materials were obtained by use of an Instron tensile testing machine using suitable jaws and attachments for each particular experiment.

The type of cell structure found in the polyurethane foams can be seen in the scanning electron photomicrograph shown in Figure 4.3. The cells are reasonably spherical, with the average diameter about 10^{-3} cm, and can clearly be seen to be interconnecting.

4.4. YOUNG'S MODULUS

The tensile stress-strain curves of foam 1 and the corresponding solid material are shown in Figure 4.4. The tensile stress for the foam is based on the cross-sectional area of rubber, including holes. The results for a typical unfilled solid natural rubber vulcanizate from previous studies[12-14] are also shown in Figure 4.4. for comparison; and it can be seen that the initial modulus of the polyurethane foam is higher, although the actual tensile strength is lower than the NR vulcanizate. The modulus of the solid polyurethane is extremely high when compared to the corresponding foam, and its tensile strength is considerably in excess of that found in the natural rubber vulcanizate. The initial linear part of the stress-strain curve for both the foam and the solid polyurethane allows a value of Young's modulus to be obtained.

It is possible to determine theoretically a value for Young's modulus of the foam, Y_F, by considering the extension of the model shown in Figure 4.1. If a small strain is applied parallel to one set of threads, Y_F can be obtained from the product of three factors: (i) Young's modulus

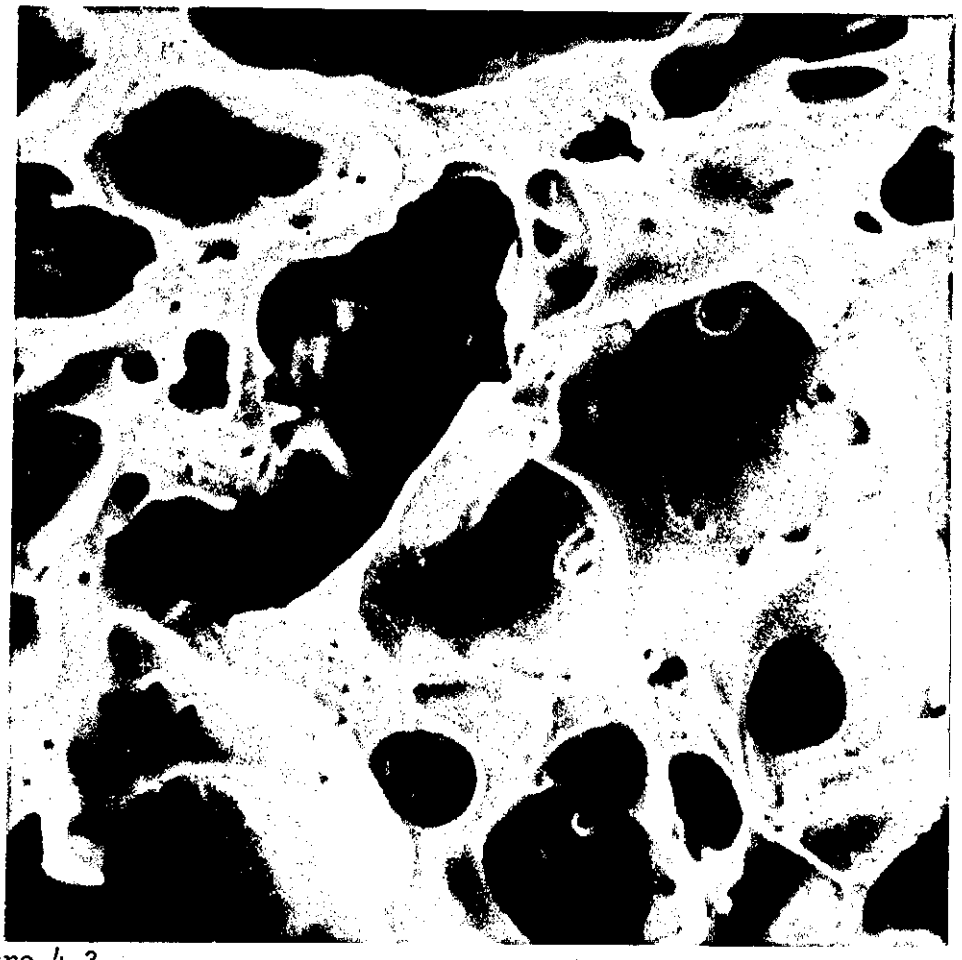

Figure 4.3.

Scanning electron microscope photograph of polyurethane foam used in poromerics showing type of cell structure (Magnification : 3,200).

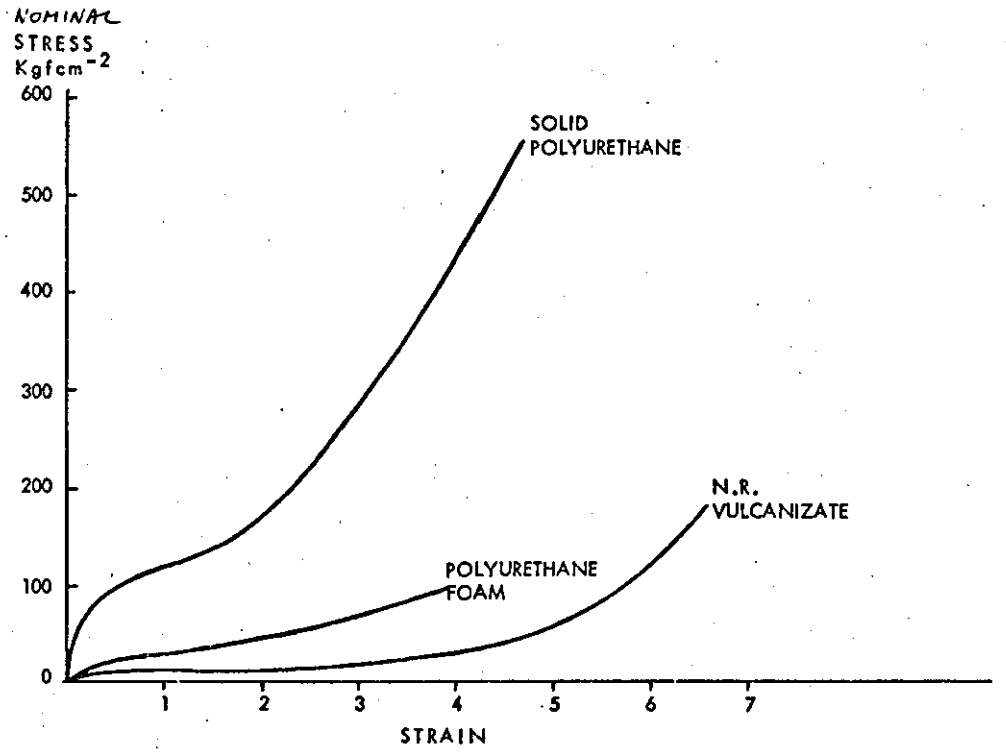

Figure 4.4.

Comparison of tensile stress-strain curves for polyurethane foam and solid and natural rubber vulcanisate.

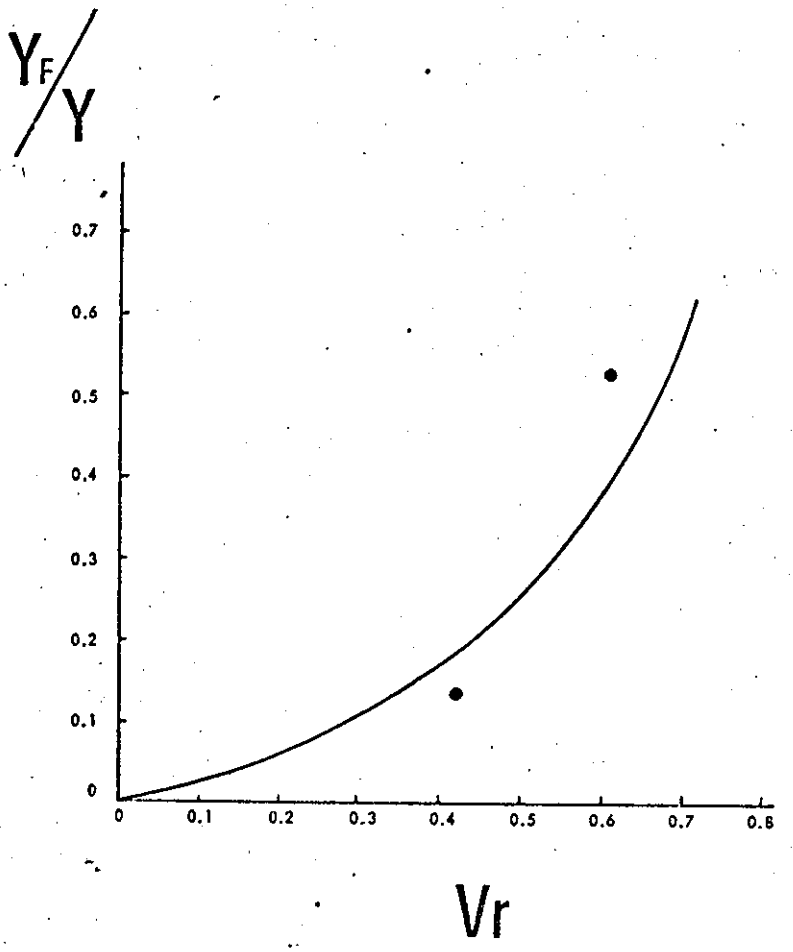

Figure 4.5.

Variation of Young's modulus of foam Y_F referred to that of the solid polyurethane Y with volume fraction of the rubber in the foam V_r. Solid line is that predicted by equation 4.5. from theory of Gent and

of the solid material, Y; (ii) the strain magnification factor, eq. 4.1.; (iii) factor representing the true load-bearing area, eq. 4.2., hence producing the equation

$$Y_F = Y \frac{\beta^2}{(1+\beta)}. \qquad 4.4.$$

Using a more complicated yet more realistic model of a system of n randomly disposed threads entering each intersection and approximating these by spheres of surface area nD^2, Gent and Thomas[56] found that the density of the foam was given by the same relation, eq. 4.3., and the equation for Young's modulus was only different by a factor of 2 from that given in eq. 4.4.

Hence, Young's modulus can be obtained from

$$Y_F = Y \frac{\beta^2}{2(1+\beta)}. \qquad 4.5.$$

The ratio Y_F/Y from the experimental results of Young's modulus for the two polyurethane foams and solid materials are plotted in Figure 4.5. against the volume rubber fraction V_r determined from measured densities on the materials. Also shown on Figure 4.5. is the theoretical line obtained from eqs. 4.3. and 4.5. The values obtained for Young's modulus are therefore in reasonable agreement with theory. There is likely to be some error in the measurement of Young's modulus of the solid polymer in view of the difficulties involved in obtaining the material.

4.5. TEAR PROPERTIES

The most convenient method of measuring tear properties of rubber-like materials is to use the "tearing energy" approach developed by Rivlin and Thomas[61] from the classical theory on the strength properties of glass developed by Griffiths[62] in 1920. Tearing energy T is defined for a strained test piece containing a crack as

$$T = -\frac{\partial U}{\partial A}. \qquad 4.6.$$

where U is the total elastically stored energy in the test piece and A is the area of the cut surface. The derivative must be taken under

conditions that the applied forces do not move and hence do not work. It thus represents the rate of release of strain energy as the crack propagates and can therefore be considered as the energy available to drive the crack through the material. It has been found that if tear or crack-growth measurements are expressed in terms of T, the results obtained from test pieces of different shapes are the same, and hence values of T are characteristic of the material and not of the form of the test piece[63]. The "trouser" tear test piece shown in Figure 4.6. was used for the present investigation, as the value of T can readily be calculated from the applied force F by the relationship [61,64]

$$T = \frac{2F}{h} \qquad \text{4.7.}$$

where h is the test piece thickness.

Measured values of tearing energy from both foams are shown in Table 4.1. A considerable difference was noted between the values of initial tearing and those for steady propagation of the tear. A similar difference in tearing energy values was also reported for latex foam rubbers by Gent and Thomas[58].

TABLE 4.1.

VALUES OF TEARING ENERGY

Foam	T (initiation), kg/cm	T (steady), kg/cm	β
1	12.7	43.5	0.816
2	20.3	54.7	1.35

The minimum theoretical value of tearing energy, T_F, for the model foam shown in Figure 4.1. is given by the energy required to break all the threads crossing a plane of unit area. The proportion of these threads to the total area of the foam structure is given by eq. 4.2.,

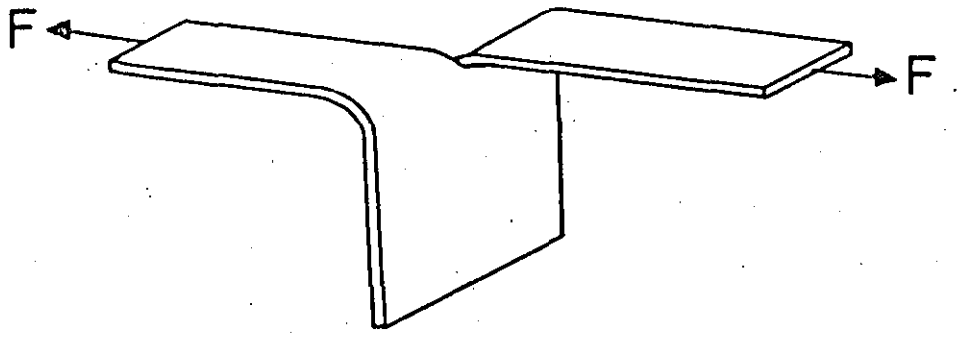

Figure 4.6.

Trouser tear testpiece used in tearing energy measurements.

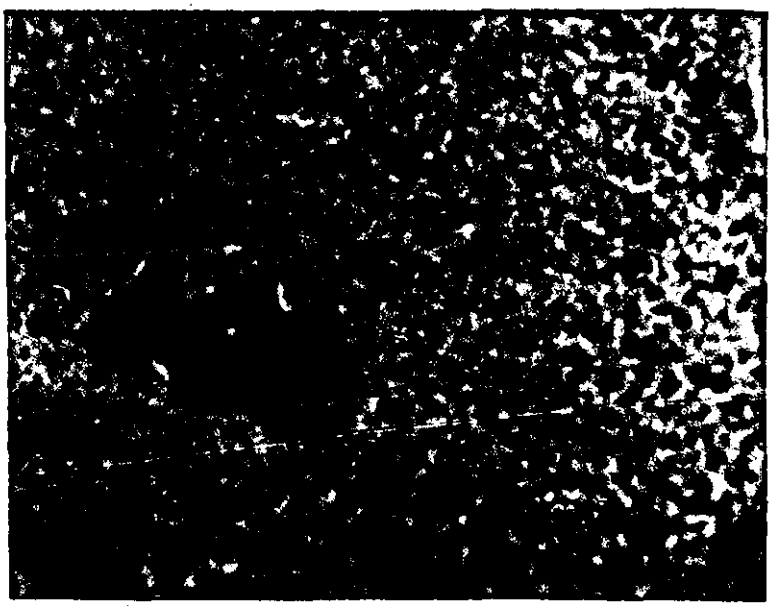

Figure 4.7.

Scanning electron microscope photograph of polyurethane foam used in this investigation showing that some pores can be of the order of 10^{-2}cm. (Magnification : 100).

and hence the tearing energy of the foam is given by

$$T_F = E_r l_o \frac{\beta^2}{(1+\beta)^2} \qquad 4.8.$$

where E_r is the breaking energy per unit volume of the bulk materials. The quantity l_o (i.e. one thread length) is assumed in the theory to be the effective "width" of the tear tip and is obviously the minimum possible value. Assuming that the model shown in Figure 4.1. can be applied to polyurethane foams, it is possible to calculate l_o and compare this with the average and largest pore diameter obtained from microscopic measurements. The value β was found from the curve shown in Figure 4.2. by measuring the densities of the solid and foam polyurethanes. Values for β for foams 1 and 2 are listed in Table 4.1. The values for E_r were found by graphically integrating the stress-strain curves for the two samples of solid polyurethane. On subsituting these values in eq. 4.8., l_o was found to be 4×10^{-2} cms for both foam 1 and foam 2. Although the average pore diameter is about 2×10^{-3} cm for both foams, odd pores as shown in the scanning electron microscope photograph in Figure 4.7. cm can be up to 2×10^{-2} cm in diameter.

Hence it can be considered that values for initiation of a tear can be obtained from eq. 4.8. by assuming that the effective width of the tear tip is about two times the largest pore diameter. This difference is probably due to imperfections in the foam causing local deviations of the tear from a linear path which gives rise to a corresponding larger effective tear width.

Gent and Thomas[57] found that the effective width of the tear tip for natural rubber foams at similar densities to the polyurethane foams in this paper was about five times the average pore diameter. Average pore diameters in their case, however, were a factor of 10 larger than those of the polyurethane foams used in this study.

4.6. TENSILE FAILURE

Following the tearing energy criterion developed by Rivlin and Thomas[61] it can be assumed that tensile rupture occurs by catastrophic tearing from a flaw in one of the test piece surfaces. The tearing energy of the foam, T_F can then be expressed as[63]

$$T_F = 2kE_FL \qquad 4.9.$$

for a test piece strained in simple extension where E_F is the energy density at failure in the bulk of the test piece for the foam, L is the depth of the flaw, and k is a numerical constant which varies slightly with strain[65] but can be taken for the purposes of this study as having a value of 2.

The depth of flaw can then be calculated by measuring the tear strength and energy density to failure of the foam and substituting these values in eq. 4.10,

$$L = \frac{T_F}{4E_F} \qquad 4.10.$$

The E_F value was obtained by measuring the area under the stress-strain curve of the foam. Using values of tear strength at initiation listed in Table 4.1., L was found to be 1.72×10^{-2} cm for foam 1 and 2.3×10^{-2} cm for foam 2. These values are very close to the largest pore diameters measured from scanning electron microscopy photographs. The numerical agreement suggests that tensile failure occurs by catastrophic tearing from a flaw of the order of the largest pore in length. This conclusion is in agreement with the work by Gent and Thomas on natural rubber foams and hence accounts for the relatively low values of tensile strengths found in foam materials in general.

4.7. UNIAXIAL COMPRESSION

The type of stress-strain curve obtained in compression for the polyurethane foams used in poromerics is shown in Figure 4.8. Similar

results have been reported previously for compression of polyurethane foams[66,67]. The type of curves obtained resemble those for the classical treatment of the buckling of a simple strut in compression. For foam 1, the ratio of thread length to width of the threads (i.e., β^{-1}) is 1.23, and hence the amount of buckling of the threads would be minimal. The classical Euler theory for buckling of struts can only be applied[68] if the length of the struts is at least 3.8 times their thickness, but it is informative to ascertain whether the assumed point of buckling (i.e., point at which curve changes slope) can be correlated with accepted "shape factor" theories of buckling from rubber engineering.

The critical compressive strain, e_c, of the individual threads of the model is given by[69]

$$e_c = \frac{\sigma_c}{Y\ (1 + 2S^2)} \qquad 4.11.$$

where σ_c is the critical compressive stress, Y is Young's modulus of the solid material, and S is the shape factor of the strut in compression as discussed by Payne[70] and others[69] in rubber engineering theory and defined as the ratio of the one loaded area to the total force-free area, and given by

$$S = \frac{D^2}{4D\,l_o} = \frac{\beta}{4} \qquad 4.12.$$

for a single rectangular strut such as those comprising the model structure shown in Figure 4.1.

For foam 1, S therefore has a value of 0.204. The value of stress at which the compression stress-strain curve in Figure 4.8. shows departure from linearity is 4.05 kgf/cm^2. The effective stress, however on each strut in the model will be much higher, as they only occupy a fractional area of the total as given by eq. 4.2. For β of 0.816, as in the case with foam 1, the threads occupy only 0.2 of the total cross-sectional

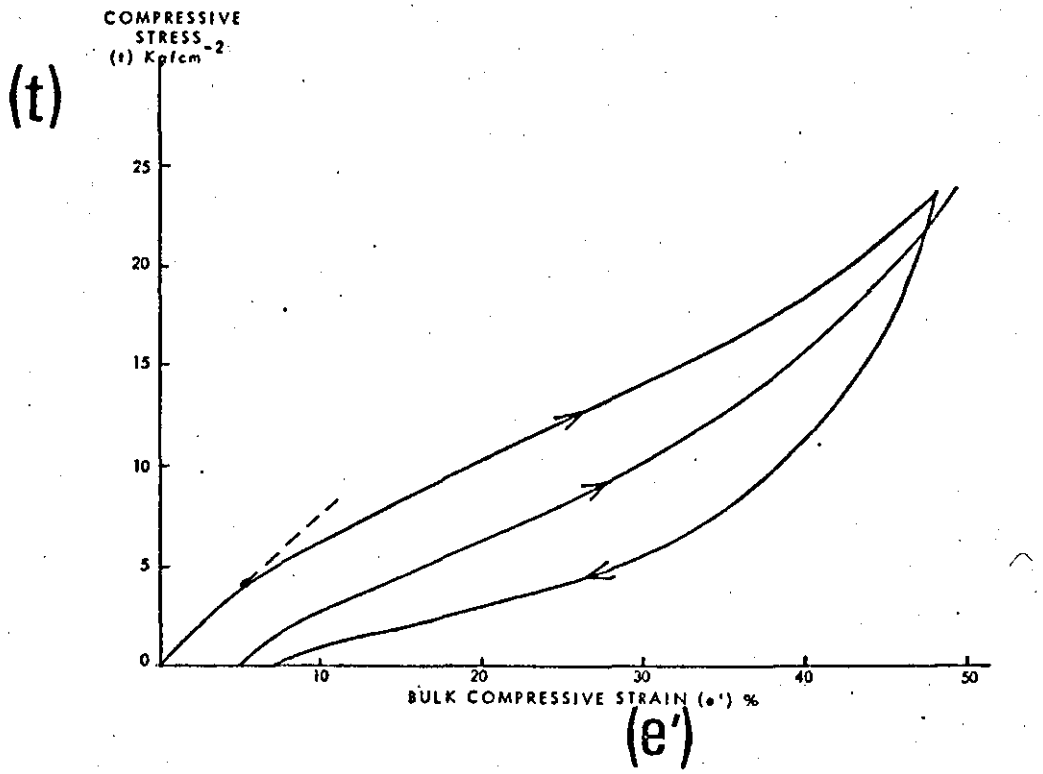

Figure 4.8.

Compressive stress-strain curve obtained for foam 1. Retraction and second compressive stress-strain curve also shown to illustrate large amount of stress softening and hysteresis.

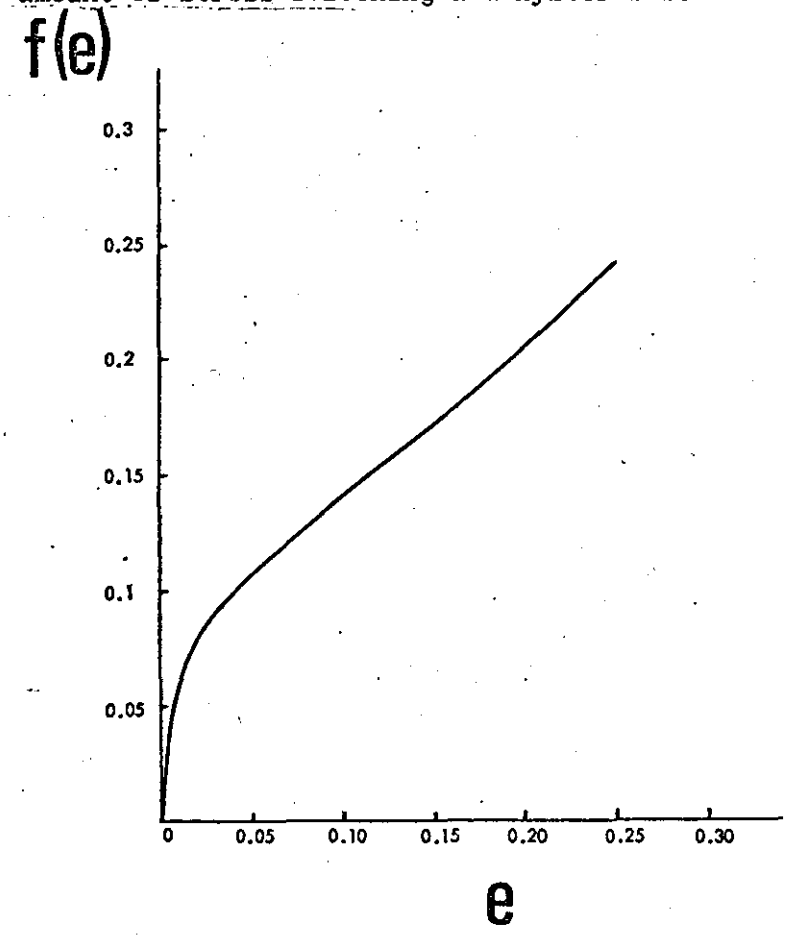

Figure 4.9.

Variation of f(e) with thread compressive strain (e) obtained from stress-strain curve shown in Figure 4.8.

area of the foam; hence the critical buckling stress σ_c for each thread in the model is 20.25 kgf/cm^2.

Using this value for σ_c and the value of 387 kgf/cm^2 predicted by eq. 4.5. for Young's modulus of the solid material from measurements of Young's modulus on the foam, a value for critical compressive strain e_c of the struts of 0.05 is obtained. The actual effective buckling strain of the foam, e_c', will be lower, however, due to the undeformable regions at thread intersections as predicted by eq. 4.1. Hence the critical compressive strain of the foam from theory is 0.03, which compares reasonably well with the experimental value of 0.056 obtained from the compression stress strain curve in Figure 4.8.

An alternative approach adopted by Gent and Thomas[58] is to include in the classical Euler strut theory an unknown function of strain, f(e). The compression is assumed to be directed parallel to one set of threads in the model structure shown in Figure 4.1. and to take place by buckling of these threads. The force F on each thread is given by

$$F = \frac{YAK^2 f(e)}{lo^2} \qquad 4.13.$$

where AK^2 is the moment of inertia of the thread cross section. For threads of similar cross section, $AK^2 = mD^4$, where m is a constant. The number of threads per unit cross sectional area is given by $(lo + D)^{-2}$, and hence the average compressive stress t is given by

$$t = \frac{F}{(lo + D)^2} = Yf(e) \frac{\beta^4}{(1 + \beta)^2} \qquad 4.14.$$

by substituting β for D/lo and absorbing the constant m in f(e).

Bulk compressive strain e′ is, however, influenced by two factors which can be considered additive: firstly the incompressibility of thread intersections as predicted by eq. 4.1. and secondly a contribution from simple compression of the threads by an amount t/Y_F. Hence the bulk compressive strain e′ will be given by

$$e' = \frac{e}{1 + \beta} + \frac{t}{Y_F}. \qquad 4.15.$$

The application of such a theory to polyurethane foams is difficult, for, as can be seen in Figure 4.8., they display a large amount of energy loss or hysteresis and also a considerable amount of stress softening (i.e., the reduction in stress on the second extension curve). Although stress softening has been extensively studied[12-14] in tension, little work appears to have been reported on stress-softening effects in compression.

Despite the large amount of hysteresis, the analysis along the lines suggested by Gent and Thomas has, however, been also adopted in this paper to ascertain the form of the function f(e).

By substituting measured values for bulk compressive stress $(\dot{t})$ and bulk compressive strain (e') from Figure 4.8. it is possible, using the derived value for β and experimental values of Young's modulus for the solid polyurethane and foam, to obtain corresponding values of f(e) and effective strain e of the threads in the model by use of eqs. 4.14 and 4.15. The relationship derived is shown in Figure 4.9. It is of the general form expected for a buckling process and is very similar to that obtained for natural rubber foams[58], although compression tests on the latter were only reported for foams with V_r less than 0.2.

4.8. CONCLUSIONS

The theoretical model proposed by Gent and Thomas which has been applied here to the mechanical behaviour of cellular polyurethane is a very idealised representation of an actual foam, which in practice must be far from homogeneous. The actual threads and intersections are of a wide range of shapes and sizes, as can be seen from the scanning electron microscope photographs. The apparent good agreement therefore obtained between experimental values of Young's modulus and theory is very satisfactory, particularly in view of the difficulties that occur with obtaining a reasonably good sample of solid material.

The measured values of breaking energy are in good agreement with those calculated on the assumption that tensile failure occurs by tearing at the tip of the largest pore, which is the same criterion as that found for natural rubber foams.

Values for tear strength at the initiation of a flaw can be obtained from the theory by assuming that the effective width of the tear tip is about twice the largest pore diameter. Tear strength results on polyurethane foams thus appear to differ from those on natural rubber foams as Gent and Thomas found that tear strength was much more dependent on the average pore diameter. In the case of the polyurethane foams examined in this paper the average pore diameter was at least a factor of 10 lower than the maximum pore diameter.

The shape of the compression stress-strain curve is similar to that obtained from the buckling of a strut in simple compression and can reasonably be described by the model proposed on the assumption that the threads in the model buckle under a compressive load. The arbitary function f(e) provides a measure of the inhomogeneity of the foam structure, and the variation of f(e) with strain is of the same form as that found for natural rubber foams. An alternative approach by use of shape factor theories predicts within a factor of 2 the value of the compressive buckling strain as compared with the value shown by the deviation in linearity of the compression stress-strain curve.

Thus, the fairly simple model of a collection of thin threads of equal length joined together to form a cubical lattice appears to predict reasonably well the mechanical behaviour of cellular polyurethanes. These materials therefore follow similar relationships to those between foam and solid vulcanised rubbers and hence the high strength of cellular polyurethanes is very dependent on the very high strength of the solid polymer.

CHAPTER 5

EFFECT OF TIME AND TEMPERATURE ON THE TENSILE PROPERTIES OF POLYURETHANES

5.1. INTRODUCTION

As shown in the previous chapter, the mechanical properties of a cellular polyurethane can be related to the corresponding solid material by use of a fairly simple model. This model was initially found to relate similar properties in cellular and solid vulcanised rubbers. The high strength of the cellular polyurethanes referred to in Chapter 1 is therefore due to the very high strength exhibited by the solid polyurethane material. The reasons for this high strength are discussed in this and some of the later chapters of the thesis.

A number of other features with regard to the properties of cellular polyurethane elastomers in poromerics were noted in Chapter 1 such as high strength over a wide temperature range, the high set and shape retention, which indicates that the material has a broad distribution of relaxation times, and the indication of some thermoplastic behaviour at temperatures above 160°C. In view of the importance of time and temperature in the final use of these polyurethanes and in order to elucidate more clearly the reason for their good mechanical properties, a full investigation into the effect of time and temperature on the tensile properties of both the cellular and solid polyurethanes is presented in this chapter.

The first part of the chapter reports an investigation into determining the relaxation spectrum of polyurethanes. The second part discusses the effect of time and temperature on the failure parameters of polyurethanes and compares these results with those obtained from vulcanised rubber and the third part of the chapter discusses the high temperature recovery of stress-softening.

5.2. EXPERIMENTAL

Ring samples of the same diameter as the samples described in Section 2.3. of the thesis were cut from the cellular polyurethane used in poromeric materials (foam 1 from Chapter 4) and the corresponding solid material. Tensile stress strain curves were obtained for both materials by use of an Instron Tensile Testing Machine at six crosshead speeds from 0.05 cm/min. to 100 cm/min. (strain rate from 0.013 to 25 per min.). This procedure was repeated at 20 degrees centigrade intervals between 21°C and 180°C. The tensile measurements for the cellular polyurethane were based in all cases on the cross sectional area including both rubber and cells.

Hysteresis and stress-softening were also measured on a number of samples where the initial extension curve was reversed before the breaking point and these are reported in section 5.7.3. The testing procedure used for all these tests was the same as described in Section 2.3. of the thesis.

For comparison with these results, ring samples of the same diameter were cut from the crosslinked polyether microporous layer of the fibrous based poromeric 'Corfam' and similar tensile stress strain curves were obtained.

5.3. VISCOELASTIC PROPERTIES

5.3.1. Theoretical Considerations

A variety of methods have been used to study the viscoelastic properties of polymeric materials in terms of the relaxation or retardation spectrum. These methods include the response to sinusoidal stress (dynamic measurements[71,72]) stress relaxation[73,74] and creep under constant load[75] and constant stress[76]. Most of this work has been reviewed by Ferry[27].

The viscoelastic properties of a polymer when subjected to a constant rate of deformation have been discussed by Alfrey[77], Sips[78]

and Smith[79,80]. The stress strain curves of a linear viscoelastic material can be conveniently related to a generalised Maxwell model which is characterised by the relaxation spectrum $H(\tau)$ and the equilibrium modulus (E_e). If the model in its relaxed state at zero time is subjected to a strain which increases linearly with time, the resulting strain and time dependent stress $\sigma(\varepsilon,t)$ is given by the equation

$$\frac{\sigma(\varepsilon,t)}{R_1} = E_e.t + \int_{-\infty}^{\infty} \tau.H(\tau).(1 - e^{-t/\tau})d.\ln.\tau \qquad 5.1.$$

where R_1 is the strain rate and τ is the relaxation time. This equation shows that $\sigma(\varepsilon,t)/R_1$ is a function only of time. Stress-strain curves measured at different strain rates will superpose to yield a single composite curve on a graph of log $\sigma(\varepsilon,t)/R_1$ against log t provided the data are reasonably <u>linear</u> viscoelastic. The slope of the stress-strain curve at $t = \varepsilon/R_1$ equals the stress relaxation modulus E(t). This interrelation results from differentiating equation 5.1. with respect to strain (ε) to yield.

$$\frac{d\sigma}{d\varepsilon} = \frac{1}{R_1}\frac{d\sigma}{dt} = E_e + \int_{-\infty}^{\infty} H(\tau)\, e^{-t/\tau}\, d.\ln\tau = E(t) \qquad 5.2.$$

The major problem however with this analysis arises because polymers only exhibit linear viscoelastic behaviour at very low deformations. The stress-strain curves shown in figure 5.1. for the cellular polyurethane tested at ~~strain~~ jaw separation rates from 0.05 cm/min. to 50 cm/min. show non-linear viscoelastic behaviour. Similar results were also found in the case of the solid materials.

This non-linear dependence of stress on strain is due firstly to the fact that under most test conditions, relaxation of stress takes place continually during a test and secondly even in the absence of stress relaxation, the stress-strain is non-linear as predicted by the statistical theory of rubber elasticity.

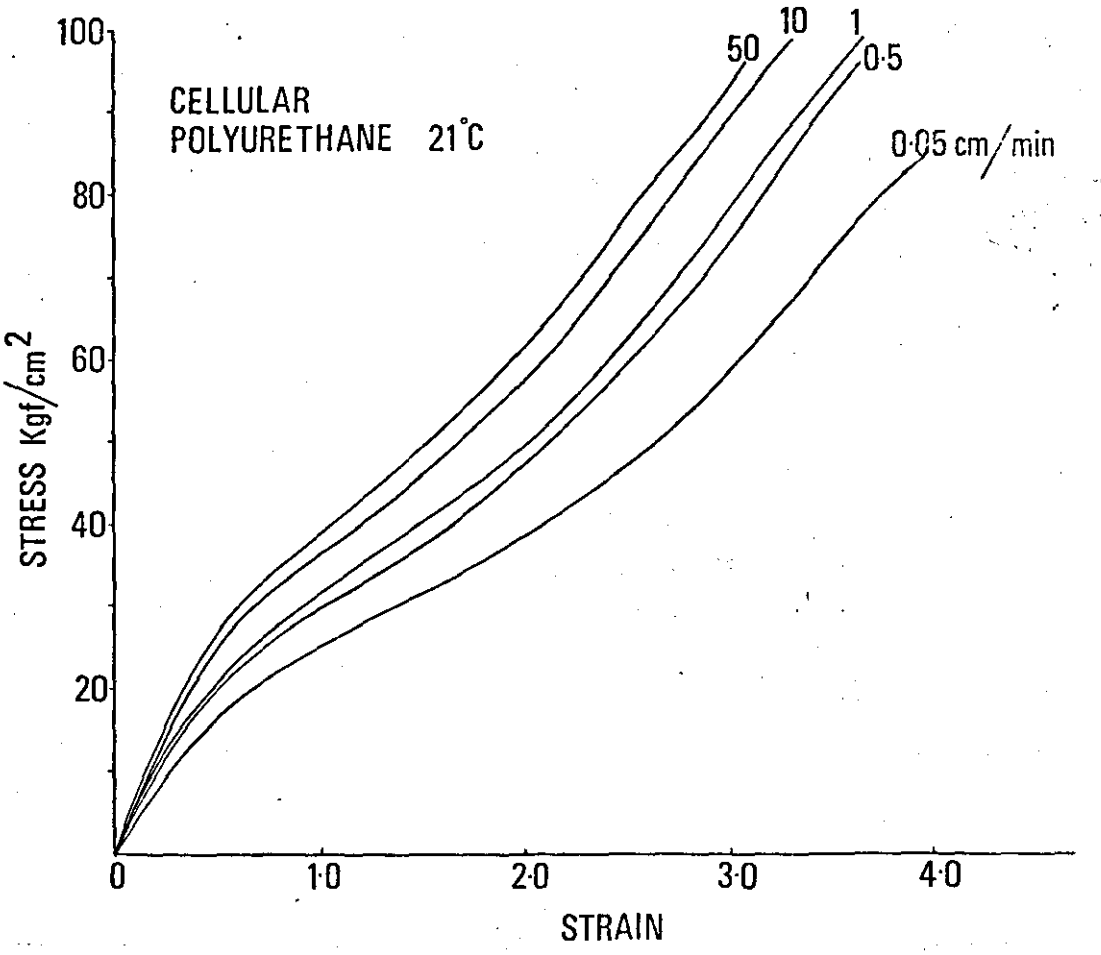

Figure 5.1.

Typical stress-strain curves for a cellular polyurethane tested at several ~~strain~~ jaw separation rates at 21°C.

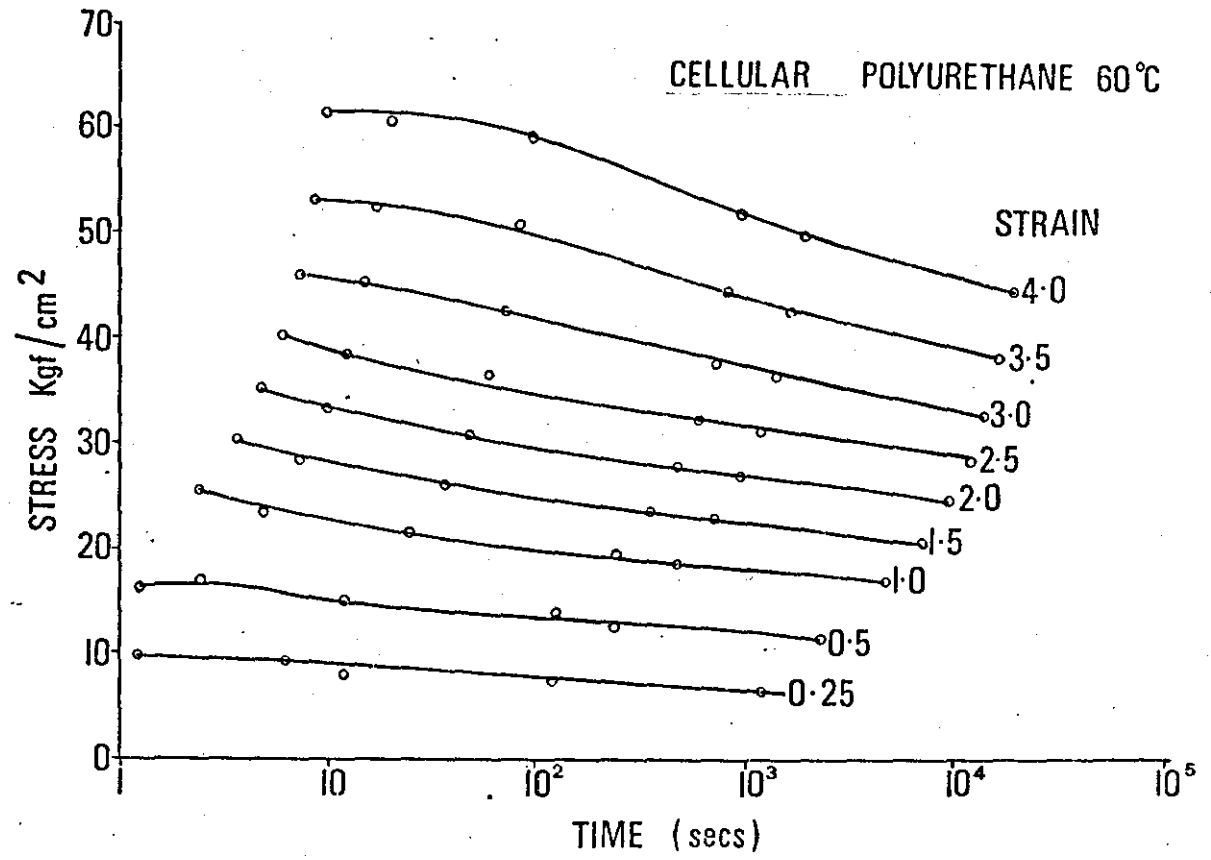

Figure 5.2.

Variation of stress at a particular strain against time to reach the strain for the cellular polyurethane at 60°C

Smith[79,80] has shown that in the case of polyisobutylene and styrene butadiene rubber (SBR), equations 5.1. and 5.2. are applicable to stress-strain data up to 100% extension provided that stress σ is replaced by real stress or the stress based on the actual cross sectional area of the stressed sample which for elastomers is equal to $\sigma(1+\varepsilon)$ or $\sigma\lambda$.

Before attempting to derive a relaxation spectrum for polyurethane, it is necessary to ascertain whether $(1+\varepsilon)$ is a suitable strain function which can be introduced into equations 5.1. and 5.2. to take account of this non-linear viscoelastic behaviour.

5.3.2. Strain Function

A number of investigators[81-85] have found it useful in tensile creep and stress relaxation measurements to express the stress $\sigma(\varepsilon,t)$ occurring after a time t at a constant extension rate from zero time as a product of a strain function and a time function which are mutually independent. A convenient method of expressing $\sigma(\varepsilon,t)$ in a tensile stress-strain curve is by the following relationship.

$$\sigma(\varepsilon,t) = F(t)\ \frac{\varepsilon}{g(\varepsilon)} \qquad 5.3.$$

where F(t) is the time function which is referred to later as the constant strain-rate modulus and $g(\varepsilon)$ is a function of strain which approaches unity as the strain goes to zero.

In order to determine whether the stress-strain curves of cellular polyurethane could be represented by equation 5.3., values of stress at strains of 0.25, 0.50, 0.75, 1.00 and at further 0.50 intervals were recorded at every strain rate and temperature.

For each temperature, a graph was drawn of the stress at a particular strain against the time to reach the particular strain. An example of these graphs is shown in figure 5.2. for the results at 60°C. The lines through the points are approximately parallel

and this indicates that equation 5.3. is obeyed. Each parallel curve is displaced along the log σ axis, by the amount log $g(\varepsilon)/\varepsilon$. A similar set of curves was found at each of the test temperatures.

This procedure indicated that a function $g(\varepsilon)$ existed which was independent of time over the range considered. It would be expected therefore that if $g(\varepsilon)$ was independent of time, it would also be independent of temperature but as an extended temperature range corresponds with many decades of time at a single temperature, it was necessary to investigate the possible temperature dependence of $g(\varepsilon)$.

Isochronal values of stress and strain were taken from plots similar to those in figure 5.2. for several temperatures and plotted as log σ against log ε as shown in figure 5.3. for data at 1,000 sec. It is observed that apart from a slight departure at higher strains for the data at 20°C, the results lie again on parallel lines as predicted by equation 5.3. and demonstrates that $g(\varepsilon)$ is temperature independent. The data between two temperatures are therefore displaced along the log σ axis by an amount which equals the difference between the logarithms of the constant strain rate modulus F(t) at the two temperatures.

Having shown that equation 5.3. is applicable to the tensile data obtained on cellular polyurethanes, it is necessary to consider the value for $g(\varepsilon)$. One of the simplest analytical expressions is the modified Hooke's Law equation,

$$\sigma\lambda = E\,\varepsilon \qquad 5.4.$$

so that the function $g(\varepsilon)$ is given by,

$$g(\varepsilon) = 1 + \varepsilon \qquad 5.5.$$

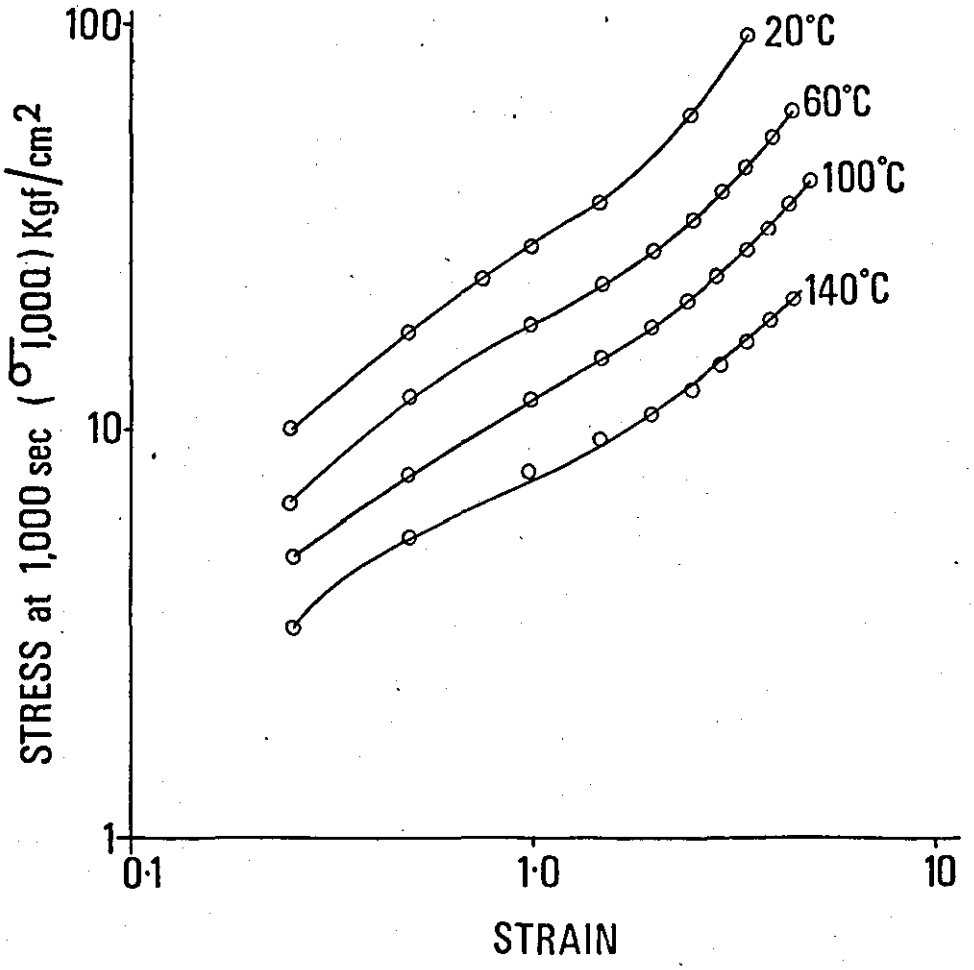

Figure 5.3.

Variation of log stress with log strain for data at 1,000 seconds taken from graphs similar to those shown in Figure 5.2.

By multiplying isochronal values of stress from graphs similar to those shown in figure 5.2. by $g(\varepsilon)$ as defined in equation 5.5. and plotting this as a function of strain as in figure 5.4., it is seen that the modified Hookes Law equation is a reasonable approximation to the isochronal stress strain-curve up to about 150-200% extension.

In order to take account of non-linear viscoelastic behaviour, it would appear appropriate therefore to put the term $\sigma(\varepsilon,t)$ equal to $\sigma\lambda$ as shown by the following equation,

$$\sigma(\varepsilon,t) = \sigma(t).\, g(\varepsilon) = \sigma(t)(1+\varepsilon) = \sigma\lambda \qquad 5.6.$$

in the calculation of the relaxation spectrum from equations 5.1. and 5.2.

5.4. RELAXATION MODULUS

5.4.1. Introduction

In order to calculate a relaxation spectrum for polyurethanes, it is necessary to determine the variation of relaxation modulus E(t) with time. Two methods for obtaining E(t) were used by Smith[79,80] in the analysis of tensile data of SBR and polyisobutylene. Both these methods have been applied to the tensile data on polyurethanes and are described in this section of the chapter.

5.4.2. Method I

The first method used by Smith[79] for analysing the stress-strain curves of polyisobutylene made use of the fact predicted by equation 5.1. that σ/R_1 was only a function of time or ε/R_1. Data obtained therefore at different strain rates should superpose to give a single curve on a graph of log σ/R_1 against log ε/R_1. Data obtained at different temperatures can be combined by use of the time-temperature reduced variable scheme of Ferry[27,86].

This scheme is based on the assumption that all the relaxation times have the same temperature dependence and that the modulus of

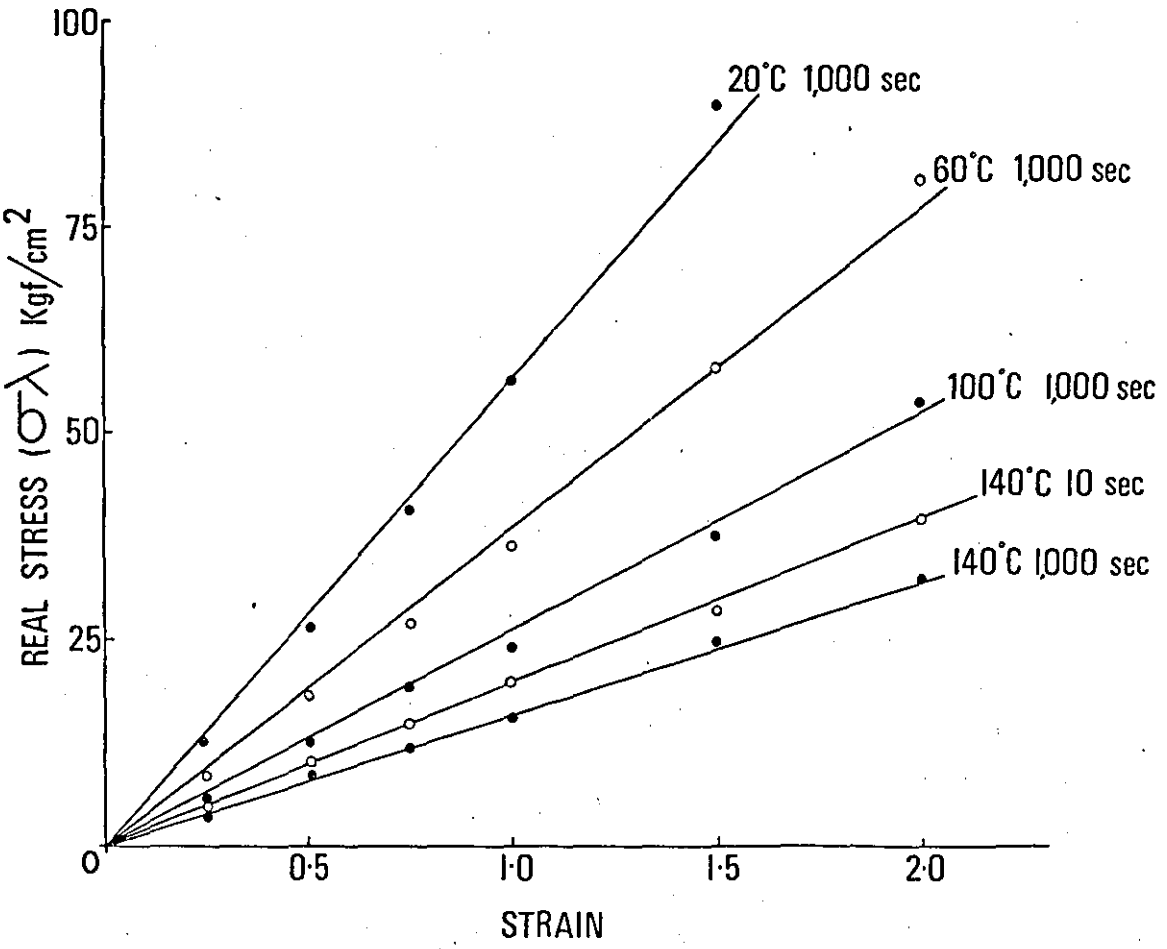

Figure 5.4.

Variation of real stress ($\sigma\lambda$) with strain at various temperatures and times indicating that the modified Hookes Law equation is obeyed up to 150 - 200% extension for isochronal data. (cellular polyurethane)

each spring in the generalised Maxwell model is proportional to absolute temperature. By including this modification and the strain function given in equation 5.6., equation 5.1. becomes

$$\frac{\sigma \lambda T_o}{R_1 a_T T} = E_e \cdot \frac{\varepsilon}{R_1 a_T} + \int_{-\infty}^{\infty} \tau . H(\tau) . \left(1 - e^{-\varepsilon / R_1 a_T \tau}\right) d.\ln \tau . \quad 5.7.$$

where T_o is an arbitrary reference temperature, T is the temperature at which σ and λ are measured and a_T is the ratio of any relaxation time at T to its value at T_o.

Data measured therefore at different temperatures and strain rates should superpose on a graph of log $(\sigma \lambda T_o / R_1 a_T T)$ against log $(\varepsilon / R_1 a_T)$. These quantities are termed reduced stress σ_r and reduced strain ε_r respectively. A graph of σ_r against ε_r therefore is a hypothetical stress-strain curve measured at unit strain rate and temperature T_o. Equation 5.7. can therefore be expressed as:

$$\sigma_r = E_e . \varepsilon_r + \int_{-\infty}^{\infty} \tau . H(\tau) . (1 - e^{-\varepsilon_r / \tau}) d.\ln . \tau \quad 5.8.$$

By differentiating equation 5.8. with respect to reduced strain, the stress relaxation modulus E(t) can be obtained as predicted by equation 5.2. By using reduced stress and strain, equation 5.2. becomes

$$\frac{d\sigma_r}{d\varepsilon_r} = E_e + \int_{-\infty}^{\infty} H(\tau) . e^{-\varepsilon_r / \tau} \, d.\ln \tau = E(t) \quad 5.9.$$

For calculation purposes, the equivalent equation can be used[79]

$$E(t) = \frac{\sigma_r}{\varepsilon_r} \left(\frac{d \ln \sigma_r}{d \ln \varepsilon_r}\right) \quad 5.10.$$

thus providing a method for obtaining the relaxation modulus-time curve for polymers from which the distribution of relaxation times or relaxation spectrum can be calculated.

Values of stress function $\left(\frac{\sigma \lambda T_o}{R_1 T}\right)$ and strain divided by rate (ε / R_1) up to 150% extension were evaluated from the experimental results for both the solid and cellular polyurethanes at the nine test

temperatures. In order to show that stress-strain data obtained at different strain rates superposed as predicted by equation 5.7., a graph of $\log \frac{\sigma \lambda T_o}{R_1 T}$ against $\log \varepsilon/R_1$ was drawn as shown for the cellular polyurethane in figure 5.5. The value of the standard reference temperature T_o was taken as 294^oA.

The results as shown in figure 5.5. follow a very shallow curve which departs at higher times from a unit slope. The data for each temperature is slightly displaced along the reduced stress axis. Values of $\log a_T$ were obtained by shifting the graphs of $\log \frac{\sigma \lambda T_o}{R_1 T}$ against $\log \varepsilon/R_1$ up a line of unit slope until all the curves for the different temperatures coincided. The distances the curves were shifted relative to the standard reference temperature 294^oA gave the actual values for $\log a_T$. These values are plotted against temperature in figure 5.6.

Measurements by Thermal Mechanical Analysis showed that the glass transition temperature of the polyurethane was approximately -30^oC. Using this value for T_g, values of a_T have been calculated by use of the Williams, Landel & Ferry (WLF) equation[27] given below.

$$\log a_T = \frac{-8.86\ (T - T_s)}{101.6 + T - T_s} \qquad 5.11.$$

where T is the test temperature and $T_s = T_g + 50$.

It is seen that the WLF equation agrees with the experimental points only over a very small temperature range and this is discussed further in Chapter 7.

Similar curves to those shown in figure 5.5. were obtained for the solid polyurethane and by using the values of $\log a_T$ calculated for the cellular polyurethane material, composite master curves of reduced stress (σ_r) against reduced strain (ε/R_1) were obtained for both the cellular and solid polyurethane and these are shown in

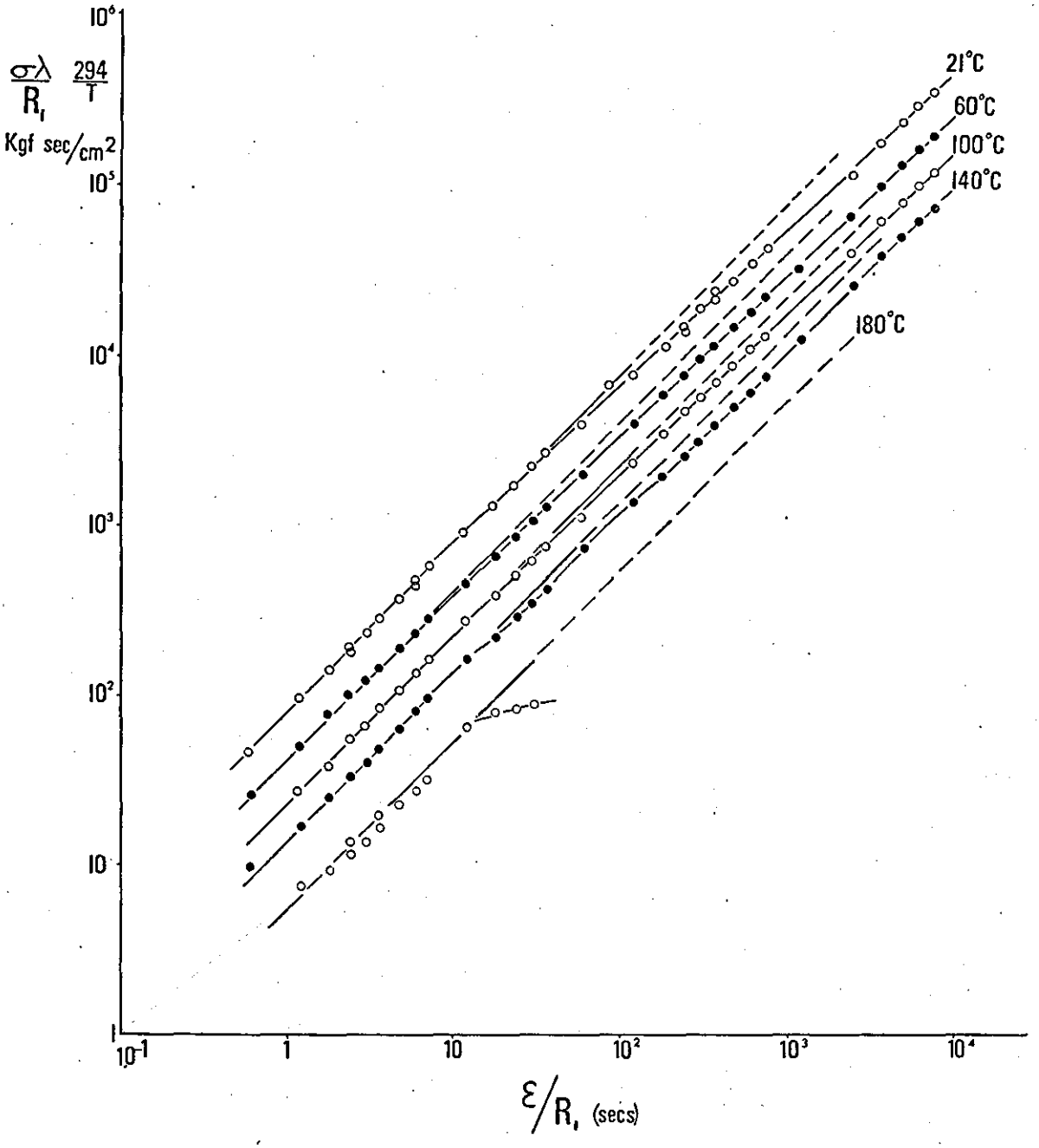

Figure 5.5.

Variation of log $(\frac{\sigma\lambda}{R_1}\ \frac{294}{T})$ with log (ε/R_1) for the cellular polyurethane. Values are for strains up to 150% extension.

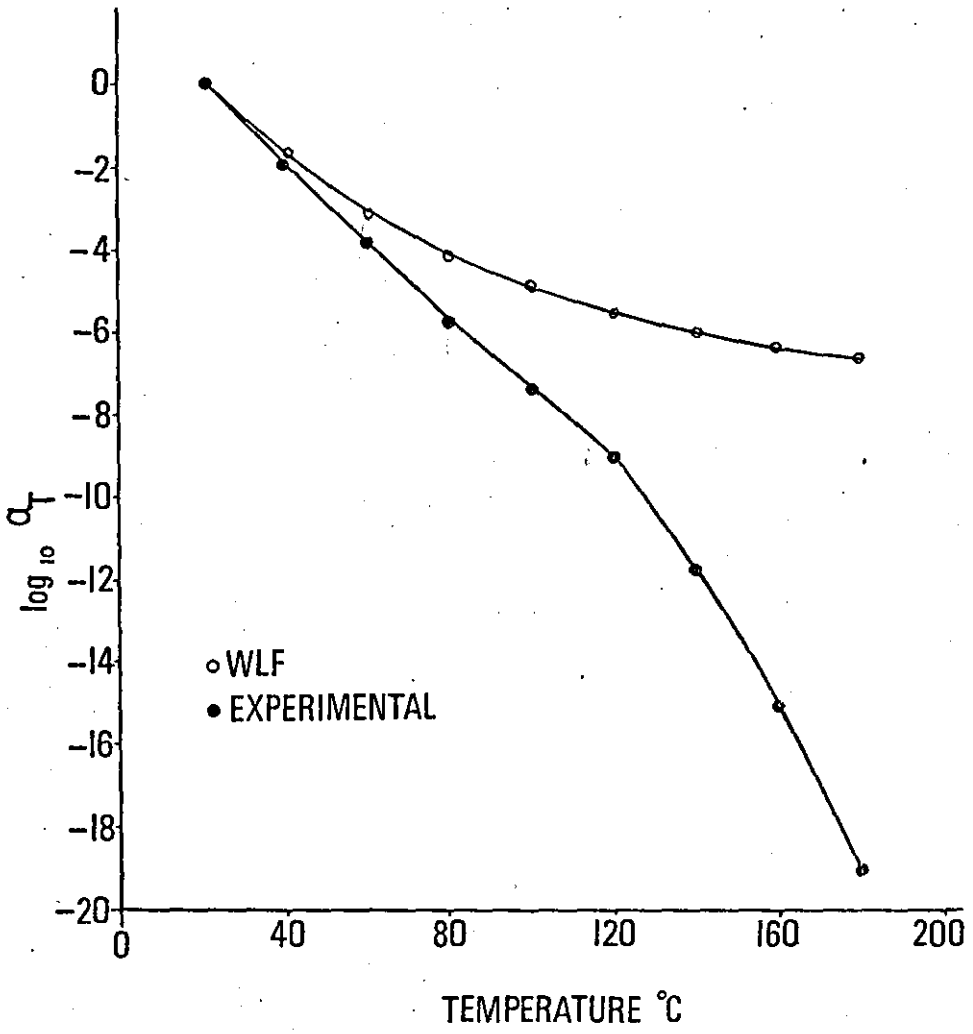

Figure 5.6.

Variation of shift distance (log a_T) with temperature from results shown in Figure 5.5. compared with that predicted by the WLF equation.

figure 5.7. It is seen that the mastercurves for the cellular and solid materials extend approximately for 20 decades of time and the results for the cellular material are, over the majority of the time scale, parallel to those for the solid polyurethane.

The slope of the lines in figure 5.7. were measured graphically at a number of values of $\varepsilon/R_1 a_T$ and by multiplying the slope by the ratio of reduced stress σ_r to reduced strain ε_r at the respective time, it was possible by use of equation 5.10. to obtain values of relaxation modulus E(t) at each particular time. The relaxation modulus - time relationship for both materials is plotted in figure 5.8. on a double logarithmic scale. It is seen that the lines for the solid and foam polyurethane are approximately parallel with a factor of 4.2 between the results. It would appear therefore that the properties of the cellular polyurethane are dependent on the corresponding solid material even at very long times.

5.4.3. Method 2

An alternative approach to the problem of analysing stress-strain curves was suggested in a later paper by Smith[80] who used it in calculating a relaxation spectrum for SBR and polyisobutylene.

If the strain rate R_1 is replaced in equation 5.1. by the equivalent function (ε/t), the rearranged equation becomes,

$$\frac{\sigma(\varepsilon,t)}{\varepsilon} = E_e + \frac{1}{t}\int_{-\infty}^{\infty} \tau.H(\tau).(1 - e^{-t/\tau})d.\ln\tau \qquad 5.12.$$

The ratio $\sigma(\varepsilon,t)/\varepsilon$, which is a function of time alone, is called the constant strain rate modulus F(t) which is related to the stress relaxation modulus E(t) by the following equation:

$$E(t) = F(t).\left[1 + \frac{d.\log F(t)}{d.\log t}\right] \qquad 5.13.$$

The relaxation modulus - time curve was recalculated for the cellular polyurethane by this method as a check on the initial

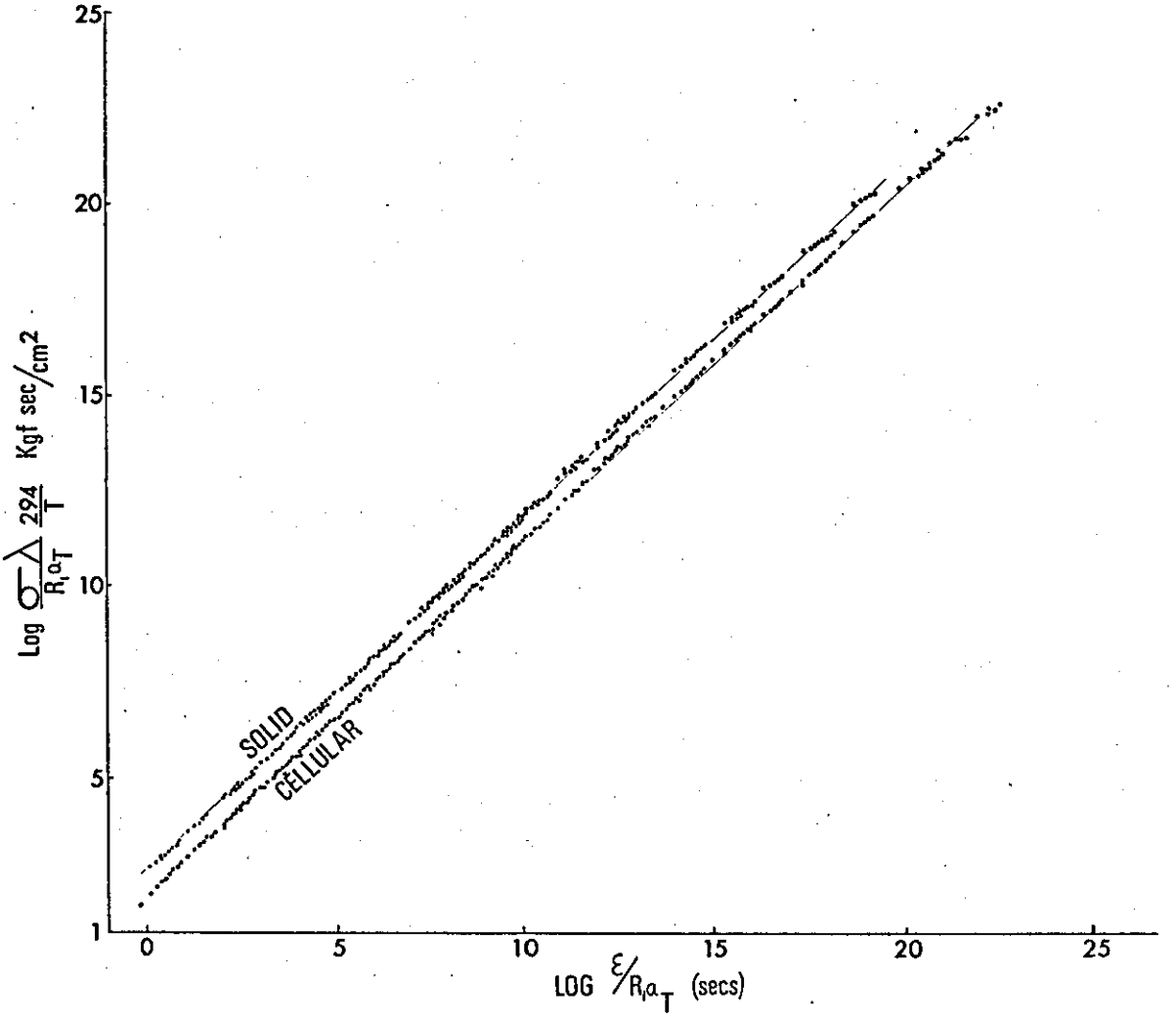

Figure 5.7.

Variation of log $\left(\frac{\sigma\lambda\ 294}{R_1\ a_T\ T}\right)$ with log $\left(\varepsilon/R_1\ a_T\right)$ for cellular and solid polyurethanes obtained by shifting curves shown in Figure 5.5.

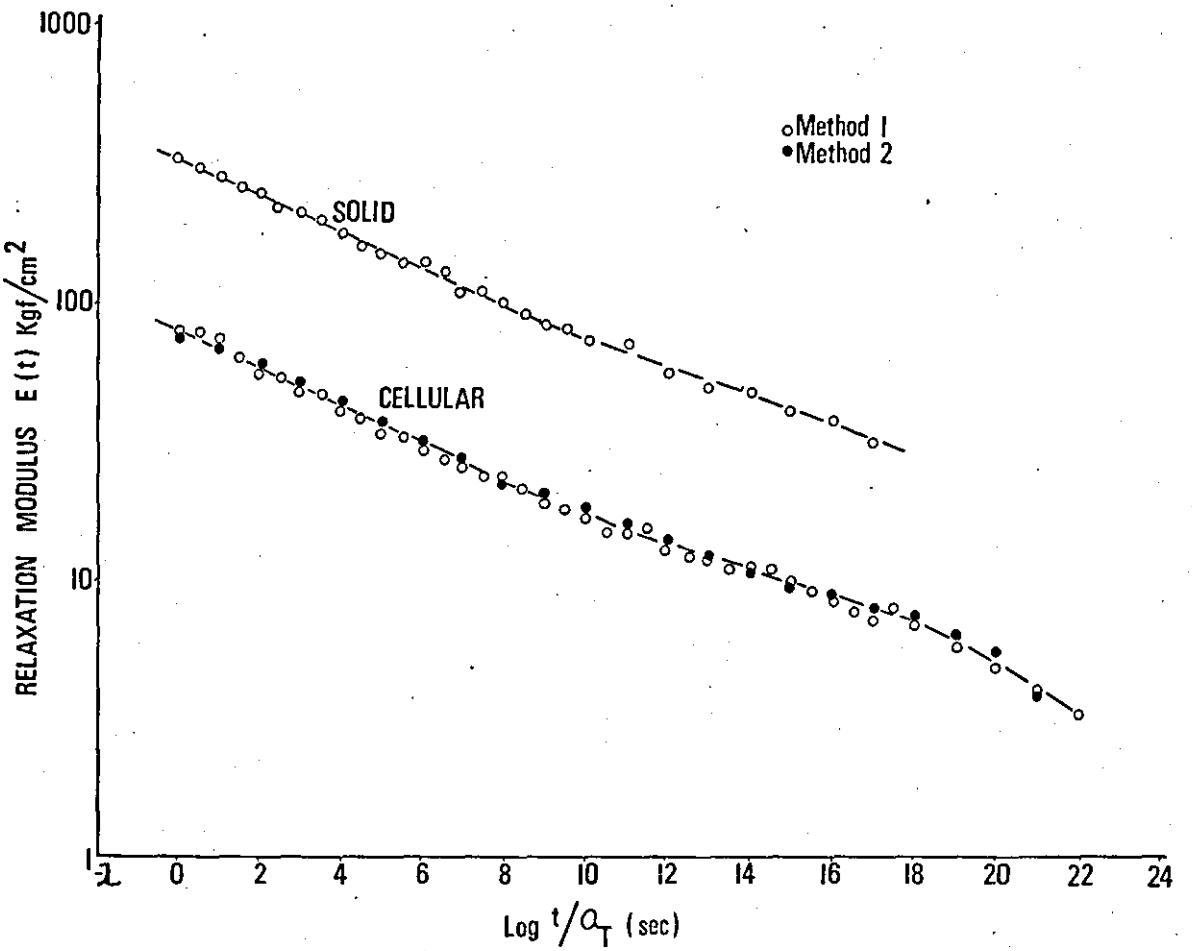

Figure 5.8.

Variation of relaxation modulus E (t) with time (t/a_T) for the cellular and solid polyurethane materials. Results from both methods 1 and 2.

calculations. Section 5.3.2. showed that it was possible to separate the stress into a time and strain function and that the strain function $g(\varepsilon)$ was equal to λ for strains at all temperatures up to 150%.

Using the same experimental data for the foam as used in the first method, the time dependence of $\sigma\lambda/\varepsilon$ (which is F(t) by definition) at temperatures between 21 and 180°C is shown in figure 5.9. by plots of $\log \frac{\sigma\lambda}{\varepsilon}.\frac{294}{T}$ against log t. The curves in figure 5.9. were shifted along the log t axis to effect superposition as shown in figure 5.10. It was found that the shift distances ($\log a_T$) were in agreement with the results obtained earlier and shown in figure 5.6.

Values of E(t) were calculated at various times from the results in figure 5.10. by use of equation 5.13. and these are compared with results obtained from the first method in figure 5.8. The agreement of the results between the two methods is very good and therefore the line drawn through the points in figure 5.8. can be taken as a reasonable description for the relaxation modulus - time curve from which the relaxation spectrum can be calculated.

5.5. RELAXATION SPECTRUM

It is possible to calculate the distribution of relaxation times $H(\tau)$ from the relaxation modulus E(t) by using various approximation methods. The most common method is due to Alfrey[77] who assumes that instead of multiplying $H(\tau)$ by the kernel function $e^{-t/\tau}$ as in equations 5.1. and 5.2. that this is approximated to by a step function going from 0 to 1 at $\tau = t$, so that

$$E(t) = \int_{\ln\tau}^{\infty} H(\tau).d \ln \tau \qquad 5.14.$$

The integral in this case would not be grossly different from equation 5.2. and hence by differentiating equation 5.14. with respect to the limit $\ln\tau$, equation 5.15. is obtained.

$$- \frac{d E(t)}{d \ln \tau}\Big)_{t=\tau} \simeq H(\tau) \qquad 5.15.$$

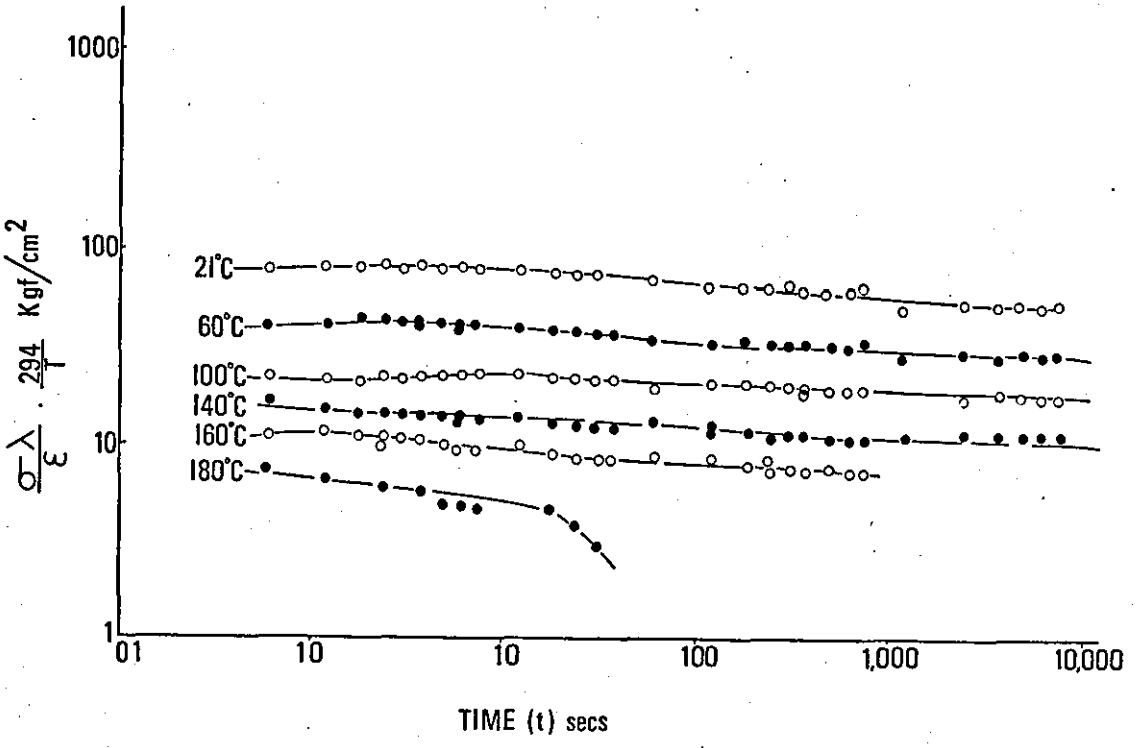

Figure 5.9.

Variation of log $(\frac{\sigma\lambda}{\varepsilon}\frac{294}{T})$ with log t for the cellular polyurethane.

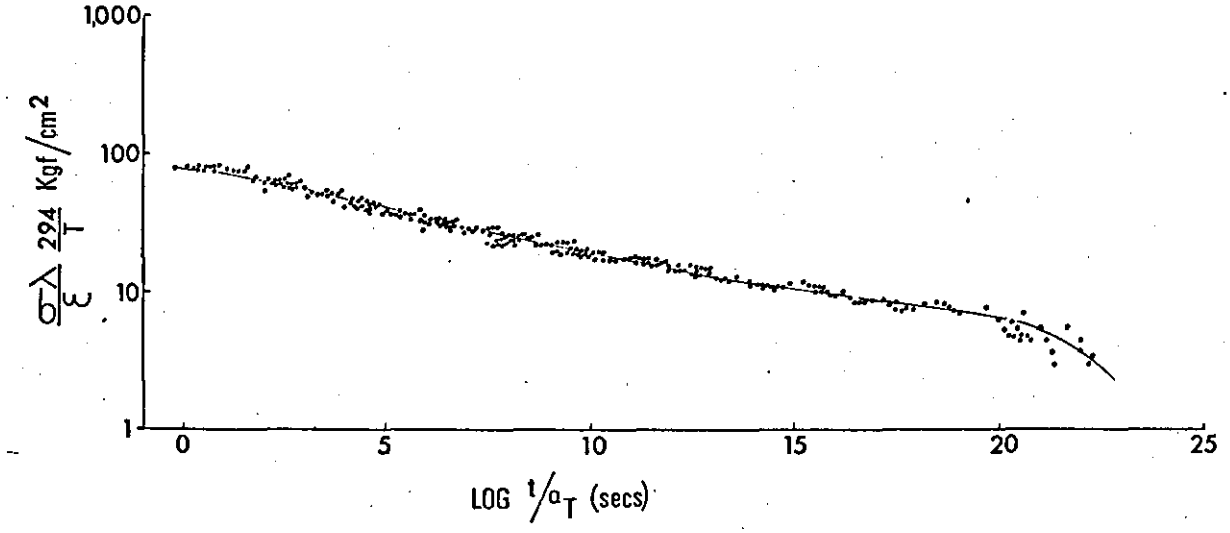

Figure 5.10.

Variation of log $(\frac{\sigma\lambda}{\varepsilon}\frac{294}{T})$ with log t/a_T for the cellular polyurethane. Graph obtained by shifting lines in Figure 5.9.

This equation provides a method for obtaining the relaxation spectrum at $\tau = t$ from the negative slope of the relaxation modulus - log time curve.

This equation is only applicable to solid materials and hence can only be used to evaluate the relaxation spectrum for the solid polyurethane but as the modulus of the foam was related to the solid material by a common factor at every time, one spectrum representing the properties of both the cellular and solid polyurethane can be derived.

The relaxation spectrum calculated from the curve shown in figure 5.8. by use of equation 5.15. is shown in figure 5.11. and compared in figure 5.12. with other typical spectra for elastomer systems from Ferry[27]. The most interesting feature of the relaxation spectrum for polyurethane compared with crosslinked amorphous rubbers is the very flat plateau which extends for over 18 decades of time. This particular relaxation spectrum is similar in shape but slightly less in magnitude than that of an amorphous polymer below its glass transition temperature or a highly crystalline polymer. In the case of the polyurethane, however, the material is flexible and above its glass transition temperature which occurs at approximately -30°C.

5.6. YOUNG'S MODULUS

5.6.1. Variation with Temperature

The normal form of stress-strain curves obtained for the cellular polyurethanes at various strain rates at 21°C are shown in Figure 5.1., the curve has an initial relatively steep slope and then flattens out at higher strains. Similar shaped curves were obtained for the solid material as shown in figure 4.4. The slope of the initial portion of the stress-strain curve permits a value of Young's modulus for the

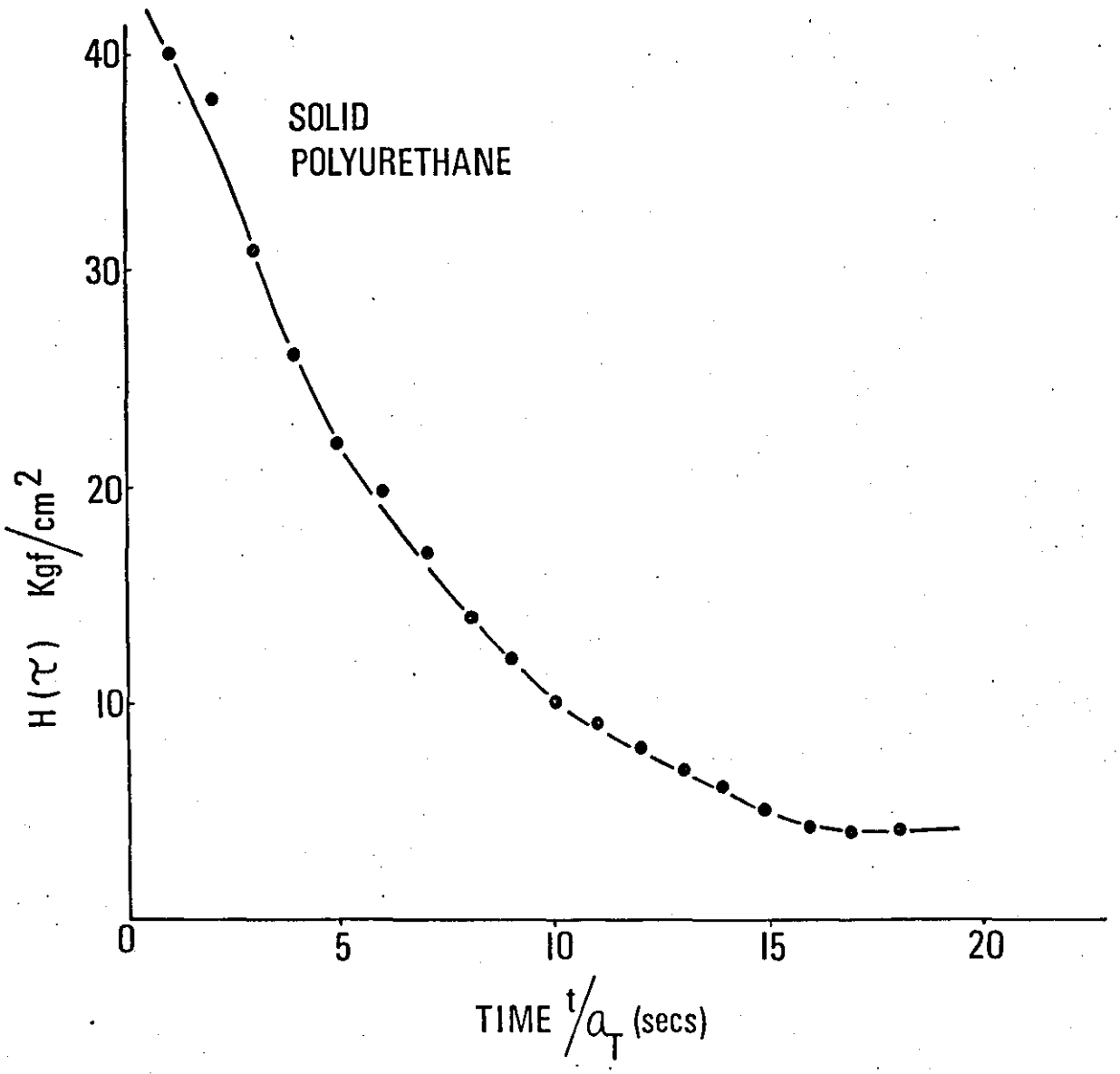

Figure 5.11.

Relaxation spectrum for solid polyurethane calculated from results in this paper.

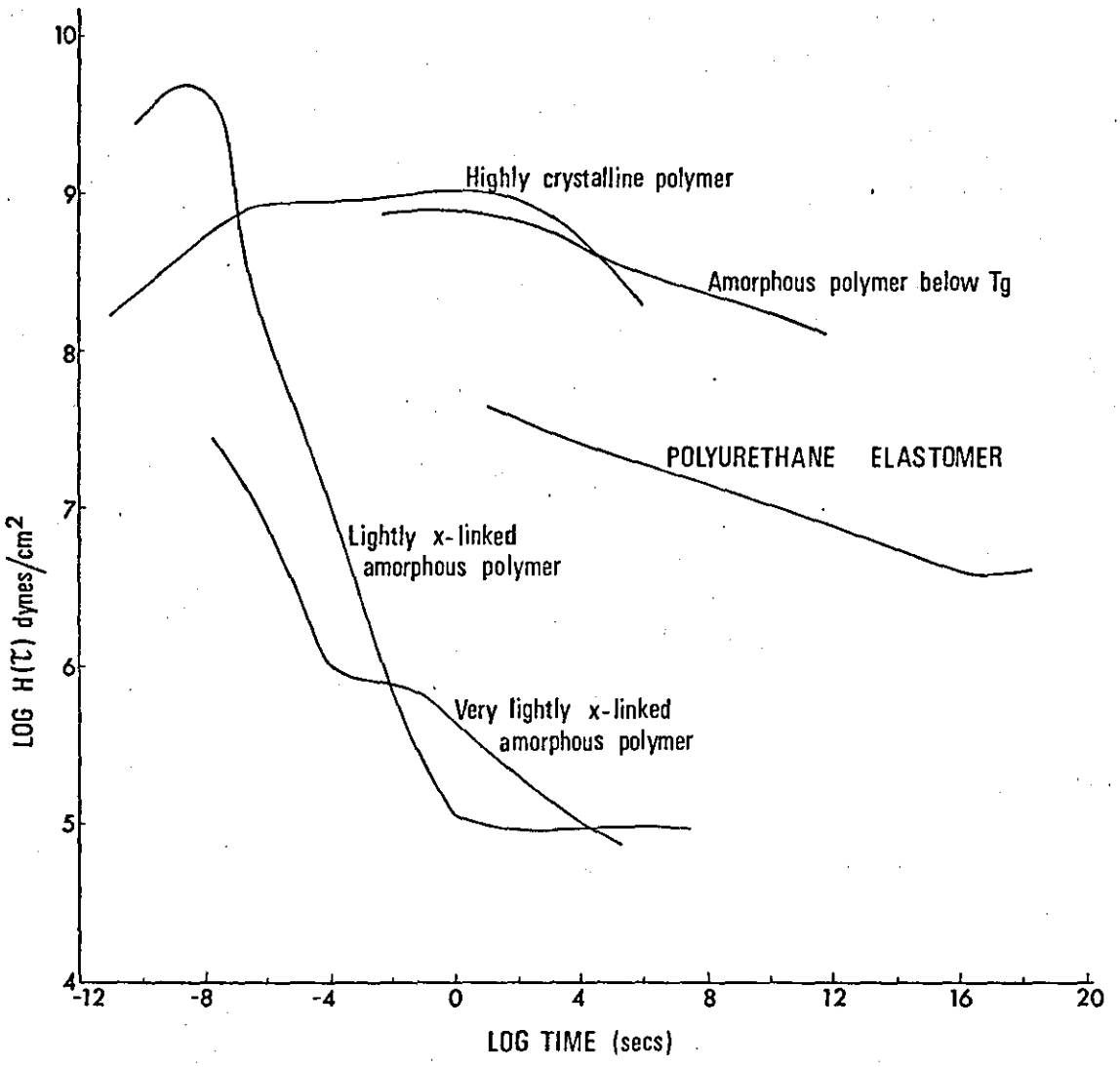

Figure 5.12.

Comparison of relaxation spectrum for elastomeric polyurethanes with spectra for other typical elastomers taken from Ferry[27].

polyurethane to be obtained. This value was measured off the stress-strain curves obtained at every strain rate and temperature for both the solid and cellular polyurethanes. The variation of the logarithm of Young's modulus with temperature for both the solid and foam polyurethane at a strain rate of 10 cm/min. is shown in figure 5.13. Up to about 160°C, the lines through the points for the foam and solid materials are parallel. The constant factor between the lines drawn through the results for the foam and solid materials is 6.1. This value is the same as found between the mechanical properties of the cellular and solid polyurethanes at 21°C in Chapter 4 and is approximately that predicted by the cubical model theory of Gent and Thomas. Figure 5.13. shows that the properties of the cellular polyurethane are dependent on the properties of the corresponding solid material and a similar model can be applied to the difference in Young's modulus even at elevated temperatures up to approximately 160°C. Above 160°C, the values of Young's modulus for the solid polyurethane begin to fall and the parallel behaviour is no longer apparent.

5.6.2. Variation with Strain Rate

Values of strain rate at which Young's modulus was measured were multiplied by the respective shift factor (log a_T) at each temperature from figure 5.6. and a composite mastercurve was drawn of the logarithm of Young's modulus with strain rate as shown in figure 5.14. Over the majority of the time scale considered, the results for the solid polyurethane are parallel to those of the cellular material. The factor between the two lines drawn being 6.1. as found in the constant strain rate graph (figure 5.13.). The data at the higher two temperatures (160°C and 180°C) appear to show a divergence from the parallel behaviour at very low rates (i.e. long times) similar to

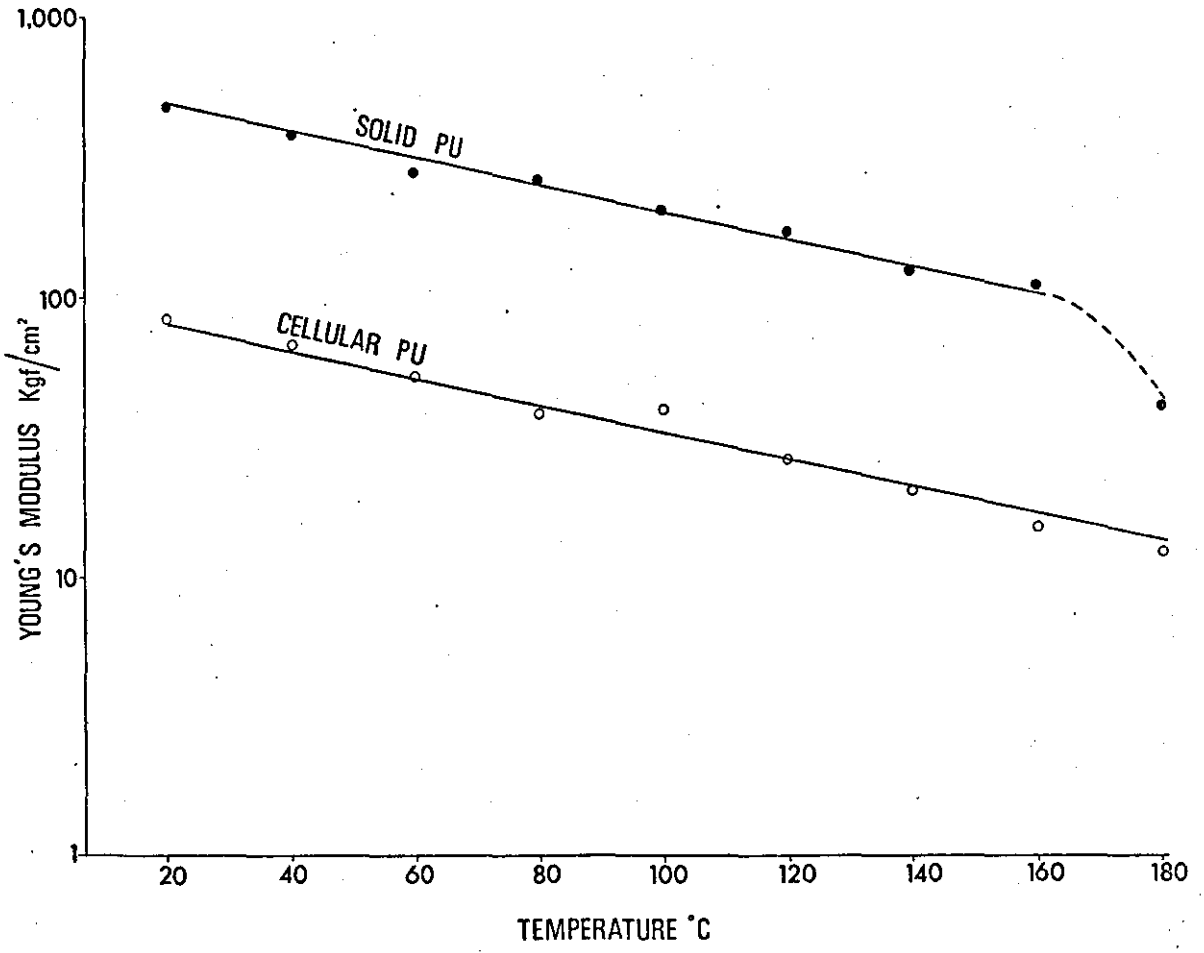

Figure 5.13.

Variation of Young's modulus with temperature for cellular and solid polyurethanes tested at a crosshead speed of 10 cm/min.

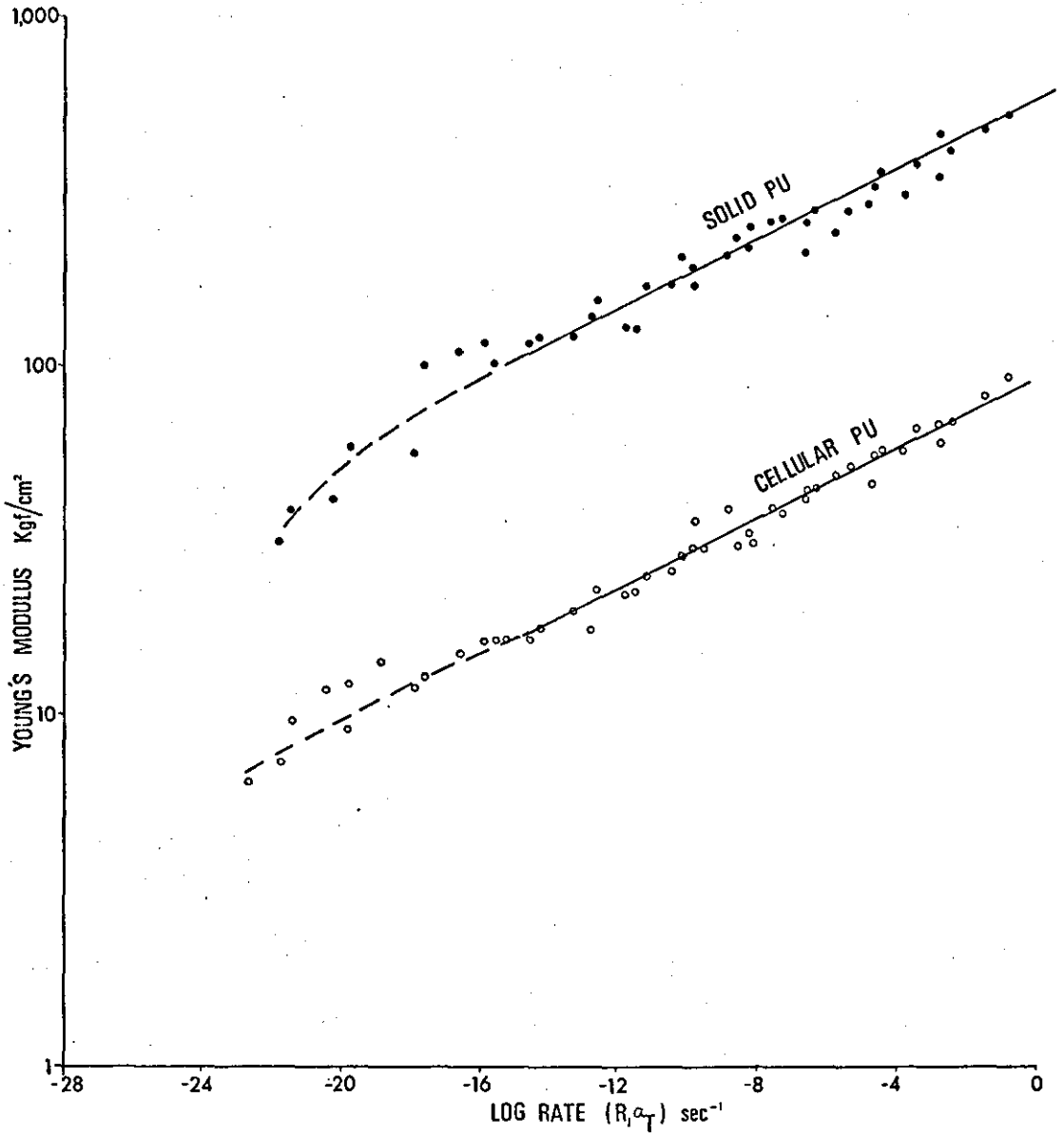

Figure 5.14.

Variation of Young's Modulus with rate of straining mastercurved to 21°C.

that shown on the temperature graph in figure 5.13. In general the data for the solid polyurethane shows more scatter than that for the foam and this is presumably due to the difficulties in obtaining a completely uniform solid sheet of the material. It would appear however that the Gent/Thomas model is applicable to values of Young's modulus for polyurethanes over a large time scale as well as over a range of temperatures.

5.7. TENSILE FAILURE PROPERTIES

5.7.1. Stress and Strain at Break

The variation of tensile stress at break (σ_B) and strain at break (ε_B) for the foam and solid polyurethanes with temperature from 0 to 180°C at a ~~strain~~ jaw separation rate of 10 cm/min. is shown in figure 5.15. The stress at break for both the foam and the solid is fairly high and slowly decreases with temperature until about 160°C when it drops suddenly. The strain at break rises to a maximum at about 100°C but again drops quite markedly above 160°C to a value of 1.40 and 0.42 for the foam and solid respectively at 180°C.

5.7.2. Energy Input to Break

A more useful measure of the strength of a polymer is the toughness or energy input to break as it combines both the contributions due to stress and strain at break. The variation of energy input to break with temperature for both the foam and solid polyurethanes at a ~~strain~~ jaw separation rate of 10 cm/min. is shown in figure 5.16. The energy input to break values for both the foam and solid polyurethanes remain fairly high and parallel up to approximately 160°C when the failure values drop quite markedly. In order to indicate the high strength and temperature stability of the polyurethane used in this investigation, typical results for styrene-butadiene rubber (SBR) with 0 and 30 phr HAF carbon black from earlier investigations[12,13] are also shown for

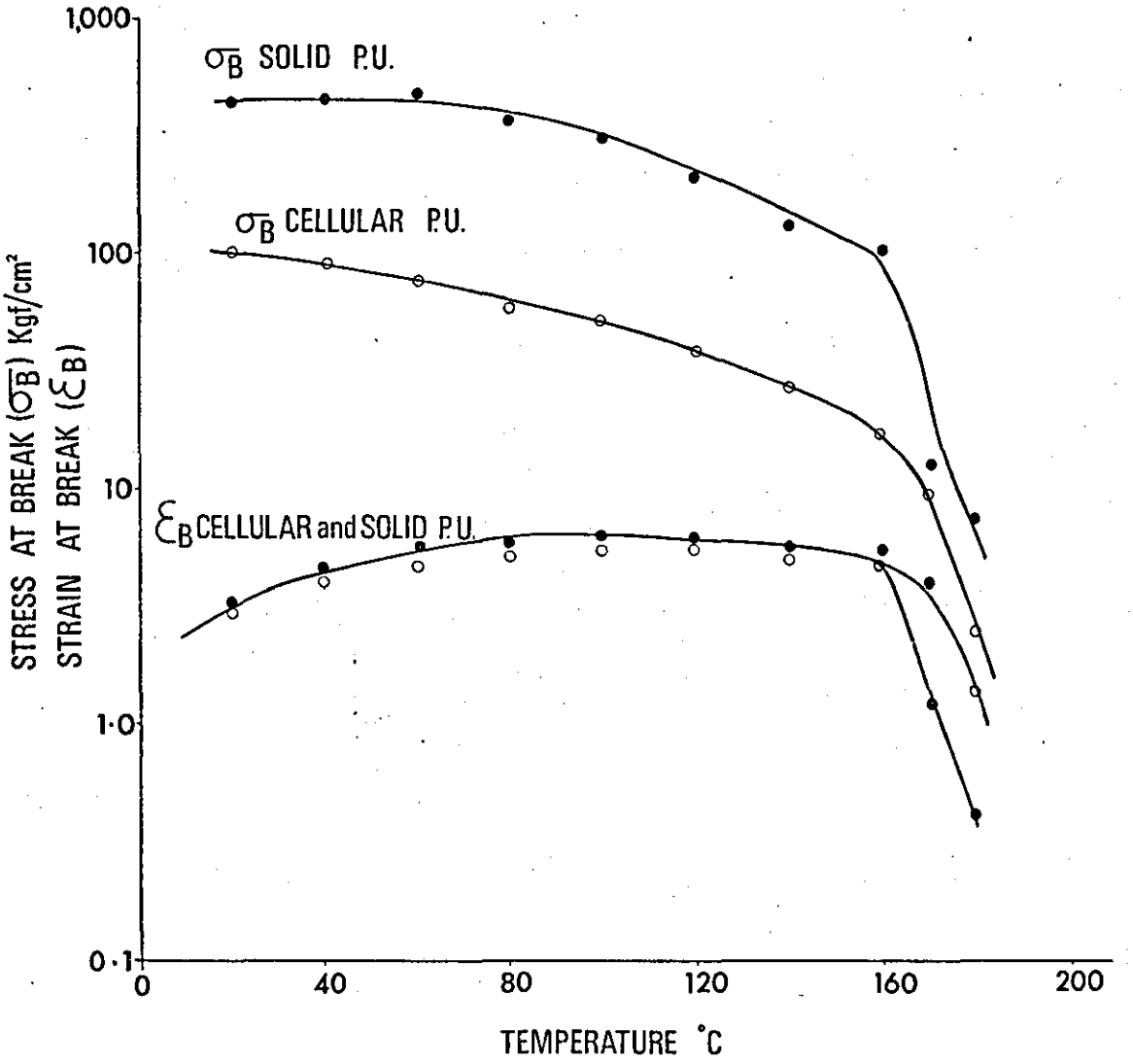

Figure 5.15.

Variation of stress and strain at break with temperature for cellular and solid polyurethane materials.

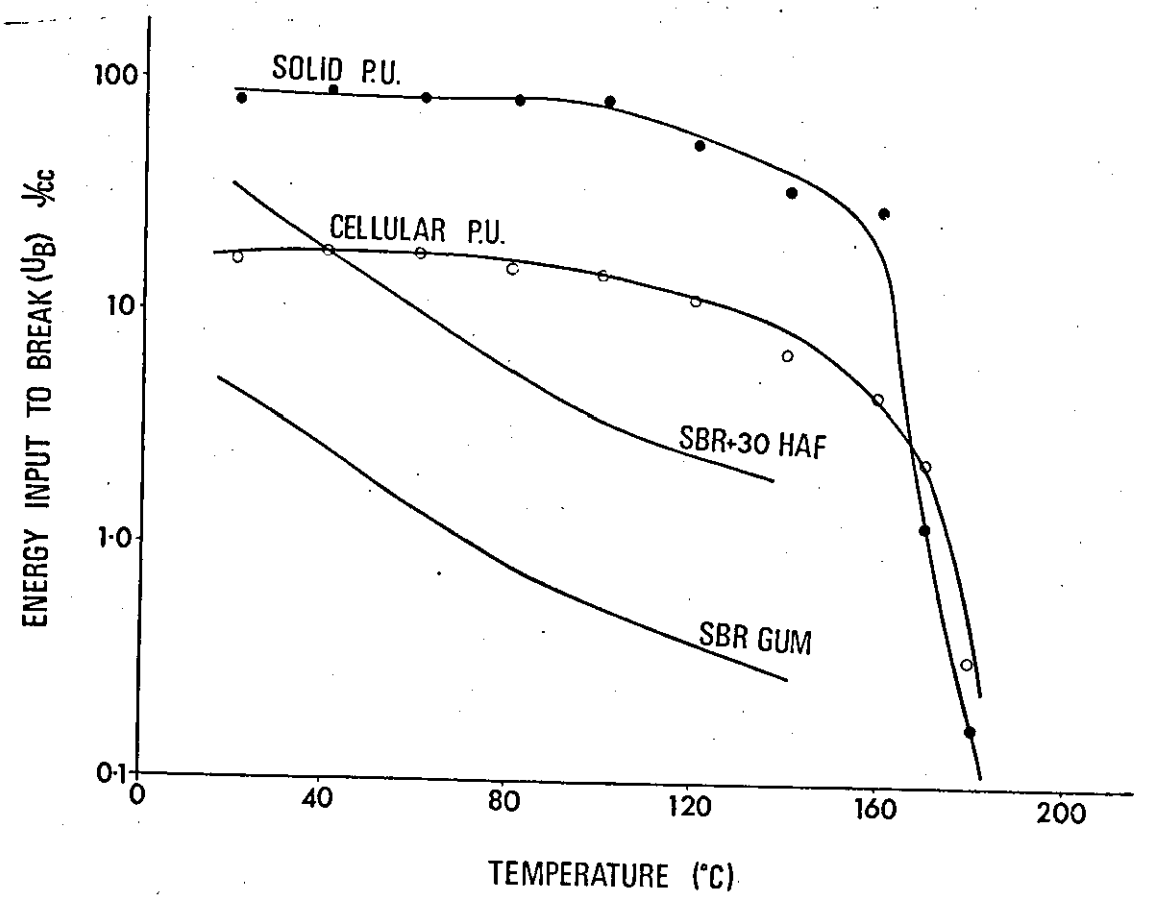

Figure 5.16.

Variation of energy input to break with temperature for cellular and solid polyurethane materials compared with results for filled and unfilled SBR vulcanisates.

comparison in figure 5.16. It is clearly seen that even the polyurethane foam has higher strength properties over the majority of the temperature range considered than the solid reinforced rubber vulcanisate.

To determine whether tensile failure data can be shifted on a time-temperature scale values of energy input to break were plotted against time to break (t_B) for each temperature. The time to break (t_B) was divided by the shift factor (a_T) at each temperature obtained from figure 5.6. and the resulting mastercurve is shown in figure 5.17. It is seen that the data superimposes remarkably well and the parallelism of the foam and solid results up to very long times is still apparent as well as the drop in energy to break at long times (or high temperatures).

5.7.3. Hysteresis at Break

Harwood, Payne and Whittaker[12-14] found for unfilled and filled amorphous vulcanised rubbers that the energy input to break in a stress-strain cycle was related to the hysteresis at break over a temperature range from -40 to 140°C by a $\frac{2}{3}$ power law relationship (equation 3.2.). The experimental results in Chapter 3 however showed that the energy input and hysteresis at and up to failure for a range of poromeric materials both with and without a fibrous base and also natural leather obeyed a 0.88 power law relationship. The variation of energy input with hysteresis for the cellular polyurethane considered in this chapter is shown in figure 5.18. This material was also included in the study reported in Chapter 3. As found in the earlier investigation, the hysteresis values up to and at break fall on a common line. The experimental results for the solid polyurethane also fall on this line. The straight line relationship shown in figure 5.18. for cellular and solid polyurethanes only is given by:

$$U_1 = 1.6\ H_1^{0.90} \qquad 5.16.$$

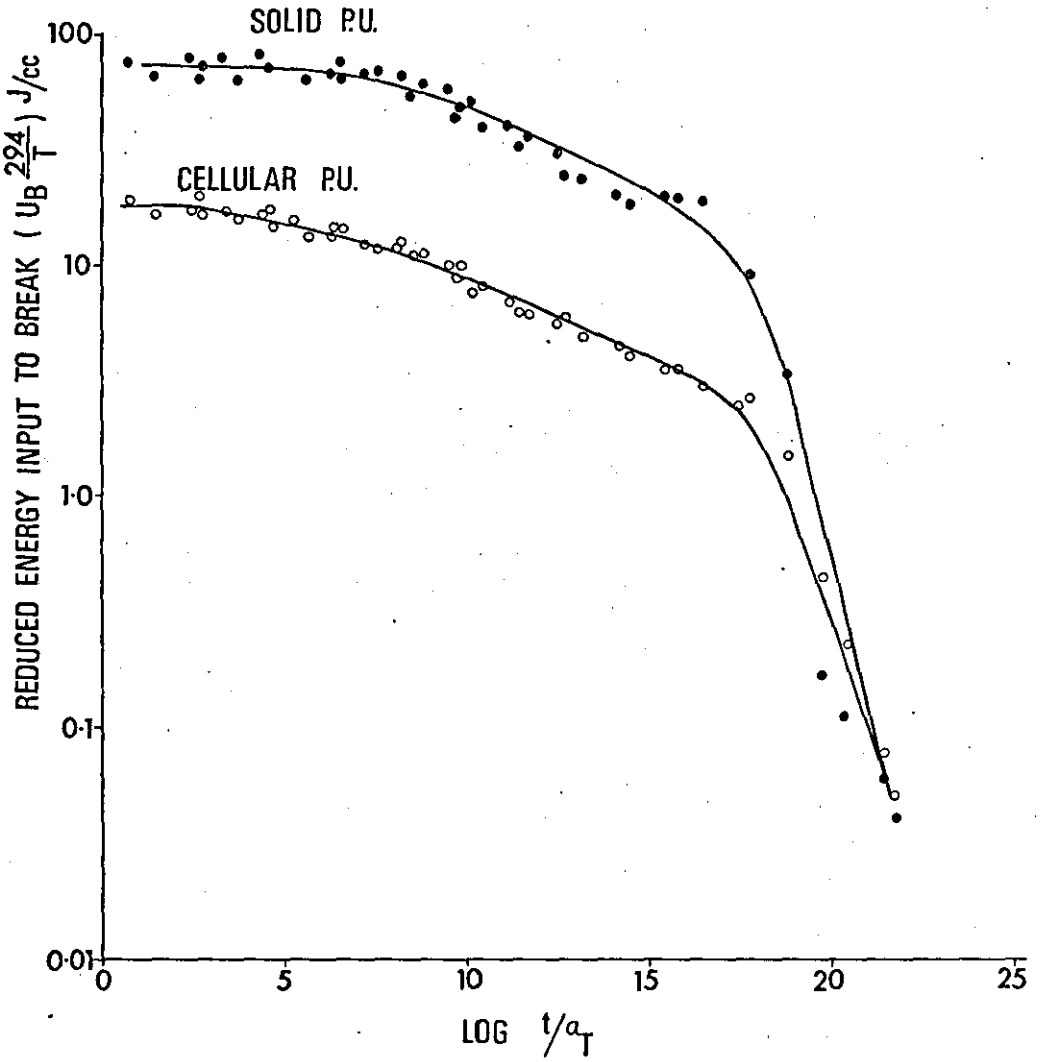

Figure 5.17.

Variation of reduced energy input to break with time to break for cellular and solid polyurethane materials mastercurved to 21°C.

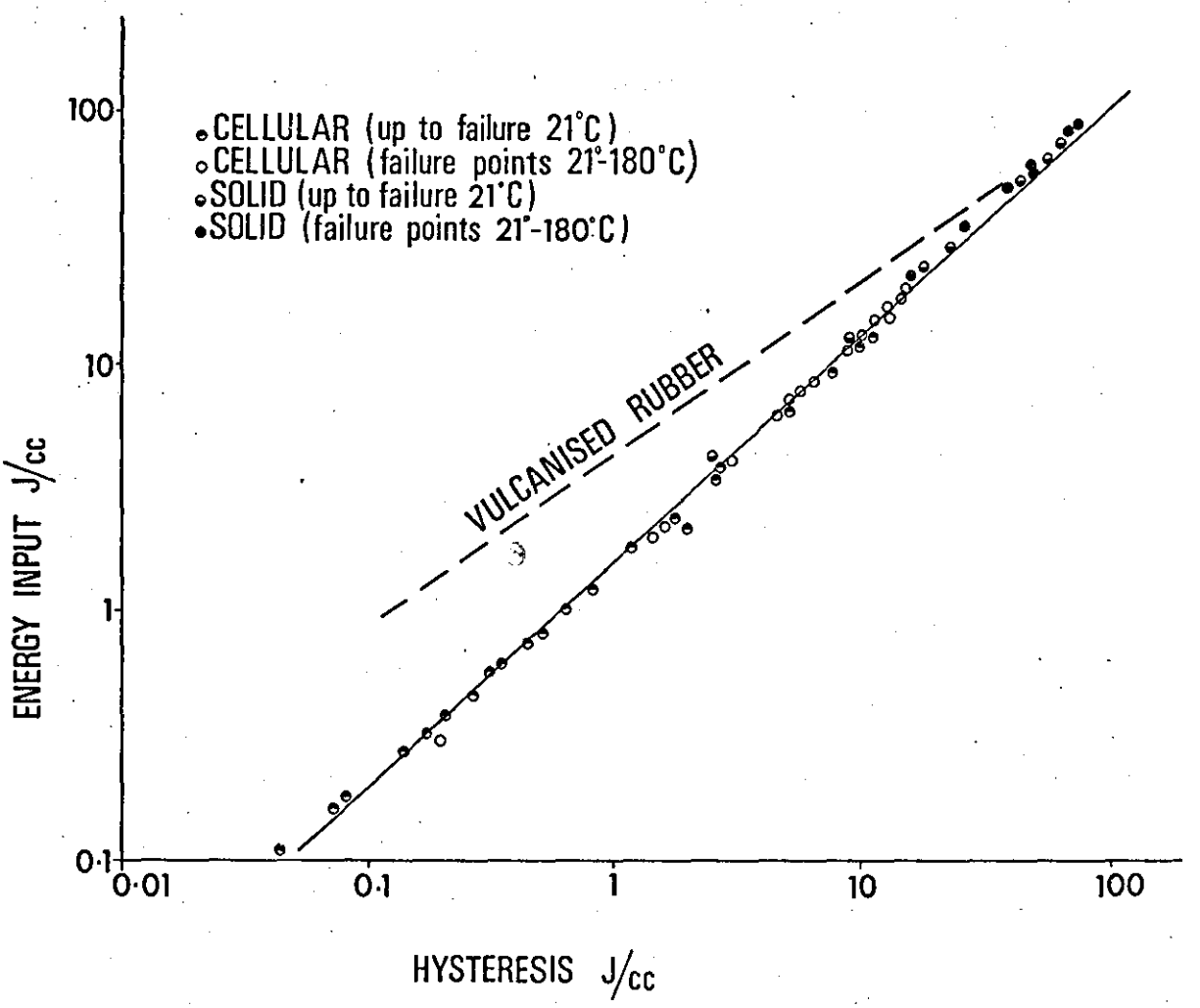

Figure 5.18.

Variation of energy input with hysteresis for cellular and solid polyurethanes both up to and at failure. Line through failure points of typical vulcanised rubber from previous studies[12-14] also shown for comparison.

A typical $\frac{2}{3}$ power relationship between the failure parameters for a vulcanised amorphous rubber (SBR) is dotted on figure 5.18. for comparison.

One of the fibrous poromerics (Corfam) used in the earlier experiments in Chapter 3 had a very thin microporous polyurethane film as the surface layer. Although when tested in total (i.e. polyurethane film + fibrous layers), this poromeric showed similar hysteresial properties to the other poromerics; it was known that the microporous layer was chemically crosslinked and based on a polyether polyurethane whereas the majority of cellular polyurethanes used in poromerics including the one considered in Chapters 4 and 5 are polyester polyurethanes with low crosslink density.

The variation of energy input with hysteresis for the crosslinked polyether polyurethane is shown in figure 5.19. ~~both~~ for values ~~of strain~~ at break and at strains up to rupture. It is seen that the results up to break fall on a different line from those at break. The slope of the line through the failure points is 0.79. It would appear therefore that as the amount of chemical crosslinking is increased, the slope on logarithmic scales of the line between energy input at break and hysteresis at break is decreased. This effect has also been noticed[21] in amorphous vulcanised rubbers such as SBR. The dotted line through the experimental points up to failure on figure 5.19. is the same line as drawn through the points for the polyurethane foam and solid materials shown in figure 5.18.

5.7.4. Strain at Break

Work[12-14] on both amorphous and strain crystallising vulcanised rubbers described in Chapter 2 and the supplementary contribution to the thesis showed that the energy input to break (U_B) is related to the strain at break (ε_B) up to the maximum extensibility of the network

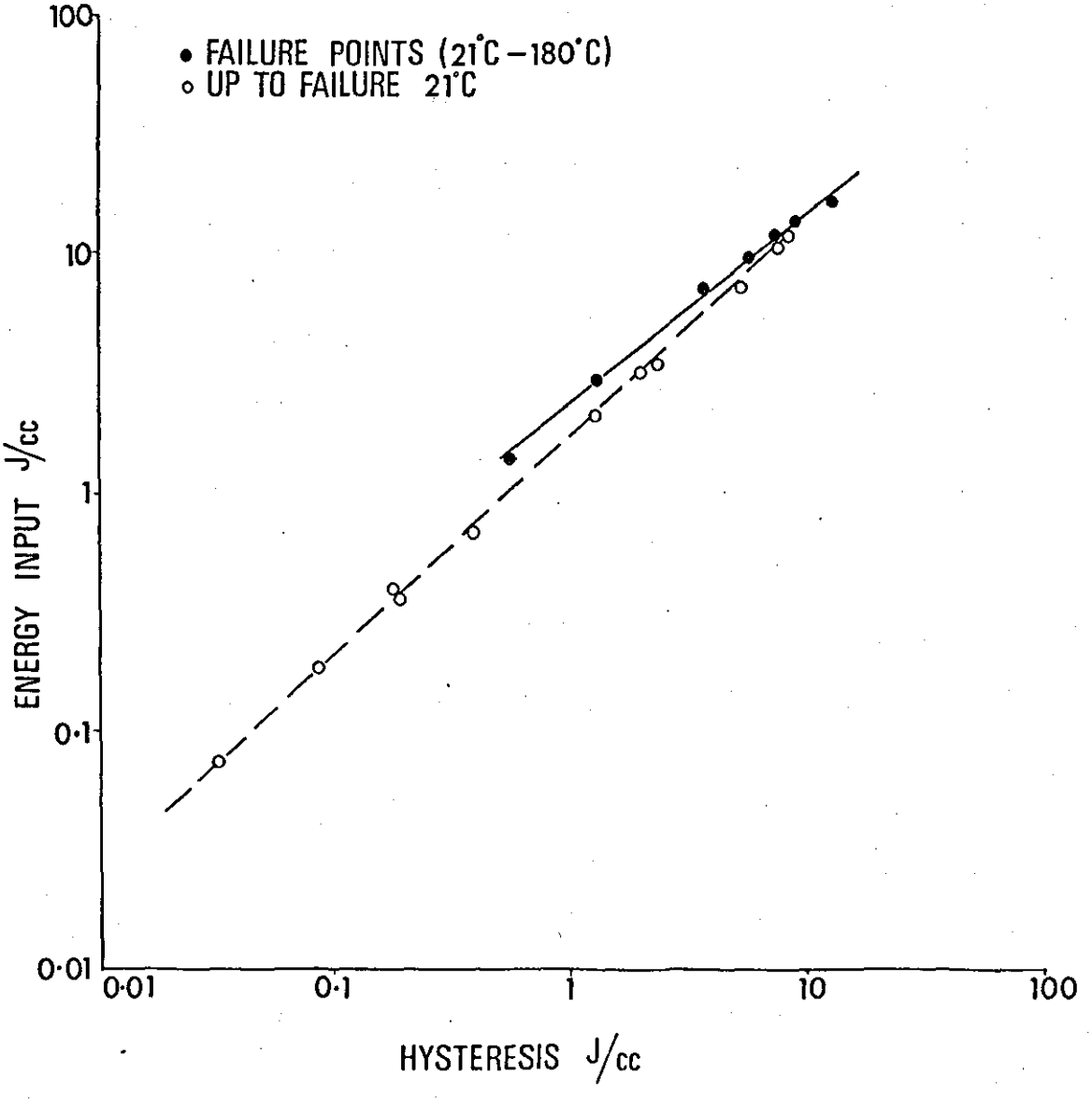

Figure 5.19.

Variation of energy input with hysteresis for crosslinked polyurethane microporous layer of poromeric "Corfam". Results both up to and at failure.

(ε_B max.) by a relationship of the following form

$$U_B \cdot \frac{294}{T} = A\,(\varepsilon_B)^2 \qquad 5.17.$$

The variation of energy input to break with strain at break for the cellular polyurethane is shown on figure 5.20a and for the solid polyurethane in figure 5.20b. The results at temperatures above 160°C are shown by open circles and it is seen that the square law relationship between the two parameters is only obeyed at these high temperatures. As shown in figures 5.15. and 5.16., the strain at break and energy at break values are fairly high except at very high temperatures. The maximum extensibility (ε_B max.) of the cellular polyurethane for example remains at a fairly constant value from 80°C to 160°C as shown in figure 5.15. This is in contrast to a normal vulcanised rubber such as a SBR which has its maximum extensibility at about 0°C.

The effect of crosslinking on the variation of energy input to break with strain at break is shown in figure 5.21a where the experimental results for the crosslinked cellular polyurethane layer of the poromeric 'Corfam' used in the previous section of the chapter are compared with the cellular polyurethane and solid results from figure 5.20. As found in the earlier investigations in Chapter 2 on branched polyurethane rubbers, increased crosslinking or branching results in the strain at break at a particular energy input to break being reduced.

Section 2.5. showed that the strains at break at the same energy input to break for various crosslinked rubbers were in the ratio of their respective $V_e^{\frac{1}{2}}$ values provided that the strains were below the maximum extensibility of the network. V_e is termed the number of network chains per unit volume of the rubber network and is usually expressed in moles/cc. Values for V_e were obtained from the

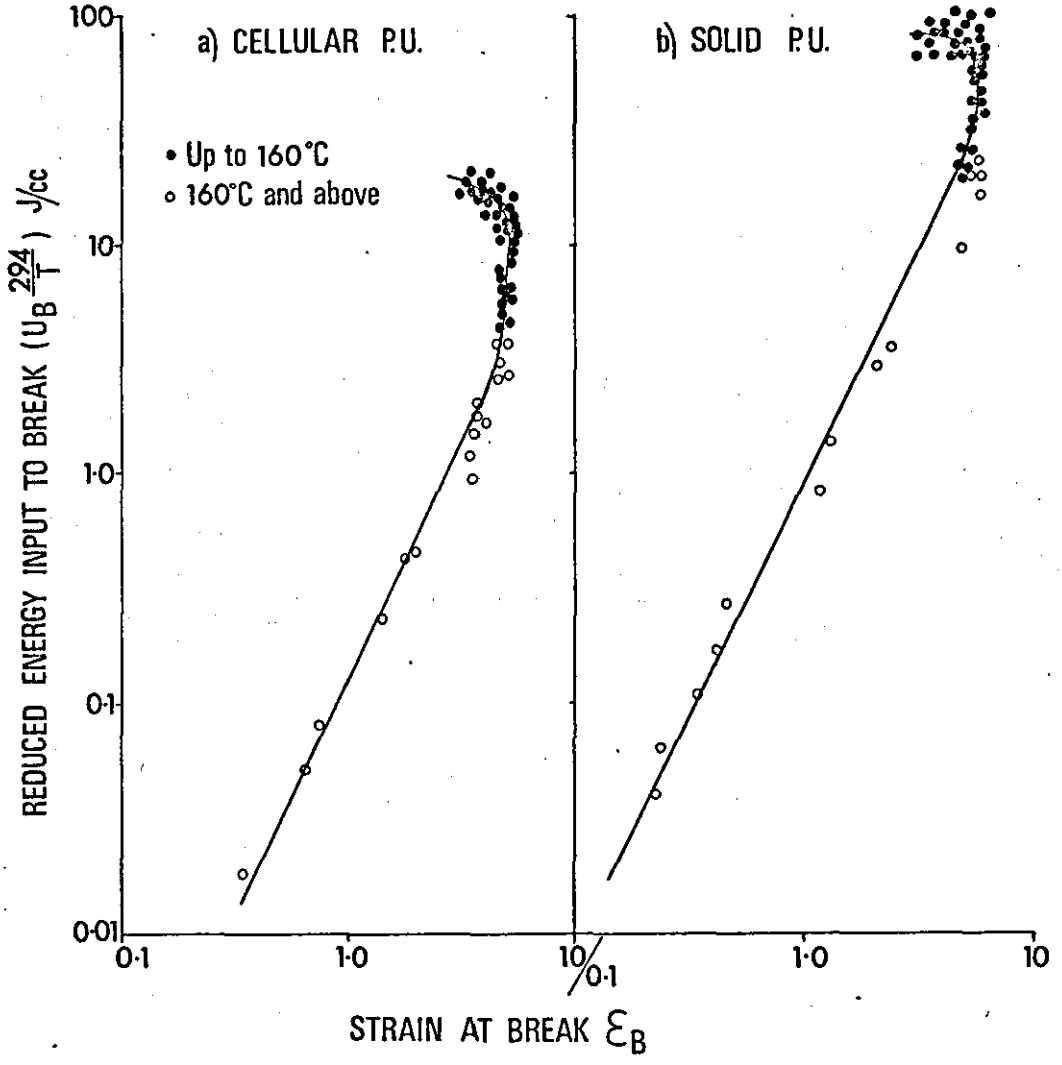

Figure 5.20.

Variation of reduced energy input to break with strain at break for (a) cellular polyurethane (b) solid polyurethane.

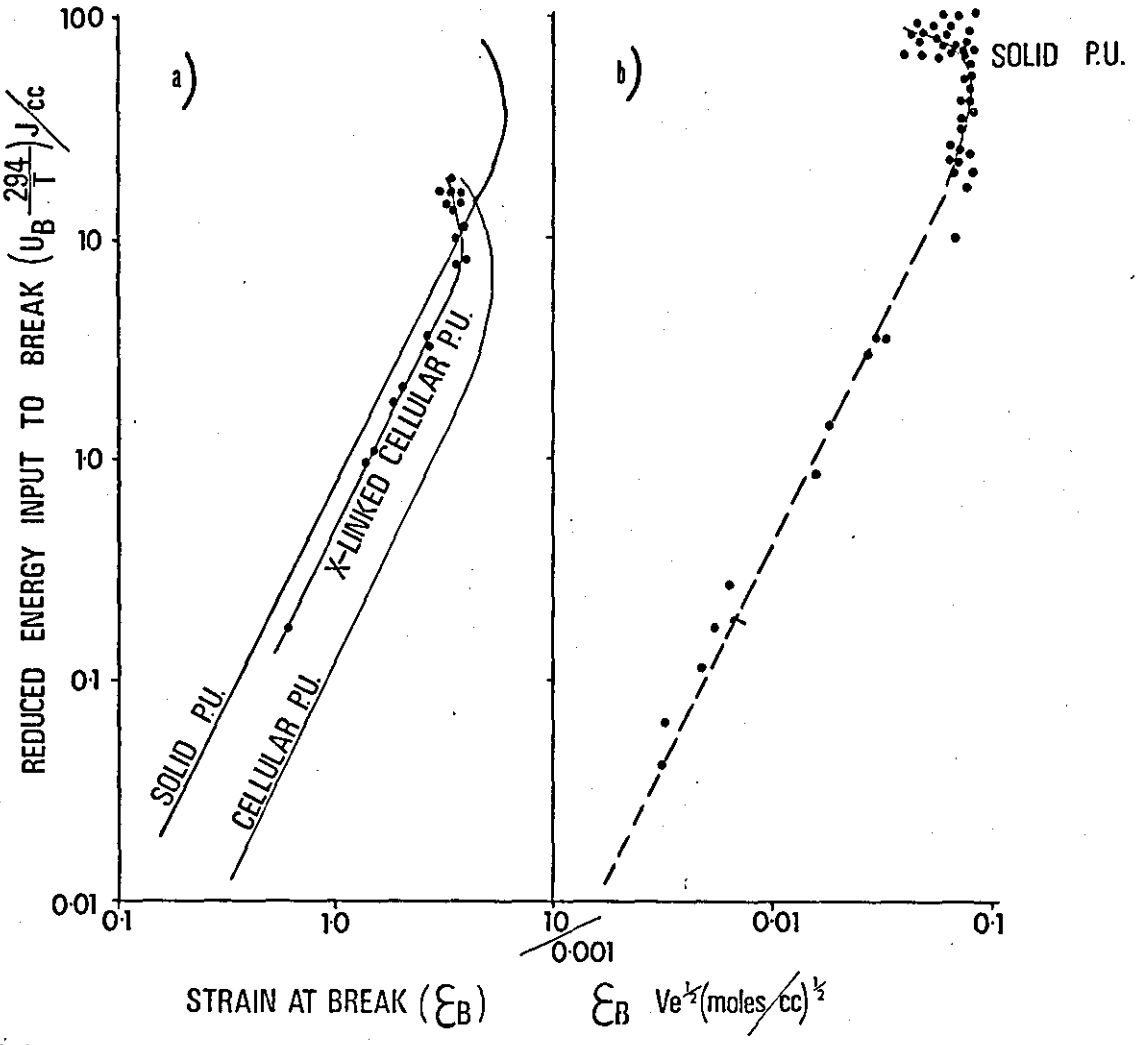

Figure 5.21.

Variation of reduced energy input to break with strain at break.

(a) Results from Figure 5.20. compared with crosslinked cellular polyurethane.

(b) Strain at break for solid polyurethane multiplied by $V_e^{\frac{1}{2}}$. Line drawn through results is the same as found for solid rubbers in Chapter 2. (Figure 2.6.).

equilibrium modulus E_e by the following relationship (equ. 2.4.).

$$E_e = 3\ V_e\ RT \qquad 5.18.$$

where R is the gas constant.

A value of equilibrium modulus (E_e) for the solid polyurethane was obtained from the limiting value of the relaxation modulus - time curve shown in figure 5.8. This value was 20 kgf/cm^2 and occurred at a temperature of about 180°C. By using equation 5.18., the value of $V_e^{\frac{1}{2}}$ was found to be 1.33×10^{-2} (moles/cc)$^{\frac{1}{2}}$.

The strains at break for the solid polyurethane shown in figure 5.21a were multiplied by this value of $V_e^{\frac{1}{2}}$ and the results are plotted in figure 5.21b. The line plotted through the points on figure 5.21b is the line for the combined results of SBR, NR and branched polyurethane elastomers from Chapter 2 (figure 2.6.) which appears to be a good approximation to the results for the solid polyurethane used in this investigation.

The equation to the line shown in figure 5.21b is given by

$$U_B \left(\frac{294}{T}\right) = (4.1 \times 10^3)\ V_e\ \varepsilon_B^2 \qquad 5.19.$$

if U_B is expressed in joules/cc. This equation therefore which was previously found applicable to branched, crystalline and amorphous polymers at various degrees of crosslinking (Chapter 2) now appears to be applicable to the type of polyurethanes used in poromeric materials. These latter materials therefore despite their very high strength and other special features appear to obey similar laws to normal rubberlike materials.

5.8. STRESS SOFTENING

The results presented in Chapter 3 showed that stress softening occurred in both natural and artificial leather materials. This is illustrated further in figure 5.22. where the cellular polyurethane,

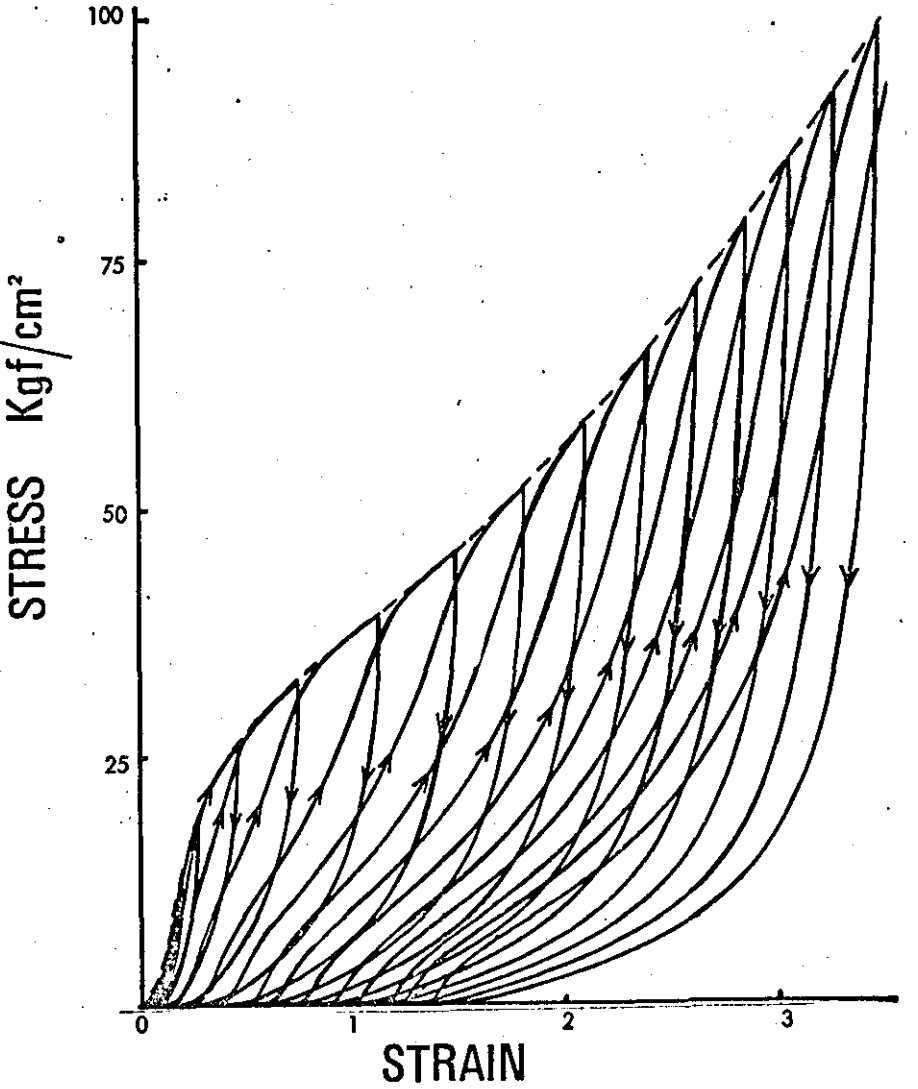

Figure 5.22.

Stress softening in the cellular polyurethane material. Dotted line shows uncycled stress-strain curve.

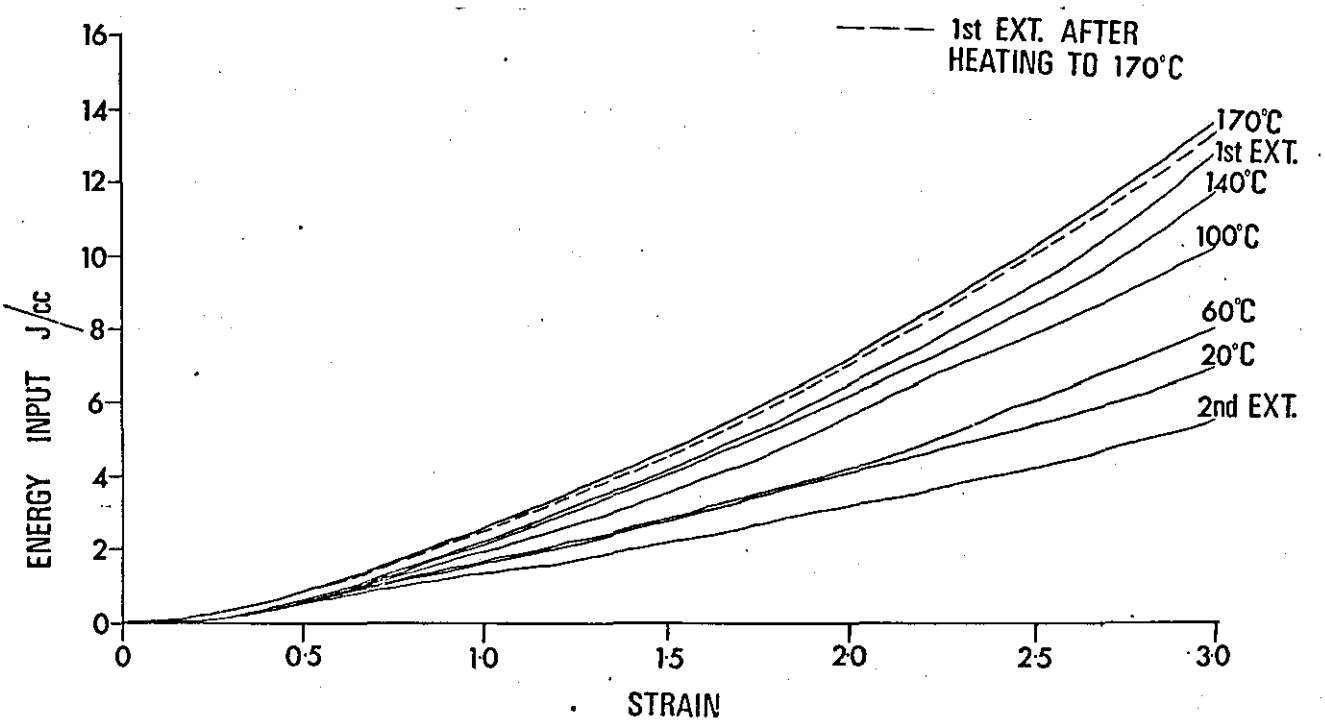

Figure 5.23.

Variation of energy input with strain for cellular polyurethane both before and after recovery of stress softening at a number of temperatures.

used in the earlier sections of this chapter, has been repeatedly cycled. Each stress-strain cycle has been taken to a higher maximum stress than the previous cycle. In all cases lower stress values are obtained at the same strain on the second extension curve than on the initial curve provided that the extension was lower than that previously applied. At strain levels higher on the second extension curve than that applied on the initial curve, the stress-strain curve was unaffected by prestraining and followed the normal (uncycled) stress-strain curve for the material which is shown by the dotted line in figure 5.22. This behaviour is very similar to that observed in an amorphous vulcanised rubber[12-14]. The earlier work on stress softening[17,87] in vulcanised rubbers which crystallise on extension such as natural rubber showed that although the rubber could be cycled in a similar manner, the second extension curve when taken past the reversal point on the initial stress-strain curve did not coincide with the uncycled curve.

The earlier sections of this chapter have shown that polyurethane retains a high strength up to about 160°C. Above this temperature the strength drops quite markedly. In order to investigate this change in properties more thoroughly and to understand the mechanism which resulted in stress softening, some experiments were undertaken where the polyurethane foam was allowed to recover at various temperatures after stress softening. Several stress-strain curves were obtained at every 50% extension up to 300% where the second extension curve was taken up to the same initial strain as on the first extension curve. Each group of samples (taken to strains from 50 to 300%) were then left at a number of temperatures up to 170°C overnight (16 hours) and then recycled to the same initial extension. Energy under the initial first and second extension curves and recovered stress-strain curve

was measured and figure 5.23. shows the variation of energy input with strain both before and after recovery at a number of recovery temperatures. Leaving the samples overnight at the testing temperature (20°C) shows only a small amount of recovery of stress softening. The amount of recovery increases as the overnight recovery temperature is increased. Even at 140°C, the stress softening is not completely recovered. At 170°C however, the stress softening is over recovered. This temperature is above the temperature at which the sharp change in mechanical properties noted in the earlier sections of this chapter occurs.

This anomalous behaviour when the polyurethane samples were heated to 170°C suggested that some stress was already put in the material during manufacture and as a check on this phenomenon, some unstressed samples of the cellular polyurethane were heated up to 170°C and then cycled to various strains. It was found that the material appeared to be stiffer after this treatment and as shown by the dotted line in figure 5.23., the results were almost identical with those samples which had been prestrained and allowed to recover at 170°C. It was concluded therefore that the over-recovery noted with the cellular polyurethane is due to inherent stresses put into the material during manufacture.

5.9. CONCLUSIONS

The two methods used by Smith to determine the relaxation spectrum of SBR and polyisobutylene from tensile stress-strain data have been shown to yield the same result and provide a satisfactory method for determining the relaxation spectrum for polyurethane elastomers. The time - temperature shift factors have been found to be higher than those predicted by the WLF equation. The relaxation spectrum for

polyurethane is a very flat plateau which extends for over 18 decades of time. The shape of the spectrum resembles that of an amorphous polymer below its glass transition temperature and is only slightly less in magnitude. The polyurethane however is still flexible and above its major glass transition temperature which occurs at about -30°C.

The cubical model relationship between the foam and solid polyurethanes described in Chapter 4 has been found to be applicable to values of Young's modulus at very high temperatures or long times. The high strength of polyurethane is shown to be reasonably temperature independent until about 160°C, when it drops quite markedly which indicates some structural change in the material. This particular feature is discussed further in Chapter 7.

Due to their essential linear or non-chemically crosslinked structure, polyurethane elastomers used in poromerics are highly hysteresial in character and their properties apart from strength resemble those of a very low crosslinked vulcanised rubber. The normal square law relationship for vulcanised rubbers between energy input to break and strain at break is obeyed by these polyurethane elastomers only at very high temperatures (above 160°C) when the sharp drop in strength occurs. By obtaining a value for equilibrium modulus, it is possible to correlate measurements on this graph with the general relationship applicable to crystalline, branched amorphous and filled vulcanised rubbers at various degrees of crosslinking described in Chapter 2.

Stress softening is also not completely recovered in these polyurethanes until the temperature is raised to about 170°C (i.e. above the point where the large drop in mechanical properties occurs).

CHAPTER 6

CUT GROWTH AND FATIGUE PROPERTIES

6.1. INTRODUCTION

The earlier chapters of this thesis have described differences in the tensile properties of polyurethanes compared with vulcanised rubbers. One of the most important properties of cellular polyurethanes for their use in the footwear industry is that they have a high resistance to cut growth. It is therefore important to consider this particular property separately and compare the cut growth resistance of polyurethane with vulcanised rubbers.

A number of investigations have been undertaken in recent years into the cut growth and fatigue properties of vulcanised rubbers. Most of the investigators have expressed these properties in terms of a parameter termed tearing energy (T). This approach has been used in determining the cut growth and fatigue properties of polyurethane and is described in this chapter.

6.2. TEARING ENERGY THEORY

6.2.1. Introduction

Cut growth in polymers, like that in metals, begins at individual points or flaws where the stress is locally very high[88-90]. The determination of the magnitude of the stresses at and around the tip of a flaw in a piece of highly strained rubber is a complex problem. It has been shown, however, for vulcanised rubbers that the consequence of this high stress concentration can be assessed by use of a simpler parameter known as Tearing Energy (T).

The concept of "Tearing Energy" for polymeric materials was originally developed to describe the tear behaviour of rubber by Rivlin and Thomas[61] and is an extension of the classical theory for the strength properties of glass developed by Griffiths[62] in 1920. The theory was briefly discussed in Chapter 4 when it was used to express the tear properties of cellular polyurethanes.

Tearing energy (T) is defined, for a strained test piece containing a crack as:

$$T = -\left(\frac{\partial U}{\partial A}\right)_e \qquad 6.1.$$

where U is the total elastically stored energy in the test piece and A is the area of the two sides of the cut surface. The derivative must be taken under conditions that the applied forces do not move and hence do no work. The suffix e denotes that the differentiation is carried out at constant deformation. It thus represents the rate of release of strain energy as the crack propagates and can, therefore, be considered as the energy available to drive the crack through the material. It has been found that if tear or crack growth measurements are expressed in terms of T, the results obtained from test pieces of different shapes can be correlated[64].

The dependence of T on flaw size, applied force or deformation can be deduced for various types of test piece. For example the tearing energy[61] for the 'trouser' tear test piece shown in Figure 6.1(a). is approximately given by:

$$T = \frac{2F}{h} \qquad 6.2.$$

where F is the applied force and h is the test piece thickness.

For a test piece in the form of a strip with a small cut of length 'C' in one edge, deformed in simple extension, as shown in Figure 6.1(b)., the tearing energy is given by:

$$T = 2KUC \qquad 6.3.$$

where U is the strain energy density in the bulk of the test piece (i.e. away from the cut) and K is a slowly varying function of strain which has been determined empirically[65] for strains up to 200%. Values of K are shown in Table 6.1.

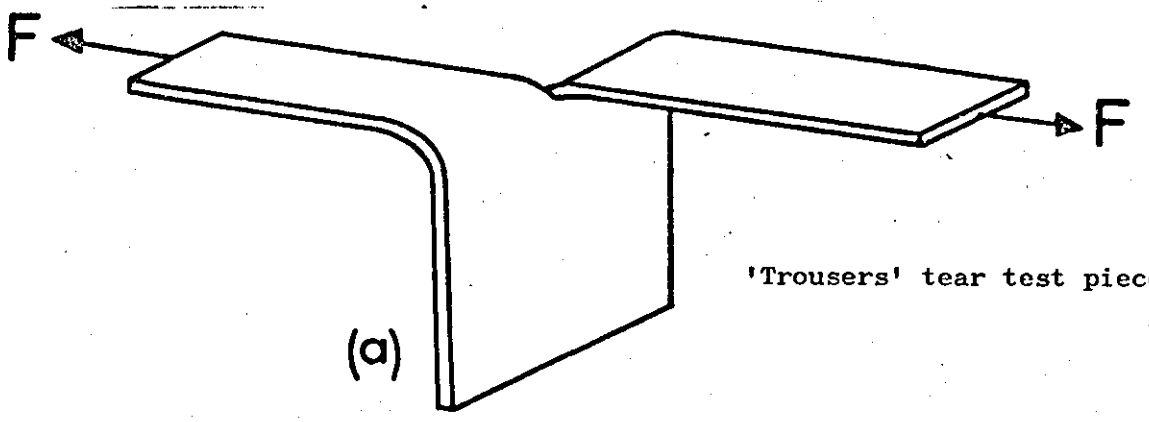

'Trousers' tear test piece

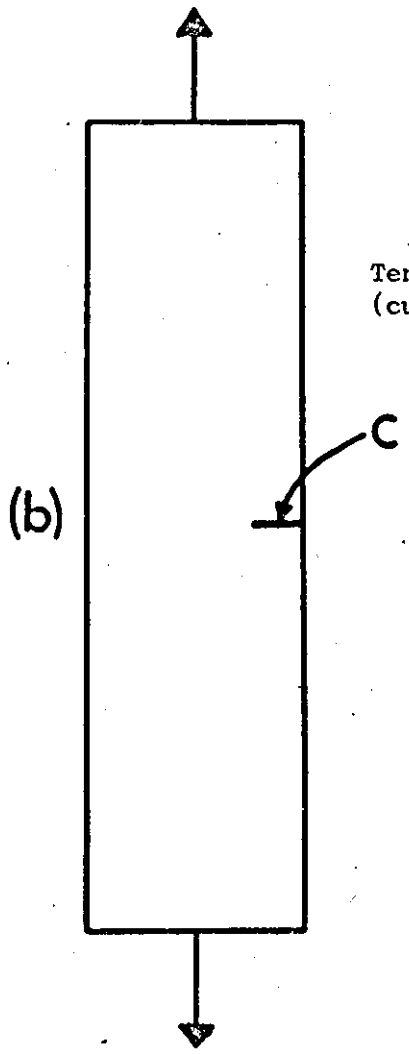

Tensile strip
(cut growth test piece)

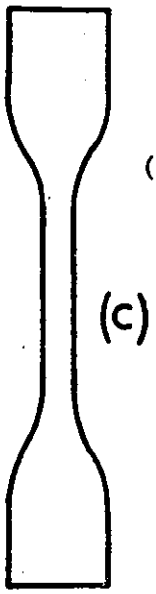

Dumb-bell
(fatigue test piece)

Figure 6.1.

Cut growth and fatigue test pieces.

This latter type of sample was used for the cut growth results described in this chapter. It has the advantage that the stress-concentrating effects of both flaw size and deformation (which govern K and U) are expressed in terms of the single parameter T.

TABLE 6.1.

VALUES OF PARAMETER K (AFTER GREENSMITH[65])

Strain	K
0	π
0.10	2.85
0.20	2.66
0.40	2.43
0.60	2.27
0.80	2.15
1.00	2.05
1.50	1.85
2.00	1.67
> 2.00	1.67

The tearing energy theory has been successfully applied to tear[91], cut growth, fatigue[88-90] and to a limited extent to tensile failure[92] of conventional vulcanised rubbers.

6.2.2. Application to Cut Growth

It has been found for vulcanised rubbers that when the tearing energy exceeds a minimum value denoted by T_o, the amount of cut growth per cycle $\left(\frac{dc}{dn}\right)$ for a tensile test piece[88-90] containing an edge crack (Figure 6.1(b).) in repeated extension test at a particular frequency depends on the maximum value of T attained in each cycle and can be expressed by an equation of the following form

$$\frac{dc}{dn} = \frac{T^m}{G} \qquad 6.4.$$

where G is a constant. This is illustrated for a number of rubbers in

Figure 6.2. The actual value of the power m is unfortunately dependent on the type of polymer[89]; for natural rubber, m = 2; for a range of synthetic rubbers (e.g. butyl, polychloroprene, polybutadiene), m = 3; and for styrene-butadiene copolymer rubber, m = 4. This type of equation has also only been shown to hold for measurements carried out at room temperature (approximately 21°C). It has been shown[88-90] that a minimum value of tearing energy (T_o) exists below which there is no mechanical cut growth, and hence this defines a fatigue limit for repeated stressing below which the life can be indefinite in the absence of any chemical effects.

6.2.3. Application to Fatigue Properties

Failure of rubber test pieces containing no artificially inserted cracks can be deduced from the cut growth behaviour[89] by assuming that naturally occurring flaws of length C_o are present in the rubber. In the case of a cellular material, C_o would be expected to be in the same order as the largest pore size.

It is possible to eliminate from equations (6.3.) and (6.4.), the parameter T and hence form the differential equation:

$$G \frac{dc}{dn} = T^m = (2KU)^m C^m \qquad 6.5.$$

The differential equation can be solved to give the number of cycles n to increase the crack from C_o to C_1.

$$n = \frac{G}{(m-1)\ (2KU)^m} \left(\frac{1}{C_o^{m-1}} - \frac{1}{C_1^{m-1}} \right) \qquad 6.6.$$

When failure occurs the final crack length will be much greater than the initial flaw size (C_o) and hence the number of cycles to failure N (e) is given by

$$N(e) = \frac{G}{(m-1)\ (2KU)^m} \frac{1}{C_o^{m-1}} \qquad 6.7.$$

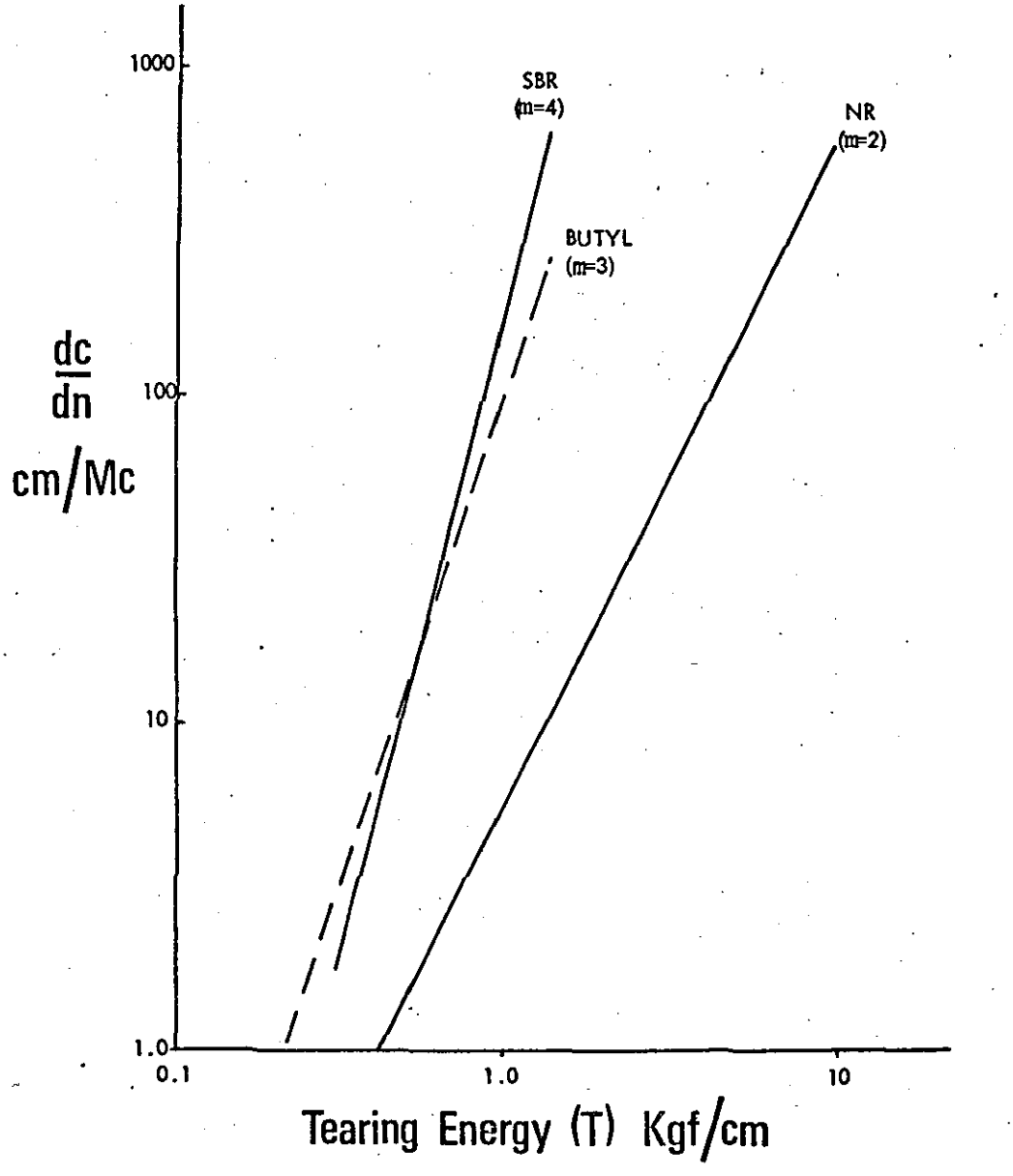

Figure 6.2.

Variation of rate of cut growth per cycle with Tearing energy for a number of vulcanised rubbers. (After Lake and Lindley[88-90])

Equation 6.7. expresses the fatigue life N (e) of a rubber when subjected to continuous cycling at constant temperature but at varying strains (e) in terms of the cut growth constant G, initial flaw size C_o and maximum strain energy U in a cycle which can be derived from the maximum strain. Good agreement has been found[88] between the predicted fatigue life from equation 6.7. and experimental data provided that the correct value of m for each particular polymer considered is substituted in the equations.

6.3. INTER-RELATION BETWEEN FATIGUE AND STRENGTH/HYSTERESIS THEORY

Before discussing the cut growth and fatigue properties of cellular polyurethanes, the author has attempted to correlate the energy input to break/hysteresis at break failure relationship for vulcanised rubbers, discussed in sections 3.4.1. and 5.7.3. with the cut growth and fatigue theory discussed in the previous section. Up to the present these two approaches to the failure of rubber have been considered separately.

Recent work[93] has also shown that if fatigue tests are carried out on synthetic rubbers at a fixed strain/amplitude but over a variable temperature range, then the fatigue life is dependent on the amount of hysteresis exhibited by the rubber at that strain/amplitude. For SBR at 175% extension and over a temperature range of $-40^{o}C$ to $+80^{o}C$ and over a frequency range 0.008 Hz to 8Hz, the fatigue life N(t) can be expressed as

$$N(t) = \frac{h^{p}}{A} \qquad 6.8.$$

where h is the hysteresis ratio raised to the power p, which was found approximately to be 6, and A is a constant.

If it is assumed that the total fatigue life N over a variable temperature and strain range can be expressed as

$$N = N(e)\ N(t) \qquad 6.9.$$

then by combining equations (6.7.), (6.8.) and (6.9.) the following relationship

can be derived

$$N = \frac{G}{(m-1)\ (2KU)^m} \quad \frac{1}{C_o^{m-1}} \quad \frac{h^p}{A} \qquad 6.10.$$

If $p = 6$ and $m = 3$ which is normally the case for amorphous polymers and $N = 1$ which is the case for a normal tensile test

$$U = \left(\frac{G}{2\ (2K)^3\ A\ C_o^2} \right)^{\frac{1}{3}} h^2 \qquad 6.11.$$

This equation can then be directly compared with the hysteresis at break failure criterion for vulcanised rubbers which when expressed in terms of hysteresis ratio at break (h_B) is given by

$$U_B = K_1^3 \quad h_B^2 \qquad 6.12.$$

if the small temperature correction factor is omitted.

The constant K_1^3 in equation 6.12. is therefore identified with constants derived from the fatigue failure equations:

$$K_1^3 = \left(\frac{G}{2(2K)^3\ A\ C_o^2} \right)^{\frac{1}{3}} \qquad 6.13.$$

If it is assumed that the parameter A remains constant for a number of amorphous polymers, then for rubbers where $m = 3$, K_1^3 is proportional to $(G/C_o^2)^{\frac{1}{3}}$. Values of K_1^3 from the data of Harwood and Payne[44] and values of C_o and G from the data of Lake and Lindley[89,95] are shown in Table 6.2.

The variation of K_1^3 with G/C_o^2 is shown in Figure 6.3. for the rubbers listed in Table 6.2. with the exception of NR which crystallizes strongly on extension and does not obey either equation 6.11. or 6.12. A line of slope $\frac{1}{3}$ predicted by equation 6.13. is shown in Figure 6.3. to be a reasonable approximation to the results. Apart from experimental error, the difference between the experimental points and the $\frac{1}{3}$ power law ~~can~~ may be ~~explained by~~ due to (a) the slightly different mixed compounds used by Harwood and Payne and Lake and Lindley, (b) the likely variation in the constant A between different polymers; (c) for some rubbers, $m = 3$ is only an approximation, and for SBR

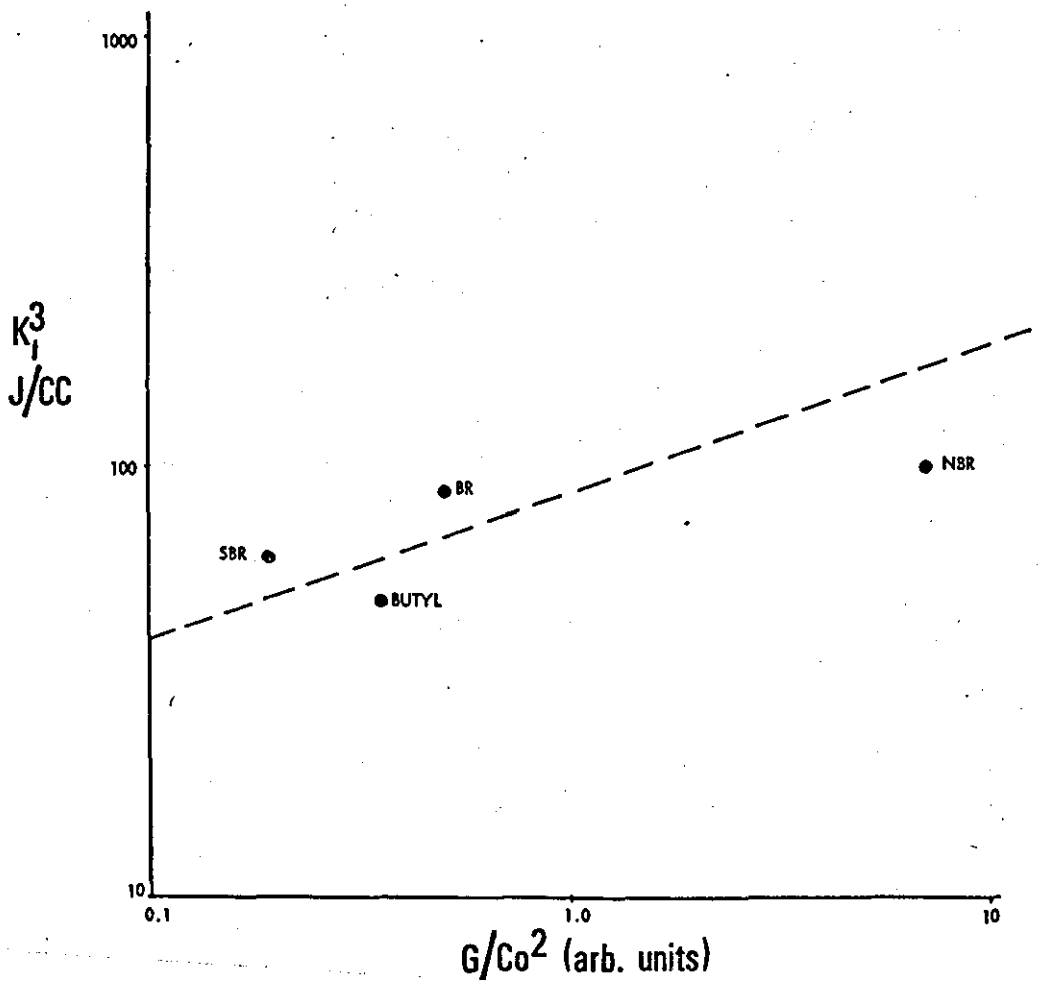

Figure 6.3.

Relationship between K_1^3 from equation 6.12. and G/C_o^2 from equation 6.11. Dotted line of slope $\frac{1}{3}$ predicted by equation 6.13. is also shown. Actual values are shown in Table 6.2.

in particular, a value of m = 4 in equation 6.11. should be used. The hysteresis failure criterion, equation 6.12. however is obeyed for SBR as well as for all other amorphous rubbers and also to a limiting extent for a strain-crystallising rubber such as natural rubber; and this possibly indicates the usefulness of the equation compared with fatigue equations which vary considerably between the different polymers.

TABLE 6.2.

COMPARISON OF TENSILE AND FATIGUE FAILURE PARAMETERS

Rubber	K_1^3 J.cm^{-3} (Ref. 94)	C_o cm X 10^3 (Ref. 95)	G arb. units (Ref. 89)	G/C_o^2, arb. units
Butyl	49	5	0.091	0.036
SBR	61	5.5	0.056	0.019
BR	88	2.5 *	0.031	0.050
NBR	97	4	1.100	0.690
NR	124	2.5	2.200	3.500

* Assumed same as NR as shows evidence of strain crystallisation on extension.

6.4. CUT GROWTH OF CELLULAR POLYURETHANES

6.4.1. Experimental

The cut growth experiments were carried out on tensile strips (shown in Figure 6.1(b).) of approximate dimensions 15 cm x 2.5 cm and about 2 mm thick. A cut about 0.5 mm long was made in the centre of one edge of the sample by use of a razor blade and the test piece was then clamped into position on a repeated extension machine and extended to a suitable strain and cycled.

The repeated extension machine which was designed for the project is shown in the photograph in Figure 6.4. The machine consists of twelve testing stations arranged six on either side of a central bar. The clamps

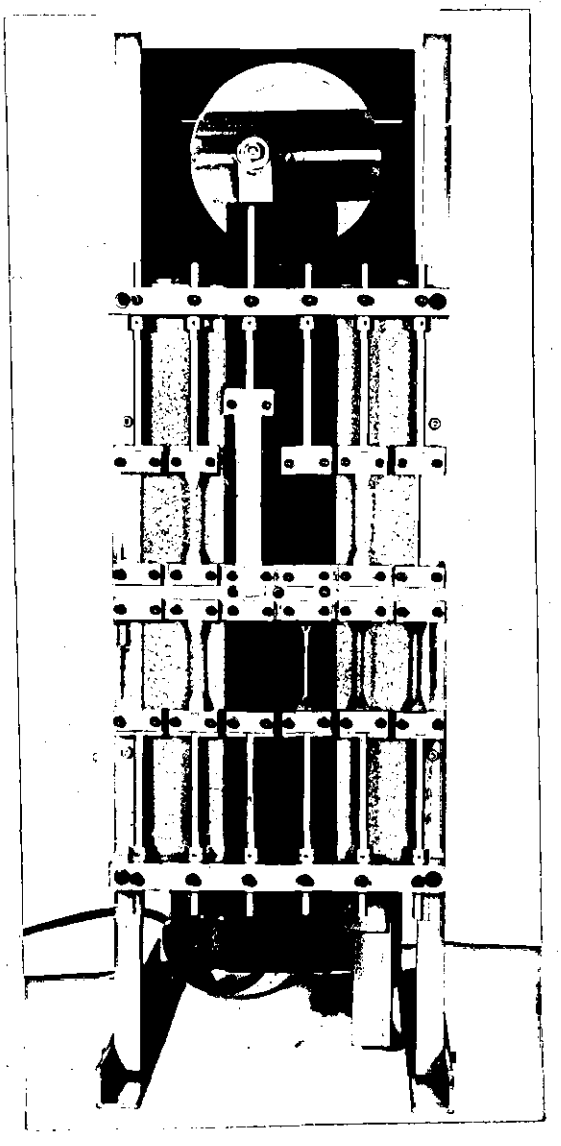

Figure 6.4.

Repeated extension machine used for all the cut growth and fatigue measurements.

on the central bar oscillate backwards and forwards between stationary clamps which could be adjusted to give extensions on the test pieces from 0 to 16 cms. The machine speed was approximately 120 cycles per minute. A six figure counter was attached to the side of the machine. Metal collars were also attached to the stationary clamps which allowed the samples to remain unloaded when the machine was left off overnight.

At each strain selected, three samples were placed on the repeated extension machine and during the test the length of cut was measured with a magnifying micrometer eyepiece. The test piece was slightly strained to facilitate observation. Readings were taken at intervals corresponding to approximately a 10% increase in cut length. Razor cuts tend to have very sharp tips and a small amount of rapid growth often occurs before the tip of the cut roughens to its steady state. This period of initial rapid growth was usually ignored. A typical example of the variation of cut length with number of cycles is shown in Figure 6.5. for a cellular polyurethane test piece strained to 70%.

6.4.2. Experimental Results

By measuring energy inputs at various strains along the stress-strain curve and using published values of 2K shown in Table 6.1., it was possible to determine the variation of 2KU with strain for the cellular polyurethane and this is shown in Figure 6.6.

Several cut growth tests were carried out at a number of extensions up to 100% maximum initial strain for the polyurethane and a number of graphs similar to Figure 6.5. were produced. For each graph, the rate of cut growth $(\frac{dc}{dn})$ was determined from the difference in cut length divided by the number of cycles between the two experimental readings. This rate was then referred to the tearing energy calculated from the average of the two cut lengths and the 2KU value obtained from Figure 6.5. at the maximum initial strain of the

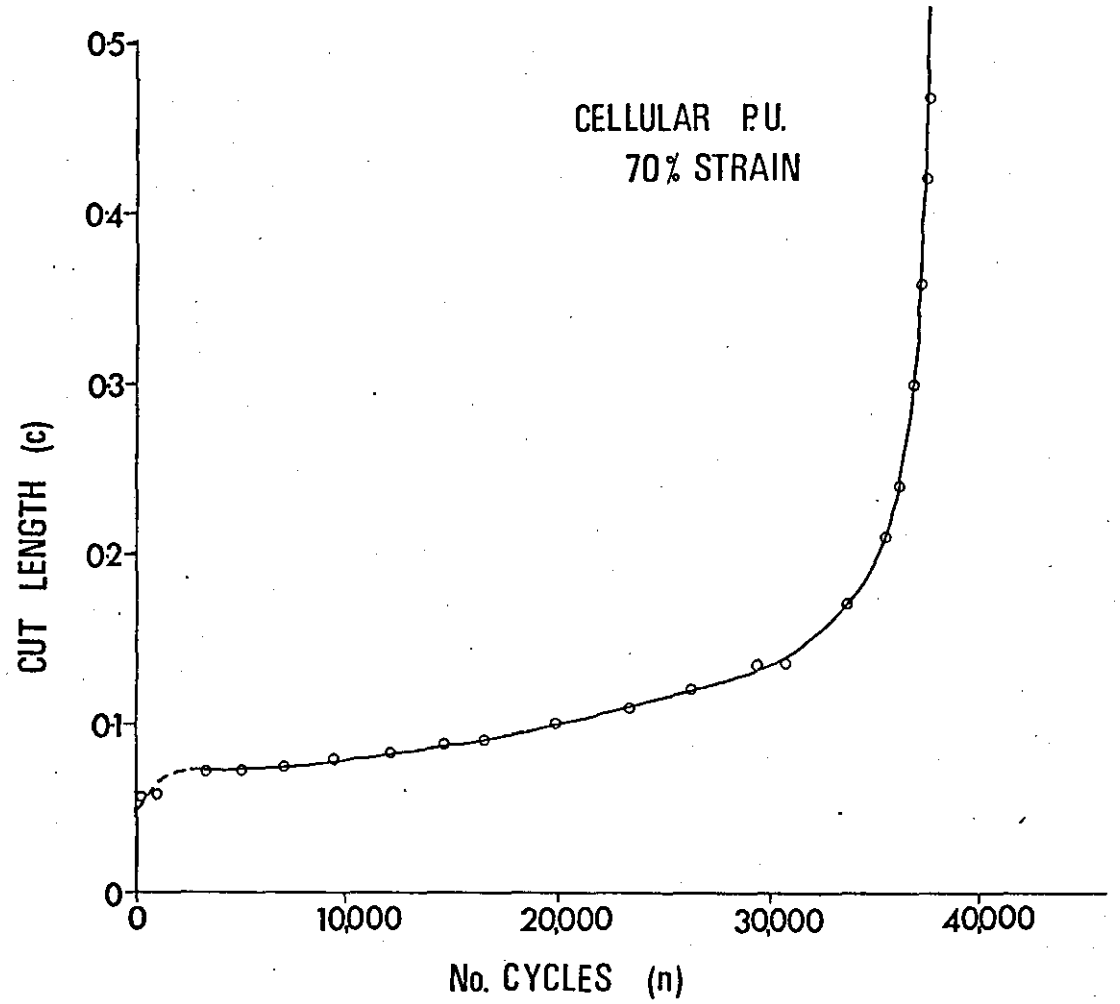

Figure 6.5.

Increase in cut length with number of cycles in a cut growth test for cellular polyurethane test piece cycled to 70% strain. Dotted line shows initial rapid growth due to razor cut.

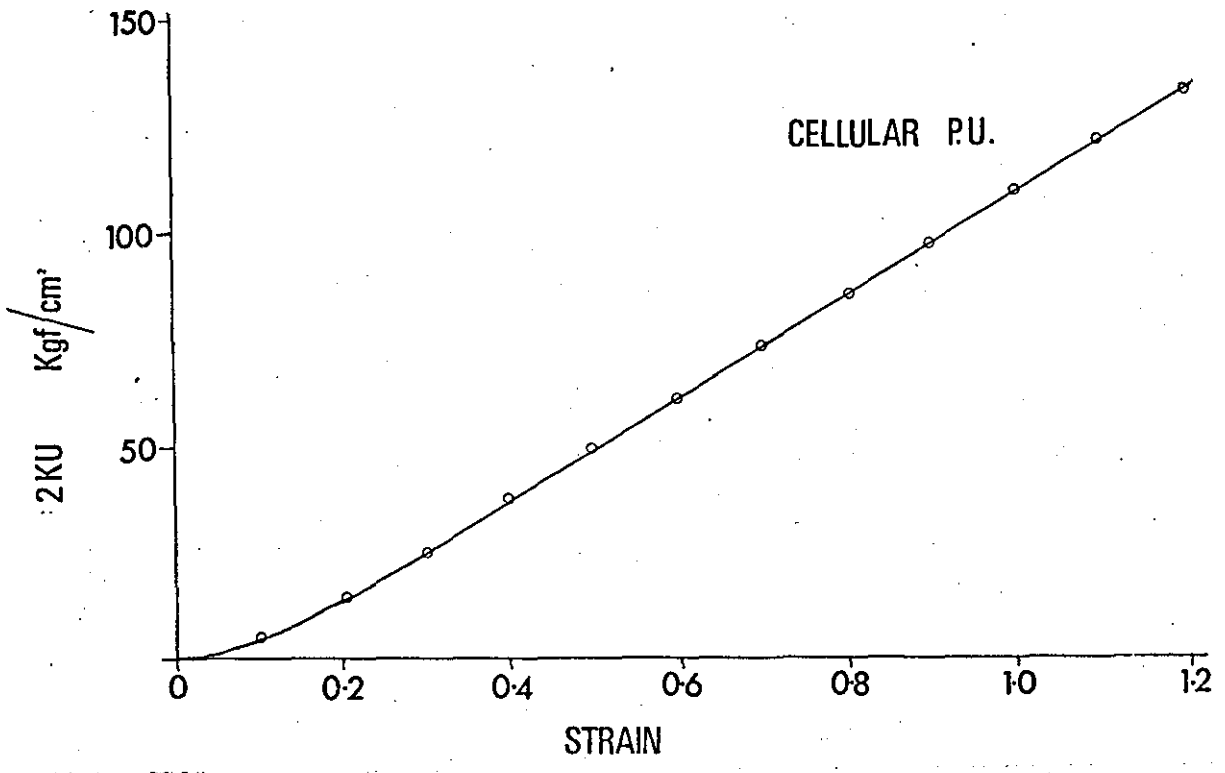

Figure 6.6.

Variation of 2KU with strain for the cellular polyurethane.

cycle. The test was stopped when the cut reached about 20% of the test piece width as the theory is inapplicable above this cut width. It was possible, however, to cover a decade of tearing energy values with one test piece. A different range of T was covered by cycling another sample to a different maximum strain, hence changing 2KU.

In all the experiments no correction was made for permanent set developed in the test piece. Provided that all the measurements were referred to the initial stress-strain curve of the material the correction was unnecessary. (This procedure differs slightly from the published work[88-90] on solid rubbers where set is usually allowed for in both the cut growth and in the stress-strain measurements).

The variation of the rate of cut growth $(\frac{dc}{dn})$ with tearing energy for the cellular polyurethane is shown in Figure 6.7. The lowest recorded value of tearing energy at which some cut growth was observed was 2.4 kgf/cm.

Cut growth samples put on the repeated extension machine at a tearing energy value of 1.7 kgf/cm showed no cut growth after repeatedly being stretched for 3 million cycles. It was therefore assumed that the value of T_o for the cellular polyurethane was approximately 2 kgf/cm.

Above T_o, however, as shown in Figure 6.7. a relationship to the power 6 is obeyed between cut growth rate and tearing energy and hence equation 6.4. can be written for this material as:

$$\frac{dc}{dn} = \frac{T^6}{G} \qquad 6.14.$$

This power is much higher than is normally found in a solid rubber polymer[88-90] but can vary according to the cellular structure as discussed later.

In order to confirm whether equation 6.14. was correct for the cellular polyurethane used in poromerics and secondly to obtain a value for the minimum

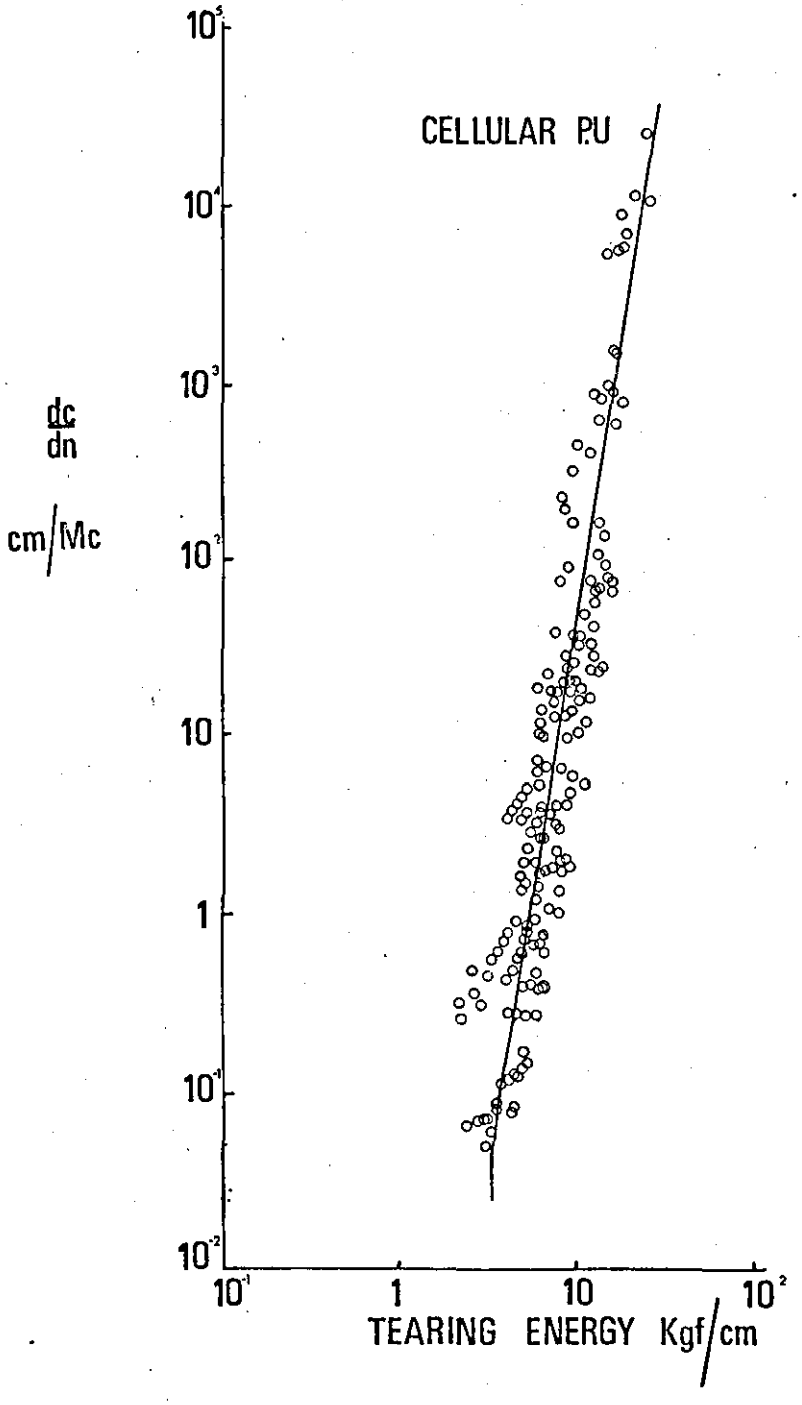

Figure 6.7.

Variation of rate of cut growth with tearing energy for cellular polyurethane.

flaw size C_o at which cut growth occurs, conventional fatigue tests where no cuts were placed in the sample were undertaken and the results of these experiments are described in the next section.

6.5. FATIGUE PROPERTIES OF CELLULAR POLYURETHANES

6.5.1. Experimental

Dumb-bell samples of the type shown in Figure 6.1(c). were cut from the cellular polyurethane used in the cut growth investigation. The samples with no inserted cuts were then placed on the repeated extension machine shown in Figure 6.4. The number of cycles to failure for each of the 12 samples repeatedly strained to the same initial strain was then recorded. The strains were calculated as a function of the original length of the parallel side centre section of the dumb-bell with no allowance being made for set in a similar manner to that described for the cut growth experiments. The whole experiment was repeated at a number of strains between 200 and 350%.

6.5.2. Experimental Results

The variation of the average number of cycles to failure for the 12 samples with strain is shown in Figure 6.8. In order however to confirm whether equation 6.14. and the cut growth theory outlined was applicable to cellular polyurethanes, the average number of cycles to failure of the twelve samples used at each strain was plotted as a function of 2KU on logarithmic scales as shown in Figure 6.9. A sixth power line has been drawn through the results in Figure 6.9. to give the relationship from equation 6.7.

$$N(e) = \frac{G}{5\,(2KU)^6}\,\frac{1}{C_o^5} \qquad 6.15.$$

From the intercept (N*) of the line on the 2KU = 1 (log 2KU = 0) axis, it is possible to derive a value for the effective flaw size C_o from

$$N^*(e) = \frac{G}{5\,C_o^5} \qquad 6.16.$$

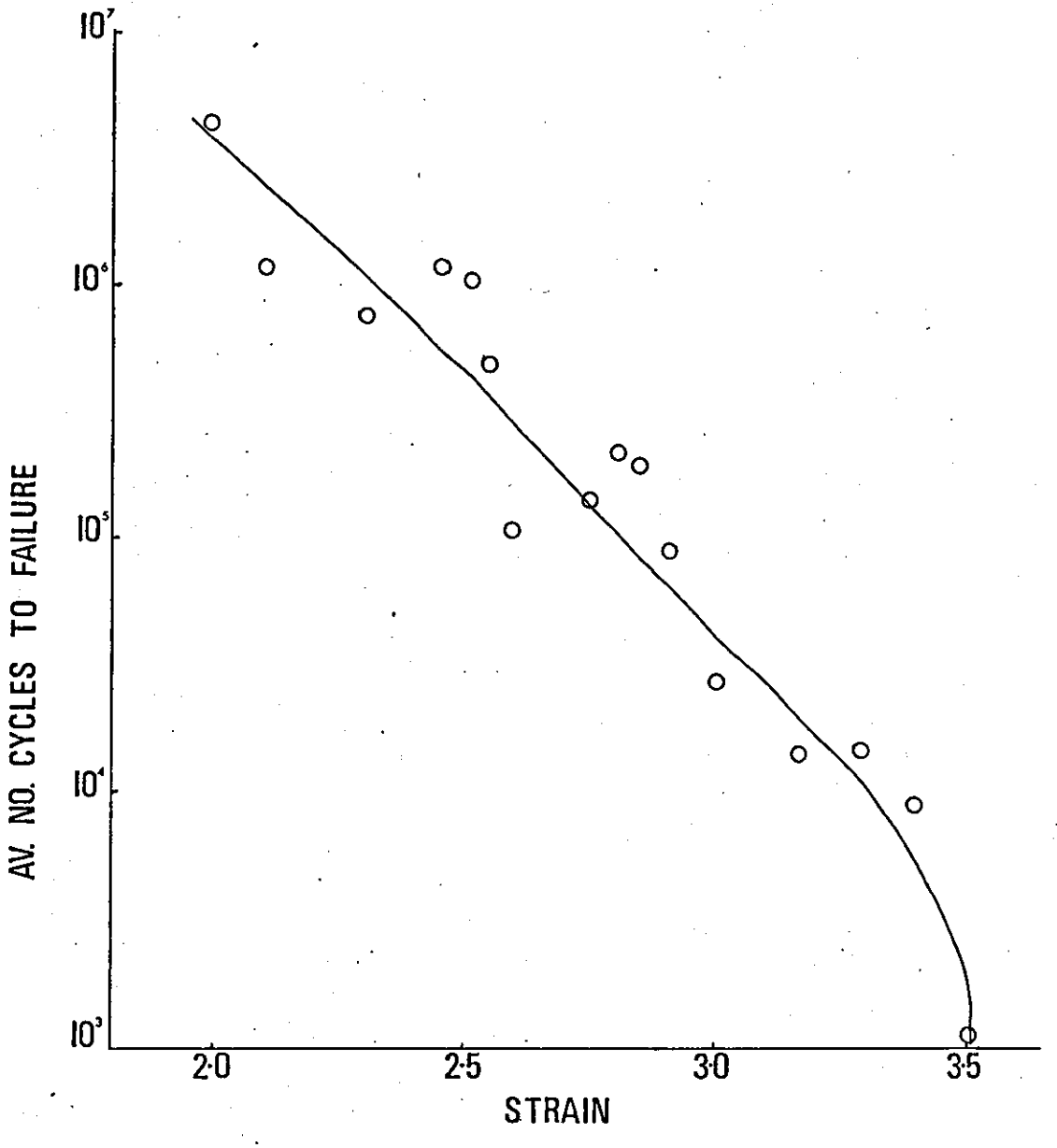

Figure 6.8.

Variation of fatigue life with strain for cellular polyurethane.

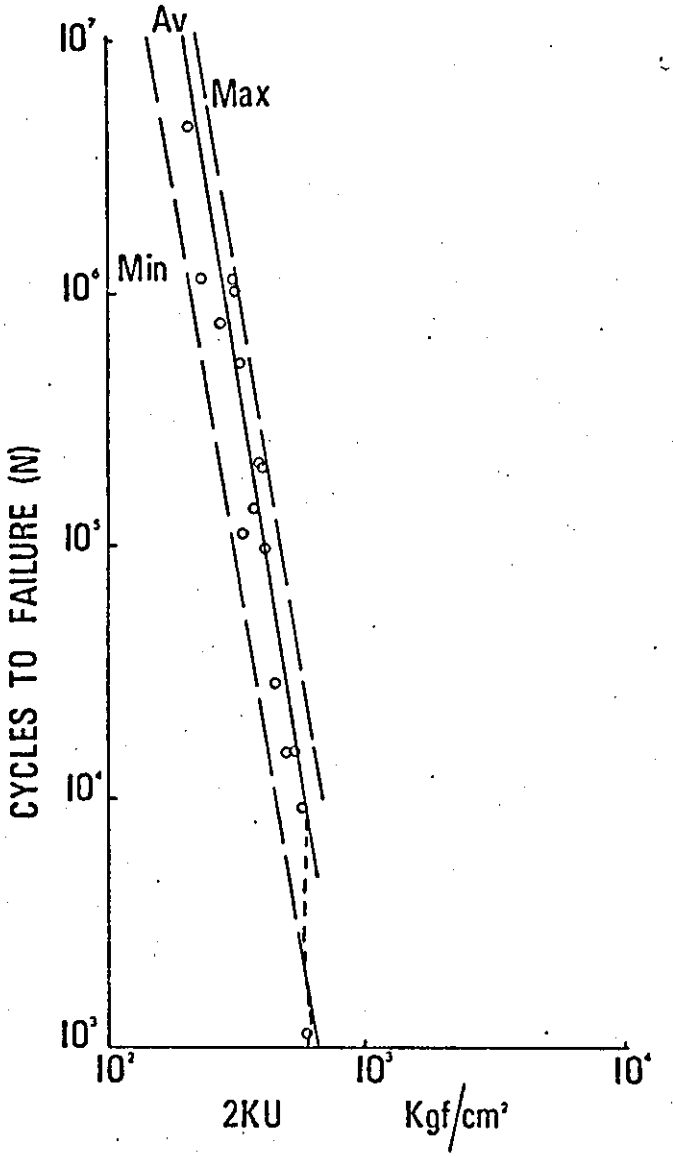

Figure 6.9.

Variation of average fatigue life of twelve test pieces with 2KU for cellular polyurethane. Dotted lines indicate maximum and minimum fatigue life of 12 samples at each 2KU value.

The value of G = 2.86×10^{10} cgs cycle units is obtained from the line shown in Figure 6.7. Using the value of N* = 4.6×10^{20} from Figure 6.9., the value of C_o is found to be 6.6×10^{-3} cms.

The scanning electron microscope photograph of the cellular polyurethane shown in Chapter 4 indicated that the average pore diameter was approximately 2×10^{-3} cm but a few cells of up to 2×10^{-2} cms in diameter were present. The calculated value for C_o appears therefore to be well within the range of cell diameters found in the cellular polyurethanes used in poromerics in practice.

The results shown in Figures 6.8. and 6.9. are the average number of cycles to failure for 12 samples of the cellular polyuretnane at various strains but the actual number of cycles for the first and last samples of the twelve to fail were very different. A sixth power law has been dotted on Figure 6.9. through the maximum and minimum number of cycles to failure of the twelve samples. From the respective N* values and equation 6.16., an indication of the maximum and minimum flaw size could be obtained and these are shown in Table 6.3.

TABLE 6.3.

VALUES OF EFFECTIVE FLAW SIZE C_o FROM FATIGUE DATA

No. Cycles to Failure	N*	C_o cms
Max.	10^{21}	5.6×10^{-3}
Av.	4.6×10^{20}	6.6×10^{-3}
Min.	8×10^{19}	9.3×10^{-3}

These values of effective flaw size are therefore within the range of cell diameters found actually in cellular polyurethanes in practice.

It is concluded therefore that the tearing energy theory developed for vulcanised rubbers appears to be applicable to cellular polyurethanes of the type used in poromerics and that fatigue failure of these materials under repeated straining is due to cut growth from the largest cell in the sample. The fatigue behaviour of cellular materials is therefore similar to that found in solid vulcanised rubbers with the size of the largest hole in cellular materials taking the place of the size of natural flaws in solid rubbers.

6.6. COMPARISON CUT GROWTH RESULTS WITH OTHER MATERIALS

6.6.1. Solid Polyurethane Elastomers

Similar cut growth measurements to those reported in Section 6.4. were also undertaken on the solid polyurethane of the same composition as the cellular material. The variation of the rate of cut growth with tearing energy for the solid polyurethane is shown in Figure 6.10.

The line through the results for the cellular polyurethane from Figure 6.7. is also dotted on Figure 6.10. for comparison. The line drawn through the results for solid polyurethane has a slope above T_o on the double logarithmic scales of $(5/2)$ to give the relationship

$$\frac{dc}{dn} \text{ (solid)} = \frac{T^{5/2}}{G^1} \qquad 6.17.$$

which is different from that for the cellular polyurethane (equation 6.14.). This is observed by the difference in slope of the two lines in Figure 6.10. The higher slope in the case of the foam polyurethane would be expected as no allowance has been made for the effect of the cells. The cut growth process in solid materials is also different as it is a continuous growth of a crack whereas in the foam polyurethane it is a repeated process of crack initiation through the polyurethane solid strands and rapid growth through the holes.

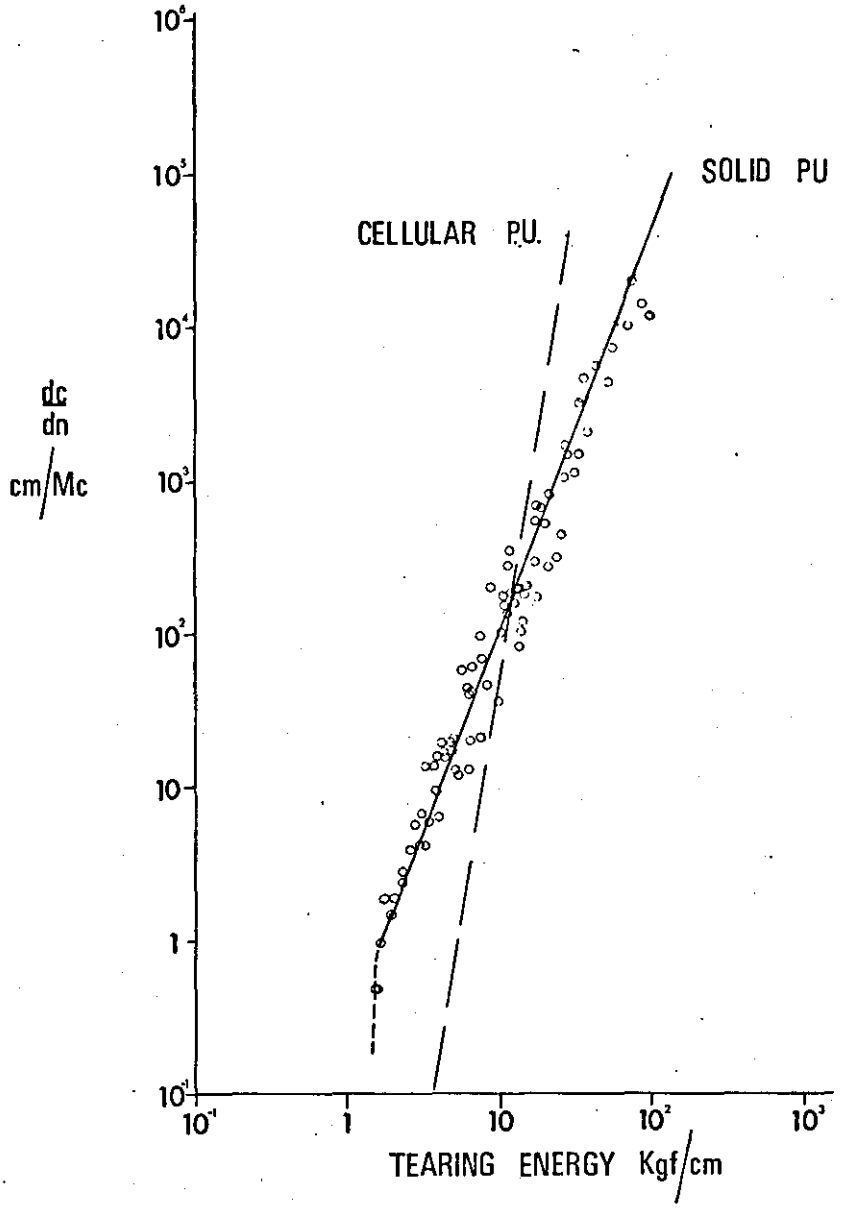

Figure 6.10.

Variation of rate of cut growth with tearing energy for solid polyurethane compared with cellular polyurethane results from Figure 6.7.

The lower limiting value of tearing energy (T_o) at which no cut growth occurs for the solid material is 1.5 kgf/cm which is approximately the same as found for the cellular polyurethane in the earlier sections of the paper. The effect of generating a cellular structure in a polyurethane material used in poromerics appears to have little effect on T_o but increases the rate of cut growth with tearing energy.

6.6.2. Effects of Chemical Crosslinking

The microporous polyurethane coating of the fibrous poromeric 'Corfam' was stripped away from the base and some cut growth measurements were made on this material. As discussed in Chapter 5, this particular polyurethane coating was different from the previous foam and the majority of poromerics in that it is based on a polyether polyurethane rather than a polyester and it was also chemically crosslinked.

The variation of rate of cut growth with tearing energy is shown in Figure 6.11. compared with the cellular polyurethane used in the earlier sections of this chapter. Although a 6th power law between cut growth rate and tearing energy is still obeyed, the effect of chemical crosslinking is to decrease the value of T_o.

6.6.3. Vulcanised Rubbers

The majority of the published[88-90] cut growth test results which are expressed in terms of the parameter 'tearing energy' have been confined to vulcanised rubbers such as natural rubber (NR) and styrene butadiene rubber (SBR). In general these test results have been calculated on a slightly different basis from the measurements discussed in this chapter. In the work on vulcanised rubbers, account has been taken of tension set developed during an experiment when calculating strain. Tearing energy values are therefore lower than those normally quoted.

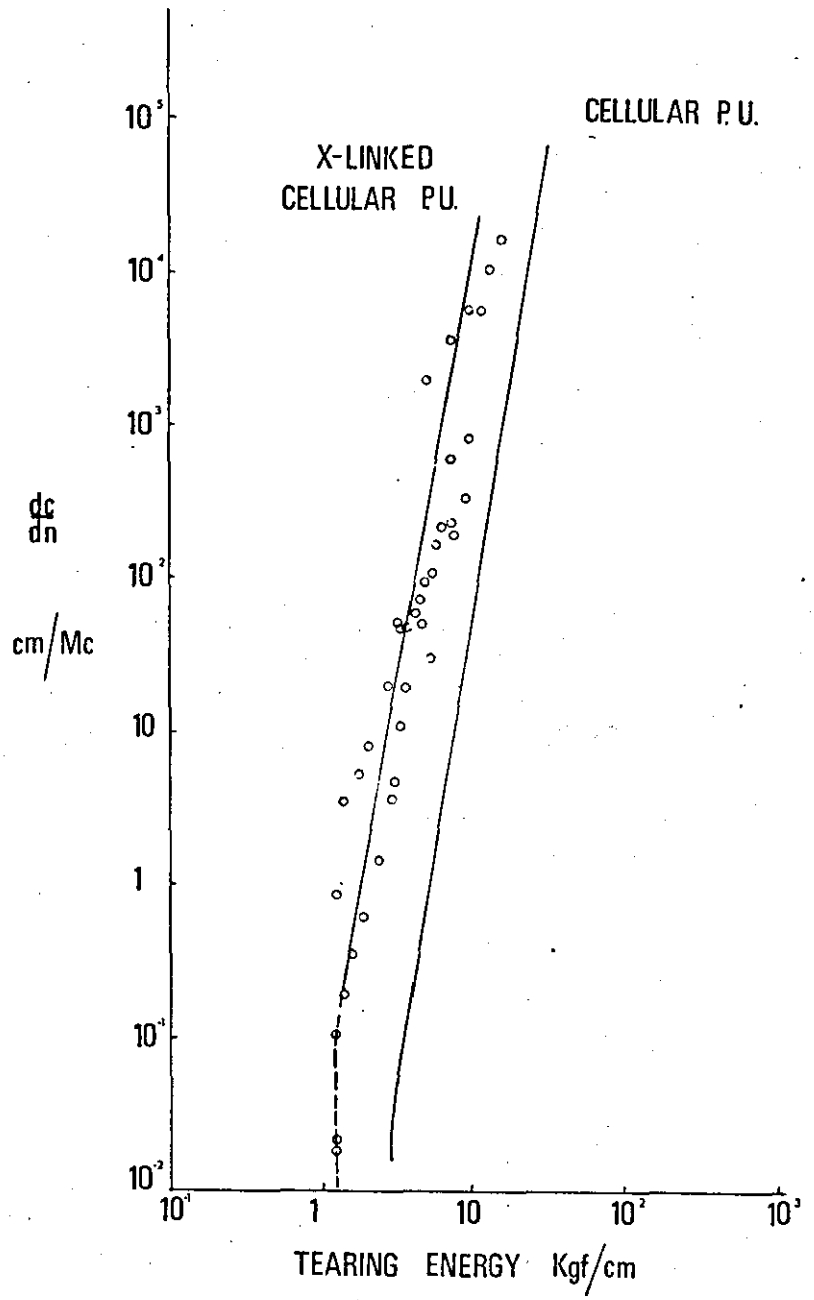

Figure 6.11.

Variation of rate of cut growth with tearing energy for chemically crosslinked microporous polyurethane surface layer from poromeric "Corfam" with cellular polyurethane results from Figure 6.7.

The cut growth results for the solid and cellular polyurethane materials were however re-calculated in this manner and are compared with solid NR and SBR data from published papers[88-90] in Figure 6.12. Although the slope of the rate of cut growth - tearing energy curve is similar for solid polyurethane and NR indicating as found in practice that both materials are highly hysteresial in character, the polyurethane is displaced along the tearing energy axis resulting in a far higher value for T_o for polyurethane than normally obtained for vulcanised rubbers. The reason for this behaviour is discussed later in the thesis.

6.6.4. Styrene-Butadiene Block Copolymer

The variation of rate of cut growth with tearing energy for a typical styrene-butadiene thermoplastic rubber is shown in Figure 6.13. The tests were performed on a 2.5 mm thickness moulded sheet of the material. Careful preparation of the sheet was undertaken to reduce anisotropy in the material to below 3%. The most interesting feature of the results shown in Figure 6.13. is that the value of T_o appears to be high compared with conventional vulcanised rubbers and is similar in magnitude to the polyurethane rubbers.

A number of investigations[96,97] have shown that the structure of thermoplastic rubbers consists of long flexible polybutadiene chains attached randomly to hard polystyrene blocks of approximately 300 Å diameter. The same thermoplastic rubber was also ~~prepared~~ cured by using 2.0 phr dicumyl peroxide as a crosslinking agent and the cut growth results for this material are also shown in Figure 6.13. It is quite clearly seen that the introduction of crosslinks considerably reduces the value of T_o. This is thought to be due to the crosslinking preventing the formation of the domain structure of the polystyrene in the polybutadiene network. This effect of crosslinking in reducing T_o is analagous to the behaviour exhibited by polyurethane described in Section 6.6.2.

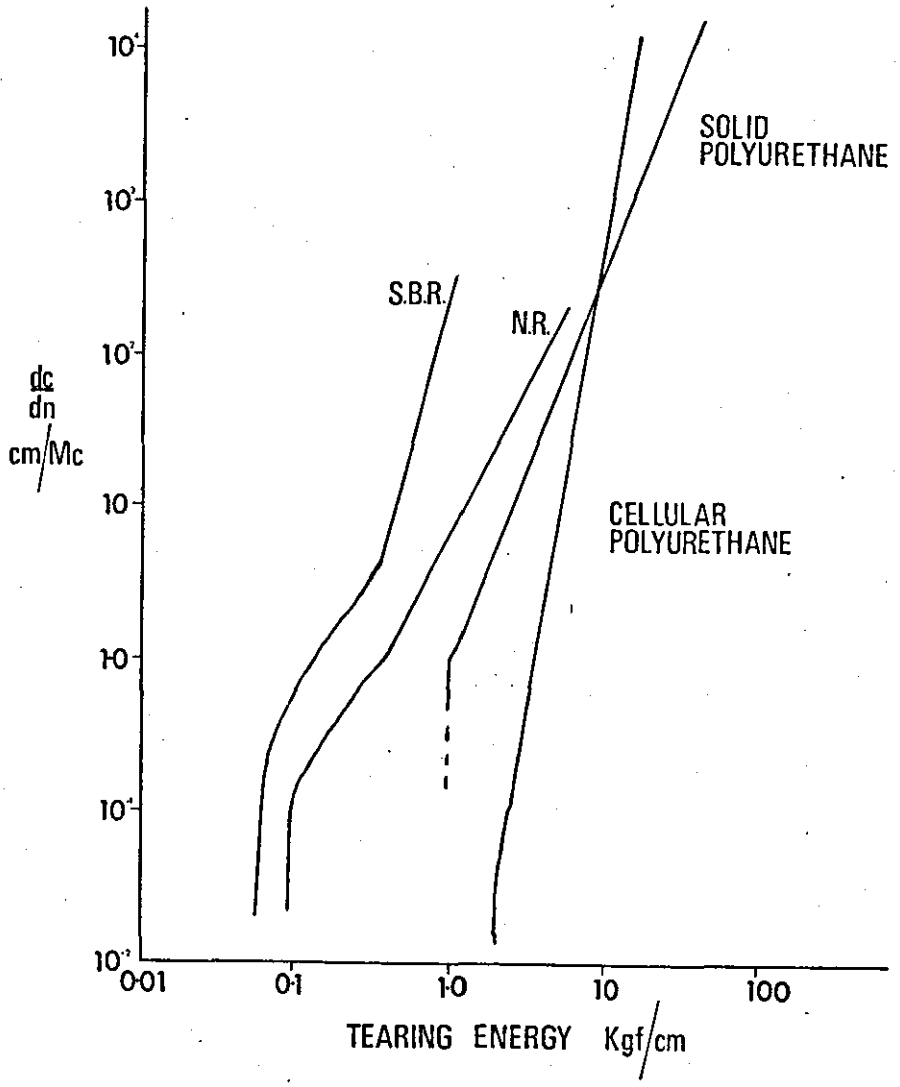

Figure 6.12.

Variation of rate of cut growth with tearing energy for NR and SBR from published data[88-90] with solid and cellular polyur-thane results from this investigation. (Results for polyurethane corrected to take account of tension set developed during course of test).

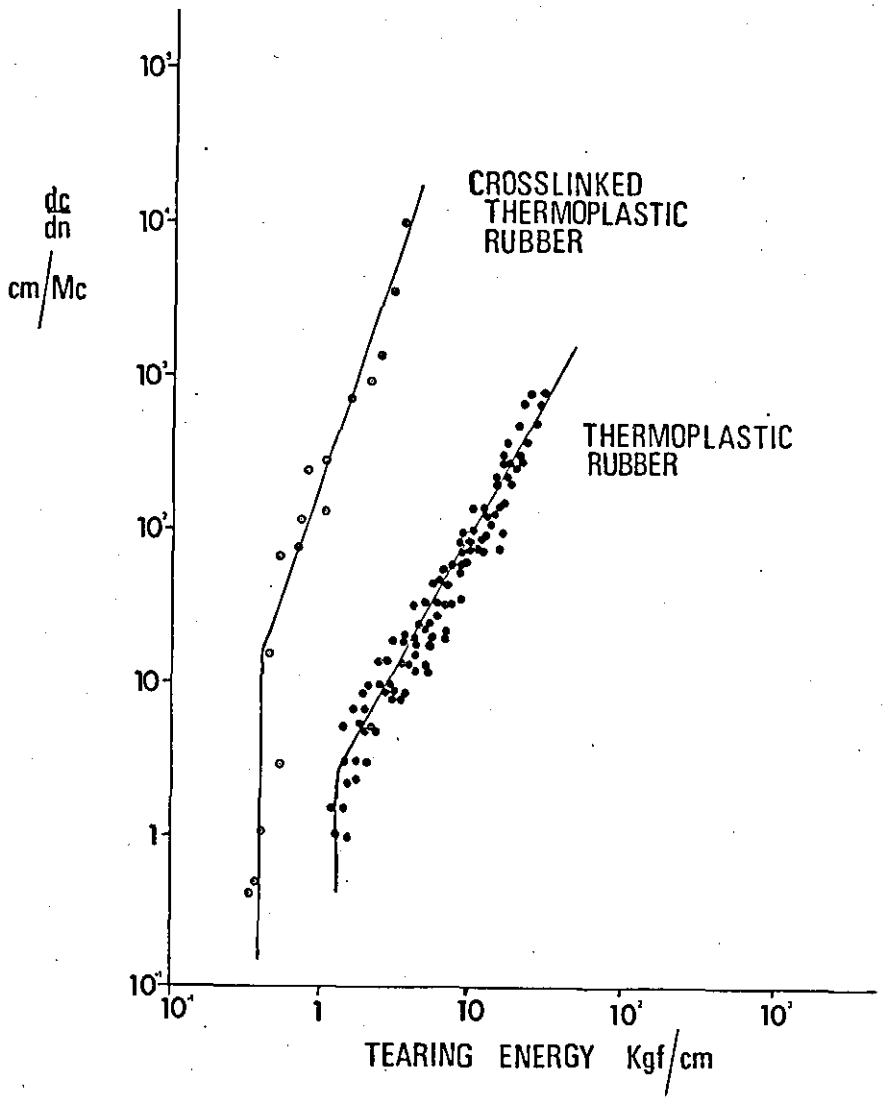

Figure 6.13.

Variation of rate of cut growth with tearing energy for normal styrene-butadiene thermoplastic rubber and for same rubber crosslinked by 2.0 phr dicumyl peroxide.

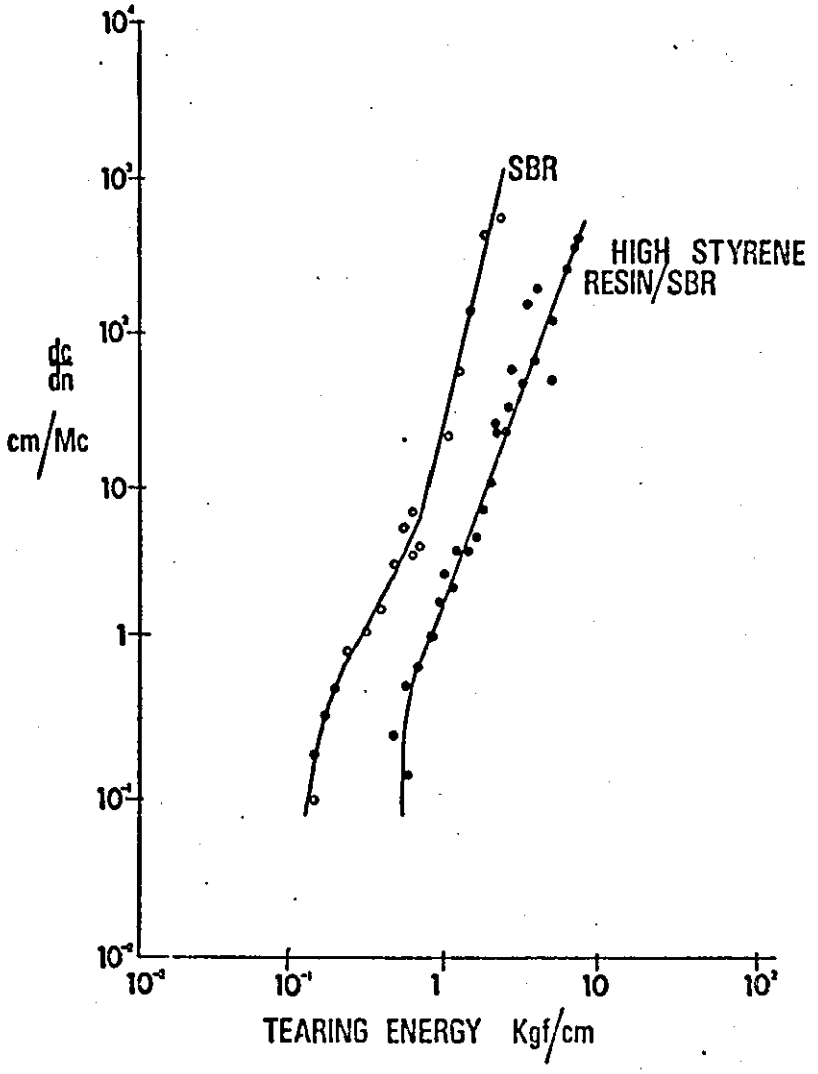

Figure 6.14.

Variation of rate of cut growth with tearing energy for styrene butadiene copolymer with approximately 80% styrene compared with conventional vulcanised styrene butadiene rubber.

6.6.5. Random Styrene Butadiene Copolymer

Limited cut growth experiments were also undertaken on a styrene butadiene copolymer with approximately 80% of styrene. The variation of rate of cut growth with tearing energy for this material compared to a conventional vulcanised styrene butadiene rubber (SBR) is shown in Figure 6.14. It is seen that the introduction of a high amount of styrene resin to the rubber increases the value of T_o. It is interesting to note that the usual type of microcellular rubber soling is manufactured from a styrene butadiene copolymer with a high styrene content and this has excellent resistance to cut growth in wear.

6.7. CONCLUSIONS

Up to the present, two main approaches to the failure of rubber have been developed, Harwood and co-workers have found quantitative failure relationships between energy input to break, hysteresis at break and strain at break. This work has been extended by the author in Chapters 2 and 5. The second approach from investigations by Lake, Lindley and Thomas into the cut growth and fatigue properties of vulcanised rubbers has been by use of the tearing energy theory. The author has attempted in Section 6.3. of this chapter to bring these two theories together and has derived a relationship between the parameters from the hysteresis failure criterion with those from the tearing energy theory of fatigue failure.

The tearing energy theory has been shown to be applicable to cellular polyurethanes. The main point emerging from this investigation is that the lower limit of tearing energies (T_o) below which no cut growth occurs in the absence of chemical effects is far higher for polyurethanes than for the majority of vulcanised rubbers. The tearing energy theory is also shown to be applicable to the fatigue properties of cellular polyurethanes. The

calculated initial effective flaw size from where the cut would appear to start is of the same magnitude as the largest hole in the cellular material. Chemically crosslinking the polyurethane is shown to decrease the value of T_o.

Experimental results on a styrene-butadiene block copolymer thermoplastic rubber also show T_o to be fairly high compared with conventional crosslinked vulcanised rubbers. The thermoplastic rubbers do show some similarity to polyurethanes, in that when the thermoplastic rubber is crosslinked, the value of T_o decreases. Similarly a styrene-butadiene copolymer with a large styrene content has a higher value of T_o than a conventional crosslinked SBR vulcanisate. It would appear therefore that the introduction of some form of domain structure into a material increases the value of minimum tearing energy (T_o). The structure of polyurethane elastomers is considered in Appendix 2.

CHAPTER 7

GENERAL CONCLUSIONS

Some of the mechanical properties of cellular polyurethane elastomers used in poromeric materials have been measured experimentally and the results are presented in this thesis. This work is supplemented in Chapter 2 by other experimental results obtained by the author on branched polyurethane elastomers. All these results are compared with those found in normal commercial vulcanised rubbers.

The major conclusion to be drawn from this work is that the polyurethanes used in poromeric materials exhibit superior mechanical properties to those found in both filled and unfilled vulcanised rubbers. A general explanation is now put forward in this chapter for these superior properties.

A number of relationships between various parameters for vulcanised rubbers such as the cubical model theory to explain the difference in mechanical properties of the foam and solid materials or secondly the variation of energy input to break with strain at break or hysteresis, have been found also to be obeyed by polyurethanes. In some properties, however, there are some large differences in magnitude, the most important being with respect to strength, hysteresis, temperature stability and cut growth resistance.

In order to provide an explanation for the good mechanical properties of polyurethanes, it is essential to refer to the structure of these elastomers. A review of published literature is given in Appendix 2. It has been shown by a number of investigators into the structure of polyurethane elastomers that they are composed of alternating hard and soft segments. The hard segments are approximately 25 - 50Å in diameter and contain urethane or urea groups whereas the soft flexible segments are in the order of 100 - 200Å and are formed

from the linear polyether or polyester chain segments. The hard segments are held together by hydrogen bonding and other intermolecular ~~physical~~ attractions.

The hard urethane segment presumably acts as a filler particle within the polyester or polyether rubber matrix. Introduction of a filler such as carbon black into an amorphous vulcanised rubber increases the modulus, hysteresis and abrasion resistance. The higher level of these properties in polyurethanes is presumably due to the very small size of the hard urethane segment. The mechanical properties of vulcanised rubbers improve as the particle size of the filler is reduced, as there is a larger particle surface area for polymer attachments and a smaller inter-particle distance. Both these effects considerably modify the relaxation behaviour of a large volume of the rubber. In vulcanised rubbers, the carbon black particles however (e.g. ~~SRF~~ SAF, ISAF) are about 300Å in diameter whereas the size of the hard segments in polyurethanes are a factor of ten smaller than this; hence the degree of reinforcement is far greater thus resulting in a high modulus and tensile strength.

The work of Harwood et al[12,14,98] showed that the introduction of 30 phr HAF carbon black into styrene butadiene rubber increased, not only the strength and hysteresis but also the temperature stability and caused a broadening of the relaxation spectrum. These features have also been demonstrated in polyurethanes as shown in Chapter 5. The introduction of a filler into an amorphous rubber resulted in the filled rubber no longer obeying the Williams, Landel and Ferry (WLF) equation and this was observed in polyurethanes. The presence of the hard segment in polyurethanes leads to additional characteristic response times as described in the theoretical work of Radok and Tai[99] on hard inclusions in viscoelastic media and produces a wide

distribution of relaxation times as found in filled vulcanised rubbers[12,14,98].

One further important feature of the physical structure of polyurethanes is that the filler particles (the hard segments) form a well dispersed molecular arrangement. Because the hard segments are formed chemically they will in general be better dispersed in the rubber matrix than the fillers (carbon black) in normal vulcanised rubbers. This is a secondary factor which must contribute to their good mechanical properties.

In a number of polymers such as natural rubber, crystallisation of the material is a main process in rendering high strength. Although some polyurethanes are known to crystallise, no evidence either from their mechanical properties or by comparing their IR spectrum with a crystalline polyurethane adhesive has been forthcoming to show crystallisation effects in the type of polyurethanes used in this investigation. Their superior mechanical properties must therefore arise mainly from their unique molecular structure.

High hysteresis at a particular energy input is a necessary condition for all materials which are to be used as artificial leathers in footwear as shown by the results on viscoelastic properties of all the fibrous poromerics and leather in Chapter 3. The hard segment arrangement in the homogeneous cellular polyurethane poromeric appears to result in the required mechanical properties which are comparable with semi-fibrous or totally fibrous materials which are used in the same application. The broad relaxation spectrum of polyurethanes is also ideal for their use in footwear where high set and hysteresis is required to give good shape retention over a very long time scale.

Studies into the high temperature transitions of polyurethanes, reported in Appendix 2 show that at about 160 - 170°C, the hydrogen bonding which normally acts as a physical crosslink between the hard segments in the polyurethane elastomer dissociates. This is the reason for the large drop in mechanical properties noticed at about these temperatures. This particular feature can be used to advantage in the footwear industry as it allows a permanently shaped article to be produced by conventional plastics fabrication techniques such as pressure or vacuum forming as described in Appendix 1. If the homogeneous cellular polyurethane is strained at 170°C, at which temperature dissociation of the hydrogen bonding between the hard segments occurs, then on cooling the hydrogen bonding reforms to physically crosslink the material in the stretched state, inducing a permanent set. The polyurethane is therefore to some extent thermoplastic in nature.

Unfortunately 170°C is too high a temperature to use in the conventional manufacture of footwear and therefore some further investigation is required into the possibility of modifying the polyurethane to reduce the temperature at which the hydrogen bonding dissociates. The reduction of this temperature to 120°C without altering any other properties could have a profound effect commercially and completely change footwear production methods.

It was shown in Chapters 3 and 5 that poromeric materials of all types display stress softening effects similar to those found in vulcanised rubbers. Before stress softening can be fully recovered in a cellular polyurethane, the material has to be heated to a temperature of approximately 170°C. It is necessary therefore to disrupt the hydrogen bonding between the hard segments before stress softening in polyurethanes is fully recovered.

One of the most remarkable features of the polyurethane used in poromerics is their very high resistance to cut growth and for this reason, this particular property has been fully investigated and reported in Chapter 6. The tearing energy theory developed by investigators[61,88-90] at NRPRA for analysing the tear, cut growth and fatigue properties of vulcanised rubbers has been found to satisfactorily describe the cut growth and fatigue behaviour of cellular polyurethanes. For example, tensile fatigue measurements on cellular polyurethanes using test-pieces with no inserted cuts, showed that failure of the cellular polymer was caused by cut growth from the largest cell in the sample. The measured large cells in the test-pieces agreed satisfactorily with those calculated theoretically from the tearing energy theory.

The most interesting feature of the cut growth results on both the foam and solid polyurethanes was the large value of T_o (i.e. the minimum value of tearing energy under which no cut growth takes place in the absence of chemical effects). Values of T_o are at least a factor of ten higher than found in vulcanised rubbers. The high value of T_o reflects the good cut growth properties of cellular polyurethanes found in practice. These measurements can be directly applied to practical problems such as flex cracking in solings as shown in Appendix 1.

Limited work has been published on the cut growth properties of filled vulcanised rubbers but it has been shown[89] that T_o is increased by about 50% with the addition of a reinforcing carbon black to a vulcanised rubber. Non reinforcing fillers have been found to have little effect on the value of T_o but they also do not alter the relaxation spectrum of the rubber. T_o is also high in a styrene butadiene block copolymer which consists of a well dispersed filler

system of polystyrene domains in the polybutadiene network. Crosslinking the block copolymer reduces the value of T_o. Similarly T_o is also increased in SBR vulcanisates when a high amount of styrene resin is introduced. It would appear therefore that the value of T_o is related to the hysteresis in the material and it is thought that the high hysteresis resulting from the "built in well dispersed filler system" in polyurethane elastomers causes the high value of T_o.

Theoretical values[100] of T_o have been derived for vulcanised rubbers from equations based on chemical bond strengths and these values agree well with those found in practice. However these theoretical equations have been derived for essentially elastic systems. Some further detailed study is now required to introduce a factor into these equations which takes account of viscoelastic effects and therefore extends the theory to filled rubber systems including polyurethane and thermoplastic elastomers.

Other investigators, as described in Appendix 2, have found that chemically crosslinking the polyurethane reduces the strength of the polymer as the crosslinking prevents the formation of the molecular arrangement of the hard and soft segments. A limited amount of work in Chapter 6 showed that T_o was lower for a crosslinked cellular polyether than for the linear cellular polyester urethane. This particular study should be extended however preferably using the same polyurethane and examining the actual change in mechanical properties, especially T_o, with increased crosslinking. Highly branched polyurethane rubbers as described in Chapter 2 are very weak in mechanical properties.

Although abrasion resistance has not been considered separately in this thesis, Schallamach[101] has shown qualitatively for vulcanised rubbers that wear decreases as the mechanical damping or hysteresis

of the rubber increases. The exceptionally high hysteresis in polyurethanes must contribute to the very good abrasion resistance of polyurethane elastomers used in poromerics as found in practice. The whole field of abrasion resistance of polyurethane however is an ideal subject for further investigation.

The high strength, abrasion resistance and good cut growth properties of the high density cellular linear polyurethanes used in the footwear industry is due to the hard urethane segments in the polyether or polyester rubber chains. These hard segments act as well dispersed minute filler particles in the rubber matrix to produce a very effective "self reinforced" elastomer.

APPENDIX 1

PRACTICAL APPLICATIONS

A1.1. FORMING OF POROMERIC UPPER MATERIALS

The high set that can be obtained in polyurethane materials by heating them to 170°C so that the hydrogen bonding between the hard segments dissociates, then stretching and subsequently cooling the material to reform the physical crosslinking (hydrogen bonding) has been utilised recently in process developments in the footwear industry.

This thermoplastic type of behaviour of poromerics which are made entirely of cellular polyurethane allows conventional plastics fabrication techniques such as vacuum and pressure forming to be used in the shaping of shoe uppers. This significant change from conventional shoemaking has potential material and labour cost savings.

The vacuum forming process developed at SATRA consists of heating to 170°C a sheet of the poromeric upper material and then forming the material over a nest of moulds by applying a vacuum. All stretching and compression of the upper takes place during moulding so that when cool, the material is permanently set to the mould shape.

Pressure forming is a further development in the preforming of shoe uppers which uses positive air pressure by which greater forces can be applied during forming than in the case of vacuum forming. In pressure forming a slightly different process concept is used, upper components are assembled in the flat prior to forming. The preclosed upper is then clamped in a jig and heated to about 170°C. A cold mould as used for vacuum forming is then forced into the hot upper to give a mechanical stretching action. Air pressure of up to 5 atmospheres is then applied to finally conform the upper to the

mould shape. The upper is cooled to set it to the mould shape by the action of the cold mould and cold air being blown on to it.

A1.2. FLEX CRACKING OF SHOE SOLINGS

One of the most common problems with shoe soles is flex cracking and a typical example is shown in figure A1.1. This particular sole was made from an experimental cellular polyurethane compound and failure has resulted from the growth of one or more cracks which either were initially present in the material or were introduced by the environment and imposed deformation on the shoe. It is interesting to note that failure has occurred at the flexing point of the sole where the imposed strain is the highest. It has been observed that the growth of these cracks is generally quite slow at first but then accelerates rapidly as the flaw size increases.

Using the same procedure as described in Chapter 6, a value of T_o (i.e. the minimum value of tearing energy under which no cut growth takes place in the absence of chemical effects) was obtained for a polyurethane soling compound. This was found to be 1 kgf/cm.

The minimum tearing energy (T_o) is a function of strain energy density (U) and initial flaw size (C_o) and hence as shown in Chapter 6 can be expressed as

$$T_o \approx 2KUC_o$$

Provided therefore that values on the right hand side of the equation remain below 1 kgf/cm, no cut growth will occur and the sole will not fail in wear. 2KU is however a function of strain as shown in Chapter 6 and therefore as the strain increases, the critical flaw to initiate failure of the sole will decrease. This relationship for the polyurethane soling material is shown by the solid line in figure A1.2.

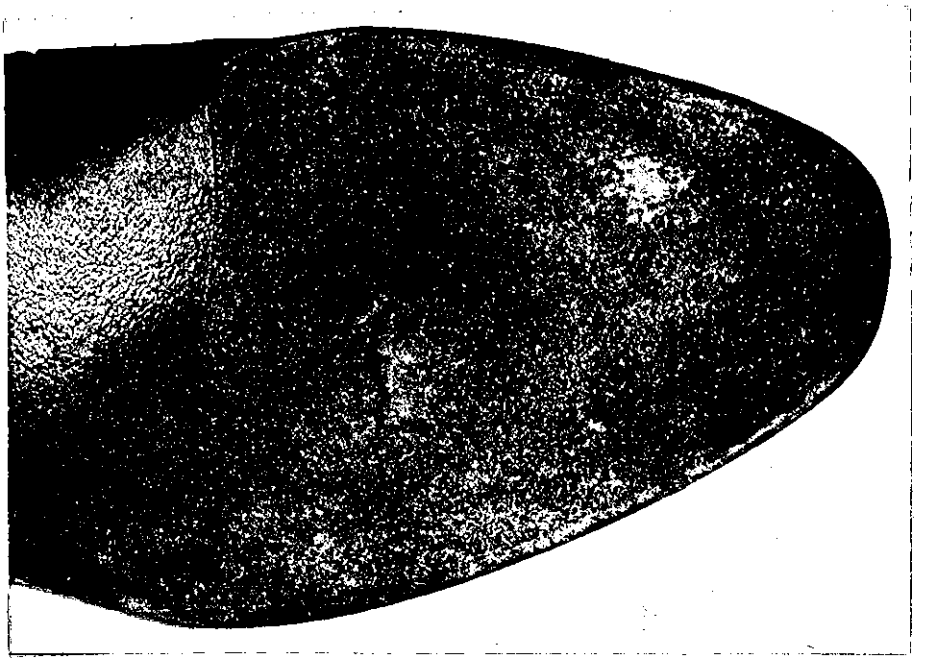

Figure A1.1.

Typical example of flex cracking in shoe soles

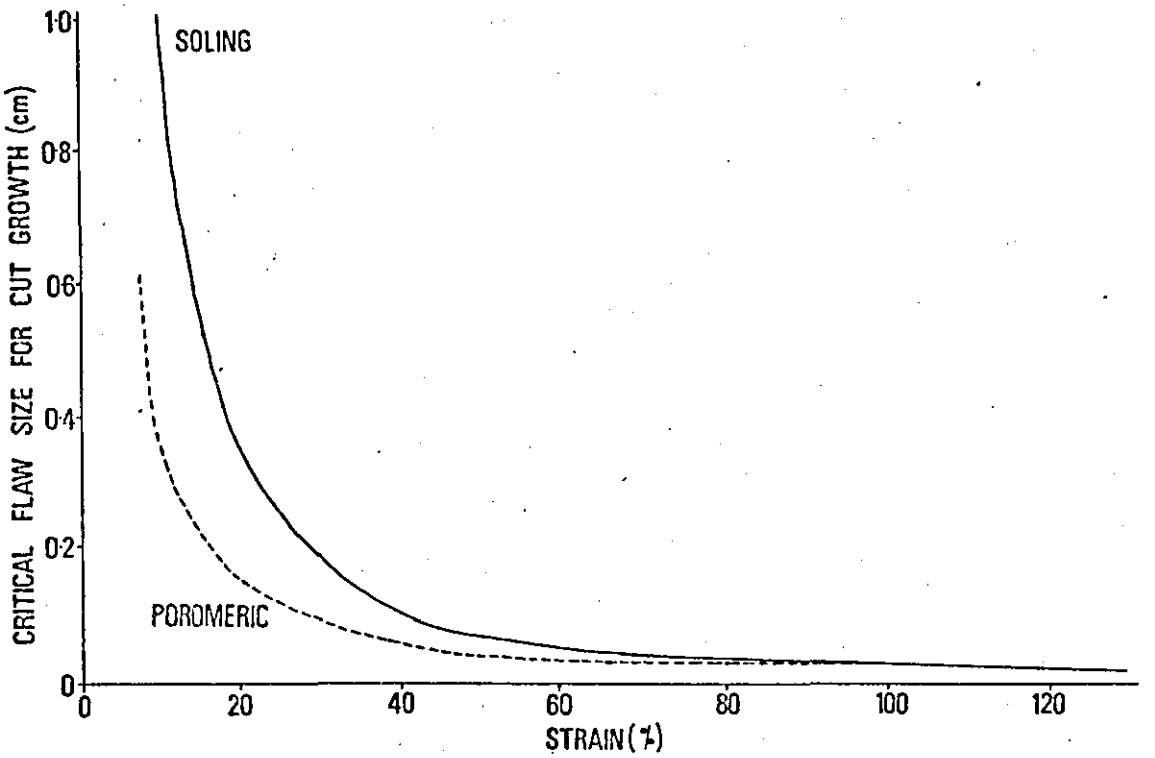

Figure A1.2.

Variation of critical flaw size to initiate failure of sole, calculated from T_o, with strain for the polyurethane soling material.

At strains less than 10%, fairly large flaws in the material can be tolerated and will show no cut growth as the line in figure A2.2. is an asymptote to the strain axis. This is observed in practice as flaws well over 1.0 cm will not generally grow in the heel or waist of a shoe sole as the strain on these parts of the sole in wear is generally less than 10%.

The critical area is in the flexing point of the sole and this is where flex cracking generally occurs. Strains on the sole in this region are often in the order of 25%, but this depends very much on the type and thickness of the sole and its pattern. Figure A2.2. predicts that flaws above 2 mm will show evidence of cut growth. This value for critical flaw size compares well with the results obtained from wear trial results on solings.

Standard tests on solings place a 2 mm cut in the sole across the flexing point and it is expected that in a satisfactory sole, no growth of the cut will occur after a reasonable period of wear. Similarly, the standard physical test to determine flex cracking of soles known as the Ross test, flexes a sample of the material with a 2 mm cut through 90°C so that strains induced in the position of maximum strain where the cut is placed are of the order of 20%. Satisfactory shoe soles are expected to show no further growth of the cut after 150 kilocycles.

If it is assumed that a cut in a shoe sole when flexed grows in a similar manner to a cut in a tensile test piece, then the tearing energy approach appears to predict a reasonable value of maximum cut length which the shoe sole can withstand in the flexing point without showing any evidence of cut growth. The critical value of 2 mm has been found from numerous wear trials on soling materials to be the acceptable standard length of cut which should show no evidence of

further growth after a reasonable period of wear and this size of cut has subsequently been used in the establishment of test methods and procedures.

The formation of cracks in a shoe sole in wear is due mainly to sharp objects such as nails, thorns, flints, drawing pins or pieces of glass getting embedded into the sole. A typical example is shown in the photograph in figure A1.3. of a cross-section of a polyurethane sole which has flex cracked. The initiating flaw was obviously the piece of sharp glass which was embedded in the position of failure on this particular sole. The length of the piece of glass across the cutting edge when removed from the sole was 3.2 mm and hence failure would be expected from consideration of the cut growth theory.

A1.3. INCLUSION OF LARGE HOLES IN SOLINGS

One feature of early expanded polyurethane soles and some experimental compounds was the inclusion of large holes in the foam structure. The problem, although not completely eliminated in the polyurethane solings produced at present, has however significantly decreased.

One particularly bad example is shown in the photograph in figure A1.4. where a cross-section cut across a cellular polyurethane sole shows some very large holes, the diameter of these holes being up to 50% of the thickness of the sole. The important feature with this particular example is that the holes are at the flexing point of the sole and hence are large enough to cause cut growth and ultimate failure of the sole as shown in the previous section. One slight difference between this type of flaw and that arising from the inclusion of some sharp glass is that, in the latter case, the flaw has a sharp tip which often causes a short period of rapid growth until the tip roughens to a steady state. Hence, possible propagation

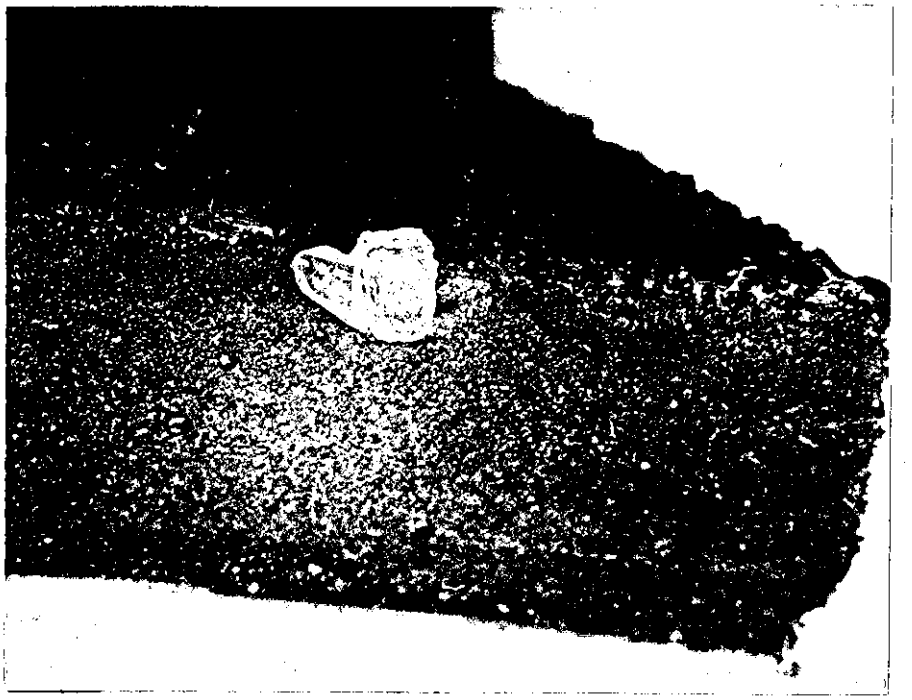

Figure A1.3.

Cross-section of sole at point where it had cracked in wear showing piece of glass which had initiated failure.

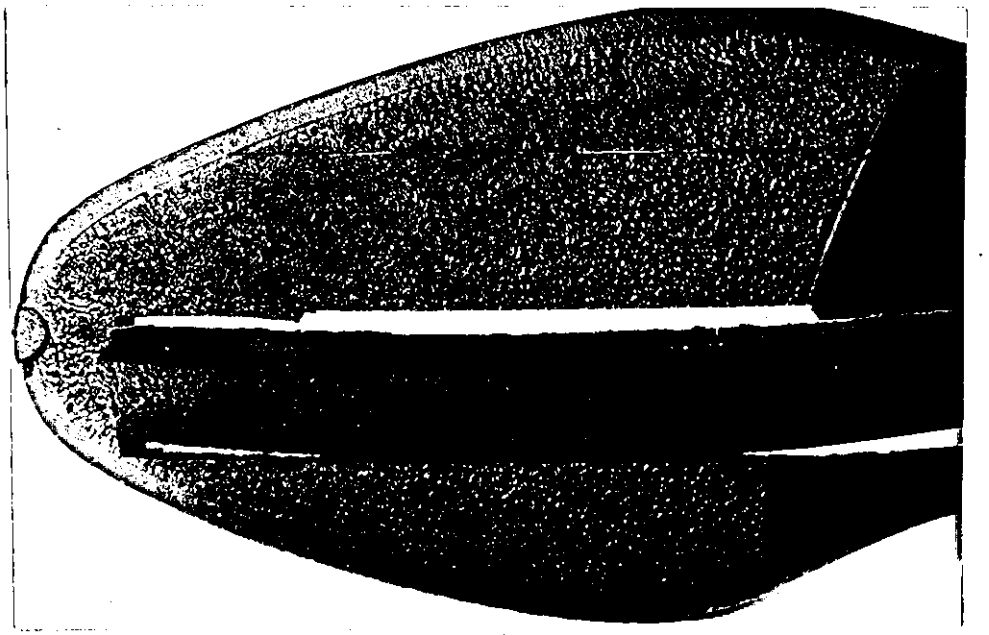

Figure A1.4.

Experimental polyurethane soling compound showing large holes at flexing point of sole.

of the flaw will be slightly less likely in the case of the large hole than in the case of the flaw from the cut glass. Nevertheless, flaws such as those shown in figure A1.4. could be a major cause of failure of solings. Flex cracking failure of a cellular polyurethane of the same compound as that shown in figure A1.4. is shown in figure A1.5. The position of cracking on the sole has been opened up and a hole measuring 4 mm in diameter is seen. Although it cannot be confirmed in this particular example that the large hole has induced cracking, it is certainly true that the hole has contributed to the weakness of the material in this area and hence the subsequent failure of the shoe sole.

In order to determine the reason for the holes, scanning electron microscope photographs were taken on samples which contained some large holes. A general photograph of the hole is shown in figure A1.6. and an enlarged photograph of the edge of the hole in the same sample is shown in figure A1.7. The regular cellular structure of the polyurethane is apparent up to the edge of the large hole and no evidence of collapsed cell structure can be seen around the hole. The most probable mechanism of hole formation is, therefore, that they are due to inclusion of air during the mixing process which results in holes being retained when the sole is moulded.

Gent and Tompkins[102] have recently suggested that a hole can be formed from a bubble of air which is trapped during the mixing and shaping processes. This is thought to be the case with the large bubbles found in the polyurethane soling compounds. During the mixing stage the rubber is a soft, highly viscous liquid, and the dominant forces on the trapped bubble would, therefore, arise from surface tension forces. The gas contained in the bubble would then dissolve into the rubber under increasingly large local pressures as the bubble

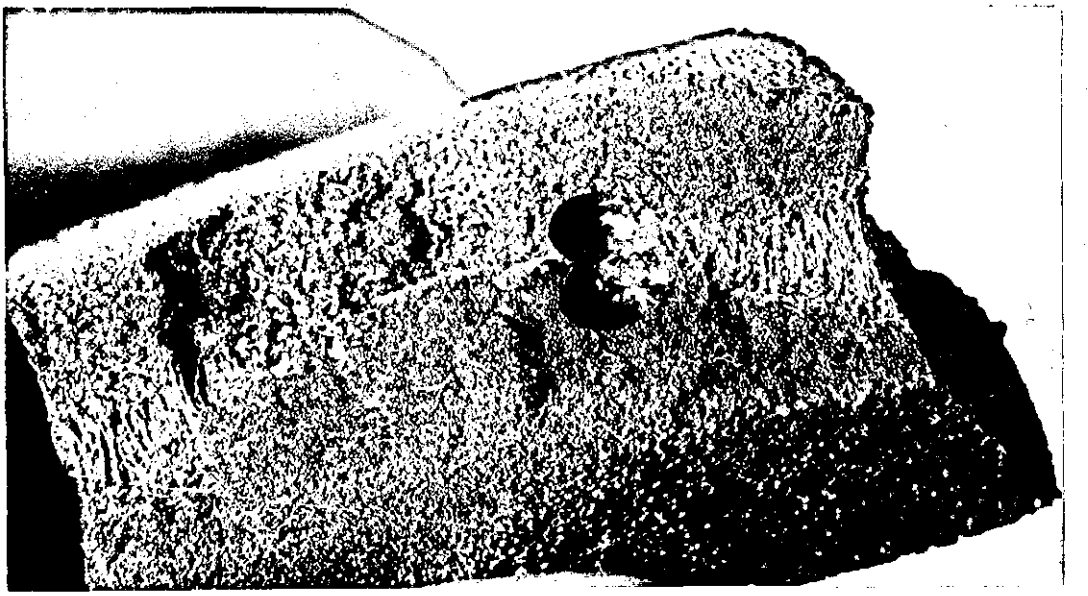

Figure A1.5.

Cross-section of polyurethane soling material across flex cracked edge showing large hole in this area.

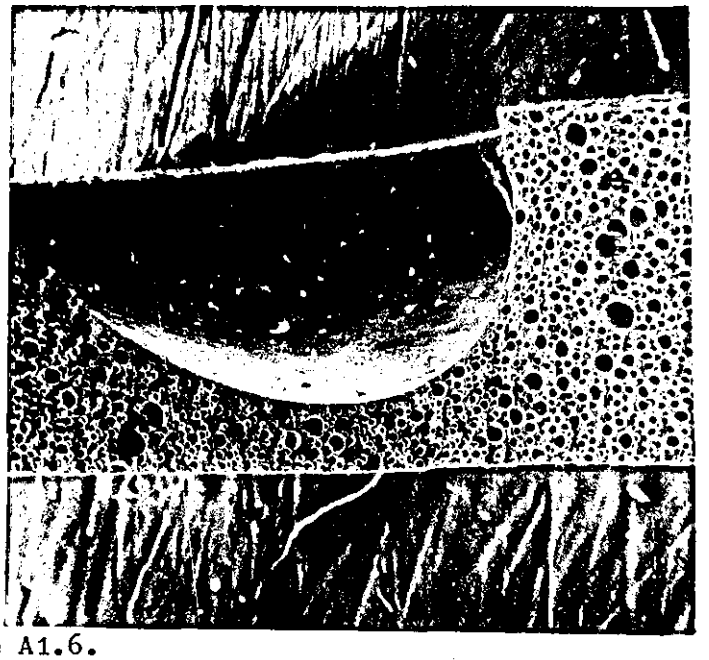

Figure A1.6.

Scanning electron microscope photograph of cross-section of typical polyurethane soling material showing a large hole. Magnification : 34.

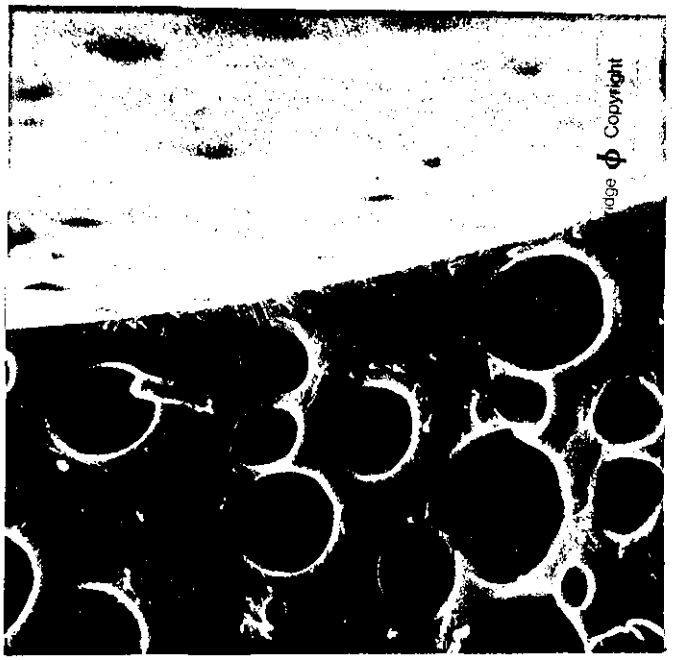

Figure A1.7.

Close up on edge of hole shown in Figure A1.6. Magnification : 525.

Figure A1.8.

Scanning electron microscope photograph at edge of a large hole of a second polyurethane soling material of lower density than the sample shown in Figure A1.7. Magnification : 120.

becomes smaller. As gas diffusion is relatively slow in rubbers, the bubbles may not have completely disappeared when crosslinking occurs and the rubber is transformed into an elastic solid. Their theory predicts that if holes have reached a small initial radius at the time of crosslinking, they decrease in size after crosslinking, but if large holes occur at the crosslinking stage, they are retained in the final product with little decrease in size.

Further confirmation that the large holes are due to air inclusions is shown by the scanning electron microscope photograph in figure A1.8. of a different polyurethane soling compound of lower density than the material shown in figure A1.7.

The photograph in figure A1.8. shows the edge of a large hole similar to that shown in figure A1.7. No sign of any collapsed cell structure around the large hole can be seen. This was also found with the earlier polyurethane compound. Another feature shown in figure A1.8. is that the normal cellular structure of the polyurethane soling which is formed during the reaction stage by either a reaction between the water and isocyanate or by the incorporation into one of the compounds of a volatile solvent has penetrated into the large hole. This would indicate that the large hole existed before the reaction stage of the process and would confirm the view that it was due to an air inclusion in the mixing stage which was retained in the final product.

A1.4. GROWTH OF CUTS FROM STITCH HOLES IN POROMERIC UPPER MATERIALS

One of the problems which is common in unreinforced or non fibrous polyurethane poromerics is growth of cuts from stitch holes in wear. A typical example is shown in figure A1.9. where failure of the shoe has resulted in cut growth from stitch holes at the tab point.

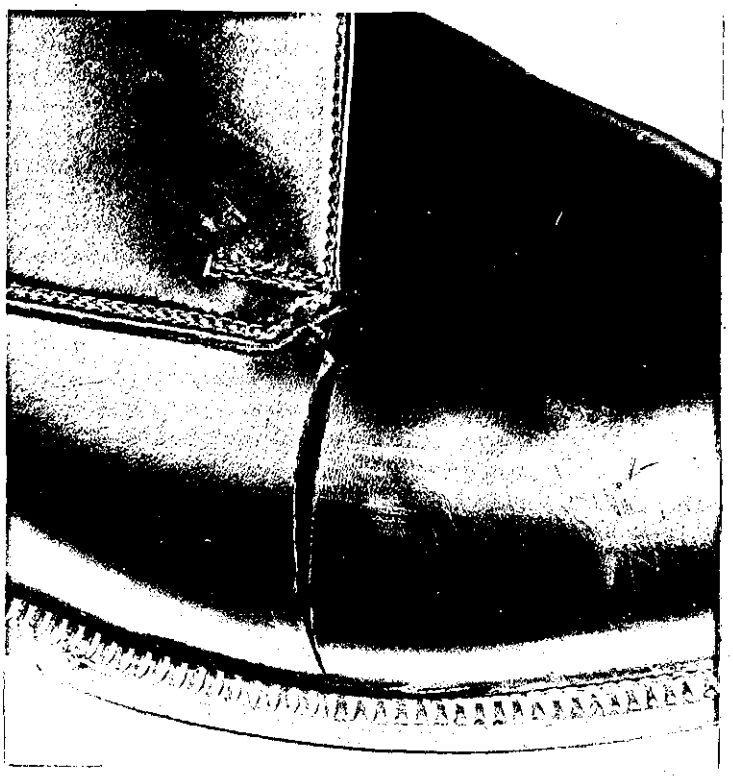

Figure A1.9.

Growth of cuts from stitch holes at tab point in a cellular polyurethane poromeric upper material.

The results are reported in Chapter 6 on the cut growth properties of the homogeneous cellular polyurethane poromeric showed that T_o was about 2 kgf/cm. Using the variation of 2KU with strain for the polyurethane shown in Chapter 6, it has been possible to determine the variation of critical flaw size for cut growth with strain and this is shown by the dotted line on figure A1.2.

The size of a stitch hole in a poromeric upper material can be up to 1 mm in diameter. The critical strain therefore for the start of cut growth from figure A1.2. assuming a 1 mm flaw would be 25%. Measurements at SATRA on upper materials in wear have shown that surface strains on shoe uppers in wear can be up to 40% on the tops of folds and up to 25% at tab points. The tearing energy theory therefore appears to predict to a reasonable degree of accuracy the type of conditions that cause failure in wear.

APPENDIX 2

REVIEW OF THE STRUCTURE OF POLYURETHANE ELASTOMERS

A2.1. INTRODUCTION

The major part of this thesis has reported experimental investigations by the author into the mechanical properties of polyurethane elastomers and has compared these properties with those obtained from vulcanised rubbers. In order to provide a satisfactory explanation for some of the superior properties of polyurethanes, it was necessary to understand their structure and a literature survey was undertaken. A brief review of this literature survey into the structure of polyurethane elastomers is presented in this Appendix.

A2.2 POLYURETHANE ELASTOMERS

The basic research work on polyurethane elastomers was carried out by Bayer and co-workers[103,104] at Leverkusen in West Germany in 1937 when they discovered the di-isocyanate addition polymerisation process. This resulted in the production of several different types of polyurethanes and polyureas and was extremely suitable for the planned build-up of elastomers with segmented structure. Although there are a number of textbooks and papers which deal with the production and properties of polyurethane elastomers in general, it is only in the last few years however that fundamental research work into the physical structure of these materials has been reported.

There are a large number of methods whereby polyurethanes can be produced but the most widely used production method is the reaction of a di- or polyfunctional hydroxyl compound, e.g. hydroxyl-terminated polyester or polyethers with di- or polyfunctional isocyanates. The general structure of a linear polyurethane[105] derived from a dihydroxyl compound HOROH and a diisocyanate OCNR'NCO

can be represented by the following general formula:

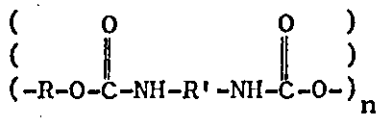

The functionality of the hydroxyl-containing component as well as of the isocyanate can be increased to three or more to form branched or cross-linked polymers such as the rubbers considered in Chapter 2. Other structural changes can also be made. The nature of R for example may be changed drastically in molecular weight or type (polyether, polyester or simple glycol). The nature of R' may also be altered (HDI, NDI, TDI or MDI).

Mainly for these reasons, polyurethanes are unique in that crosslinking, chain flexibility and intermolecular forces can be varied widely and almost independently so that the class of materials known as polyurethane include fibres, soft and hard elastomers, flexible and rigid foams, miscellaneous coatings and highly crosslinked plastics.

Urethane elastomers are usually prepared from a long chain diol such as linear polyester or polyether of molecular weight 1,000 to 2,000, a diisocyanate and a low molecular weight chain extender such as a glycol or diamine. One of the most successful reaction sequences used is that of the prepolymer method[105]. In the first stage of the process, the diol is caused to react with an excess of diisocyanate to produce either a moderate molecular weight liquid or low melting solid termed the prepolymer.

The second step in the process is the addition of a low molecular weight glycol or diamine. The final curing step involves the reaction of the terminal isocyanate groups with active hydrogen-containing groups in the polymer chain, e.g. urethane groups to give allophanate branch points.

A large variety of structures can be built into the polymer chain depending on the nature and molecular weight of the diol and ratios of reactants. The interpretation of the chemistry of elastomer structure was made by Bayer and co-workers[103,104,106,107]. One of the first references to the physical structure of urethane elastomers was by Saunders and Frisch[105] in 1962 who suggested that they should be considered as block copolymers where the length and structure of each block could be controlled within certain limits. A typical elastomer is represented by figure A2.1. in which E designates the repeating ester unit, A the aromatic portion of the isocyanate, U the urethane group, G a glycol extender and UU the allophanate branch point. Thus, the polymer contains a moderately flexible, long, linear polyester segment, then a relatively stiff segment composed largely of aromatic and urethane groups. Branching can occur only at these stiff segments (if the polyester or polyether is linear).

The average length of the stiff aromatic-urethane segment can be controlled, as can the number of branch points. Furthermore, the flexibility of the linear portion may be controlled by the choice of a very flexible polyether or polyesters of moderate to low flexibility. The stiffness of the aromatic-urethane portion may be controlled in part by the choice of isocyanate, e.g. 1, 5-naphthalene diisocyanate providing greater rigidity than 2, 4-tolylene diisocyanate (or, in an extreme case, than 1, 6-hexamethylene diisocyanate). The urethane portion may also serve as a means of control, with greater rigidity being obtained from glycol extenders which contain aromatic nuclei, compared to aliphatic glycols. Even greater rigidity is obtained if an aromatic diamine is used as an extender, giving urea groups in the chain. The amount of crosslinking may be controlled by

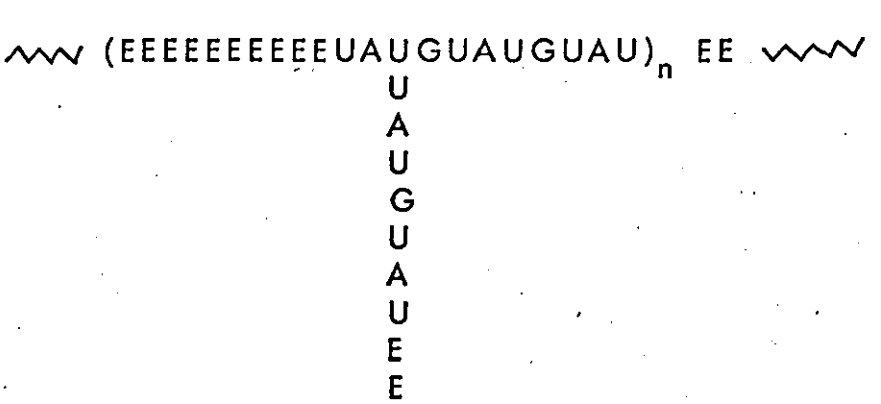

Figure A2.1.

Structure of Urethane Elastomer (After Saunders and Frisch[105])

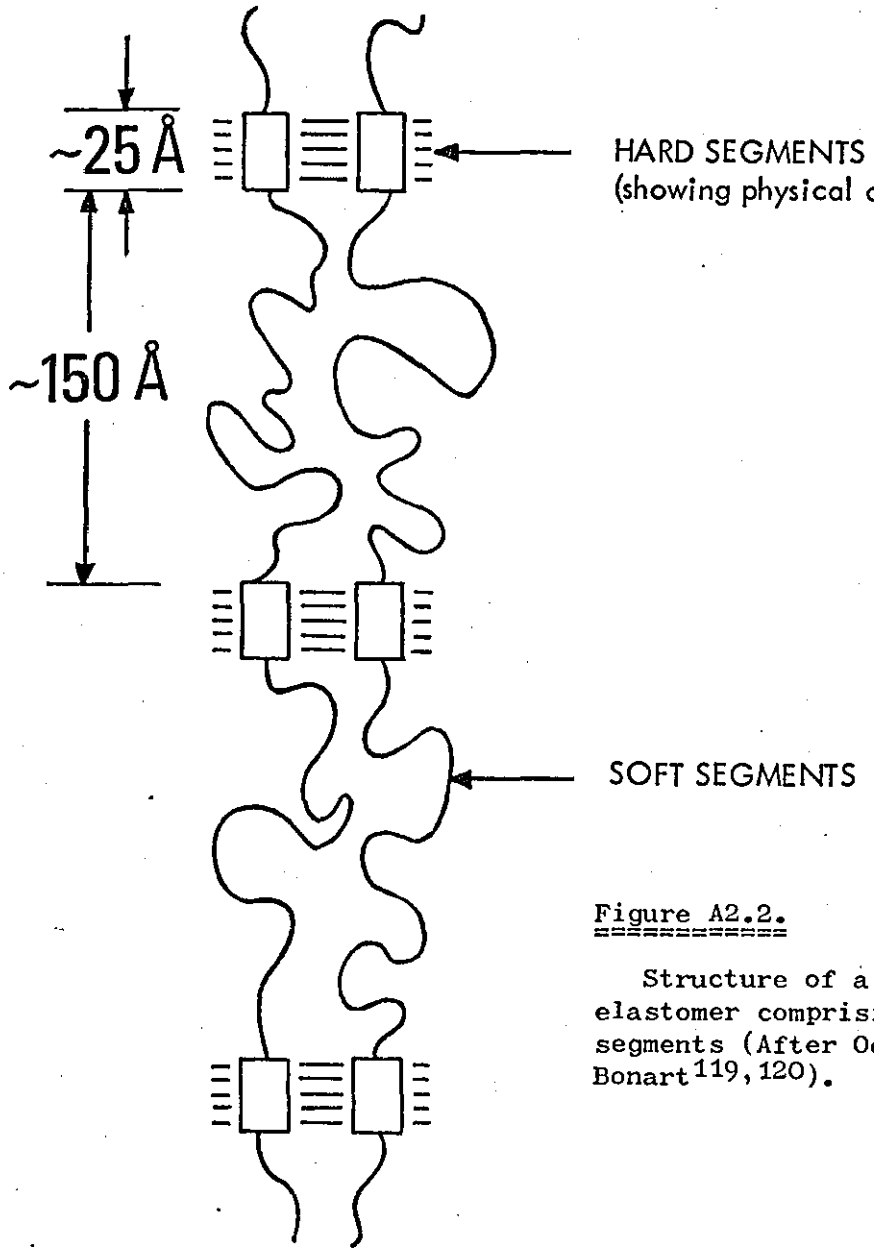

Figure A2.2.

Structure of a segmented urethane elastomer comprising hard and soft segments (After Oertel[114,115], Bonart[119,120]).

adjusting the ratio of isocyanate groups to the total of all active hydrogen groups in the reactants, or by using tri (or higher) functional chain extenders, such as triols.

In terms of polymer interactions, Saunders and Frisch considered that the properties of these elastomers were the result of a combination of segment flexibility, chain entanglement, orientation of segments, hydrogen bonding and other van der Waals forces, the rigidity of aromatic units and crosslinking. The urethane elastomers differ from the more familiar olefin-derived elastomers in that hydrogen bonding and other van der Waals forces play a much more pronounced role in the urethane systems.

One further difference noted in polyurethane elastomers initially by Pigott et al[108] was that increased chemical crosslinking caused a reduction in modulus and strength whereas in hydrocarbon elastomers an increase in degree of crosslinking results in increased modulus. Saunders and Frisch[105] suggested that this was due to a reduction in orientation of the chains and hence a reduction in the probability of obtaining hydrogen bonding and benefit of other intermolecular attractive forces. Therefore with increased chemical crosslinking, a spatial separation of the chains occurs which reduces effective intermolecular attractions. A similar interpretation of the phenomenon has been given by Quant[109]. This observation supports the view that the major portion of the strength of urethane elastomers is due to forces other than primary valence bonding and was confirmed by Schollenberger et al[110].

More recently Dieterich and co-workers[111] at Bayer when discussing the basic chemistry of polyurethane ionomers have suggested that the anomalous increase in permanent elongation with increasing degree of crosslinking is due to the breakage and reformation or slippage of

hydrogen bonds between the hard segments when the polyurethane elastomer is stretched.

Following these early investigations, the physical structure of polyurethanes was discussed by Rinke[112,113], Oertel[114-116] and others[117-120] which led to the general picture for the structure of a segmented urethane elastomer shown in figure A2.2. of hard and soft segments.

The soft segments were formed from the linear polyether or polyester chain segments about 100 - 200Å long which at service temperatures are sufficiently high above their second-order transition temperature, or in the case of crystallisable soft segments above their melting temperature, to give the material an extensibility of several hundred per cent.

The hard segments originate from a diisocyanate and a chain extender or crosslinking agent (e.g. diol or diamine) and hence contain urethane or urea groups. These hard segments are at service temperatures below their second order glass transition point and cause physical interchain reaction which prevents the material from flowing so that elasticity is maintained.

A2.3. X-RAY INVESTIGATIONS

In 1966, on the basis of a fairly detailed study, Shimanskii et al[121], using a range of polyfunctional alcohols and isocyanate noted a specific X-ray diffraction band corresponding to angles of diffraction between 10° and 12° which originate from the hard segments. They went on to postulate that the diffraction band was caused by urethane bridges.

Shimanskii et al also considered the orientation of the macromolecules (presumably hard segments) during the extension of the elastomer and made reference to earlier work by Kazarayan and Tsvankin[122]. They made X-ray studies at zero, 300% and 500%

extension and found an increased ordering of the macromolecules with increase in extension of the polyester urethane.

A similar but more detailed study than that of Shimanskii et al was made independently by Bonart[120] in 1968 who studied the physical structure of crosslinking in two polyurethane elastomers: a mixed polyester and a polyether using the chain extenders ethylene-diamine and hydrazine.

Both in the case of the polyether-based material which showed elongation crystallisation of the soft polyether segment and in the case of the polyester polyurethane which showed a paracrystalline chain arrangement of the soft segments when stretched, an intense 12Å interference line was found. The crystal reflexes associated with the soft segments were only of low intensity. When both polyurethane samples were stretched to about 500% and placed in warm water at 80°C for about 30 minutes, the 12Å interference line still remained fairly intense while the crystallinity in the soft segments disappeared completely. Bonart concluded that the 12Å interference line must be associated with the hard segments and he then proceeded to demonstrate that the interference line was due to a system of hydrogen bridges between the hard segments.

Some of these conclusions were confirmed in the work of Heikens et al[123]. They found that when using diamines as chain extenders, an alternation of the elastic properties occurred corresponding to the number n of the CH_2 groups of the diamine. This led to the conclusions that physical crosslinking between the hard segments not only depends on the concentration of urethane or urea segments but also on the spatial characteristics which either favour or hinder the intermolecular action thus indicating a structural problem which was not only chemical but also physical.

Bonart, Morbitzer and Hentze[124] followed these studies by considering the structure of the crosslinking which results from the use of butanediol - 1, 4 chain extender. By varying isocyanate content, they found from their X-ray measurements that the higher the hard segment content of polyurethane, the less was the likelihood of the soft segment showing stress-induced crystallisation. They postulated that the hard segment content of the material acted as a crystallisation-inhibiting filler.

A2.4. ELECTRON MICROSCOPY INVESTIGATIONS

Considerable attention in recent years has been directed to using the electron microscope for studying the rather complex morphology of block copolymers. Some electron microscopy has been done using surface replication techniques[125-127] but the most extensive work has been done using transmission electron microscopy through thin films. Kato's technique[128-130] of using osmium tetroxide as a chemical staining agent has been applied by many authors studying block copolymers[131-135].

Koutsky et al[136] reported in 1970 some transmission electron microscopy measurements on thin films of segmented polyester and polyether urethane elastomers. They found dark domains of 30 - 100Å width in polyester urethanes and from 50 - 100Å in polyether urethanes which they presumed to be due to the hard aromatic-urethane microphase. The dark domains were similar to those observed in styrene-butadiene block copolymers but the latter were about 300Å in size.

This work provided direct evidence for the existence of a domain structure in polyurethanes which was in agreement with the results discussed above on X-ray, thermal scanning and mechanical properties of polyurethanes.

A2.5. HIGH TEMPERATURE TRANSITIONS

Early work[108,110,137-140] on the modulus-temperature relationships was reviewed by Saunders and Frisch[105]. Of particular importance was that the modulus-temperature curves showed two marked transitions, one occurring below room temperature and one well above 100°C with unusually high modulus values (approx. 10^8 dynes/cm^2) between these temperatures. The low temperature transition is presumably due to the onset of rotation in the flexible polyester or polyether segments whereas the high temperature transition has been ascribed to the dissociation of secondary bonding between the hard segments. The high modulus between the two transition temperatures has also been ascribed to the intermolecular hydrogen bonding between the hard segments.

Clough and Schneider[141] in 1968 made a study of structural ordering and transitions in both polyether and polyester-based compounds by use of rapid scanning thermal methods, light scattering and X-ray diffraction. As well as finding a transition T_1 at -10 to -20°C and the normal transition at about 140°C which they termed T_3, they also found a transition at about 80°C nearer the middle or upper end of the rubbery plateau region which they termed T_2. The T_2 transition had not been shown up in any mechanical measurements reported earlier.

T_1 is usually taken as the major glass transition temperature which is related to the onset of rotation about bonds in the flexible polyester or polyether chains. This has been shown in volume expansion measurements[138] as well as in mechanical measurements[105,142,143] as discussed later, although Miller[144] has suggested that the true glass transition actually occurs at a lower temperature and T_1 only reflects the change from viscoelastic to elastomer mechanical behaviour.

Clough and Schneider[141] considered that T_2 and T_3 should be interpreted in terms of a dissociation of intermolecular secondary bonding. This suggestion is supported by the work of Andrews[145], Tanaka et al[146], Boyarchuk et al[147] and Cooper and Tobolsky[142,143]. The T_2 transition occurring at 80°C is associated with H-bonding between the urethane secondary amine group and the ester carbonyl or ether oxygen of the prepolymer, while the T_3 transition occurring at about 140°C or above is ascribed to interurethane H-bonding. Clough and Schneider[141] suggested that the extent of interurethane bonding and domain structure was higher in polyether than in polyester polyurethanes. They further suggested, however, the larger amount of H-bonding between the urethane and the groups of the polyester chain leads to higher but more temperature-dependent modulus values than in the equivalent polyether-based polyurethane. This they suggest would lead to greater hysteresis in the stress-strain curve in the polyester urethanes compared with the polyether types.

In a later paper, Clough, Schneider and King[148] confirmed by the use of small angle X-ray scattering techniques, the conclusions found in the study above. They found that samples which exhibited a strong T_3 showed relatively strong scattering between T_2 and T_3 which did not diminish in intensity when measurements were made between these two temperatures. They also found that longer urethane segments led to a more intense scattering and thus to a higher degree of domain structure.

A note added to the proof of Clough et al's[148] paper confirmed the view that the transition T_3 was associated with the dissociation of urethane structure. They found a 80% reduction in scattering intensity at 25°C after an Estane 5707 sample had been heated to 180°C for 1 minute compared with that obtained before heating.

Bonart, Morbitzer and Hentze[124] found in their differential thermal analysis (DTA) studies on urethane elastomers using butanediol - 1, 4 as the chain extender that an endothermal transformation at approximately 230°C indicated the melting of the hard segment crystallites whereas the heat distortion temperature (HDT) occurred at about 170°C well below the hard segment melting points and hence was connected with the thermal instability of physical crosslinking in agreement with the work of Clough et al.

In a study of modulus-temperature behaviour, Cooper and Tobolsky[143] in 1966 compared two polyester urethanes with a polystyrene-butadiene block copolymer. For comparison the modulus-temperature behaviour of a typical linear amorphous polymer is shown in figure A2.3. Above the glass transition temperature (T_g), the modulus decreases by a factor of one thousand and approximately at 10^7 dynes/cm^2, there is a slight plateau region due to entanglement interactions. The plateau region generally is strongly altered by changes in molecular weight of the polymer and by crosslinking. A semi-crystalline polymer as shown in figure A2.3. retains a very high modulus until the crystallites melt at T_m. The linear polyester urethanes examined by Cooper and Tobolsky, however, have a high value of plateau modulus as shown in figure A2.3. which was unaccounted for by either crosslinking or primary chemical bonds or the presence of a crystalline phase. The modulus-temperature profile is similar to that found in the polyurethane elastomers in Chapter 5.

Similar results to those obtained on the polyester polyurethane were found in polybutadiene-styrene block copolymers when a high amount of styrene was incorporated and this led Cooper and Tobolsky[143] to conclude that in both systems a similar physical interaction takes place which reinforces the structure until the T_g of the higher

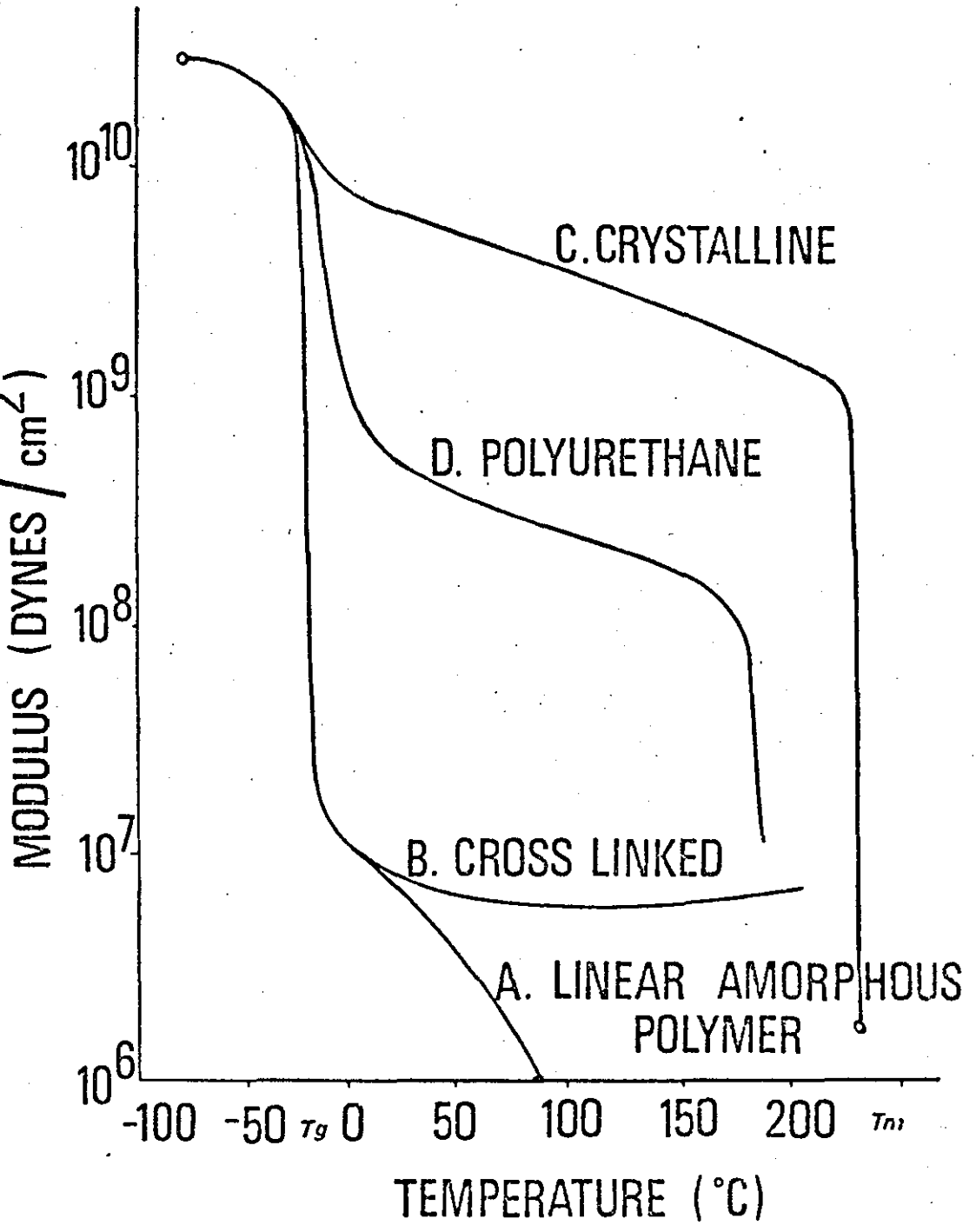

Figure A2.3.

Characteristic modulus-temperature relationships for a number of polymer systems (After Cooper and Tobolsky[142,143]).

modulus block is reached. Moreover, they suggested that hydrogen bonding could not alone account for the general phenomenon but also a proper molecular association of hard and soft regions must occur in amorphous segmented systems in agreement with the earlier work of Bayer[103] and others[105,123] referred to previously. The association of the hard segments in the solid state is required for the occurrence of the second higher temperature T_g which is responsible for the reinforcement of the system, whereas a similar association of the flexible polyester segments influences the low temperature properties.

A similar study on a range of polyurethanes produced by different isocyanates and differing composition and structure of the hard and soft segments was reported by Williams et al[149] in 1968. Their conclusions agreed in general with those presented by Cooper and Tobolsky of the soft segment having its greatest effect on the transition region whereas the hard segment influenced the rubbery plateau and flow behaviour. They found, however, that the modulus-temperature profiles for various linear chain extenders in the MDI capped polyurethanes were different and hence it was thought that hydrogen bonding could not be the only mechanism which held the hard segments together and acted as the points for the soft segments or "pseudo crosslinks". They suggested that the proper molecular association of the hard segments must also be relevant to explaining the properties. They compared the properties obtained from the polyurethane system with those of styrene-isoprene block copolymer in a similar manner to that of Cooper and Tobolsky.

A2.6. STRESS SOFTENING AND BIREFRINGENT MEASUREMENTS

The experimental results presented in Chapters 3 and 5 showed that linear polyurethanes of the type used in poromerics displayed stress softening effects similar to that observed in vulcanised

rubbers. As early as 1960, Trick[150] showed that the modulus of a linear diamine-cured polyurethane decreased on repeated extension whereas a similar system containing crosslinking via triol linkages showed no such effect[151]. This latter material had much lower modulus and tensile properties. These observations have been confirmed in this thesis as the branched polyurethane elastomers referred to in Chapter 2 showed negligible hysteresis and stress softening in direct contrast with the linear polyurethane from poromeric materials.

An interesting investigation into the effect of crosslinking on the stress softening characteristics of styrene-butadiene-styrene and polyester-urethane block copolymer elastomers was made by Cooper et al[152] in 1968. They found that crosslinking had little effect on the stress softening characteristics of these materials until the crosslinking disrupted the aggregated hard segments of the block copolymer. At high levels of crosslinking, reversible stress-strain curves were observed. They concluded that the "modulus enhancement" observed in these block copolymer elastomers appears to lessen as the material exhibits less stress softening.

Birefringence techniques have in recent years been applied to studying styrene-butadiene and styrene-isoprene block copolymers[153,154]. Puett[155] in 1967 used birefringence-stress measurements to demonstrate that the stress-strain behaviour of polyurethanes is partially influenced by the presence of ordered microcrystalline regions.

Estes et al[156] in 1969 showed typical stress-softening behaviour in a polyester-urethane and compared these results with birefringence measurements. The main conclusions from their work were; (1) The birefringence-stress curves were non-linear making the stress optical coefficient stress-dependent; (2) The birefringence-strain curves were remarkably linear up to high strain levels and (3) Considerable

stress softening occurred causing hysteresis in the stress-strain, birefringence-stress and to a smaller degree in the birefringence-strain curves. The similarity in mechanical and optical properties of polyurethanes with other known block copolymer systems led to the overall conclusion that polyurethane elastomers possess a segregated domain structure comparable with that observed in hydrocarbon block copolymers by electron microscopy.

A2.7. CONCLUSIONS

A number of investigations by X-ray diffraction patterns, rapid scanning thermal methods, differential thermal analysis, birefringence and mechanical data have been referred to in this review to show that polyurethane elastomers are composed of hard and soft segments. The hard segments are approximately 25 - 50Å in diameter and contain urethane or urea groups while the soft flexible segments are in the order of 100 - 200Å and are formed from the linear polyether or polyester chain segments. There are therefore similarities in the structure of polyurethane elastomers with other block copolymers such as butadiene-styrene although the size of the hard segments in the latter are of the order of 300Å.

Crosslinking in polyurethane elastomers is obtained by the aggregation of the hard urethane segments through hydrogen bonds, Van der Waal's forces and other intermolecular physical attractions. To obtain high strength, a proper molecular arrangement of hard and soft segments must occur in addition to the hydrogen bonds and other forces between the hard segments. Chemically crosslinking the polyurethane appears to disrupt the molecular arrangement and over a certain critical level, significantly decreases the strength of the material.

Various measurements at high temperatures have shown that two major transitions occur in polyurethane elastomers. The first occurs around -10°C to -20°C and is due to the onset of rotation in the flexible polyether or polyester chain, whereas the second transition at about 160°C is due to the dissociation of the interurethane hydrogen bonding. Two further transitions have also been noted. One at 80°C is ascribed to hydrogen bonding between the urethane secondary amine group and ester carbonyl or ether oxygen of the prepolymer, and the other at 230°C to the melting of the hard urethane segments.

The aggregation of the hard segments also accounts for the high modulus of polyurethanes in the rubbery plateau region. The transition at about 150°C due to the dissociation of the interurethane bonding gives the material a certain degree of thermoplasticity.

REFERENCES

1. A. R. Payne and R. E. Whittaker
J. Inst. Rubb. Ind. 4 107 (1970)

2. R. E. Whittaker
Polymer Age 2 21 (1971)

3. K. F. Buchel
J. of BBSI 17 63 (1970)

4. P. H. Kellett
Rubb. J. 152(4) 61 (1970)

5. L. G. Hole and R. E. Whittaker
J. Materials Sci. 6 1 (1971)

6. A. R. Payne and R. E. Whittaker
Paper 18 in "Non Wovens '71" Edited by P. Lennox Kerr
Textile Press (1971)

7. L. G. Hole
Rubb. J. 152(4) 72 (1970)

8. P. R. Austin
US Patent 2,302,167 (Nov. 17th, 1942)

9. M. Sittig
"Synthetic Leather from Petroleum" Chem. Proc. Review
no. 29 (1969).

10. A. R. Payne and R. E. Whittaker
Rubb. J. 152(4) 89 (1970)

11. A. R. Payne, R. W. T. Skelham and R. E. Whittaker
J of BBSI 17 200 (1970)

12. J. A. C. Harwood, A. R. Payne and R. E. Whittaker
Paper presented to IRI Conference "Advances in Polymer
Blends and Reinforcement" Loughborough (1969)
(Supplementary Contribution to Thesis)

13. A. R. Payne and R. E. Whittaker
J. Composites 1 203 (1970)

14. J. A. C. Harwood, A. R. Payne and R. E. Whittaker
J. Macromol Sci. - Phys. B5 473 (1971)

15. A. R. Payne and R. E. Whittaker
Rubb. Chem. Tech. 44 440 (1971)

16. A. R. Payne and R. E. Whittaker
Trans. Faraday Soc. 66 2383 (1970)

17. J. A. C. Harwood, A. R. Payne and R. E. Whittaker
J. Appl. Poly. Sci. 14 2183 (1970)

18. G. Trappe
Chap. 2 in "Advances in Polyurethane Technology" Edited by J. M. Buist and H. Gudgeon. Maclaren (1968)

19. J. M. Buist and A. Lowe
Br. Polym. J. 3 104 (1971)

20. J. A. C. Harwood and A. R. Payne
J. Appl. Poly. Sci. 12 889 (1968)

21. R. E. Whittaker
To be published

22. J. D. Ferry, E. R. Fitzgerald, L. D. Grandine and M. L. Williams.
Ind. Eng. Chem. 44 703 (1952)

23. T. L. Smith
J. Appl. Phys. 35 27 (1964)

24. T. L. Smith
Rubb. Chem. Tech. 40 544 (1967)

25. F. N. Kelley
Appl. Poly. Symp. No. 1 299 (1965)

26. L. R. G. Treloar
"Physics of Rubber Elasticity" Clarendon Press, London (1958)

27. J. D. Ferry
"Viscoelastic Properties of Polymers" Wiley (1970)

28. A. J. Staverman
Handbuch Der Physik. Edited by S. Flugge Vol. 13 p.432 (1962)

29. K. Dusek and W. Prins
Adv. Poly. Sci. 6 1 (1969)

30. P. J. Flory, C. A. J. Hoeve, and A. Ciferri
J. Poly. Sci. 34 337 (1959)

31. A. V. Tobolsky, D. W. Carlson and N. Indictor
J. Poly. Sci. 54 175 (1961)

32. E. Guth
J. Polymer Sci. C12 89 (1966)

33. W. Prins
"Physics of Non-Crystalline Solids" North Holland Publishing Co., Amsterdam, p.360 (1965).

34. A. J. Chompff and J. A. Duiser
J. Chem. Phys. 45 1505 (1966)

35. M. R. Porter
Private Communication

36. E. Guth and O. Gold
Phys. Rev. 53 322 (1968)

37. R. G. Mitton
J. Soc. Leather Trades Chem 29 169 (1945)

38. G. O. Conabere and R. H. Hall
J. Soc. Leather Trades Chem 30 214 (1946)

39. W. Grassman and E. Zeschitz
Das Leder 5 145 (1954)

40. J. G. Butlin
J. Soc. Leather Trades Chem 43 3 (1963)

41. D. Popplewell and A. G. Ward
J. Soc. Leather Trades Chem 47 502 (1963)

42. R. E. Whittaker
Paper presented to Intersat Conf. "Artificial Leathers"
Blackpool (1971) Published in proc. conference.

43. R. E. Whittaker
Awaiting publication in J. Coated Fibrous Materials

44. P. J. Upstone and A. G. Ward
J. Soc. Leather Trades Chem. 53 361 (1969)

45. R. G. Mitton and C. Price
J. Soc. Leather Trades Chem. 54 44 (1970)

46. F. H. Church,
Trans. Inst. Rubber Ind. 4 533 (1928)

47. H. P. Stevens
Trans. Inst. Rubber Ind. 4 486 (1929)

48. S. A. Brazier
Trans. Inst. Rubber Ind. 6 526 (1931)

49. W. H. Chapman
Rubber Age (London) 28 144 (1947)

50. C. S. Yoran
Rubber Age 63 199 (1948)

51. F. S. Conant and L. A. Wohler
India Rubber World 121 179 (1949)

52. J. A. Talalay
Ind. Eng. Chem. 46 1530 (1954)

53. S. L. Dart and E. Guth
J. Appl. Phys. 17 314 (1946)

54. S. L. Dart and E. Guth
J. Appl. Phys. 18 470 (1947)

55. S. L. Dart, E. Guth and H. A. Robinson
J. Appl. Phys. 18 474 (1947).

56. A. N. Gent and A. G. Thomas
J. Appl. Polym. Sci. 1 107 (1959)

57. A. N. Gent and A. G. Thomas
J. Appl. Polym. Sci. 2 354 (1959)

58. A. N. Gent and A. G. Thomas
Rubber Chem. Technol. 36 597 (1963)

59. A. N. Gent and K. C. Rusch
J. Cell Plast. 2 46 (1966)

60. A. N. Gent and K. C. Rusch
Rubber Chem. Technol. 39 389 (1966)

61. R. S. Rivlin and A. G. Thomas
J. Polym. Sci. 10 291 (1953)

62. A. A. Griffiths
Phil. Trans. Roy. Soc. (London) A221 163 (1920)

63. A. G. Thomas
J. Polym. Sci. 31 467 (1958)

64. H. W. Greensmith and A. G. Thomas
J. Polym. Sci. 18 189 (1955)

65. H. W. Greensmith
J. Appl. Polym. Sci. 7 993 (1963)

66. J. M. Buist
Trans. Inst. Rubber Ind. 33 102 (1957)

67. K. C. Rusch
J. Appl. Polym. Sci. 13 2297 (1969)

68. C. Atkins and D. G. Franks
J. Inst. Rubber, Ind. 3 214 (1969)

69. A. N. Gent and P. B. Lindley
J. Mech. Eng. Sci. 6 318 (1964)

70. A. B. Davey and A. R. Payne
"Rubber in Engineering Practice", Maclaren (1965)

71. J. D. Ferry, L. D. Grandine and E. R. Fitzgerald
J. Appl. Phys. 24 911 (1953)

72. E. R. Fitzgerald, L. D. Grandine and J. D. Ferry
J. Appl. Phys. 24 650 (1953)

73. A. V. Tobolsky and J. R. McLaughlin
J. Poly. Sci. 8 543 (1952)

74. E. Catstiff and A. V. Tobolsky
J. Colloid Sci. 10 375 (1955)

75. W. Aiken, T. Alfrey, A. Janssen and H. Mark
J. Polymer Sci. 2 179 (1947)

76. R. S. Marvin
Proc. Second Intern. Congress Rheology p.156 (1954)

77. T. Alfrey
"Mechanical Behaviour of High Polymers" Interscience (1948)

78. R. Sips
J. Poly. Sci. 5 69 (1950)

79. T. L. Smith
J. Poly. Sci. 20 89 (1956)

80. T. L. Smith
Trans. Soc. Rheol. 6 61 (1962)

81. E. Guth, P. E. Wack and R. L. Anthony
J. Appl. Phys. 17 347 (1946)

82. A. V. Tobolsky and R. D. Andrews
J. Chem. Phys. 13 3 (1945)

83. R. D. Andrews, N. Hofmann-Bang and A. V. Tobolsky
J. Poly. Sci. 3 669 (1948)

84. R. F. Landel and P. J. Stedry
J. Appl. Phys. 17 1884 (1960)

85. J. T. Bergen, D. C. Messersmith and R. S. Rivlin
J. Appl. Poly. Sci. 3 152 (1960)

86. J. D. Ferry
J. Am. Chem. Soc. 72 3746 (1950)

87. J. A. C. Harwood and A. R. Payne
J. Appl. Poly. Sci. 11 1825 (1967)

88. G. J. Lake and P. B. Lindley
J. Appl. Poly. Sci. 8 707 (1964)

89. G. J. Lake and P. B. Lindley
Rubb. J. 146 (10) 24 (1964)

90. A. N. Gent, P. B. Lindley and A. G. Thomas
J. Appl. Poly. Sci. 8 455 (1964)

91. L. Mullins
Trans. Inst. Rubb. Ind. 35 213 (1959)

92. A. G. Thomas
Inst. Phys. and Phys. Soc. Conf. Series no. 1 p.134 (1967)

93. A. G. James
Paper presented at DKG Conference, Weisbaden (1971)

94. J. A. C. Harwood and A. R. Payne
J. Appl. Poly. Sci. 12 889 (1968)

95. G. J. Lake and P. B. Lindley
J. Appl. Poly. Sci. 9 1233 (1965)

96. G. Holden
J. Elastoplastics 2 234 (1970)

97. E. T. Bishop and S. Davison
J. Poly. Sci. C26 59 (1969)

98. J. A. C. Harwood, A. R. Payne and J. F. Smith
Kaut u. Gummi 10 548 (1969)

99. J. R. M. Radok and C. L. Tai
J. Appl. Poly. Sci. 6 518 (1962)

100. G. J. Lake and A. G. Thomas
Proc. Royal Soc. A300 108 (1967)

101. A. Schallamach
Rubb. Chem. Tech. 33 857 (1960)

102. A. N. Gent and D. A. Tompkins
J. Poly. Sci. A2 7 1483 (1969)

103. O. Bayer
Angew Chem. A59 257 (1947)

104. O. Bayer, E. Muller, S. Petersen, H. Piepenbrink and E. Windemuth
Angew Chem. 62 57 (1950)

105. J. H. Saunders and K. C. Frisch
"Polyurethanes, Chemistry and Technology". Interscience (1962)

106. E. Muller, O. Bayer, S. Petersen, H. Piepenbrink, W. Schmidt and E. Weinbrenner.
Angew Chem. 64 523 (1952)

107. O. Bayer and E. Muller
Angew Chem. 72 934 (1960)

108. K. A. Pigott, B. F. Frye, K. R. Allen, S. Steingiser, W. C. Darr, J. H. Saunders and E. E. Hardy
J. Chem. Eng. Data 5 391 (1960)

109. A. J. Quant
SPE Jnl. 15 298 (1962)

110. C. S. Schollenberger, H. Scott and G. R. Moore
Rubb. World 137(4) 549 (1958)

111. D. Dieterich, W. Keberle and H. Witt
Angew Chem. (Int. Edition) 9 40 (1970)

112. H. Rinke
Angew Chem. 74 612 (1962)

113. H. Rinke
Chimia 16 93 (1962)

114. H. Oertel
Textil - Praxis 19 820 (1964)

115. H. Oertel
Melliand Textilber 46 51 (1965)

116. H. Oertel
Bayer Fabrenrev 11 1 (1965)

117. A. F. Smith
Mod. Textiles Mag. 44 47 (1963)

118. A. J. Ultee
Textilindustrie 67 453 (1965)

119. R. Bonart
Kolloid Z 211 14 (1966)

120. R. Bonart
J. Macromol. Sci-Phys. B2 115 (1968)

121. V. M. Shimanskii, S. I. Shkolnik and S. B. Kozakov
Soviet Rubb. Tech. 26 20 (1967)

122. L. G. Kazaryan and D. Y. Tsvankin
Polym. Sci. USSR 5 25 (1964)

123. D. Heikens, A. Meijers and P. H. van Reith
Polymer 9 15 (1968)

124. R. Bonart, L. Morbitzer and G. Hentze
J. Macromol. Sci-Phys. B3 337 (1969)

125. M. Morton, J. E. McGrath and P. C. Julians
J. Polym. Sci. C26 99 (1969)

126. B. D. Gesner
Appl. Polym. Symp. 7 53 (1968)

127. R. Blockland and W. Prins
J. Polym. Sci. A2 7 1595 (1969)

128. K. Kato
Polym. Lett. 4 35 (1966)

129. K. Kato
Polym. Eng. and Sci. 6 38 (1967)

130. K. Kato
Polymer 9 225 (1968)

131. E. Vanzo
J. Polym. Sci. A1 4 1727 (1966)

132. E. B. Bradford and E. Vanzo
J. Polym. Sci. A1 6 1661 (1968)

133. H. Hendus, K. H. Illers and E. Ropte
Kolloid Z 216 110 (1967)

134. J. F. Beecher, L. Marker, R. D. Bradford and S. L. Aggarwal
J. Polym. Sci C26 117 (1969)

135. R. P. Kambour
Poly Lett. 7 573 (1969)

136. J. A. Koutsky, N. V. Hein and S. L. Cooper
Poly Lett. 8 353 (1970)

137. C. H. Smith and C. A. Peterson
Modern Plastics 38 125 (1961)

138. T. L. Smith and A. B. Magnusson
J. Polym. Sci. 42 391 (1960)

139. T. L. Smith and A. B. Magnusson
J. Appl. Polym. Sci. 5 218 (1961)

140. R. F. Landel
J. Colloid Sci. 12 308 (1957)

141. S. B. Clough and N. S. Schneider
J. Macromol. Sci-Phys. B2 553 (1968)

142. S. L. Cooper and A. V. Tobolsky
J. Appl. Polymer Sci. 10 1837 (1966)

143. S. L. Cooper and A. V. Tobolsky
Textile Res. J. 36 800 (1966)

144. G. Miller
Polym. Preprints 8 1072 (1967)

145. R. D. Andrews
J. Polymer Sci. 14 261 (1966)

146. T. Tanaka, T. Yokoyama and K. Kaku
Mem Fac. Eng. Kynshu Univ. 23(2) 113 (1963)

147. Y. M. Boyamhuk, L. Y. Rappoport, V. N. Nikitin and N. P. Apukhtina
Polym. Sci. USSR 7 859 (1965)

148. S. B. Clough, N. S. Schneider and A. O. King
J. Macromol Sci-Phys. B2 641 (1968)

149. B. L. Williams, L. Weissbein and A. Singh
Rubb. Age 100 57 (1968).

150. G. S. Trick
J. Appl. Poly. Sci. 3 252 (1960)

151. R. J. Athey
Rubb. Age 85 77 (1959)

152. S. L. Cooper, D. S. Huh and W. J. Morris
Ind. Eng. Chem. 7 248 (1968)

153. J. F. Henderson, K. H. Grundy and E. Fischer
J. Poly. Sci. C16 3121 (1968)

154. E. Fischer and J. F. Henderson
Rubb. Chem. Technol 40 1373 (1967)

155. D. Puett
J. Poly. Sci. A2 5 839 (1967)

156. G. M. Estes, R. W. Seymour, D. S. Huh and S. L. Cooper
Polym. Eng. Sci. 9 383 (1969).

SUPPLEMENTARY CONTRIBUTION

"Particulate Reinforcement of Polymers".

by

J. A. C. Harwood, A. R. Payne and R. E. Whittaker

Paper presented to the Inst. Rubb. Ind. Conference "Advances in Polymer Blends and Reinforcement" Loughborough. Sept. 1969. Published in the proceedings of the conference.

Particulate Reinforcement of Polymers

By J. A. C. HARWOOD
Avon Rubber Company Ltd.
and A. R. PAYNE
and R. E. WHITTAKER
Shoe and Allied Trades Research Association

Synopsis

This paper mainly reviews the studies of the authors into the mechanisms of strength, reinforcement and hysteresis of fillers in polymers. The subjects discussed include low strain amplitude dependence of modulus and hysteresis, stress-softening effects, the energetics at rupture over a wide temperature range and rate of straining, energy failure envelopes, as well as proposing a physical interpretation of the phenomenon of reinforcement by small particles.

Introduction

Over recent years, studies have been undertaken by many investigators including the authors, into the reinforcement of polymers with fine particulate fillers.

The authors believe that the behaviour of filler particles in rubber at low strains is a completely different mechanism from that occurring at high strains. Moreover they contend that stress-softening in filled vulcanizates, an energy dissipative mechanism at high strains is not to be associated with any rubber-filler breakdown, but can be explained by changes that take place in the rubber phase of the filled vulcanizate. The effect of adding the filler particles to rubber has been to increase the hysteresis exhibited by the rubber both hydrodynamically and visco-elastically. The total hysteresis exhibited by a rubber has been shown to influence greatly the strength, and quantitative relationships between hysteresis and strength have been derived.

This paper presents a review of these studies which previously have only been presented in separate publications, and shows how the combination of these separate studies has led to confirming a previously proposed theory of reinforcement.

Hysteresis Effects at Low Strains

The application of low amplitude sinusoidal oscillations on a rubber vulcanizate results in the ensuing strain lagging behind the stress. This is because of the viscoelastic nature of rubber. The complex shear modulus (G*) of rubber can be expressed in terms of an elastic (in-phase) shear modulus (G') and a viscous (out-of-phase) shear modulus (G'') which for low amplitude sinusoidal strain are related by the following two equations:—

$$G^* = G' + i\,G'' \qquad (1)$$

and

$$\text{Tan } \delta = G''/G'$$

where δ is the phase angle between the sinusoidal stress and strain and tan δ gives a measure of the hysteresis exhibited by a rubber at low strains.

The variation of these dynamic parameters for rubbers containing carbon black filler with strains up to about 10% in shear has been the subject of numerous papers by Payne[1–5]. The in-phase shear modulus (G') decreases with small sinusoidal strain oscillations as shown in Fig. 1 for butyl rubber containing increasing concentrations of HAF carbon black. The effect increases with increasing concentration of carbon black and is associated with properties of the filler particle.

The in-phase shear modulus appears to have a limiting value both at low strains (G_o') and at high strains (G'_∞). The difference between these two limits ($G'_o - G'_\infty$) has been shown to correlate with dispersion of the carbon black filler within the rubber vulcanizate. ($G'_o - G'_\infty$) decreases with improvement in dispersion[6] as estimated from electron microscope and conductivity[7, 8] measurements on filler-loaded vulcanizates.

The variation of out-of-phase shear modulus (G'') with strain is shown in Fig. 2 for a typical series of vulcanizates. G'' passes

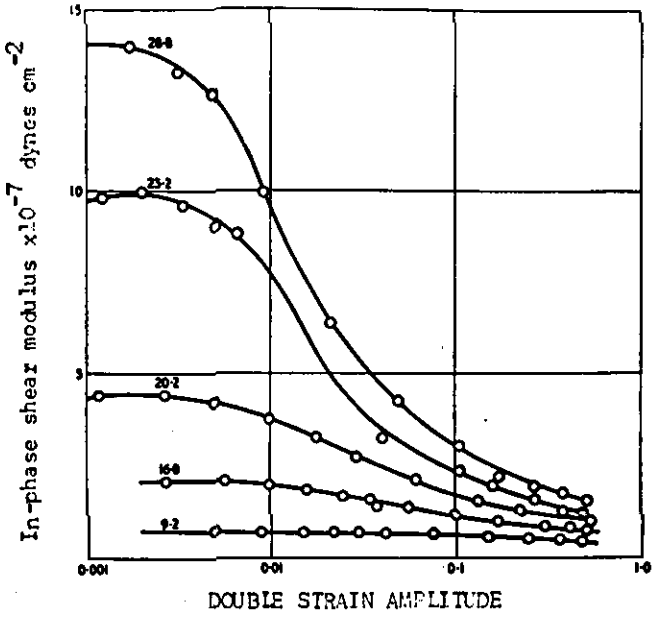

Fig. 1. Variation of in-phase shear modulus (G') with double strain amplitude for a series of Butyl vulcanizates containing HAF carbon black

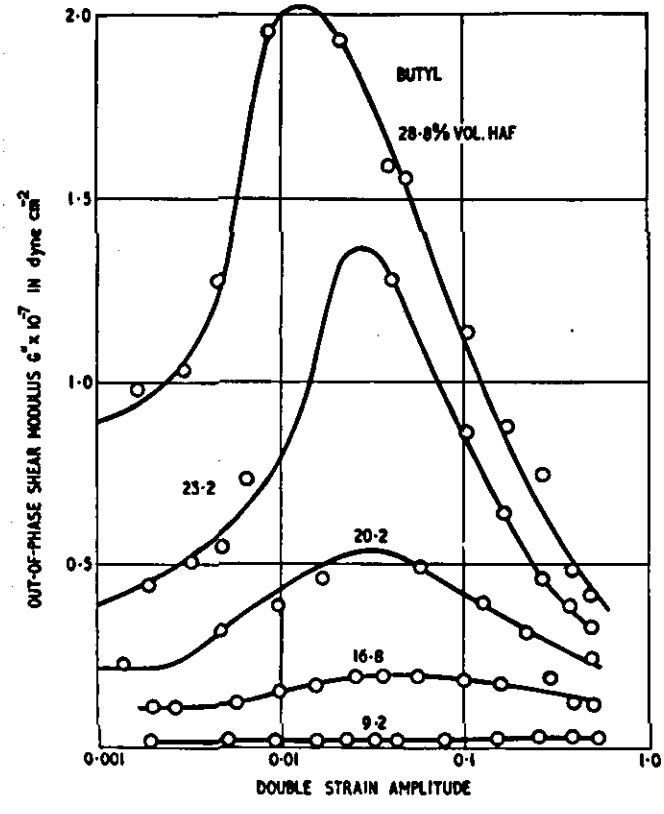

Fig. 2. Variation of out-of-phase shear modulus (G'') with double strain amplitude for a series of Butyl vulcanizates containing HAF carbon black

through a maximum value (G" max.) in the region of strain where G' changes most rapidly. Values of G" max. correlate well with resilience and heat build-up data and are linearly related to the modulus change ($G'_o - G'\infty$) by an equation of the following form

$$G'' \text{ max} = A + B\,(G'_o - G'\infty) \qquad (2)$$

The value of B ranges from 0·1—0·2 depending on the type of mix being used and A is assumed to be the "out-of-phase" modulus of an ideally dispersed vulcanizate. A recent study[9] showed that A had a value of 5×10^5 dynes.cm^{-2}. This effect is the result of a mechanism causing energy dissipation and is attributed to the breakdown and reformation of the three-dimensional or aggregated carbon black structure during the imposed oscillation.

The breakdown and reformation of the carbon black structure has been more clearly demonstrated in a recent paper[10]. It is found that the hysteresis-strain behaviour exhibited by filled rubber vulcanizates can be described by a domain theory proposed by Everett and co-workers[11, 12] which was applied by them to adsorption hysteresis. Fig. 3 shows typical sequences of boundary loops and ascending and descending scanning curves which demonstrate the existence of independent domains within carbon black filled rubber vulcanizates. It should be noted here, however, that there is evidence of stress-softening in the first two cycles at these low strains, but the effect is small and can be neglected compared with the overall effect of the carbon black particle. Stress-softening is much more important at higher strains and will be discussed separately in the next section.

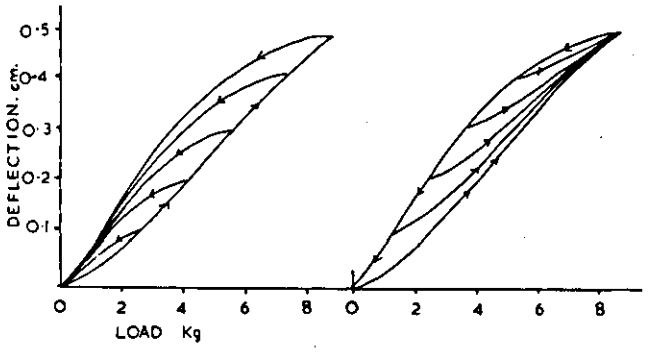

Fig. 3. Typical load-deflection boundary and scanning loops for NR vulcanizate with 60 phr HAF carbon black

Filler agglomeration effects have also been recently demonstrated in other two-phase systems such as carbon-black in low viscosity paraffin[13] and bentonite and stockalite clays in both rubber[14] and water[15]. Fig. 4 shows the effect of bentonite and stockalite clays in water. The shape of the curves are similar to those shown in Fig. 1: $G'_o - G'\infty$ increasing with increasing concentration of clay as observed in the carbon black filled rubber results. Bentonite and stockalite clays are known to form three-dimensional structures when suspended in liquids and the shape of the curves in Fig. 4 is most certainly due to this effect and gives credence to the hypothesis that this effect is the same as that encountered in rubber-filler composites.

A more striking example of this effect was obtained by swelling crystals of phenyl-β-naphthylamine (PBN) into rubber and evaporating off the solvent[16, 17]. The PBN formed fern-like crystal structures within the rubber as shown in Fig. 5 and, on the deformation of this material, produced effects (Fig. 6) analagous to those obtained in the other two-phase systems considered above.

The magnitude of the energy lost (hysteresis) results from the breakdown of this filler structure is difficult to measure accurately but, for an NR vulcanizate containing 50% by volume of carbon black, it has been estimated to be less than 1 joule cm^{-3}. This energy loss, however, is of great importance in the heat build-up of filled rubbers when undergoing rapid flexing at these small strains. Improved methods of dispersing the filler particles within the vulcanizate reduce the effect and measurements of the modulus change at these low strains is being used increasingly in technological development work as a reliable index of dispersion in rubber-filler composites.

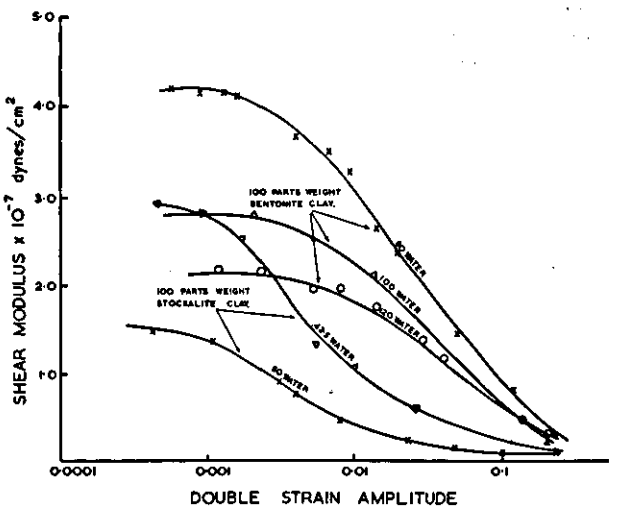

Fig. 4. Variation of shear modulus with double strain ampl for bentonite and stockalite clays suspended in different centrations of water

Fig. 5. Photograph of fern-like crystals of PBN in rubber. Le of line shown 0·1 mm

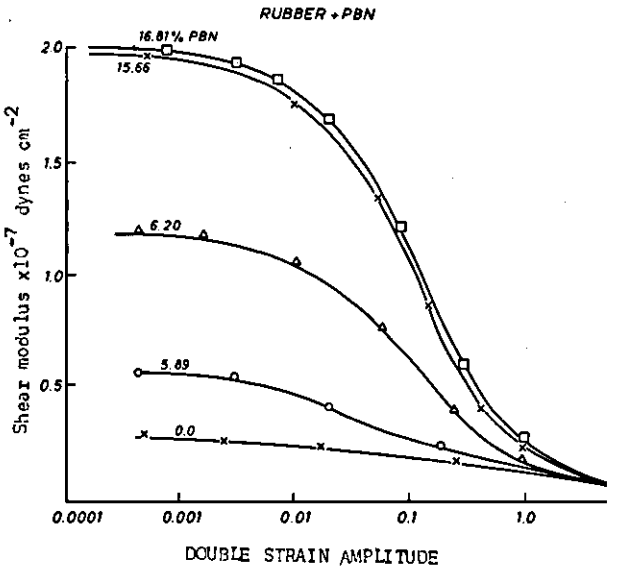

Fig. 6. Variation of shear modulus with double strain ampl for NR containing different amounts of PBN crystals

Stress-Softening Effects

All rubbers, vulcanized or unvulcanized, filled or unfilled, require a greater stress to produce a given elongation in the first extension curve than during subsequent extensions. This well-known phenomenon called stress-softening, which causes an appreciable amount of energy dissipation, is often referred to as "Mullins Effect" in view of the study by Mullins[18, 19] to the phenomenon in filled rubber vulcanizates.

One of the first references to stress softening was by Bouasse and Carriere[20] in 1903 and many investigations into the phenomenon have been reported since. Several recent theories have been proposed to explain stress-softening behaviour in filled rubber vulcanizates. Dannenberg[21], Boonstra[22] and co-workers[23, 24] envisage a slippage of the rubber network chains over the surface of the carbon black particles whilst Kraus *et al.*[25] consider the effect to be the result of several mechanisms, thixotropy involving transient carbon black structures, rupture of network chains connecting filler particles and disruption of the "permanent structure" of the carbon black. Harwood and Payne, however, in a series of recent papers[26–30], claim that most of the stress-softening occurs in the gum phase of filler-loaded vulcanizates leaving little to be explained in terms of breakage or slippage of rubber to filler bonds. The various theories will not be considered in great depth here as the whole phenomenon of stress-softening was the subject of a fairly comprehensive review recently[31].

A typical set of stress-strain cycles are shown in Fig. 7 for NR gum and NR containing 60 phr HAF carbon black. When the curves for the gum and filled rubbers are taken up to the same stress level, it is shown that the amount of stress-softening between the first and third extension cycles (curves 1 and 5) is remarkably similar. Stress-softening in NR has been attributed to crystallisation[23] but the same effect has also been shown to occur in amorphous polymers such as butadiene-acrylonitrile rubber[31] (NBR) and styrene-butadiene rubber[32] (SBR) and in a whole host of other non-crystallising materials.

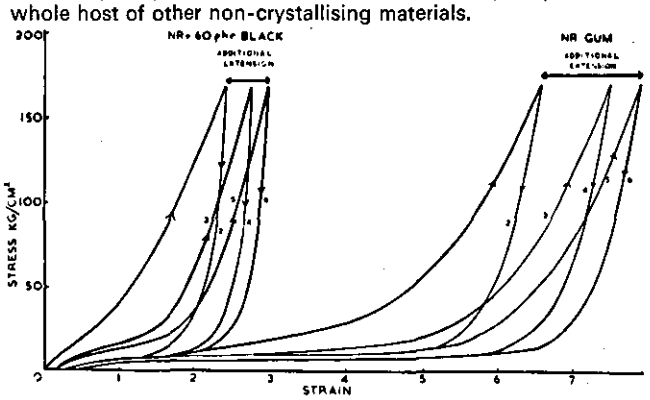

Fig. 7. Stress-strain curves for gum NR and NR containing 60 phr HAF carbon black showing similar stress-softening behaviour

Stress-Softening in Other Materials

Stress-softening has been observed in a wide range of other polymers and fibres. Puett *et al.*[33] showed the normal characteristics of stress-softening occurring in nylon, certain wool fibres and in unfilled, uncrosslinked ethylene propylene block co-polymer films of different degrees of crystallinity.

Recent studies[34] have shown that stress-softening is exhibited in certain shoemaking materials. Fig. 8 shows both the virgin stress-strain curve and a cycled stress strain curve for full chrome leather. Clearly the Mullins Effect or stress-softening is evident here and in this respect leather can be regarded as showing similar properties to polymer. Leather consists of a network of interlaced protein (collagen) fibres[35] which are made up of various interconnected sub-units known as fibrils, photofibrils and filaments. In addition to molecular bonds connecting the molecules in the fundamental chains, other bonds known as hydrogen bonds tie the chains, fibrils, photofibrils, etc. together. These bonds are not as strong as the molecular bonds but they do provide sufficient cross-ties between the sub-units. In the presence of moisture the interchain H-bonds being fairly weak often rupture. On drying in an extended or distorted condition, there is reformation of the interchain H-bonds and hence a new secondary network is produced. This behaviour is completely analagous to the labile crosslinks obtained in a polysulphide vulcanizate as discussed below.

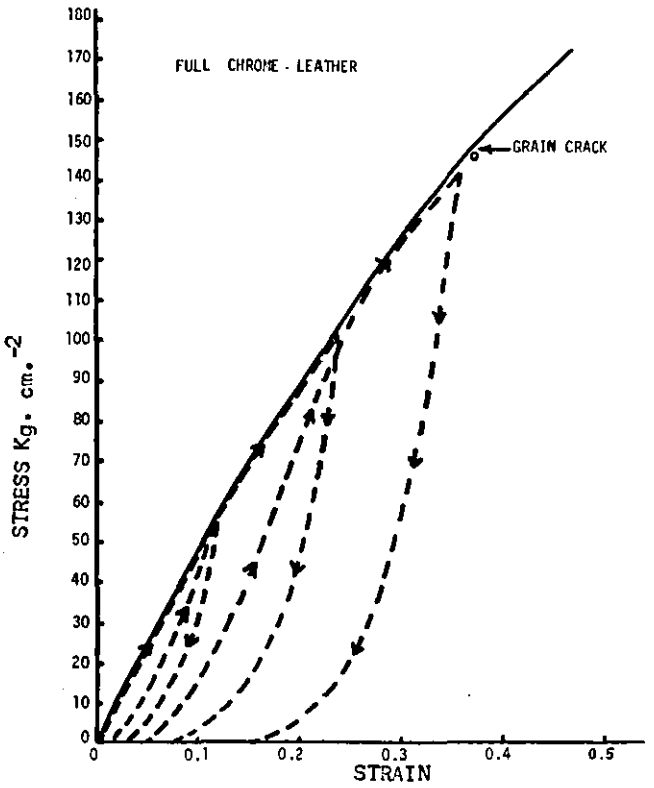

Fig. 8. Stress-strain curves for full chrome leather showing stress-softening behaviour

The stress-softening effect has also been demonstrated in a poromeric material[34] such as "Corfam"* or "Clarino"* shown in Fig. 9. These materials exhibit similar properties to leather and are being used increasingly in the shoemaking industry. These materials are based on viscoelastic polyurethane but are different from rubber in that they have a non-uniform structure. Corfam, for example, consists of a polyurethane foam layer, a fabric interlayer consisting of mainly polyester fibres with a little cotton and a base layer consisting of randomly orientated polyester fibres held together by a polyurethane binder. The energy losses observed in a poromeric material are associated with the movement of polymer chains, crosslinks and entanglement points when the poromeric is stressed. The permanent set obtained is due to the very wide distribution of relaxation times exhibited by the viscoelastic response of the polyurethane molecule and the presence of hydrogen bonds between neighbouring chains which break under mechanical stress[36] and in presence of moisture as discussed for leather.

Mechanism of Stress-Softening

Harwood and Payne[28] have shown that stress-softening in unfilled rubber vulcanizates can be partially recovered by heating the samples in vacuo for about twenty-four hours. They further found that it was possible to recover completely the stress-softening in unfilled vulcanizates containing predominantly monosulphide crosslinks and carbon-carbon crosslinks. However, only partial recovery was observed in polysulphide crosslinked rubbers. The recovery of stress-softening indicates that no basic breakdown process has occurred and is hence attributed to quasi-irreversible rearrangement of molecular networks due to localised non-affine deformation. This results from short chains reaching the limit of their extensibility leading to a relative displacement of the network junctions from their initial random state. The incomplete recovery in the case of polysulphide vulcanizates is attributed to the breakage of crosslinks and their reformation in the extended state to create a secondary network[37–40]. Similar behaviour is expected in poromeric materials due to the weak hydrogen bonds in polyurethane.

The recovery of stress-softening in filled vulcanizates by both heating and swelling treatments is demonstrated in Fig. 10. The stress on the second extension curve and on the curves after heat and swelling treatments is plotted against the stress occurring at the same strain on the initial extension curve, hence

*Registered Trade Marks

providing a convenient method of comparison for an NBR rubber filled with 60 phr ISAF carbon black. At low stresses recovery is complete and in fact in the case of NBR, over-recovery is obtained but at the higher stresses there is only partial recovery and permanent stress-softening still remains.

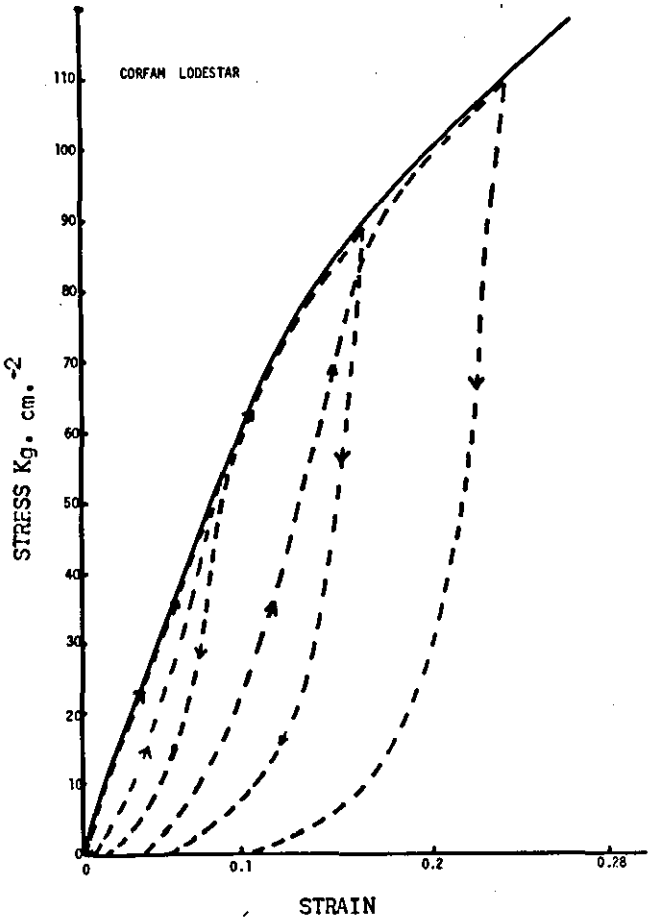

Fig. 9. Stress-strain curves for Corfam Lodestar showing stress-softening behaviour

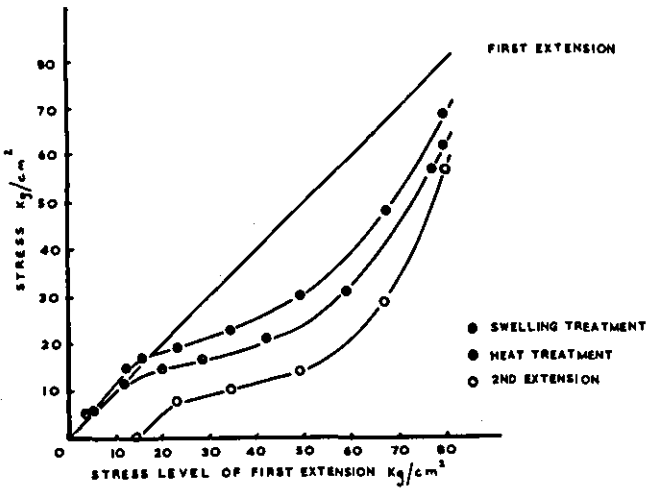

Fig. 10. Partial recovery of stress-softening by heat and solvent treatments for NBR filled with 60 phr ISAF carbon black

The recovery at low stresses is presumably the recovery of the carbon black aggregates referred to previously. The recovery of the molecular network after rearrangement at the higher stresses is very likely hindered by the presence of the filler particles and complete recovery is not obtained. The formation of the filler structure in the extended state limits recovery presumably in a similar way to the secondary network produced by labile crosslinks.

Stress-softening, therefore, in filler-loaded vulcanizates with weak crosslinks, can be accounted for by three main mechanisms:

1. Rearrangement of the rubber network associated with slip of entanglements and non-affine displacement of net junctions in the rubber matrix. This occurs in gum vulcani and the gum phase of filler-loaded vulcanizates.
2. Structural changes of the carbon black aggregates. Th associated with the possible breakdown and reformatic filler domains.
3. Breakage of weak crosslinks such as hydrogen bonds, type links and polysulphide crosslinks.

The other mechanisms proposed by Boonstra and Dan berg[21–24] of the slippage of rubber chains on the carbon l surface or breakage of rubber to filler bonds proposed by Beu Kraus[25], therefore, can only account for a very small fraction c energy losses and are hence thought unlikely.

Fig. 11 shows a photograph of a network of string which pro an interesting model for stress-softening in unfilled vulcaniz Knots have been tied between two pieces of string so that a acts as a tetrofunctional crosslink point. The lengths of s between the knots are randomly varied so that some piec string between the crosslinks are short whilst others are lengthy. The network of string was inserted between the of an Instron Tensile testing machine and stress-cycle produce the curve shown in Fig. 12. The type of curves sh in Fig. 12 are clearly similar to those obtained on material sys referred to earlier.

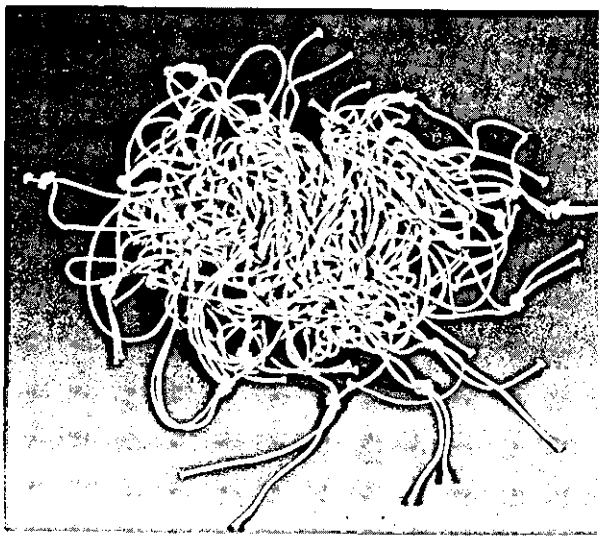

Fig. 11. Model system of knots tied in string to demon stress-softening effects

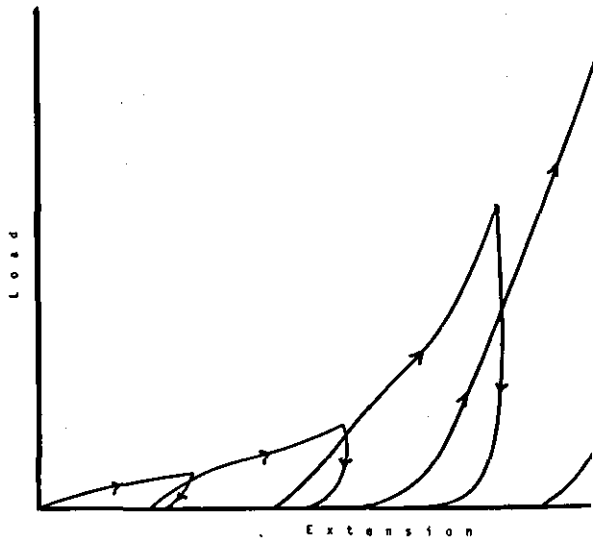

Fig. 12. Stress-strain curves obtained from model system of in string shown in Fig. 11

Effect of Fillers on Strain at Break

T. L. Smith[42] and others[43] over recent years have developed the concept of a "failure envelope" which is a unique curve peculiar to each polymer relating the stress at break (σ_B) or real stress at break $\sigma_B(1 + \varepsilon_B)$ to the strain at break (ε_B) over a wide range of temperature and rate of strain. It was found by Harwood and Payne[44, 45] that a quantitative relationship between the failure parameters could be obtained by using work done (or energy density) to break (U_B) instead of stress at break.

Fig. 13a shows the energy input to break plotted against the strain at break for SBR containing increasing amounts of HAF carbon black. The energy input to break is multiplied by the ratio between the chosen reference temperature (294°K) and the experimental temperature to allow for the temperature dependence of rubber-like elasticity as predicted by the kinetic theory[46]. It is found that as the temperature is increased, the failure points for the gum rubber move clockwise around an envelope passing through a maximum strain (ε_a (max)) at a temperature of about 0°C. The results for the filled rubbers lie along lines parallel to the gum rubber.

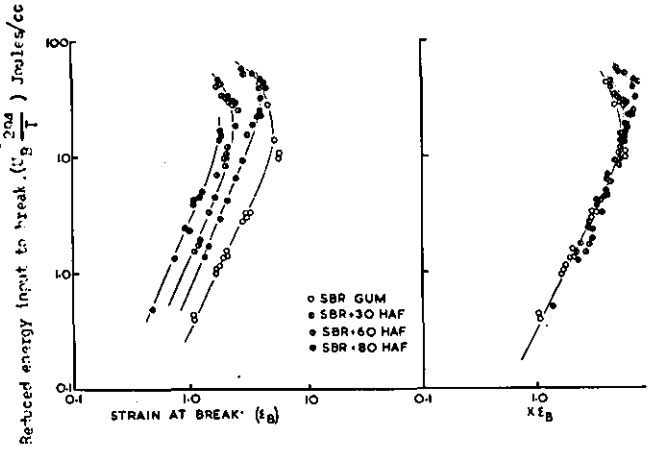

Fig. 13. Variation of reduced energy input to break with (a) strain at break, (b) strain at break corrected by hydrodynamic factor for SBR with 0, 30, 60 and 80 phr HAF carbon black

Mullins and Tobin[47] have shown that Young's modulus of carbon black filled rubber vulcanisates can be expressed in terms of the modulus of the unfilled rubber by use of an expression from hydrodynamic theory developed by Guth and Gold[48] relating the viscosity of a liquid containing hard spherical particles to that of the liquid alone

$$X = 1 + 2{\cdot}5c + 14{\cdot}1c^2 \qquad (3)$$

where c is the volume concentration of filler.
It was found by applying this factor X to the strain axis in Fig. 13a, the gum and filler loaded results coincided as shown in Fig. 13b for strains up to ε_B (max.). The slope of the graph on the log scales was found to be 2 and hence the relationship between energy input and strain at break can be expressed as

$$\left(\frac{294}{T}\right)U_B = A\left(X\,\varepsilon_B\right)^2 \qquad (4)$$

where A is a constant. This type of relationship has also been found to hold both in other amorphous polymers such as NBR and also in crystalline polymers such as natural rubber[49].

Mullins and Tobin[47] have suggested that when the factor X is applied to filled vulcanizates, it takes account of both the disturbance of the strain distribution and the absence of deformation in that fraction of material composed of filler. It is shown in Fig. 13b that the results at low temperatures do not coincide and this indicates that the hydrodynamic correction factor X is too large when the moduli of the filler and rubber approach parity[50]. The bulk strains at break, therefore, of the filled and unfilled rubbers are related by a factor X under conditions of constant energy input. It must be remembered that when this type of agreement is obtained, the temperature of the filler loaded rubber is always higher than that of the unfilled rubber.

Effect of Changing Degree of Crosslinking

In view of the apparent good agreement between data from filled and unfilled rubbers by using the failure envelope approach outlined above, it was decided to investigate[47] the effect of changing the degree of crosslinking on this type of graph.

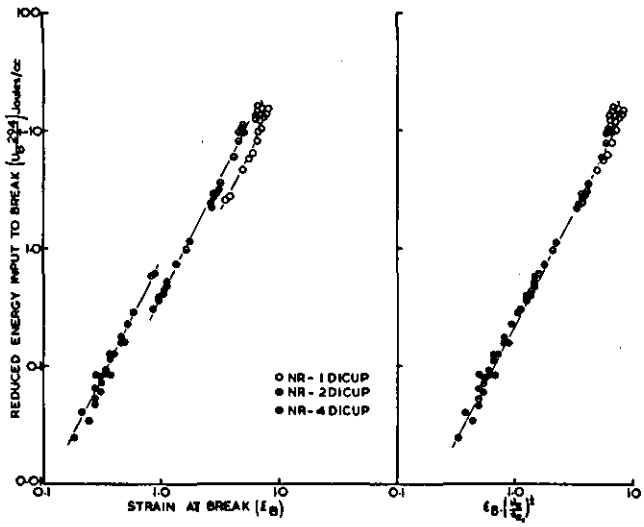

Fig. 14. Variation of reduced energy input to break with (a) strain at break, (b) strain at break multiplied by crosslinking correction factor for NR vulcanized with 1, 2 and 4 phr dicumyl peroxide

Fig. 14a shows results of energy input and strain at break for three NR gum compounds vulcanized with 1, 2 and 4 phr dicumyl peroxide ("dicup") to produce carbon-carbon crosslinks tested over a range of temperatures from 21°C to 140°C. The crosslinks in a dicup vulcanizate are non-labile and have no extra linkages such as the cyclic sulphides that occur in polysulphide vulcanizing systems. The results as in the case of the polysulphide rubbers shown above produce a square law relationship up to the finite extensibility of the network ε_B (max.) but the individual lines for the three vulcanizates are displaced along the strain axis. It has been shown[51] that the maximum elongation of the rubber network is proportional to $N^{\frac{1}{2}}$ where N is the number of links in a monomer chain and is, therefore, inversely proportional to $\sqrt{e^{\frac{1}{2}}}$ where $\sqrt{e}$ is the number of chains per unit volume of the rubber network. As the lines in Fig. 14a are parallel up to the maximum elongation of the rubber network, their strains up to this position should, therefore, be in the ratios of their respective $\sqrt{e^{\frac{1}{2}}}$ values. Porter[52] has obtained values of $\sqrt{e^{\frac{1}{2}}}$ from measurements of C_1 in the well-known Mooney-Rivlin equation and the ratios for the three dicup rubbers used there are given as

$$\sqrt{e_4}/\sqrt{e_1} = 3{\cdot}08$$

$$\sqrt{e_2}/\sqrt{e_1} = 1{\cdot}67$$

where $\sqrt{e_1}$ refers to value of $\sqrt{e}$ for the 1 phr dicup vulcanizate.

The strains at break for the 2 and 4 phr dicup vulcanizates were multiplied by the square root of this ratio and the results are shown in Fig. 14b. The agreement between the vulcanizates on this type of plot is good and the equation of the line for different crosslink densities can be expressed as

$$\left(\frac{294}{T}\right)U_B = C\left(\frac{\sqrt{e}}{\sqrt{e_1}}\right)\varepsilon_B^2 \qquad (4)$$

when the rubbers are referred to the 1 phr dicup vulcanizate and where C is a constant.

This type of relationship was also found to hold for polysulphide vulcanized NR and hence by combining equations (3) and (4) it can be shown that the equation

$$\left(\frac{294}{T}\right)U_B = D\left(\frac{\sqrt{e}}{\sqrt{e_1}}\right)\left(X\varepsilon_b\right)^2 \qquad (5)$$

is applicable to all vulcanizates of different degrees of crosslinking of one curing system both filled and unfilled with carbon black when referred to the 1 phr vulcanizate and where D is a constant.

Effect of Fillers on Total Hysteresis

When a viscoelastic material such as rubber is deformed by the application of a force, some of the mechanical work required is stored in the material and the remainder is dissipated as heat. This energy dissipation or hysteresis results from several different mechanisms which are dependent on the type of material and the

experimental conditions. A measure of this quantity can be obtained from the area of the loop between the extension and retraction curves in a single tensile stress-strain cycle.

The major sources of hysteresis in filled rubbers can be listed as follows:

1. Viscoelasticity
   This becomes increasingly important as the temperature of test is lowered.
2. Crystallisation
   This occurs in some rubbers (e.g. natural rubber) when they are stretched and the molecules align.
3. Breakdown of filler aggregates
4. Changes in network configurations (stress-softening)
5. Changes in network structure (i.e. the breakage of weak crosslinks such as a polysulphide crosslink).

The last three processes have been discussed in the previous sections. Processes (1) and (2) are well documented[53–55] and will not be discussed further in this review.

It has been found that the strength of a rubber vulcanizate is not dependent on any individual contribution to the energy dissipation but is dependent on the combined effect of all the processes which are applicable to the particular rubber and experimental conditions used.

The energy input to break (U_B) is related to the hysteresis at break (H_B) for amorphous polymers by the relationship[44, 56]

$$\left(\frac{294}{T}\right)^{\frac{1}{2}} U_B = K H_B^{\frac{3}{2}} \qquad (6)$$

where K is a constant.

This is demonstrated in Fig. 15 where log $U_B\frac{294}{T}$ is plotted against log $H_B\frac{294}{T}$ for SBR containing increasing amounts of HAF carbon black.

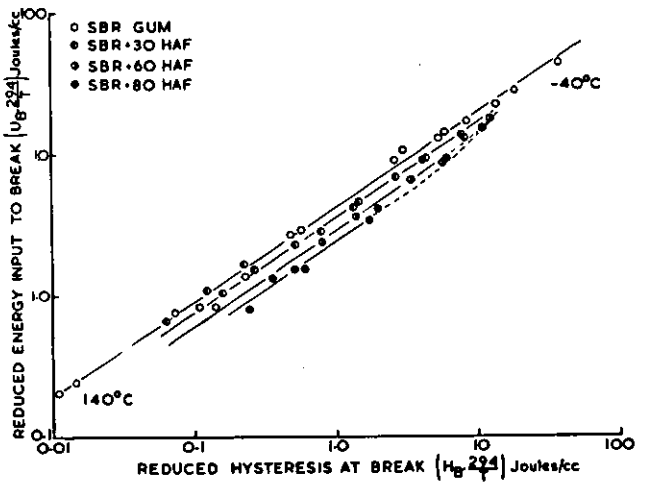

Fig. 15. Reduced energy input to break as function of reduced hysteresis at break for SBR containing 0, 30, 60 and 80 phr HAF carbon black

Equation (6) can be rewritten in terms of hysteresis ratio (h_B) where

$$h_B = H_B/U_B$$

to yield

$$\left(\frac{294}{T}\right) U_B = K^3 h^2_B \qquad (7)$$

The maximum value of $U_B\frac{294}{T}$, therefore, occurs when all the work done in stretching the rubber is dissipated ($h_B = 1$) and is, therefore, equal to K^3. This is thought to occur at the glass transition temperature of the polymer[44].

The results for the filled rubbers are displaced from the gum rubber, the displacement increasing with increasing concentration of carbon black and it was found that by dividing the hysteresis by the factor X used in the previous section, the results for the gum and filler-loaded rubbers coincided[44, 45]. Some disagreement is noticed at higher energies (low temperatures) and this is presumably due again to the hydrodynamic correction being too large when the moduli of the rubber and filler particle approach parity. The relationship therefore for gum and filler-loa rubbers can be expressed as

$$\left(\frac{294}{T}\right)^{\frac{1}{2}} U_B = K\left(\frac{H_B}{X}\right)^{\frac{3}{2}}$$

Values of energy density and hysteresis measured before fa have been shown not to obey any of the above equations and hence equations (6) to (8) have been found to represer excellent description of failure.

The lowest values of U_B recorded agree with values rece given in a theory by Lake and Thomas[57] for a lower limit of tea energies (To).

(To) can be expressed as the energy required to produce area of new surface and defines a fatigue limit below which fatigue life under repeated stressing can be virtually indefi

(To) has values ranging from $1—5\times10^4$ ergs and is related minimum value of energy input to break (U_B (min.)) for a te test piece by the following relationship[58, 59]

$$U_B\,(\text{min}) = \frac{To}{2\pi Co}$$

Co is the "characteristic flaw size" and for SBR is give $5{\cdot}5\times10^{-8}$ cm. Hence for SBR, values of U_B (min) range 0·04 to 0·15 joules cm^{-3}. The lowest experimental value SBR gum has been found to be approximately 0·15 joules c

The failure equations, therefore, appear to represent a criterion of failure between the upper limit of a totally hyster system and a lower limit which is in accordance with calcul values of other limiting parameters.

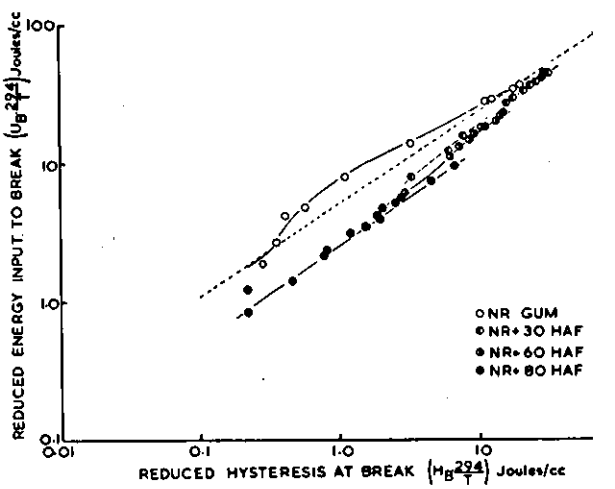

Fig. 16. Reduced energy input to break as function of red hysteresis at break for NR containing 0, 30, 60 and 80 phr carbon black

Equations (6) to (8) are not applicable to natural rubber[30], in the temperature range 80°C—140°C as demonstrated in Fi Within this temperature region, the hysteresis at break has found to be less than predicted. This anomalous behavio not obtained in non-crystallising isomerised natural rubber indicated by the dotted failure line on Fig. 16, and is h attributed to the ability of NR to crystallise at high strains i region 80°C—140°C. The bulk of the polymer remains a phous whilst the highly strained regions around the inh flaws in the sample crystallise[60]. Outside this temperature r the rubber is either predominantly crystalline (low temperat or predominantly amorphous (high temperatures). The re for NR with 30 and 60 phr HAF carbon black show si anomalous behaviour[49] and only follow curves of slope app mately $\frac{2}{3}$ at temperatures above 100°C. The addition of 8 carbon black in natural rubber appears to suppress or co the anomalous crystallisation behaviour and yield a line of $\frac{2}{3}$ similar to that obtained in amorphous polymers.

The correction factor X can be eliminated by combining equa (3) and (8) to yield

$$\left(\frac{294}{T}\right)^{\frac{1}{2}} \qquad U_B = F\left(H\varepsilon_B\right)^{\frac{1}{2}}$$

where F is a constant. This equation unlike equations (6) t is not a sensitive description of failure but is applicable rubbers both filled and unfilled and eliminates uncer associated with a hydrodynamic correction factor.

The Application to Reinforcement Theory

At the same reduced energy input to break, the bulk hysteresis of gum and filler-loaded rubbers are related by a hydrodynamic correction factor as indicated by equation (8). This can also be expressed by the fact that at the same reduced energy input to break, the bulk hysteresis of the gum rubber and the hysteresis of the rubber phase of the filler-loaded rubber is the same. An important point, however, is that this relationship only applies when the temperatures of the gum and filler loaded rubbers are different. This is demonstrated in Fig. 17 where the temperature difference between SBR gum and SBR with 30 phr HAF carbon black to obtain the same energy input to break is plotted against the temperature of the gum rubber. Hence it is shown that in order to obtain agreement by the hydrodynamic correction factor both in the case of the strain at break (equation 4) and in the case of hysteresis at break (equation 8), the temperature of SBR with 30 phr HAF carbon black must be at least 40°C above that of the unfilled rubber.

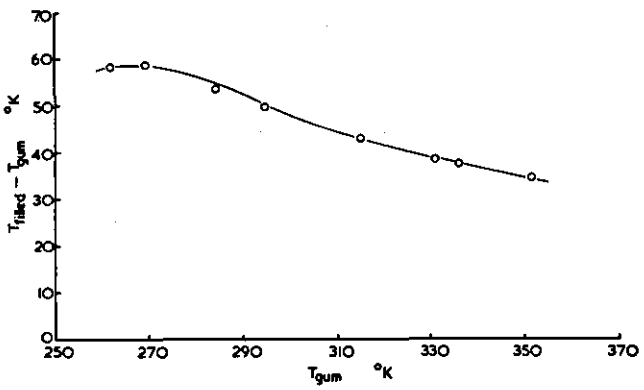

Fig. 17. Temperature difference between SBR gum and SBR containing 30 phr HAF carbon black as function of temperature of the gum rubber when both vulcanizates exhibit the same energy input to break

The effect of temperature is better demonstrated in Fig. 18 where log energy input to break (U_B) is plotted against temperature for SBR gum and SBR filled with 30 phr HAF carbon black. At temperatures above room temperature the energy input to break of the filled rubber is approximately an order of magnitude above that of unfilled SBR. Similar results have also been shown[45] to occur when stress at break is plotted against temperature.

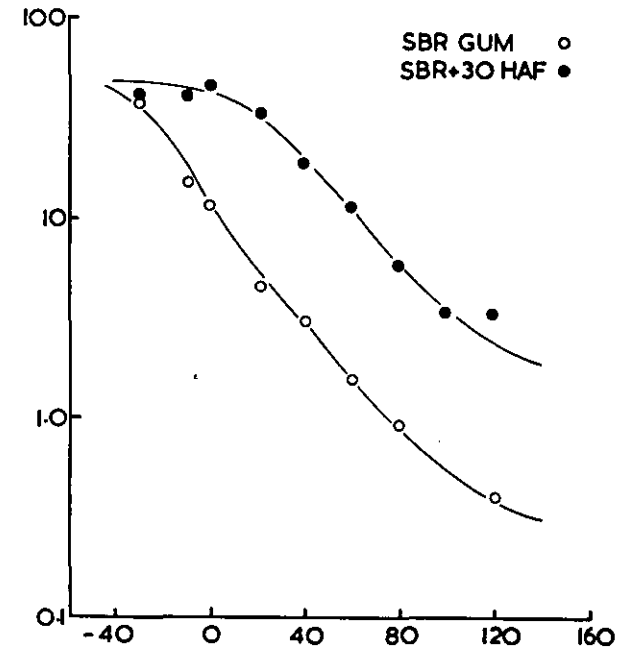

Fig. 18. Energy input to break as function of temperature for SBR and SBR containing 30 phr HAF carbon black at a strain rate of 300% per sec.

Because of the interdependence of time and temperature[58] in viscoelastic materials, the curves shown in Fig. 18 were of necessity obtained at one extension rate (300% per minute). The behaviour of filled and gum SBR vulcanizates with respect to extension rate, or time as distinct from temperature is illustrated in Fig. 19. Reduced energy input to break is plotted as a master function of the logarithm of reduced time to break (log t_b/a_T) in a tensile test. To obtain the master function, isothermal curves relating reduced energy to break to log time at break (t_b) obtained by stretching the rubber at different extension rates, were shifted along the log time axis to produce a master curve for the reference temperature 294°K. The shifts along the log t_b scale (log a_T) were similar to those predicted by the well-known WLF equation[61]. Again it is noticed that the difference between the energy input to break values for the gum and filler loaded rubbers at the higher times to break are an order of magnitude.

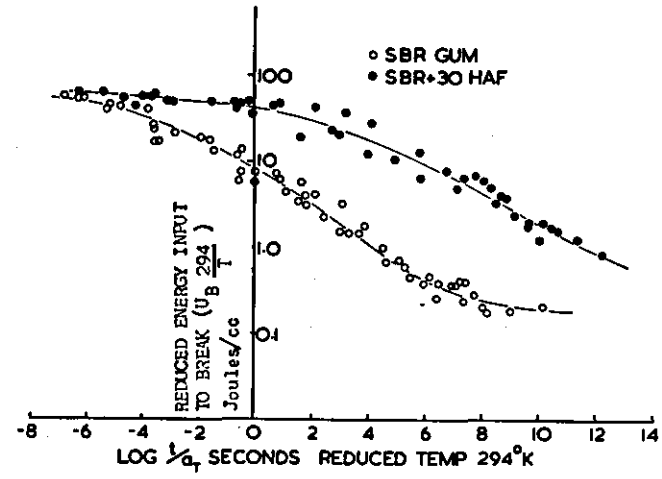

Fig. 19. Reduced energy input to break as function of reduced time to break for SBR gum and SBR containing 30 phr HAF carbon black

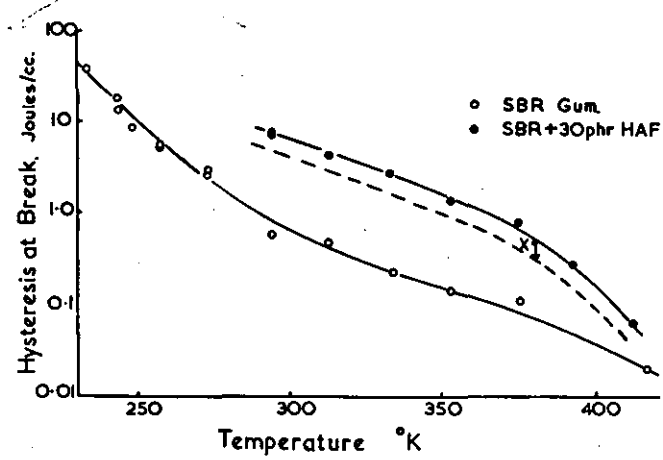

Fig. 20. Hysteresis at break as function of temperature for SBR gum and SBR containing 30 phr HAF carbon black

These results suggest that the rubber phase of filler loaded vulcanizates exhibit more hysteresis than the corresponding gum vulcanizate when compared isothermally. Fig. 20 illustrates this point more clearly where the bulk hysteresis of the two vulcanizates are plotted as a function of temperature. Unification of the isothermal gum and filler loaded results by the hydrodynamic correction factor does not succeed. After correction by equation (4) the filled rubber still exhibits more hysteresis at break than the gum rubber at the same temperature of test, although the difference does decrease as the temperature of the test is raised. A small correction could be applied to take account of the breakdown of the filler structure but this would by no means unify the results. The hydrodynamic correction factor, therefore, can only be applied in cases where the rubber phase of the filler loaded vulcanizate is in the same viscoelastic condition as the gum rubber. This necessitates the temperature of test for SBR with 30 phr HAF carbon black to be at least 40°C above the temperature of test of the unfilled SBR.

In an attempt to investigate more clearly the role of time and temperature in reinforcement of rubbers, Harwood, Payne and Smith[45] have considered a more fundamental approach. The tensile stress of a rubber (σ) can be factorized[62, 63] into a strain factor $f(\varepsilon)$ and a time-dependent modulus function $\phi(t)$

$$\sigma = f(\varepsilon) \times \phi(t) \qquad (11)$$

This type of analysis has been applied to SBR gum and filler loaded vulcanizates by using an empirical relationship due to Martin, Roth and Stiehler[64] (MRS equation) which has been shown to be applicable to SBR by Smith[62] and Landel and Stedry[65]. The MRS equation is given by

$$f(\varepsilon) = \frac{\lambda - 1}{\lambda^2} \exp A\left[\lambda - \frac{1}{\lambda}\right] \qquad (12)$$

where λ is the extension ratio equal to $(1 + \varepsilon)$ and A is a constant.

Harwood *et al.* have concluded from their investigations that the strain function for filled rubbers is the more temperature-sensitive parameter. It is found that the constant A is independent of temperature for the gum rubber but does increase very slightly with increasing temperature for the filled vulcanizate. There is, however, at least a factor of 2 between A for the filled and unfilled rubbers. This increase in A for filled rubbers is similar to the increase in A obtained with increasing crosslink density[66] and implies that the presence of the filler particles tightens the network but that the "tightness" decreases with increasing temperature. Two possible explanations of this behaviour are:

1. The rubber chains adhering to the surface of a carbon black particle, desorb from the surface of the filler particle as the temperature is raised

   or

2. There is a shell of rubber chains immobilised around each filler particle, which decreases in thickness with increasing temperature.

It is conditional, however, to the derivation of the hydrodynamic correction factor (equation 3) by Guth and Gold[48] and Smallwood[67] from the initial findings of Einstein[68] that there is complete wetting of the filler surface by the rubber. This correction factor has been shown to be applicable to the ultimate strains and hysteresis at break provided the test conditions are favourable and this, together with the conclusions from stress-softening, of there being strong adhesion between the filler particle and the rubber discussed earlier, and the electron microscope investigations by Hess[69], confirm that rubber-filler breakdown can be neglected with reinforcing fillers.

It is thought, therefore, that explanation (2) is the more probable mechanism which is compatible with the widely-held concept of a region of restricted rubber surrounding the filler particles.

Conclusion

This review has discussed in some depth hysteresial mechanisms that have been studied in recent years. Others such as crystallisation and viscoelasticity have been widely discussed previously.

The most interesting feature of the work is the influence that the combined hysteresis due to all the mechanisms has on the strength of rubber. The finding of a unique relationship between hysteresis and strength is of great importance and the general applicability of the relationship to filled rubbers by use of a hydrodynamic correction factor when test conditions are suitable is most useful.

Hysteresis is increased by the presence of fillers viscoelastically as well as hydrodynamically but it is not until data are expressed in terms of time or temperature that the viscoelastic contribution is noticed. The concept of a filler particle surrounded by a layer or shell of rubber, with properties different from that of the rubber continuum, is not a new one, but the approach to reinforcement by the consideration of bulk energies is novel. Other evidence for rubber chain hindrance close to the filler surface is forthcoming from the investigations of Westlinning[70], Schoon[71], Grosch[72] and Smit[73]. Radok and co-workers[74] in a series of papers on the theory of inclusions in viscoelastic materials have shown that if the conclusions are non-rigid but possess a modulus differing from that of the bulk rubber, then the bulk rubber acquires additional characteristic response times which is equivalent to increasing the hysteresis exhibited by the rubber.

This approach, therefore, provides a physical explanation of why the strength of amorphous polymers with 30—60 phr carbon black filler can be anything from 10 to 20 times greater the corresponding unfilled amorphous polymer at or temperatures.

Acknowledgement

The majority of the authors' own work reported in this re was done at the Rubber and Plastics Research Associ Shawbury, Shropshire, the Natural Rubber Producers' Res Association, Welwyn Garden City, Herts., and the Sho Allied Trades Research Association, Kettering, Northants thanks go to the Boards and Councils of the Research As tions for the facilities provided for this work.

References

1. Payne, A. R., J. Appl. Poly. Sci., **6**, 57 (1962).
2. Payne, A. R., J. Appl. Poly Sci., **7**, 873 (1963).
3. Payne, A. R., J. Appl. Poly Sci., **8**, 2661 (1964).
4. Payne, A. R., Trans. IRI, **40**, T135 (1964).
5. Payne, A. R., Chapter 3 in "Reinforcement of Elastomers". Edited by G. Kraus, Interscience (1965).
6. Payne, A. R., J. Appl. Poly Sci., **9**, 2273 (1965).
7. Boonstra, B. B., and Medalia, A. I., Rubb. Age, **92**, 892 (1963).
8. Payne, A. R., J. Appl. Poly Sci., **9**, 1073 (1965).
9. Payne, A. R., Swift, P. M., and Wheelans, M. A., Paper presented to "Natural Rubber Conference", Kuala Lumpur, Malaysia (1968).
10. Payne, A. R., and Whittaker, R. E., SATRA publication, I.P.12.
11. Everett, D. H., and Whitton, W. I., Trans. Farad. Soc., **48**, 749 (1952).
12. Everett, D. H., and Smith, F. W., Trans. Farad. Soc., **50**, 187, (1954).
13. Payne, A. R., J. Colloid Sci., **19**, 744 (1964).
14. Payne, A. R., Paper presented at Brit. Soc. Rheol. Conference, Shrivenham (1968). SATRA publication, SA.2135.
15. Payne, A. R., Paper presented at Brit. Soc. Rheol. Conference, Shrivenham (1968). SATRA publication, SA.2134.
16. Harwood, J. A. C., and Payne, A.R., Cahiers du Groupe Français de Rheologie, **1**, 207 (1967).
17. Payne, A. R., J. Appl. Poly Sci., **11**, 383 (1967).
18. Mullins, L., J. Rubb. Res., **16**, 275, (1947).
19. Mullins, L., J. Phys. and Colloid Chem., **54**, 239 (1950).
20. Bouasse, H., and Carriere, Z., Annales de la Faculte des Sciences de Toulouse, **5**, 257 (1903).
21. Dannenberg, E. M., Trans. IRI, **42**, T26 (1966).
22. Boonstra, B. B., Chapter 16 in "Reinforcement of Elastomers". Edited by G. Kraus, Interscience (1965).
23. Dannenberg, E. M., and Brennan, J. J., Paper No. 22, ACS Div. Rubb. Chem., Philadelphia (1965).
24. Brennan, J. J., Jermyn, T. E., and Perdagio, M. F., Paper No. 36, ACS Div. Rubb. Chem., Detroit (1964).
25. Kraus, G., Childers, C. W., and Rollman, K. W., J. Appl. Poly Sci., **10**, 229 (1966).
26. Harwood, J. A. C., Mullins, L., and Payne, A. R., J. Appl. Poly Sci., **9**, 3011 (1965).
27. Harwood, J. A. C., and Payne, A. R., J. Appl. Poly Sci., **10**, 315 (1966).
28. Harwood, J. A. C., and Payne, A. R., J. Appl. Poly Sci, **10**, 1203 (1966).
29. Harwood, J. A. C., and Payne, A. R., Trans. IRI, **42**, T14, (1966).
30. Harwood, J. A. C., and Payne, A. R., J. Appl. Poly Sci., **11**, 1825 (1967).
31. Harwood, J. A. C., Mullins, L., and Payne, A. R., J. of IRI, **1**, 17 (1967).
32. Harwood, J. A. C., and Payne, A.R., Unpublished work.
33. Puett, D., Smith, K. J., and Ciferri, A., J. Phys. Chem., **69**, 141 (1965).
34. Payne, A. R., and Popplewell, D., Paper presented to SATRA "Poromerics Symposium", Corby, (1968). SATRA publication, RR.204.
35. Jackson, E. G., Tech. J. Nat. Footwear Manuf. Assn., **4**, 130 (1968).
36. Trick, G. S., J. Appl. Poly Sci., **3**, 252 (1960°.
37. Brucksch, W. F., Rubb. Chem. Tech., **35**, 453 (1962).
38. Brucksch, W. F., Rubb. Chem. Tech., **36**, 975 (1963).
39. Bateman, L., *et al.* Chapter 19 in "Chemistry and Physics of Rubber-like Substances". Edited by L. Bateman, Maclaren, London (1963).
40. Brown, H. P. Rubb. Chem. Tech. **36**, 931 (1963).
41. Bueche, F., Chapter 1 in "Reinforcement of Elastomers". Edited by G. Kraus, Interscience (1965).
42. Smith, T. L., J. Appl. Phys., **35**, 27 (1964).
43. Kelley, F. N., Appl. Poly Symp. No. 1, 229 (1965).
44. Harwood, J. A. C., and Payne A. R., J. Appl. Poly Sci., **12**, 889 (1968).
45. Harwood, J. A. C., Payne, A. R., and Smith, J. F., Paper presented at DKG conference, Berlin (1968). Awaiting publication in Kaut. u. Gummi.
46. Ferry, J. D., Fitzgerald, E. R., Grandine, L. D., and Williams, M. L., Ind. Eng. Chem., **44**, 703 (1952).
47. Mullins, L., and Tobin, N. R., J. Appl. Poly Sci., **9**, 2993, (1965).
48. Guth, E., and Gold, O., Phys. Rev., **53**, 322 (1938).
49. Harwood, J. A. C., Payne, A. R., and Whittaker, R. E., To be published.
50. Landel, R. F., Trans. Soc. Rheol., **2**, 53 (1958).
51. Treloar, L. R. G., "The Physics of Rubber Elasticity", Clarendon Press (1958).
52. Porter, M., private communication.
53. Ferry, J. D., "Viscoelastic Properties of Polymers", Wiley, (1961).
54. Grosch, K. A., and Mullins, L., Rev. Gen. Caoutch., **39**, 1781, (1962).
55. Harwood, J. A. C., and Schallamach, A., J. Appl. Poly Sci. **11**, 1835 (1967).
56. Grosch, K. A., Harwood, J. A. C., and Payne, A. R., Inst. Phys. and Phy. Soc. Conf., Series No. 1, "Physical Basis of Yield and Fracture", p. 144 (1966).
57. Lake, G. J., and Thomas, A. G., Proc. Royal Soc., **A300**, 108, (1967).
58. Lake, G. J., and Lindley, P. B., J. Appl. Poly Sci., **9**, 1233, (1965).
59. Lake, G. J., and Lindley, P. B., Rubb. J., **146**, 24, 30, (1964).
60. Andrews, E. H., J. Mech. Phys. Solids, **11**, 231 (1963).
61. Williams, M. L., Landel, R. F., and Ferry, J. D., J. Am. Chem. Soc., **77**, 3701 (1965).
62. Smith, T. L., Trans. Soc. Rheol., **6**, 61 (1962).
63. Halpin, J. C., J. Poly Sci., B, **2**, 959 (1964).
64. Martin, G. M., Roth, F. L., and Stiehler, R. D., Trans. IRI, **32**, 189 (1956).
65. Landel, R. F., and Stedry, P. J., J. Appl. Phys., **31**, 1885, (1960).
66. Harwood, J. A. C., CNAA Ph.D. Thesis, NCRT (1968).
67. Smallwood, H. M., J. Appl. Phys., **15**, 758 (1944).
68. Einstein, A., Ann. Physik., **19**, 289 (1906).
69. Hess, W. M., private communication.
70. Westlinning, H., Paper read at DKG conference, Freiburg i Bresgau (1962).
71. Schoon, T. G. F., and Alder, K., Paper read at DKG conference, Munich (1965).
72. Grosch, K. A., J. Appl. Poly Sci., **12**, 915 (1968).
73. Smit, P. P. A., Rheol. Acta, **5**, 277 (1966).
74. Radok, J. R. M., and Tai, C. L., J. Appl. Poly Sci., **6**, 518, (1962).